AD-A154 121 BASIC EMC (ELECTROMAGNETIC COMPATIBILITY) TECHNOLOGY ADVANCEMENT FOR C3 S..(U) SOUTHEASTERN CENTER FOR ELECTRICAL ENGINEERING EDUCATION INC S.. 1/3

UNCLASSIFIED Y H SUTU ET AL. FEB 85 F/G 20/14 NL

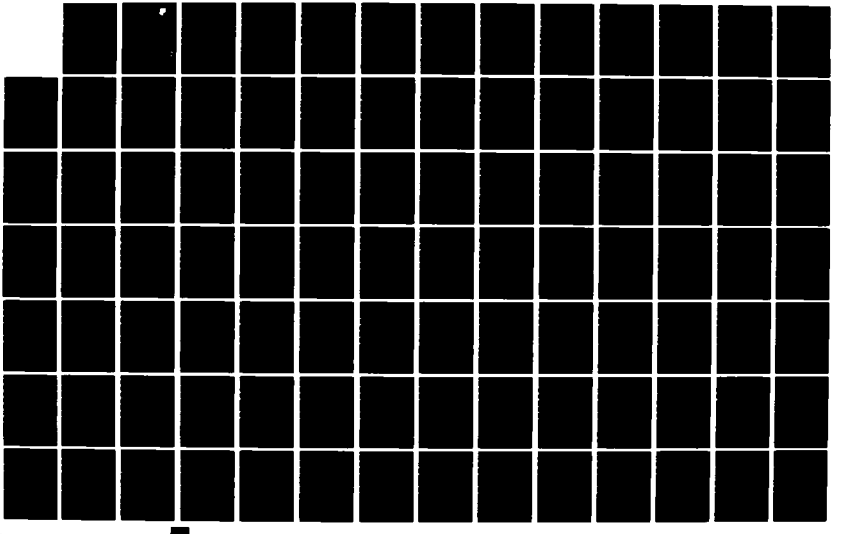

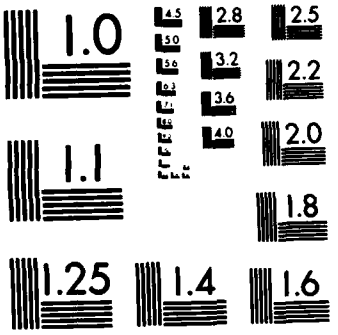

RADC-TR-82-286, Vol Ib (of six)
Final Technical Report
February 1985

BASIC EMC TECHNOLOGY ADVANCEMENT FOR C^3 SYSTEMS - Demodulation Radio Frequency Interference Effects in Operational Amplifier Circuits

Southeastern Center for Electrical Engineering Education

Yue-Hong Sutu and James J. Whalen

ROME AIR DEVELOPMENT CENTER
Air Force Systems Command
Griffiss Air Force Base, NY 13441-5700

This report has been reviewed by the RADC Public Affairs Office (PA) and is releasable to the National Technical Information Service (NTIS). At NTIS it will be releasable to the general public, including foreign nations.

RADC-TR-82-286, Vol Ib (of six) has been reviewed and is approved for publication.

APPROVED: Roy F. Stratton

ROY F. STRATTON
Project Engineer

APPROVED: W. S. Tuthill

W. S. TUTHILL, Colonel, USAF
Chief, Reliability & Compatibility Division

FOR THE COMMANDER: John A. Ritz

JOHN A. RITZ
Acting Chief, Plans Office

If your address has changed or if you wish to be removed from the RADC mailing list, or if the addressee is no longer employed by your organization, please notify RADC (RBCT) Griffiss AFB NY 13441-5700. This will assist us in maintaining a current mailing list.

Do not return copies of this report unless contractual obligations or notices on a specific document requires that it be returned.

UNCLASSIFIED
SECURITY CLASSIFICATION OF THIS PAGE

REPORT DOCUMENTATION PAGE

1a. REPORT SECURITY CLASSIFICATION UNCLASSIFIED	1b. RESTRICTIVE MARKINGS N/A
2a. SECURITY CLASSIFICATION AUTHORITY N/A	3. DISTRIBUTION/AVAILABILITY OF REPORT Approved for public release; distribution unlimited.
2b. DECLASSIFICATION/DOWNGRADING SCHEDULE N/A	
4. PERFORMING ORGANIZATION REPORT NUMBER(S) N/A	5. MONITORING ORGANIZATION REPORT NUMBER(S) RADC-TR-82-286, Vol Ib (of six)
6a. NAME OF PERFORMING ORGANIZATION Southeastern Center for Electrical Engineering Education 6b. OFFICE SYMBOL (If applicable)	7a. NAME OF MONITORING ORGANIZATION Rome Air Development Center (RBCT)
6c. ADDRESS (City, State and ZIP Code) 1101 Massachusetts Ave. St. Cloud FL 32706	7b. ADDRESS (City, State and ZIP Code) Griffiss AFB NY 13441-5700
8a. NAME OF FUNDING/SPONSORING ORGANIZATION Rome Air Development Center 8b. OFFICE SYMBOL (If applicable) RBCT	9. PROCUREMENT INSTRUMENT IDENTIFICATION NUMBER F30602-81-C-0062
8c. ADDRESS (City, State and ZIP Code) Griffiss AFB NY 13441-5700	10. SOURCE OF FUNDING NOS. PROGRAM ELEMENT NO. 62702F; PROJECT NO. 2338; TASK NO. 03; WORK UNIT NO. 35

11. TITLE (Include Security Classification)
BASIC EMC TECHNOLOGY ADVANCEMENT FOR C^3 SYSTEMS - Demodulation Radio Frequency Interference Effects in Operational Amplifier Circuits

12. PERSONAL AUTHOR(S)
Yue-Hong Sutu, James J. Whalen

13a. TYPE OF REPORT	13b. TIME COVERED	14. DATE OF REPORT (Yr., Mo., Day)	15. PAGE COUNT
Final	FROM Sep 82 TO Dec 83	February 1985	252

16. SUPPLEMENTARY NOTATION
Work was performed at the State University of New York at Buffalo, Buffalo NY 14226.
Project Engineers: Gerard T. Capraro and Roy F. Stratton

17. COSATI CODES		
FIELD	GROUP	SUB. GR.
09	03	
09	01	

18. SUBJECT TERMS (Continue on reverse if necessary and identify by block number)
Electromagnetic Compatibility, Macromodel, Electromagnetic Interference, Nonlinear Response, Operational Amplifiers, Nonlinear Transfer Function

19. ABSTRACT (Continue on reverse if necessary and identify by block number)

Since monolithic integrated operational amplifier (op amps) have become important building blocks in today's control and communication systems, a series of investigations have been carried out to determine RFI effects in analog circuits using op amps as active devices. The specific RFI effect investigated is demodulation of amplituder-modulated (AM) RF signals in op amp circuits to produce undesired low frequency responses at the AM-modulation frequency. Subsequently, the undesired demodulation responses may be processed in a manner similar to a desired low frequency signal by the low frequency components that follow the op amp. The undesired demodulation responses were shown to be characterized by a second-order nonlinear transfer function.

Four representative op amp types investigated were the 741 bipolar op amp with its conventional npn input transistors, the LM10 bipolar op amp with its less conventional pnp input transistors, the LF35 JFET-Bipolar op amp with its JFET input transistors, and

20. DISTRIBUTION/AVAILABILITY OF ABSTRACT UNCLASSIFIED/UNLIMITED ☒ SAME AS RPT. ☐ DTIC USERS ☐	21. ABSTRACT SECURITY CLASSIFICATION UNCLASSIFIED
22a. NAME OF RESPONSIBLE INDIVIDUAL Roy F. Stratton	22b. TELEPHONE NUMBER (Include Area Code) (315) 330-2563 22c. OFFICE SYMBOL RADC (RBCT)

DD FORM 1473, 83 APR EDITION OF 1 JAN 73 IS OBSOLETE.

UNCLASSIFIED
SECURITY CLASSIFICATION OF THIS PAGE

the CA081 MOS-Bipolar op amp with its MOSFET input transistors.

Two op amp circuits were investigated. The first op amp circuit configuration was the unity voltage gain buffer circuit known as a voltage follower. The circuit configuration is also called noninverting because both the intended signal and the RFI signal are injected into the noninverting input. The second circuit was an inverting op amp configuration. The intended signal voltage gain is determined by the ratio of the feedback resistor R2 and the input resistor R1. The investigation includes the effects of an RFI suppression capacitor in the feedback path.

Approximately 30 units of each op amp type were tested to determine the statistical variations of the RFI demodulation effects in the two op amp circuits. Statistical parameters such as mean and standard deviation provide quantitative measures on variations in op amp RFI susceptibility.

The Nonlinear Circuit Analysis Program, NCAP, was used to simulate the demodulation RFI response. In the circuit simulation, the op amp was replaced by its incremental macromodel. Values of macromodel parameters were obtained from previous investigations and from manufacturer's data sheets. Sensitivity analysis of the effects of variations of model parameters upon RFI susceptibility was performed for the unity gain buffer circuit in which critical parameters were identified. The effects of the RFI suppression capacitor in the inverting op amp circuit were also simulated. The simulated results were compared to measurements and satisfactory agreement has been achieved.

Some key results of this work are: (1) The RFI demodulation effects are 10 to 20dB lower in CA081 and LF355 FET-bipolar op amp than in 741 and LM10 bipolar op amp except above 40 MHz where the LM10 RFI response begins to approach that of CA081. (2) The experimental means values for 30 741 op amps show that RFI demodulation responses in the inverting amplifier with a 27 pF feedback capacitor were suppressed from 10 to 35 dB over the RF frequency range 0.1 to 150 MHz except at 0.15 where only 3.5 dB suppression was observed. (3) The computer program, NCAP, can predict RFI demodulation responses in 741 and LF355 unity gain buffer circuits within 6 and 7 dB respectively for RF frequencies 0.1 to 400 MHz except near the resonant frequencies for the LF355 circuit. (4) The NCAP simulations suggest that the resonances of the LF355 unity gain buffer circuit are related to small parasitic capacitance values of the order of 1 to 5 pF. (5) The NCAP sensitivity analysis indicates that variations in a second-order transfer function are sensitive to some macromodel parameters. In the 741 unity gain buffer circuit, the parameters V_{CBO}, I_C, and C_{je} are critical BJT model parameters; the parameters C_E, R_e, C_2 and G_a are critical linear macromodel parameters. In the LF355 unity gain buffer circuit, the parameters V_p, I_{Dmax}, and ψ are critical JFET model parameters; the parameters R_d, G_a, R_s, C_2 and C_s are critical linear parameters.

TABLE OF CONTENTS

TABLE OF CONTENTS (continued)

LIST OF ILLUSTRATIONS

LIST OF TABLES

LIST OF TABLES (Continued)

ACKNOWLEDGEMENTS

I wish to thank my major professor, Dr. James J. Whalen, for his guidance and encouragement throughout the dissertation research. Thanks are also due to committee members, Dr. Wayne A. Anderson and Dr. Darold C. Wobschall, for their comments and suggestions, and to outside reader, Dr. Roy Stratton, for his careful review and helpful criticisms.

In addition, I would like to express my gratitude to the many who have helped me in preparing this dissertation. Mrs. Mary Hill typed the table of contents, the list of illustrations, and most of the text. Mrs. Joan Bennett typed Chapters Four and Seven. Mrs. Marylin Hutching typed some of the tables in Appendices B and D. Their expert typing is deeply appreciated. Mr. Tom Whalen, Miss Cathy Whalen, and Miss Andrea Luong prepared the drawings and proof-read most of the tables in the Appendices. Their assistance is very much appreciated.

Finally, I would like to thank all the other people who have made my four years in SUNY/Buffalo worthwhile and memorable.

CHAPTER ONE

INTRODUCTION

In recent years, wideband monolithic analog integrated circuits (ICs) such as operational amplifiers (op amps) have become important building blocks in control and communication systems. These amplifiers, although designed to be linear, are not perfectly linear because of the inherent nonlinearities of the devices in the circuits. These nonlinear devices include diodes, bipolar junction transistors (BJTs), junction field-effect transistors (JFETs) and metal-oxide-semiconductor field-effect transistors (MOSFETs). When the control and communication systems built with these ICs are operated in a multi-signal radio frequency interference (RFI) environment, nonlinear effects can severely degrade system performance.

Some of the major nonlinear interference effects in electronic circuits are intermodulation, desensitization, cross modulation, and gain compression/expansion. Intermodulation is the process by which two or more signals combine in a nonlinear manner so as to produce new frequency components. Desensitization is the nonlinear effect by which a strong interfering signal at frequency f_2 reduces the apparant gain of a desired signal at frequency f_1. Cross modulation is the nonlinear effect whereby modulation from one signal is transferred to another. Gain compression/expansion occurs when the gain of an amplifier does not remain constant as the input signal amplitude is varied.

As an example, let us briefly consider nonlinear elements described by a power series. If the input and output are denoted by x and y

respectively, the power series description assumes the form

$$y = a_1x + a_2x^2 + a_3x^3 + \cdots \tag{1-1}$$

Suppose that the input x(t) is composed of a desired signal s(t) and unwanted modulated signal i(t)

$$s(t) = S\cos\omega_1 t \tag{1-2}$$

$$i(t) = I(1 + m(t))\cos\omega_2 t\ , \quad |m| < 1 \tag{1-3}$$

where ω_1 and ω_2 are angular frequencies, S and I are amplitudes, and m(t) is a modulation function. After substituting x(t) = s(t) + i(t) into Eq. (1-1), the output signal y(t) will include the following terms:

$$y(t) = \cdots + a_1S[1 + (3a_3/4a_1)S^2 + (3a_3/2a_1)I^2 + (3a_3/a_1)m(t)I^2]\cos\omega_1 t$$
$$+ \cdots + SI\cos(\omega_1 - \omega_2)t + SI\cos(\omega_1 + \omega_2)t + \cdots \tag{1-4}$$

where the terms with factors $(3a_3/4a_1)S^2$, $(3a_3/2a_1)I^2$, $(3a_3/a_1)m(t)I^2$ are called the gain compression/expansion, desensitization, cross modulation terms respectively, and $SI\cos(\omega_1 - \omega_2)t$ and $SI\cos(\omega_1 + \omega_2)t$ are two of the intermodulation terms.

This dissertation investigates mainly a subset of the intermodulation effects, namely demodulation effects, in op amp circuits. The intermodulation effect which causes demodulation is illustrated in Figure 1-1. Two sinusoidal RF signals at frequencies f_1 and f_2 respectively, which are outside the passband of an amplifier, combine nonlinearly to produce second-order nonlinear components at frequencies

f_1-f_2, $2f_2$, f_1+f_2, and $2f_1$. It is possible that the frequency component at f_1-f_2 falls within the passband of the amplifier. If this occurs, interference results. Consider the case in which a single interfering signal $v_i(t)$ is an amplitude-modulated (AM) RF signal with RF carrier f_{RF}, amplitude A, modulation frequency f_{AF}, and modulation index m. Then the interfering signal can be expressed as

$$v_i(t) = A(1 + m\cos 2\pi f_{AF}t)\cos 2\pi f_{RF}t$$

$$= A\cos 2\pi f_{AF}t + (mA/2)\cos 2\pi(f_{RF} - f_{AF})t + (mA/2)\cos 2\pi(f_{RF} + f_{AF})t \quad (1\text{-}5)$$

Defining the frequencies f_1 and f_2 of Figure 1-1 to be the RF carrier frequency and the lower sideband frequency respectively, we have

$$f_1 = f_{RF}, \quad (1\text{-}6)$$

$$f_2 = f_{RF} - f_{AF}, \quad (1\text{-}7)$$

$$f_{AF} = f_1 - f_2 \quad (1\text{-}8)$$

The second-order nonlinearities of the amplifier cause an intermodulation product (IMP) at the frequency f_{AF} which may fall inside the passband of the amplifier. This IMP may also be interpreted as being the demodulation RFI response of the amplifier at the AM frequency f_{AF}.

Electronic equipment being constructed for today's control and communication systems include integrated circuits (ICs) of various complexity. As the complexity of ICs increases, the need for computer-aided procedures in the analysis and prediction of various RFI effects in these electronic circuits becomes necessary.[1, 35-38] The computer-aided procedures include the use of nonlinear models for semiconductor

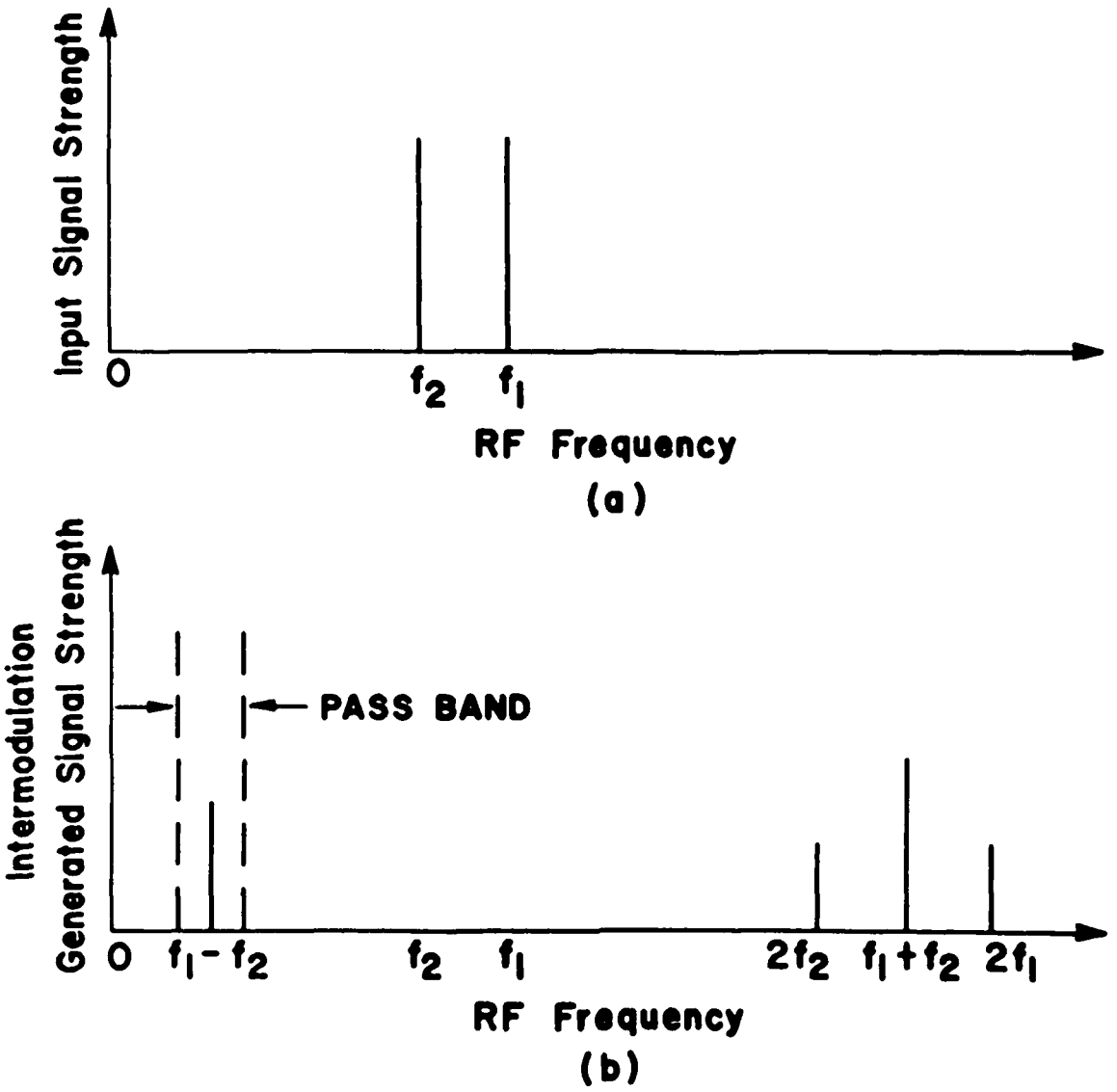

Fig. 1-1. Intermodulation type of RFI arising from a second degree nonlinearity in an amplifier.

(a) frequency content at input

(b) frequency content generated by second degree nonlinearity

devices and nonlinear transfer functions to characterize various nonlinear effects in electronic circuits.[2,3]

The Nonlinear Circuit Analysis Program (NCAP) was developed during 1972-1977 through the joint efforts of government, industry, and universities to provide the Electromagnetic Compatibility (EMC) community with a usable procedure for analyzing electronic equipment which must operate in a multi-signal RFI environment.[3,35] The program NCAP includes nonlinear circuit models for semiconductor diodes, BJTs, FETs, and also for vacuum diodes, triodes and pentodes. Nonlinear models for resistors, capacitors and inductors are also available. Recently, a nonlinear MOSFET model [4,5] has been developed for NCAP. When this model is incorporated into NCAP, then NCAP can be used to analyze circuits that include MOSFETs. NCAP uses a circuit oriented procedure based upon frequency domain analysis to predict the nonlinear transfer functions which characterize many nonlinear effects in electronic circuits. Among the nonlinear effects NCAP can predict are intermodulation and demodulation, desensitization, cross modulation, and gain compression/expansion.

In 1979, Fang demonstrated that NCAP can be used to predict how audio frequency modulated RF signals with radio frequencies up to 100 MHz are demodulated in bipolar ICs to cause undesired low frequency responses.[6-9] The ICs reported upon were the differential pair CA3026 which was used in a broadband cascode amplifier and the μA741 operational amplifier which was used in a unity gain buffer configuration. Among the significant contributions of Fang is a set of nonlinear BJT T model parameter values for NCAP simulations of μA741 op amp circuits.[3,10]

The set of parameter values could also be used in NCAP simulations of other bipolar ICs. Fang used a full (device-level) model when he analyzed μA741 op amp circuits.[6-7]

In 1980, G.K.C. Chen, in modeling the 741 and LM10 bipolar op amps, applied the macromodeling procedures by Boyle et al.[11] The advantage of using a macromodel over a full model is a saving of nearly an order of magnitude of computer analysis time and cost. Chen provided at least a partial justification for replacing a full model with a macromodel.[12] He applied the macromodel to predict demodulation RFI in two types of op amps: the 741 and LM10. Both types were used in a unity gain buffer amplifier configuration. The predicted results, presented as values for a second-order nonlinear transfer function, were compared to measurements made on a few (1-3) op amps.

In 1981, K.N. Chen compared demodulation RFI effects in bipolar and JFET-bipolar operational amplifiers based on NCAP simulation results using macromodels.[13] The op amps compared were the bipolar 741 and the JFET-bipolar LF355. Each was connected in a unity gain buffer amplifier configuration. The incremental macromodel for the LF355 op amp was derived from the large-signal macromodel of Krajewska and Holmes.[14] No experimental data for the LF355 were available at that time.

In 1982, K.N. Chen developed a four-terminal nonlinear incremental MOSFET model for predicting low level RFI in analog MOS circuits.[4,5] He used this model to investigate low level RFI effects in three analog MOS circuits. Chen investigated demodulation RFI effects in a CD4007 MOS amplifier and in a CA081 MOSFET-bipolar (BiMOS) op amp unity gain

buffer amplifier. He also investigated third-order intermodulation products (IMPs) in the CD4007 CMOS amplifier with a buffer stage. The experimental and predicted values of a second-order transfer function, which characterizes demodulation RFI effects for the first two circuits, were in very good agreement. The experimental and predicted values of third-order nonlinear transfer functions, which characterize third-order IMPs in the third circuit, were in good agreement.

In those previous op amp investigations, the emphasis was to compare predicted demodulation RFI effects to RFI measurements made on a very small number (1-3) of each op amp type. No measurements were made for the LF355. The only op amp configuration investigated was the unity gain buffer amplifier.

In a monolithic integrated circuit, all components are made simultaneously. The process, therefore, can be optimized for one type of component only e.g. the npn transistor. Furthermore, the parameters of each component in an integrated circuit cannot be pretested. As a result, the parameters of the components in a monolithic integrated circuit are subjected to wide variations. None of the previous investigations focused on this important fact.

The research work reported in this dissertation has the following objectives:

(1) To carry out an experimental investigation to determine the statistical variations of demodulation RFI effects in two op amp circuit configurations. One configuration is the unity gain buffer amplifier with each of the four op amp types previously mentioned (741, LM10,

LF355, CA081). Another configuration is an inverting amplifier with a voltage gain of 10. For the unity gain buffer amplifier, approximately 30 units of each op amp type have been tested. For the inverting amplifier, the same 30 units of 741 op amps have been tested. The op amps tested were purchased in groups of five over an extended time duration in order to obtain units with different date codes.

(2) To compare predicted values for a second-order nonlinear transfer function, which characterizes a demodulation RFI effect, to the mean value of measured data for the two op amp configurations. The circuits, with the op amps replaced by macromodels, were analyzed using NCAP. Values for op amp macromodel linear elements were based upon values provided in manufacturers' data sheets. The values for the model parameters of the nonlinear transistors in the macromodel were obtained from publications.[6,14,17] Since macromodel linear parameters were derived from typical values, the predicted values for the second-order transfer functions are best interpreted as typical or mean values. Hence, they will be compared to the measured mean values.

(3) To identify the critical macromodel input parameters. Sensitivity analyses of two types of op amps (741 and LF355) in the unity gain buffer amplifier configuration were performed. Each of the nonlinear device parameters and the macromodel linear parameters was varied independently by ± 10% from its original value. Variations in a second-order transfer function resulting from variations in op amp macromodel parameters were compared at corresponding RF frequencies.

(4) To study experimentally the effect of a RFI suppression capacitor on the inverting amplifier, especially its influence on the demodulation RFI statistics. A 27 pF capacitor was connected in the feedback path between output and inverting input of the op amp.

(5) To discuss some of the experimental observations. These observations include lower demodulation RFI effects in CA081 and LF355 op amps than in 741 and LM10 op amps and two resonances in the unity gain buffer configuration when LF355 op amps were used.

This dissertation is organized in the following manner. In Chapter Two, an analysis of weakly nonlinear circuits using the nonlinear transfer function approach is presented. This approach is employed by NCAP to characterize nonlinear effects in electronic circuits. In Chapter Three, op amp macromodels for RFI predictions are described. Chapter Four presents statistics of measured demodulation RFI effects in an op amp unity gain buffer configuration. Chapter Five presents statistics of measured demodulation RFI effects in an op amp inverting amplifier configuration. Results of NCAP simulations and sensitivity analyses are discussed in Chapter Six. Chapter Seven includes a summary, conclusions, and recommendations for future work.

CHAPTER TWO

ANALYSIS OF WEAKLY NONLINEAR CIRCUITS: NONLINEAR TRANSFER FUNCTION APPROACH

The analysis of nonlinear circuits is complicated, and no single analytical tool is generally applicable. However, various approaches are available for specific classes of nonlinear circuits. For the special case of weakly nonlinear circuits, whose nonlinearities are characterized by gradual, rather than abrupt variations, the Volterra functional series has proven to be an effective method.[15,16] The frequency domain transformations of Volterra functional series are called nonlinear transfer functions.

2.1 Nonlinear Transfer Function Approach

Consider a nonlinear circuit with input x(t) and output y(t), as shown in Figure 2-1a. Using the Volterra series method, the output y(t) may be written as[16]

$$y(t) = y_1(t) + y_2(t) + \cdots = \sum_{n=1}^{\infty} y_n(t) \tag{2-1}$$

where

$$y_n(t) = \int_{-\infty}^{\infty} \int_{-\infty}^{\infty} \cdots \int_{-\infty}^{\infty} h_n(\tau_1,\tau_2,\cdots,\tau_n) \prod_{i=1}^{n} x(t-\tau_i)d\tau_i \tag{2-2}$$

The kernel of Eq. (2-2), $h_n(\tau_1,\tau_2,\cdots,\tau_n)$, is called the nonlinear impulse response of order n. The n-dimensional Fourier Transform of y_n can be expressed as

$$Y_n(f_1,f_2,\cdots,f_n) = H_n(f_1,f_2,\cdots,f_n) \cdot \prod_{i=1}^{n} X(f_i) \tag{2-3}$$

where the nth-order nonlinear transfer function[16]

$$H_n(f_1,f_2,\cdots,f_n) = \int_{-\infty}^{\infty}\int_{-\infty}^{\infty}\cdots\int_{-\infty}^{\infty} h_n(\tau_1,\tau_2,\cdots,\tau_n)\cdot$$

$$\exp[-j2\pi(f_1\tau_1 + f_2\tau_2 + \cdots + f_n\tau_n)]d\tau_1 d\tau_2\cdots d\tau_n \qquad (2\text{-}4)$$

is the Fourier Transform of the nonlinear impulse response.

For a weakly nonlinear circuit, the output can be adequately approximated by including only the first few terms of the Volterra series. Therefore, Equation (2-1) reduces to

$$y(t) = \sum_{n=1}^{N} y_n(t) \qquad (2\text{-}5)$$

where $y_n(t)$ is given by Eq. (2-2). Terms above the Nth-order have been omitted from the infinite series because they are assumed to contribute negligibly to the output. Thus, the output of a weakly nonlinear circuit can be modeled as a sum of N individual responses, as shown in Figure 2-1b. This model consists of a parallel combination of N blocks with each block having the same excitation x(t).

For the sinusoidal steady state case, let the input x(t) be a sum of Q sinusoidal signals with amplitudes E_q, frequencies f_q and phase angles θ_q.

$$x(t) = \sum_{q=1}^{Q} |E_q| \cos(2\pi f_q t + \theta_q) \qquad (2\text{-}6)$$

We define the complex amplitude E_q as

$$E_q = |E_q| \exp(j\theta_q) \qquad (2\text{-}7)$$

with $E_{-q} = E_q^*$, $E_0 = 0$, and $f_{-q} = -f_q$ (2-8)

where E_q^* is the complex conjugate of E_q. Now Equation (2-6) can be written as

$$x(t) = (1/2) \sum_{q=-Q}^{Q} E_q \exp(j2\pi f_q t) \tag{2-9}$$

After substituting Eq.(2-9) into Eq. (2-2) and manipulating, we obtain[2]

$$y_n(t) = (1/2^n) \sum_{q_1=-Q}^{Q} \cdots \sum_{q_n=-Q}^{Q} E_{q_1} \cdots E_{q_n} H_n(f_{q_1}, \cdots, f_{q_n}) \cdot \exp[j2\pi(f_{q_1} + f_{q_2} + \cdots + f_{q_n})t] \tag{2-10}$$

where $H_n(f_{q_1}, \cdots, f_{q_n})$ is the nth-order nonlinear transfer function as described in Eq. (2-4). It is of nth-order in the sense that multiplication of the input x(t) by a constant A results in multiplication of the output $y_n(t)$ by the constant A^n. Based on the nonlinear transfer function approach, a weakly nonlinear circuit can be modeled as shown in Figure 2-2. Figure 2-2 is the frequency domain analogy of Figure 2-1b.

Of particular interest in this dissertation is the two-tone input case where Q = 2. The first-order, second-order and third-order components of the response, denoted as $y_1(t)$, $y_2(t)$ and $y_3(t)$ respectively, are given by

$$y_1(t) = (1/2) \sum_{q_1=-2}^{2} E_{q_1} H_1(f_{q_1}) \cdot \exp(j2\pi f_{q_1})t \tag{2-11}$$

$$y_2(t) = (1/4) \sum_{q_1=-2}^{2} \sum_{q_2=-2}^{2} E_{q_1} E_{q_2} H_2(f_{q_1}, f_{q_2}) \cdot \exp[j2\pi(f_{q_1} + f_{q_2})t] \tag{2-12}$$

$$y_3(t) = (1/8) \sum_{q_1=-2}^{2} \sum_{q_2=-2}^{2} \sum_{q_3=-2}^{2} E_{q_1} E_{q_2} E_{q_3} H_3(f_{q_1}, f_{q_2}, f_{q_3}) \cdot \exp[j2\pi(f_{q_1} + f_{q_2} + f_{q_3})t] \tag{2-13}$$

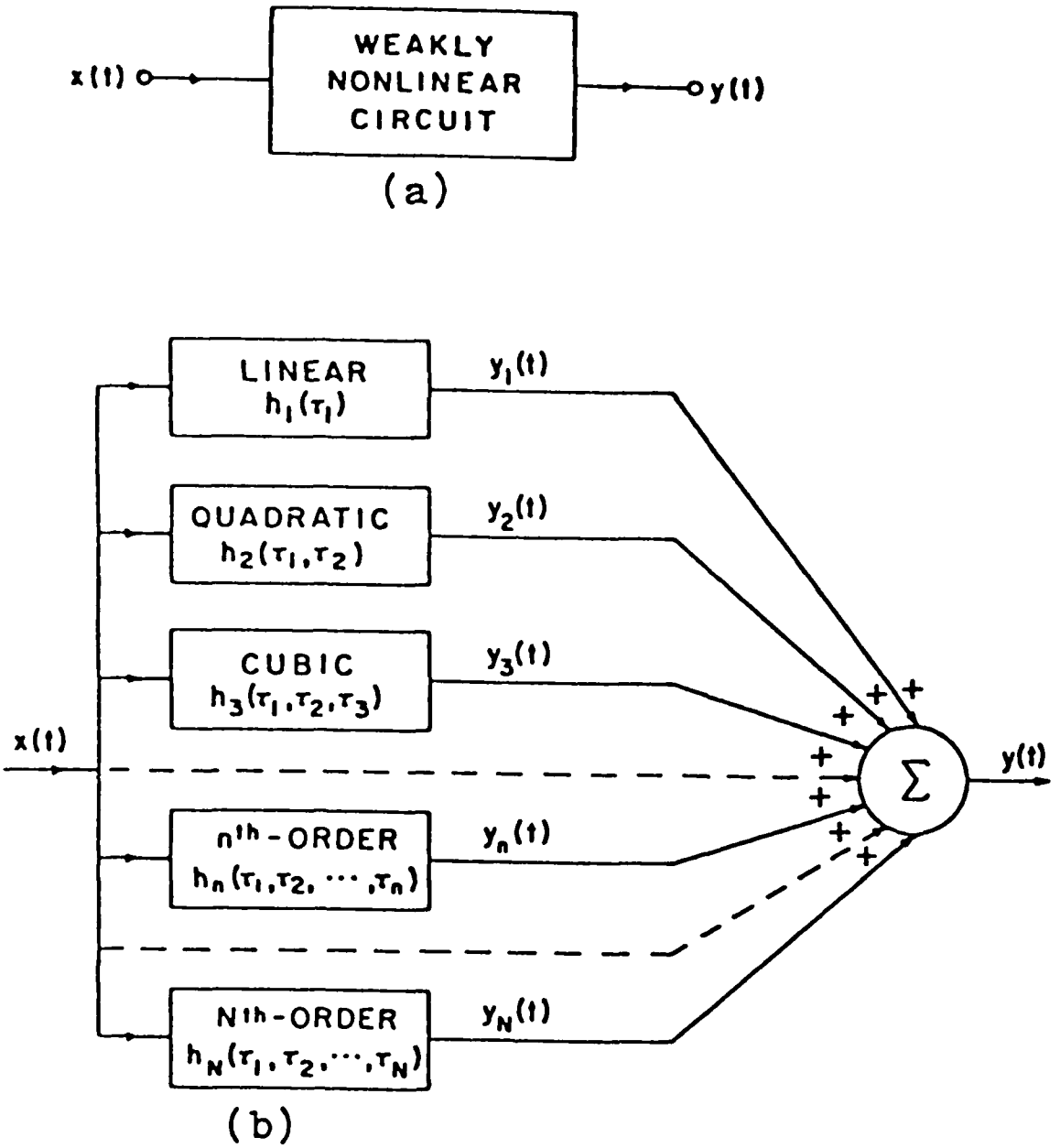

Figure 2-1. (a) Weakly nonlinear circuit with input x(t) and output y(t).
(b) Model of weakly nonlinear circuit suggested by the Volterra series time domain representation. (After Ref.[15,16])

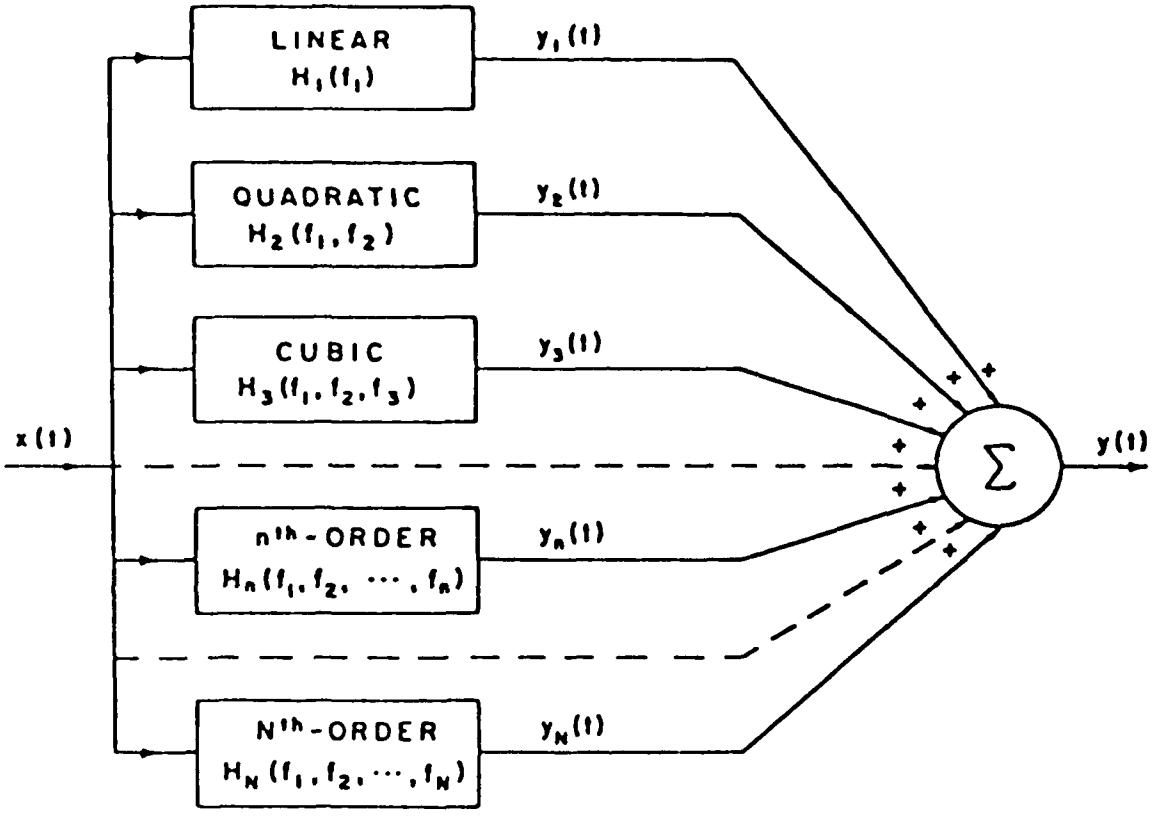

Fig. 2-2. Model of weakly nonlinear circuit suggested by the Volterra series frequency domain representation: the nonlinear transfer function approach. (After Ref.[2]).

All nonlinear transfer functions that differ by a permutation of arguments are equivalent, i.e. they are symmetrical functions of their arguments. Also, the nonlinear transfer functions of real systems are conjugated when the signs of all arguments are changed. For example,

$$H_2(f_1,f_2) = H_2(f_2,f_1) \tag{2-14}$$

$$H_2(-f_1,-f_2) = H_2^*(f_1,f_2) \tag{2-15}$$

Because the output response of a real system to real inputs is real, $y_n(t)$ is real. Thus the complex terms in Eqs. (2-11), (2-12), and (2-13) appear in conjugate pairs. For example, for the second-order response at frequency $(-f_1 + f_2)$, there are four terms in Eq. (2-12) that contribute: i.e., $(q_1,q_2) = (-1,2)$, $(q_1,q_2) = (2,-1)$, $(q_1,q_2) = (1,-2)$, and (q_1,q_2) $(-2,1)$. Therefore the output term $y_2(t)$ at frequency $(-f_1 + f_2)$ may be expressed as

$$\begin{aligned} y_2(t)\big|_{-f_1+f_2} &= (1/4)\{E_1^*E_2H_2(-f_1,f_2)\cdot\exp[j2\pi(-f_1+f_2)t] + \\ &\quad E_2E_1^*H_2(f_2,-f_1)\cdot\exp[j2\pi(f_2-f_1)t] + \\ &\quad E_1E_2^*H_2(f_1,-f_2)\cdot\exp[j2\pi(f_1-f_2)t] + \\ &\quad E_2^*E_1H_2(-f_2,f_1)\cdot\exp[j2\pi(-f_2+f_1)t]\} \\ &= (1/2)\{E_1^*E_2H_2(-f_1,f_2)\cdot\exp[j2\pi(-f_1+f_2)t] + \\ &\quad E_1E_2^*H_2(f_1,-f_2)\cdot\exp[j2\pi(f_1-f_2)t]\} \\ &= |E_1||E_2||H_2(-f_1,f_2)|\cos[2\pi(f_2-f_1)t + \theta_2 - \theta_1 + \\ &\quad \gamma_2(-f_1,f_2)] \end{aligned} \tag{2-16}$$

where $H_2(-f_1,f_2) = |H_2(-f_1,f_2)|\exp[j\gamma_2(-f_1,f_2)]$.

Outputs at other frequencies can be calculated similarly. A list of outputs at all frequencies generated is given in Table 2-1 up to the third order.[4,16] In Table 2-1, the input and output voltages are related by the nonlinear transfer functions. When the corresponding voltage components at the input and output are measured, the expressions in Table 2-1 can be used to calculate experimental values of the nonlinear transfer functions.

2.2 Nonlinear Models for Basic Circuit Elements

In Section 2.1, we have shown how nonlinear effects in weakly nonlinear circuits are characterized by nonlinear transfer functions. In order to facilitate the calculation of nonlinear transfer functions, nonlinear devices in a nonlinear circuit are replaced by equivalent nonlinear models. Some basic nonlinear circuit elements are the nonlinear resistor, nonlinear capacitor, nonlinear inductor, and nonlinear controlled sources. These are adequate for modeling the nonlinearities of most electronic devices such as diodes, vacuum tubes, transistors, integrated circuits, etc. In weakly nonlinear circuits, electronic devices are typically operated over a localized region of their characteristics. Therefore, it is possible to expand the nonlinearities in power series about the quiescent operating point in terms of incremental variables.

(1) Nonlinear resistor

Let $e_r(t)$ and $i_r(t)$ denote the incremental voltage and current

TABLE 2-1

RESPONSES OF A WEAKLY NONLINEAR CIRCUIT FOR THE TWO TONE INPUT CASE[a]

Order	Frequency Combination	Amplitude of Response	Type of Response
1	f_1	$\|E_1\|\|H_1(f_1)\|$	Linear
1	f_2	$\|E_2\|\|H_1(f_2)\|$	
2	f_1-f_2	$\|E_1\|\|E_2\|\|H_2(f_1,-f_2)\|$	Second-order intermodulation
2	f_1+f_2	$\|E_1\|\|E_2\|\|H_2(f_1,f_2)\|$	
2	$2f_1$	$0.5\|E_1\|^2\|H_2(f_1,f_1)\|$	Second harmonics
2	$2f_2$	$0.5\|E_2\|^2\|H_2(f_2,f_2)\|$	
3	$2f_1-f_2$	$0.75\|E_1\|^2\|E_2\|\|H_3(f_1,f_1,-f_2)\|$	Third-order intermodulation
3	$2f_2-f_1$	$0.75\|E_1\|\|E_2\|^2\|H_3(-f_1,f_2,f_2)\|$	
3	$3f_1$	$0.25\|E_1\|^3\|H_3(f_1,f_1,f_1)\|$	Third harmonics
3	$3f_2$	$0.25\|E_2\|^3\|H_3(f_2,f_2,f_2)\|$	

[a]After K.N.Chen,[4] a more complete table can be found in Refs. [2] and [15].

associated with a nonlinear resistor. The incremental current through the resistor may be expressed as[2]

$$i_r(t) = \sum_{k=1}^{\infty} g_k [e_r(t)]^k \qquad (2\text{-}17)$$

where g_1 is the conductance of the linear resistor normally included in a linear incremental equivalent circuit, and the g_k for $k > 1$ are usually referred to as nonlinear coefficients.

(2) Nonlinear capacitor

Let $e_c(t)$ and $i_c(t)$ denote the incremental voltage and current associated with a nonlinear capacitor. The incremental current through the capacitor is given by[2]

$$i_c(t) = \sum_{k=0}^{\infty} C_k [e_c(t)]^k de_c(t)/dt \qquad (2\text{-}18)$$

where C_0 is the capacitance of the linear capacitor to be inserted into a linear incremental circuit, and the C_k for $k > 1$ are usually referred to as nonlinear coefficients.

(3) Nonlinear inductor

Let $e_\ell(t)$ and $i_\ell(t)$ be the incremental voltage and current associated with a nonlinear inductor. The series representation of the incremental current through the inductor is[2]

$$i_\ell(t) = \sum_{k=1}^{\infty} \Gamma_k \left[\int_{-\infty}^{t} e_\ell(z)dz\right]^k \qquad (2\text{-}19)$$

where Γ_1 is the reciprocal inductance of the linear inductor in a linear incremental equivalent circuit, and the Γ_k for $k > 1$ are usually referred to as nonlinear coefficients.

(4) Nonlinear controlled sources

Nonlinear controlled sources occur frequently in electronic device models and are two-terminal elements whose terminal voltage or current is a nonlinear function of either the control voltage e_x or the control current i_x from some other part of the circuit. There are four simple types of nonlinear controlled sources which depend upon one variable. Their series representations are:

(4a) Voltage-controlled voltage source[2]

$$e_{cs}(t) = \sum_{k=1}^{\infty} \mu_k [e_x(t)]^k , \tag{2-20}$$

(4b) Current-controlled voltage source[2]

$$e_{cs}(t) = \sum_{k=1}^{\infty} r_{ks} [i_x(t)]^k , \tag{2-21}$$

(4c) Voltage-controlled current source[2]

$$i_{cs}(t) = \sum_{k=1}^{\infty} g_{ks} [e_x(t)]^k , \tag{2-22}$$

(4d) Current-controlled current source[2]

$$i_{cs}(t) = \sum_{k=1}^{\infty} \alpha_k [i_x(t)]^k . \tag{2-23}$$

The linear term in each expansion defines the linear controlled source to be used in linear incremental equivalent circuits. The linear coefficients μ_1, r_{1s}, g_{1s}, and α_1 are referred to as the voltage amplification factor, the mutual resistance, the mutual conductance, and the current amplification factor respectively. The coefficients with $k > 1$ are usually referred to as nonlinear coefficients, e.g. μ_2, r_{2s},

etc. The incremental equivalent circuit models for the nonlinear resistor, capacitor, inductor, and the four nonlinear controlled sources are shown in Figure 2-3 and Figure 2-4 respectively.

In addition to the four simple types of nonlinear controlled sources, some circuit device models require controlled sources that are a function of more than one independent control variable. For example, in the nonlinear incremental MOSFET model developed by K.N. Chen[4,5] the nonlinear drain current is a function of the gate-source voltage v_{gs}, the drain-source voltage v_{ds}, and the substrate-source voltage v_{bs}. When the source and substrate terminals are ac shorted so $v_{bs} = 0$, the series representation of this nonlinear controlled source may be expressed as

$$i_{ds} = \sum_{j=0}^{\infty} \sum_{k=0}^{\infty} g_{jk}(v_{gs})^j(v_{ds})^k \quad \text{where} \quad g_{00} = 0 \qquad (2\text{-}24)$$

The incremental equivalent circuit model for a voltage-controlled current source that is a function of two independent control voltages is shown in Figure 2-5.

2.3 NCAP Procedure for Determination of Nonlinear Transfer Functions

The Nonlinear Circuit Analysis Program NCAP was developed to provide the EMC community with usable procedure for analyzing nonlinear effects in electronic circuits in terms of nonlinear transfer functions. The NCAP procedure uses nodal analysis to solve for the nonlinear transfer functions. Nodal analysis is preferred to loop analysis because electronic circuits tend to have fewer nodes than loops. In order to perform nodal analysis, it is necessary that each nonlinear resistor, capacitor, and inductor have an admittance representation in which the element current

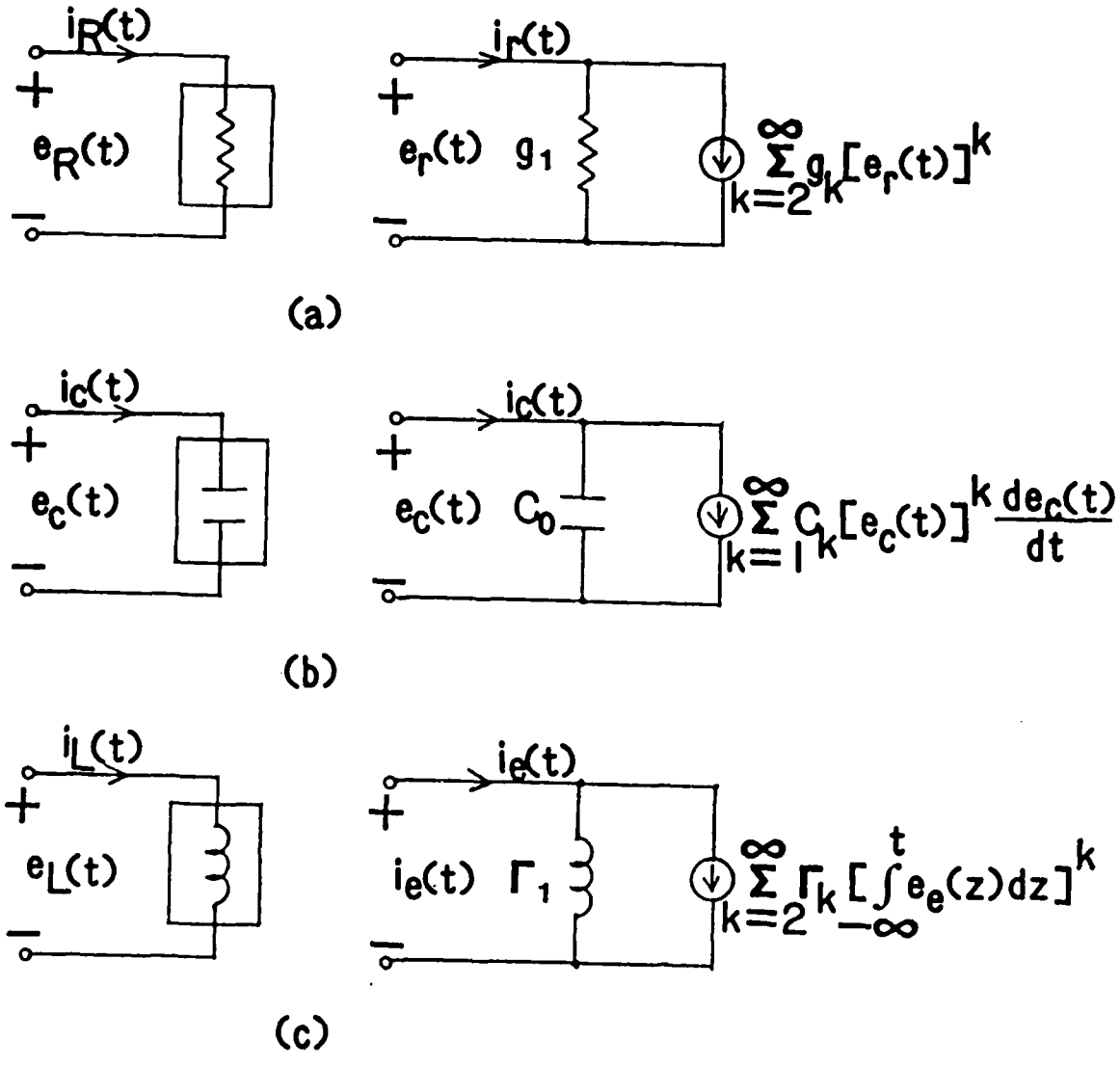

Fig. 2-3. Circuit symbols and incremental equivalent circuit models. (a) Nonlinear resistor. (b) Nonlinear capacitor. (c) Nonlinear inductor.

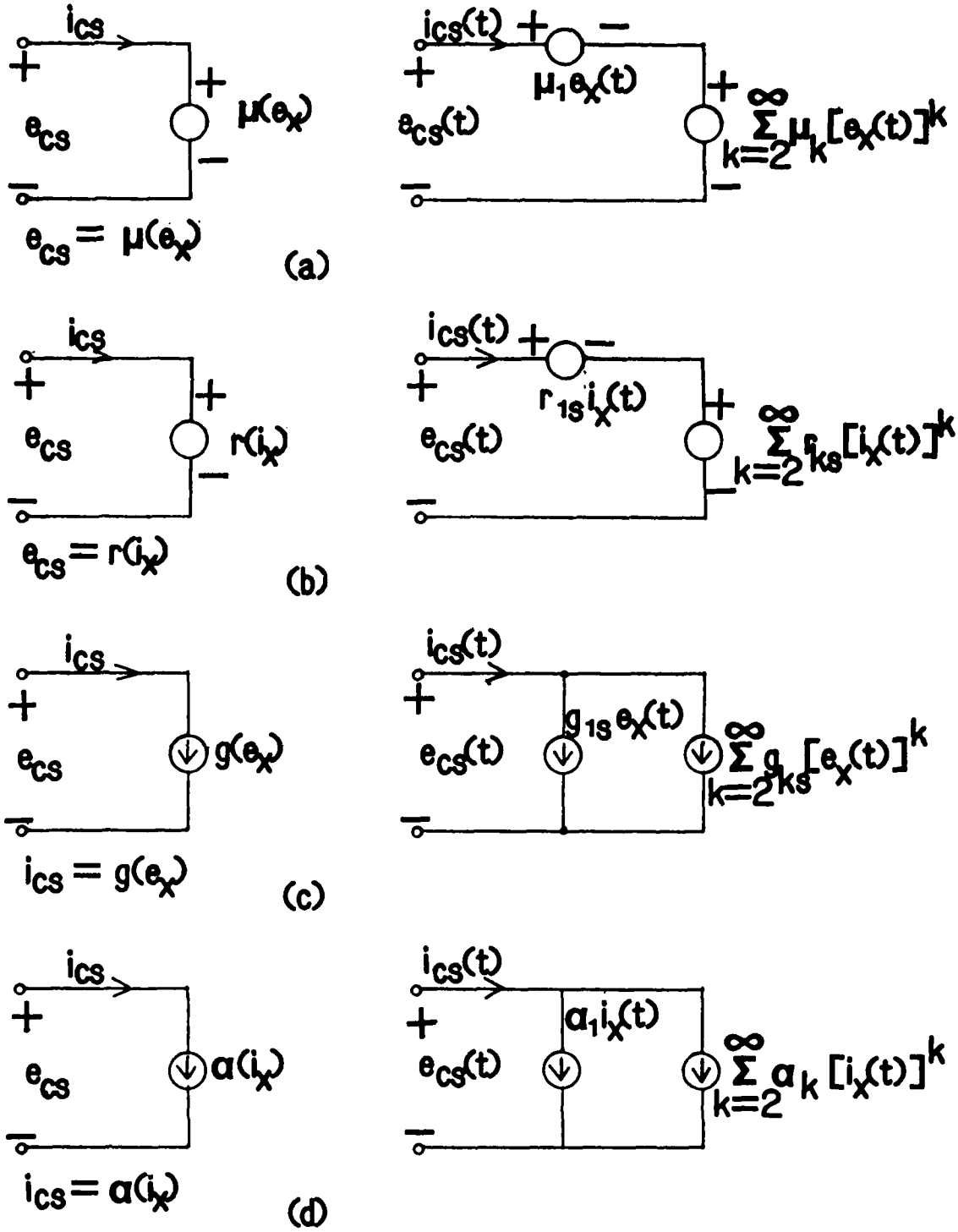

Fig. 2–4. Controlled source circuit symbols and incremental equivalent circuit models. (a) Voltage–controlled voltage source. (b) Current–controlled voltage source. (c) Voltage–controlled current source. (d) Current–controlled current source.

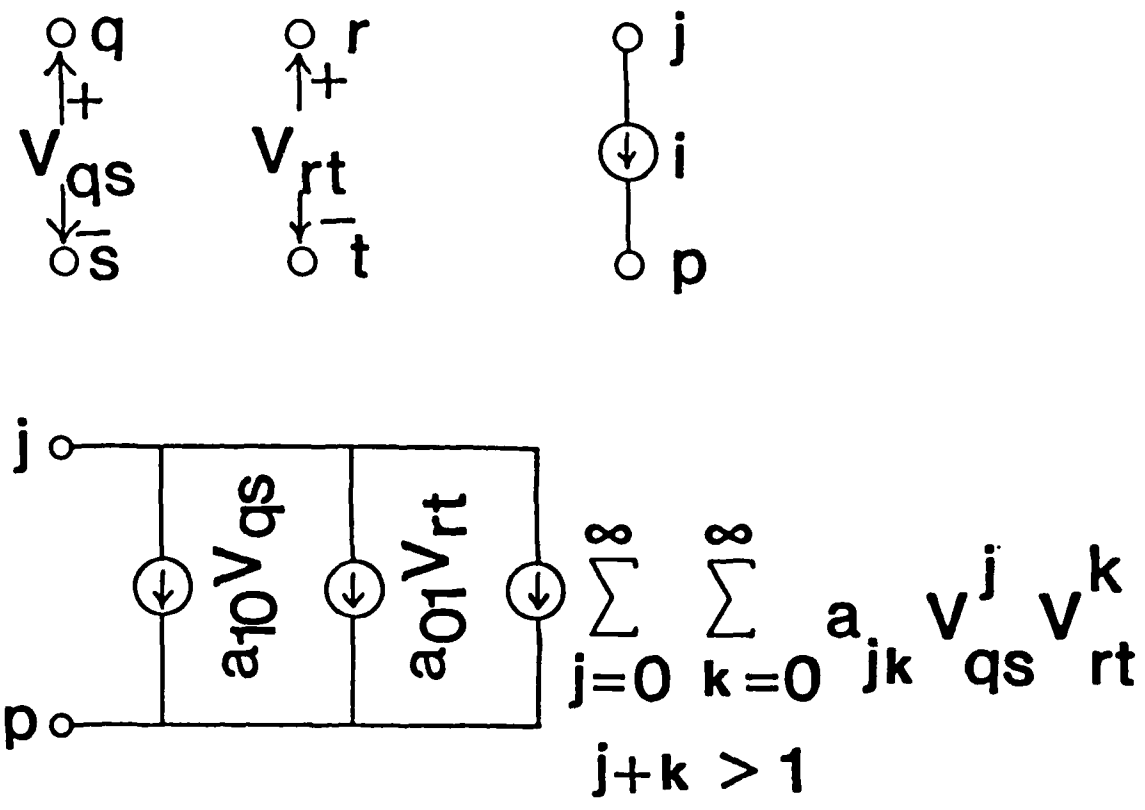

Figure 2-5. Nonlinear current source dependent upon two voltages.

is expressed as a function of the element voltage. Should an admittance representation not exist, as in the case of a current-controlled resistor, nodal analysis cannot be used directly. As far as controlled sources are concerned, only voltage-controlled current sources have an admittance representation. However, techniques are available by which other types of controlled sources can be converted to equivalent voltage-controlled current sources.[2]

Assume that an input which is the sum of n complex exponentials,

$$v_g(t) = \exp[j2\pi f_1 t] + \cdots + \exp[j2\pi f_n t] \qquad (2\text{-}25)$$

is applied to a nonlinear circuit with K + 1 nodes. The first step in the procedure is to write Kirchhoff's current law at each of the K nodes (one node is the reference node). The current through each nonlinear circuit element is then expressed as a power series where the independent variables are node-to-datum voltages. The linear term in each series can be represented by a linear circuit element. These are grouped with the linear portion of the network to form the incremental linear network. In terms of the K Kirchhoff current law equations, the second step is to arrange the equations such that only terms linear in node-to-datum voltage appear on the left-hand side. The right side of the equations then contains only the independent source terms and the nonlinear current sources. The nonlinear current sources are the nonlinear terms from the power series expansions of the nonlinear circuit elements. These equations can be expressed by the matrix equation

$$[Y(f_1 + \cdots + f_n)]\underline{H}_n(f_1,\cdots,f_n) = \underline{I}_n(f_1,\cdots,f_n) , \quad n \geq 2 \qquad (2\text{-}26)$$

where $[Y(f_1 + \cdots + f_n)]$ is the admittance matrix of the incremental linear network at frequency $f_1 + \cdots + f_n$, $\underline{H}_n(f_1, \cdots, f_n)$ is the nth-order nonlinear transfer function vector with components corresponding to each of the K nodes, and $\underline{I}_n(f_1, \cdots, f_n)$ is the nth-order nonlinear current source vector which can be determined from lower order transfer functions as will be shown in Section 2.4. For n = 1, the first-order transfer functions for various nodes are simply the conventional linear transfer functions obtained by solving the matrix equation

$$[Y(f_1)]\,\underline{H}_1(f_1) = [1/Z_g(f_1) \quad 0 \quad 0 \cdots\cdots \quad 0]^T \tag{2-27}$$

where $Z_g(f_1)$ is the independent source impedance, and T denotes the transpose operator. Thus, the first-order transfer function may be obtained from Eq. (2-27), and the second and higher order transfer functions are determined by solving Eq. (2-26) recursively. The computer-aided procedures used by NCAP to calculate nonlinear transfer functions up to the third order is illustrated by a flow chart in Figure 2-6.

2.4 Nonlinear Current Sources

The key step in the procedures are the calculations of the nth-order ($n \geq 2$) nonlinear current sources which are used to drive the incremental linear circuit to generate the nth-order nonlinear responses. A systematic algorithm has been developed for the computation of the nth-order current sources. See Ref. [2]. Results up to the third order are

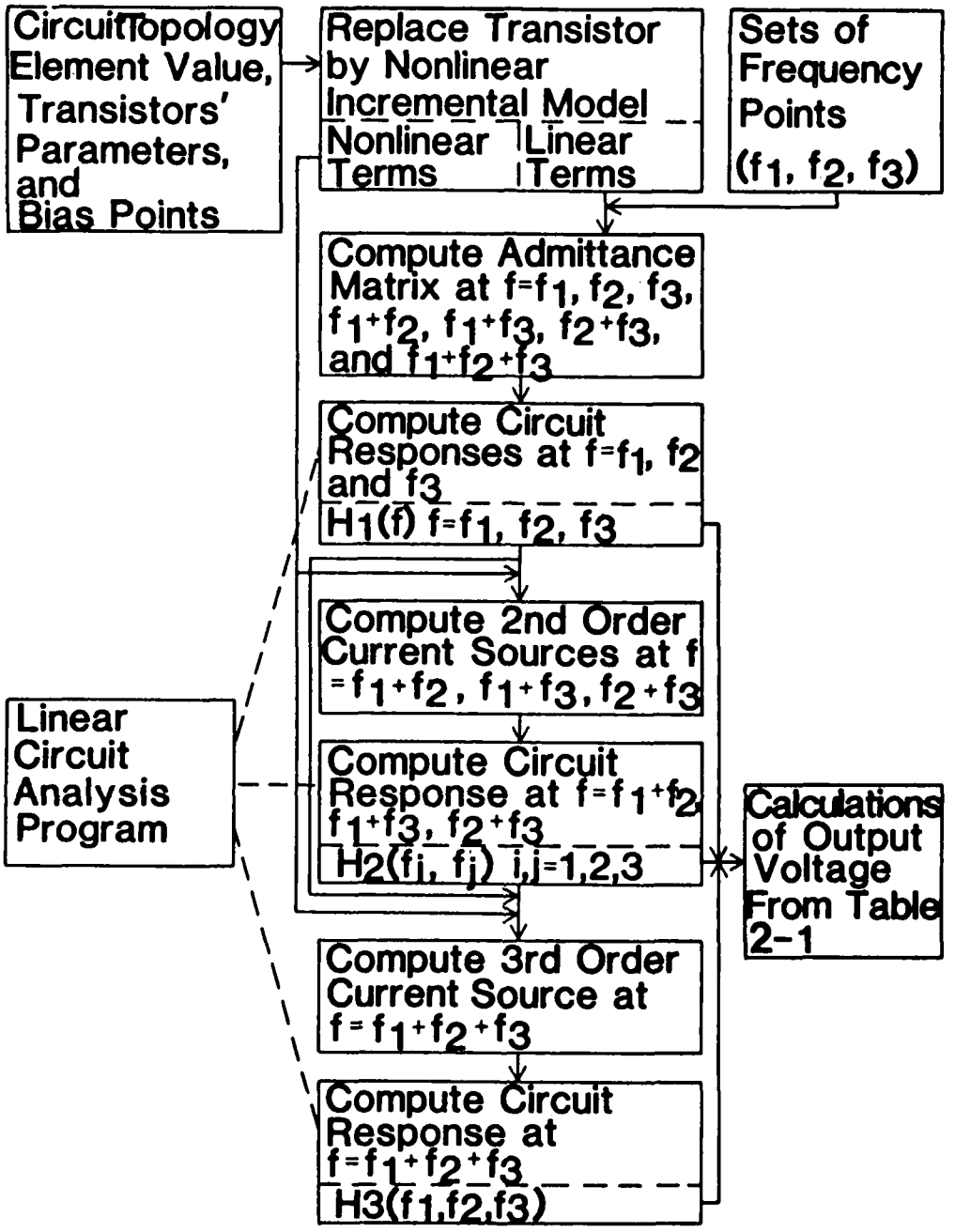

Figure 2-6. Flow chart of the computer-aided procedure for the calculation of the nonlinear transfer functions and the output responses of a weakly nonlinear circuit. (After Ref.[4])

summarized here for the four nonlinear elements described by Eqs. (2-17) - (2-19) and (2-22). The exact form of the nonlinear current source depends upon whether the nonlinear element has a zero-memory nonlinearity (i.e. a nonlinear resistor or a nonlinear controlled source), a capacitive nonlinearity or an inductive nonlinearity.

Second-order current sources at $f_1 + f_2$:

(1) Nonlinear resistor

$$I_2^{jp}(f_1,f_2) = g_2 H_1^{jp}(f_1) H_1^{jp}(f_2) \tag{2-28}$$

(2) Nonlinear capacitor

$$I_2^{jp}(f_1,f_2) = j2\pi(f_1+f_2)(C_1/2) H_1^{jp}(f_1) H_1^{jp}(f_2) \tag{2-29}$$

(3) Nonlinear inductor

$$I_2^{jp}(f_1,f_2) = \Gamma_2 \frac{H_1^{jp}(f_1)}{j2\pi f_1} \frac{H_1^{jp}(f_2)}{j2\pi f_2} \tag{2-30}$$

(4) Nonlinear voltage-controlled current source

$$I_2^{jp}(f_1,f_2) = g_{2s} H_1^{rt}(f_1) H_1^{rt}(f_2) \tag{2-31}$$

where I_2^{jp} is the second-order current source associated with the nonlinear circuit element connected between nodes j and p, $H_1^{jp}(f_1) = H_1^{j}(f_1) - H_1^{p}(f_1)$, and $H_1^{j}(f_1)$ is the first-order transfer function at node j which is evaluated at frequency f_1. When NCAP is used to analyze a circuit, the circuit is excited by a voltage source of unit amplitude at frequency f and $H_1(f)$ is the complex voltage at node j.

Third-order current sources at $f_1 + f_2 + f_3$:

(1) Nonlinear resistor

$$I_3^{jp}(f_1,f_2,f_3) = 2g_2\overline{H_1^{jp}(f_1)H_2^{jp}(f_2,f_3)} + g_3H_1^{jp}(f_1)H_1^{jp}(f_2)H_1^{jp}(f_3) \tag{2-32}$$

(2) Nonlinear capacitor

$$I_3^{jp}(f_1,f_2,f_3) = j2\pi(f_1+f_2+f_3)[2(C_1/2)\overline{H_1^{jp}(f_1)H_2^{jp}(f_2,f_3)} + (C_2/3)H_1^{jp}(f_1)H_1^{jp}(f_2)H_1^{jp}(f_3)] \tag{2-33}$$

(3) Nonlinear inductor

$$I_3^{jp}(f_1,f_2,f_3) = 2\Gamma_2\overline{\frac{H_1^{jp}(f_1)}{j2\pi f_1}\frac{H_2^{jp}(f_2,f_3)}{j2\pi(f_2+f_3)}} + \Gamma_3\frac{H_1^{jp}(f_1)}{j2\pi f_1}\frac{H_1^{jp}(f_2)}{j2\pi f_2}\frac{H_1^{jp}(f_3)}{j2\pi f_3} \tag{2-34}$$

(4) Nonlinear voltage-controlled current source

$$I_3^{jp}(f_1,f_2,f_3) = 2g_{2s}\overline{H_1^{rt}(f_1)H_2^{rt}(f_2,f_3)} + g_{3s}H_1^{rt}(f_1)H_1^{rt}(f_2)H_1^{rt}(f_3) \tag{2-35}$$

where the overbar denotes the arithmetic average of the 3! terms generated by all possible permutations of the 3 frequencies. For example,

$$\begin{aligned}\overline{H_1^{jp}(f_1)H_2^{jp}(f_2,f_3)} &= (1/6)[H_1^{jp}(f_1)H_2^{jp}(f_2,f_3) + H_1^{jp}(f_1)H_2^{jp}(f_3,f_2) + \\ &\quad H_1^{jp}(f_2)H_2^{jp}(f_1,f_3) + H_1^{jp}(f_2)H_2^{jp}(f_3,f_1) + \\ &\quad H_1^{jp}(f_3)H_2^{jp}(f_1,f_2) + H_1^{jp}(f_3)H_2^{jp}(f_2,f_1)] \\ &= (1/3)[H_1^{jp}(f_1)H_2^{jp}(f_2,f_3) + H_1^{jp}(f_2)H_2^{jp}(f_1,f_3) + H_1^{jp}(f_3)H_2^{jp}(f_1,f_2)]\end{aligned} \tag{2-36}$$

From Eqs. (2-28) - (2-35), we observe that the nth-order nonlinear current sources may be expressed as functions of lower order nonlinear transfer functions (n-1, n-2, etc.). In summary, the calculations of the nth-order nonlinear transfer functions ($n \geq 2$) involve the evaluations of the linear response of the incremental linearized circuit driven by the nth-order nonlinear current sources at frequencies $f_1 + \cdots + f_n$.

2.5 An Example

We illustrate the procedure described in Section 2.3 with the circuit shown in Figure 2-7.[2] For simplicity, the nonlinear resistor is assumed to be characterized by

$$i_r(t) = g_1 a(t) + g_2 a^2(t) \tag{2-37}$$

The objective is to determine the nonlinear transfer functions associated with the node-to-datum voltage a(t).

For this purpose, we need consider only the solutions to a set of equivalent sinusoidal steady-state linear circuit problems. The equivalent circuits required for the first-order, second-order, and third-order transfer functions are also shown in Figure 2-7. Note that the desired nonlinear transfer functions appear as unknown complex node-to-datum voltages. The independent current source is used as an excitation only in the equivalent circuit used to calculate the first-order transfer function. It does not occur in the equivalent circuits used to calculate the higher order transfer functions. There the excitations are provided by the nonlinearities that manifest themselves

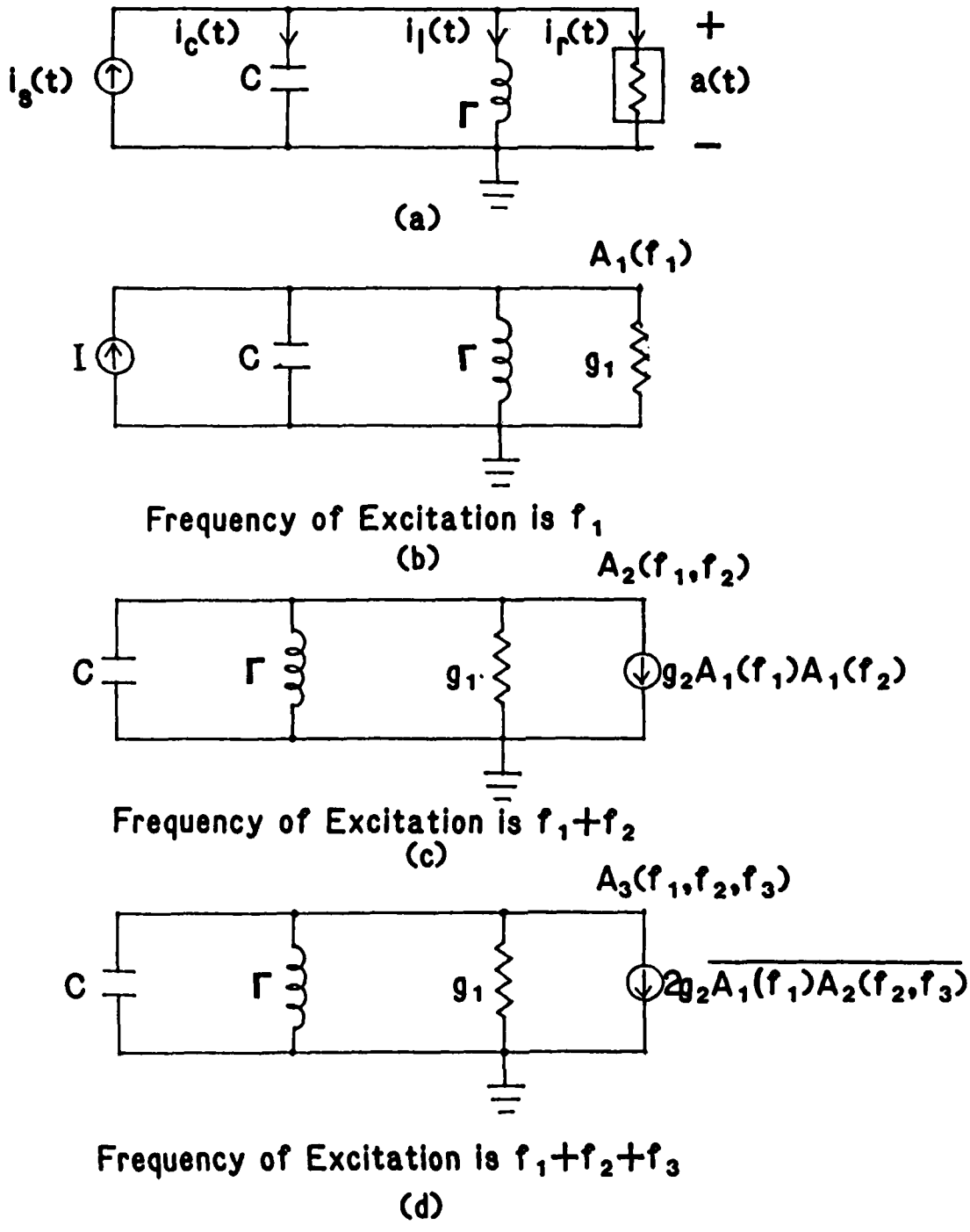

Fig. 2-7. A simple nonlinear circuit for use to illustrate the NCAP calculation procedure. (After Ref.[2])

as current sources driving the linearized network. Observe that, except for the sources, the same linearized circuit is used in each case.

The first-order transfer function is determined by assigning unit amplitude to the independent current source I in Figure 2-7b. Applying nodal analysis at frequency f_1, we obtain the expression for the voltage amplitude $A_1(f_1)$ given by

$$A_1(f_1) = 1/Y(j2\pi f_1) \ , \tag{2-38}$$

where $Y(j2\pi f) = g_1 + j2\pi fC + 1/j2\pi fL$.

One of the second-order transfer functions is determined by carrying out the nodal analysis at frequency $f_1 + f_2$. The excitation is a second-order current source of the form shown in Figure 2-7c. It is expressed in terms of linear transfer functions evaluated at f_1 and f_2 and the nonlinear series coefficient g_2. Solving the circuit shown in Figure 2-7c for the voltage amplitude A_2 at $f_1 + f_2$ yields the expression

$$A_2(f_1+ f_2) = - \frac{g_2 A_1(f_1)A_1(f_2)}{Y[j2\pi(f_1+ f_2)]} = A_2(f_1,f_2) \tag{2-39}$$

The same procedure is performed for the third-order transfer function at frequency $f_1 + f_2 + f_3$ using the circuit shown in Figure 2-7d. The excitation is a third-order current generator, and it can be expressed in terms of first-order and second-order transfer functions and the nonlinear coefficient g_2 as shown in Figure 2-7d. Solving the circuit shown in Figure 2-7d for the voltage amplitude A_3 at $f_1 + f_2 + f_3$ yields the expression

$$A_3(f_1+f_2+f_3) = -\frac{\overline{2g_2A_1(f_1)A_2(f_2,f_3)}}{Y[j2\pi(f_1+f_2+f_3)]} = A_3(f_1,f_2,f_3) \qquad (2\text{-}40)$$

The process can be extended to calculate the higher order transfer functions (n > 3).

CHAPTER THREE

MODELING OF DEMODULATION RFI IN OP AMP CIRCUITS

Recent advances in integrated circuit technology have pushed circuit complexity, measured in terms of number of transistors, far beyond the limitations of computer circuit analysis programs. The limitations, which are usually specified in terms of the maximum number of circuit nodes, devices, etc., are imposed either by computer memory size or by convergence problems. The circuit of a typical operational amplifier consists of about 30 devices. If the limit for the maximum number of devices (FET's, BJT's, and diodes) is 50, then circuits containing two or more op amps cannot be analyzed using device-level models for each op amp. (A device-level model is also called a full or complete model.) Furthermore, even if a computer system with large enough capacity is available, the simulation time required may be so long as to make the analysis too costly. These problems can often be circumvented by using an operational amplifier macromodel, which has significantly reduced complexity compared to the actual op amp circuit.

3.1 Macromodeling of Operational Amplifiers

The purpose of the macromodel is to represent adequately the electrical characteristics of the operational amplifier. Each relevant performance specification of the op amp is modeled separately with only limited consideration of the internal circuitry of the op amp. A macromodel for all bipolar operational amplifiers has been developed by Boyle et al.[11] Based on this bipolar op amp macromodel, macromodels for both the MOS-bipolar and JFET-bipolar op amps were developed by

Krajewska and Holmes.[14] Shown in Figure 3-1 is the circuit diagram of the 741 type op amp. Its macromodel is shown in Figure 3-2.

The circuit model in Figure 3-2 can be divided into three stages: the input stage, the interstage, and the output stage. It has been developed using two basic macromodeling techniques: simplification and build-up. In the simplification technique, representative portions of op amp circuitry are successively simplified by using simple ideal elements to replace numerous real elements. The final model using this approach bears some resemblance to the real circuit. The input stage circuit in Figure 3-2 is an example of the simplification technique. In the build-up technique, a circuit configuration composed of ideal elements is proposed to meet external circuit specifications without necessarily resembling a portion of an actual op amp circuit configuration. The build-up technique was employed in the development of the output stage shown in Figure 3-2.

Two npn bipolar transistors are employed in the input stage of the circuit model in Figure 3-2 to model the linear and nonlinear differential -mode and common-mode input characteristics. The input stage voltage gain is arbitrarily set to unity. The differential-mode and common-mode voltage gain are provided by the second stage. The macromodel includes the following elements related to dc operation: I_{EE} accounts for the dc bias current source in the input stage; the resistor R_p accounts for the dc power dissipation; the output stage elements G_C, R_C, D_1, D_2, and R_{01} provide dc current limiting, whereas V_E, V_C, D_3, and D_4 provide dc voltage limiting. The small-signal operation is controlled by the parameters G_a for the differential voltage gain, G_{cm}

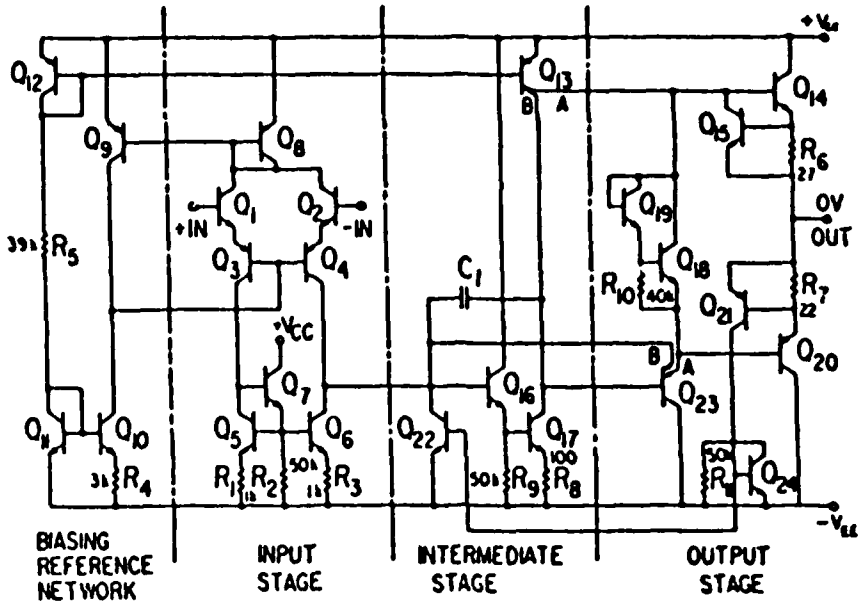

Fig. 3-1. Circuit diagram of the 741 bipolar op amp.[11]

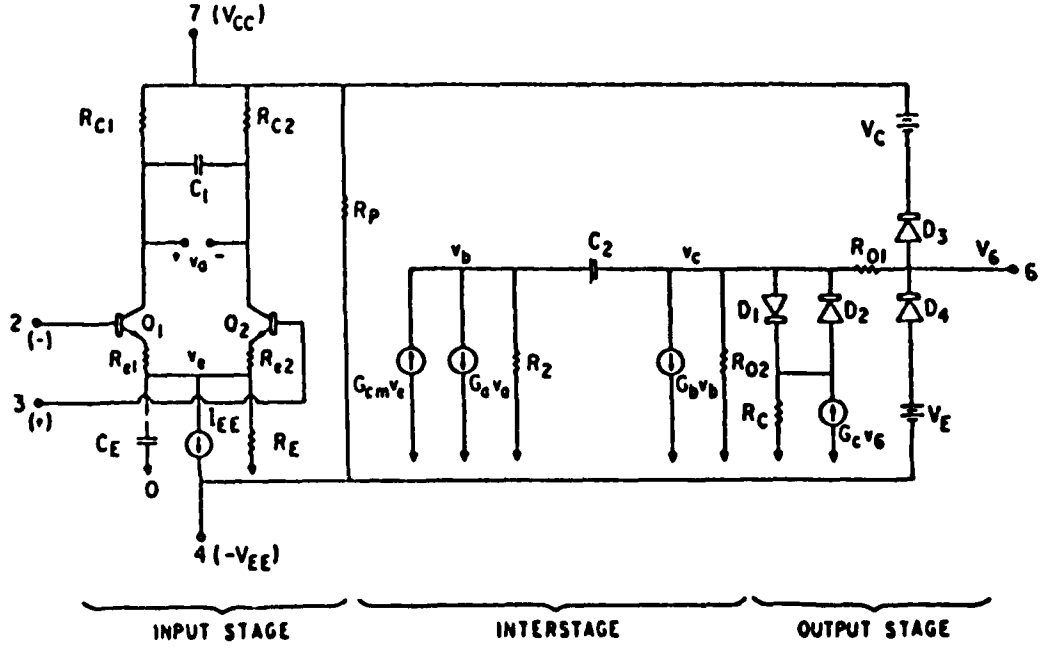

Fig. 3-2. Circuit diagram of the bipolar op amp macromodel.[11]

for the common-mode voltage gain, R_{02} for the frequency-dependent output resistance, C_1 for the excess phase shift at the 0-dB frequency, and C_2 for the upper 3-dB frequency. The slew rate is related to the amount of current available to charge C_2. The difference in positive slew rate S_R^+ and negative slew rate S_R^- which is caused by charge-storage effects in the input stage is modeled by C_E.[18] The resistors R_{c1} and R_{c2} ($R_{c1} = R_{c2}$) are determined by the requirement that the 0-db frequency $f_{0dB} = 1/2\pi R_{c1}C_2$.[11] The resistors R_{e1} and R_{e2} ($R_{e1} = R_{e2}$) model the emitter degeneration for slew rate enhancement.[18]

The macromodel developed by Boyle et al. can be used for dc, small-signal and transient analysis. This macromodel may be further simplified for RFI analysis since the equivalent circuit used by NCAP is a nonlinear incremental model. Elements in the macromodel which account for dc bias currents, dc power dissipation, dc current limiting and dc voltage limiting can be omitted. The omitted elements are R_p, I_{EE}, D_1, D_2, R_C, $G_C v_6$, V_E, V_C, D_3, and D_4. Nodes which are connected to dc supply voltages (V_{CC} and V_{EE}) are ac grounded. The simplified bipolar op amp macromodel for RFI analysis is shown in Figure 3-3.[12]

3.2 Macromodel Parameters for 741 Type Op Amp

The macromodel parameters for the all-bipolar 741 type op amp have been determined using the procedures given by Boyle et al.[11] and manufacturer's specifications extracted from the 1982 Fairchild Linear Data Book.[19] The relevant specifications which are believed to be typical values are summarized in Table 3-1.

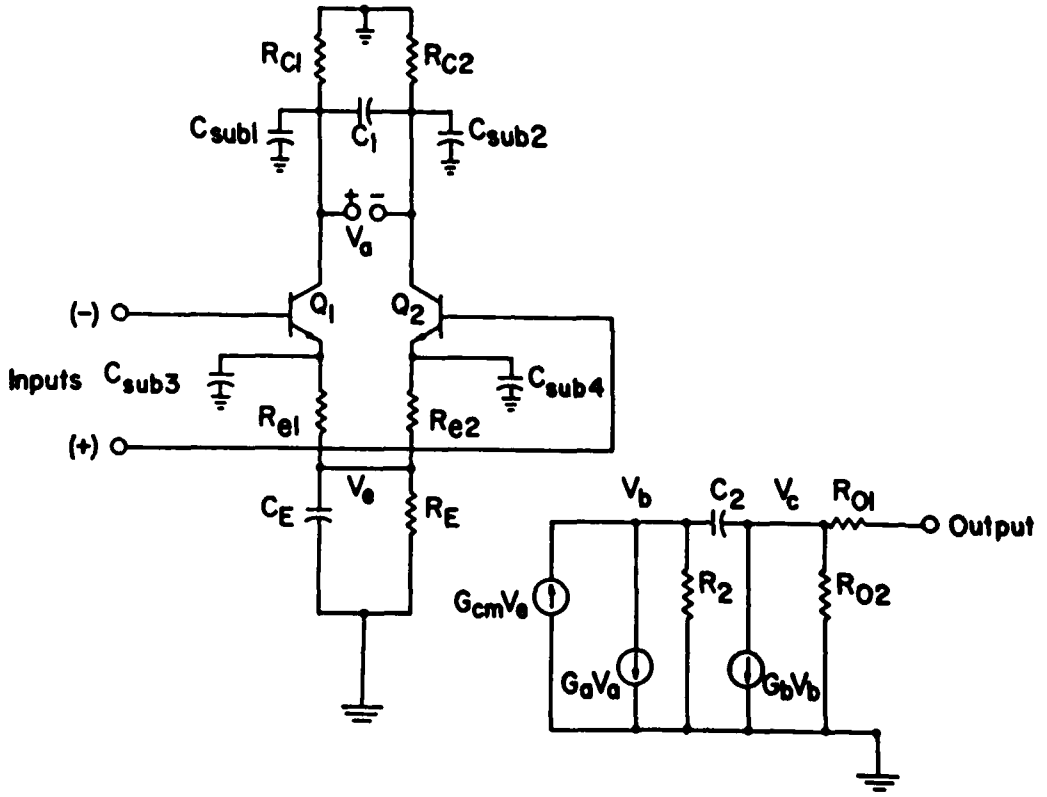

Fig. 3-3. Nonlinear macromodel for the BJT IC op amp in small-signal operation. Note that G. K. C. Chen has added four capacitors C_{sub1}, C_{sub2}, C_{sub3}, and C_{sub4} to account for parasitic effects.[12]

TABLE 3-1

SUMMARY OF RELAVANT CHARACTERISTICS OF THE 741 OP AMP

Symbols	Characteristics	Typical Values[a]	Units
S_R^+	Positive going slew rate	0.53	V/μs
S_R^-	Negative going slew rate	0.48	V/μs
C_2	Compensation capacitor	30	pF
I_B	Input bias current	80	nA
I_{Bos}	Input offset current	20	nA
f_{0dB}	Zero dB frequency	1	MHz
$\Delta\phi$	Excess phase shift	9	Degree
CMRR	Common-mode rejection ratio	90	dB
a_{VD}	Open-loop voltage gain	200,000	
R_{Oac}	AC output resistance (1kHz)	10[b]	Ω
R_{Odc}	DC output resistance (1Hz)	75[b]	Ω

[a] All values are from Fairchild Linear Databook, 1982 except for R_{Oac} and R_{Odc}.

[b] Obtained by measurement.

TABLE 3-2

SUMMARY OF 741 OP AMP MACROMODEL PARAMETERS[a]

Parameter	Value
I_{C1}, I_{C2} (μA)	7.95
C_E (pF)	3.13
β_1	88.3
β_2	113.6
R_{c1}, R_{c2} (kΩ)	5.3
R_{e1}, R_{e2} (kΩ)	2.05
R_E (MΩ)	11.2
C_1 (pF)	2.38
G_a (μU)	189
R_2 (kΩ)	100
G_{cm}(nU)	5.97
R_{O1} (Ω)	10
R_{O2} (Ω)	65
G_b (U)	163
C_2 (pF)	30

[a] All except I_{C1}, I_{C2}, β_1, and β_2 are linear macromodel parameters.

The calculations of values for the macromodel linear parameters shall now be described.* The value of the dc collector current, I_{C1} of the first stage is established by the slew rate of the op amp. If the op amp is connected as a voltage follower, the positive slew rate S_R^+ is given by [11]

$$S_R^+ = 2I_{C1}/C_2 \quad \text{for} \quad S_R^+ > S_R^- \tag{3-1}$$

Rearranging this expression and using the data in Table 3-1, we obtain

$$I_{C1} = (1/2)C_2 S_R^+ = 7.95\ \mu A \tag{3-2}$$

The quiescent collector currents of transistors Q1 and Q2 in the input stage are assumed equal ($I_{C2} = I_{C1}$). The negative slew rate S_R^- is smaller than S_R^+ because of the charge-storage effects in the input stage which are modeled by C_E.[18] The appropriate expression for S_R^- is [11]

$$S_R^- = 2I_{C1}/(C_2 + C_E) \quad \text{for} \quad S_R^- < S_R^+ \tag{3-3}$$

Rearranging this expression and using the data in Table 3-1, we obtain

$$C_E = (2I_{C1}/S_R^-) - C_2 = 3.13\ pF \tag{3-4}$$

The values of the common-emitter dc short-circuit current gains β_1 and β_2 for the two input transistors are obtained from the specifications for the typical input bias current I_B and input current offset I_{Bos}.

*The subscripts 1 and 2 will be used to denote transistors Q1 and Q2 in Figure 3-3.

The appropriate expressions for dc base currents I_{B1} and I_{B2} are given by

$$I_{B1} = I_B + I_{Bos}/2 \ , \qquad I_{B2} = I_B - I_{Bos}/2 \tag{3-5}$$

Using the definitions for β_1 and β_2, Eq. (3-5), and the data given in Table 3-1, we obtain

$$\beta_1 = I_{C1}/I_{B1} = 88.3 \ , \qquad \beta_2 = I_{C2}/I_{B2} = 113.6 \tag{3-6}$$

Values for the resistors R_{c1} and R_{c2} ($R_{c1} = R_{c2}$) can be related to the specified value of the 0-dB frequency f_{0dB} of the fully compensated op amp. The 0-dB frequency is approximately the product of the low frequency differential-mode (DM) voltage gain a_{VD} and the upper 3-dB frequency f_{3dB} of the gain function. The appropriate expression is[11]

$$f_{0dB} = a_{VD} f_{3dB} \tag{3-7}$$

The upper 3-dB frequency can be estimated using a Miller effect[20,21] approximation in the interior stage. The appropriate expression is[11]

$$f_{3dB} \approx 1/[2\pi R_2 C_2 (1 + G_b R_{02})] \approx 1/(2\pi R_2 C_2 G_b R_{02}) \tag{3-8}$$

The differential voltage gain at low frequencies is given by[11]

$$a_{VD} = (G_a R_2)(G_b R_{02}) \tag{3-9}$$

The gain G_a is chosen so that $G_a = 1/R_{c1}$ in order to obtain a convenient slew rate expression as in Eq. (3-1). Using Eqs. (3-7) to (3-9), we obtain the expression[11]

$$f_{0dB} = 1/(2\pi R_{c1} C_2) \tag{3-10}$$

Rearranging this expression and using the data in Table 3-1, we obtain,

$$R_{c1} = 1/(2\pi f_{0dB} C_2) = 5.3\ k\Omega \tag{3-11}$$

The emitter resistors R_{e1} and R_{e2} ($R_{e1} = R_{e2}$) can be determined using an expression for the differential voltage gain of the first stage, which for convenience was previously set to be unity. The appropriate expression is[11]

$$\frac{v_a}{v_{in}} = \frac{\beta_1 R_{c1} + \beta_2 R_{c2}}{\beta_1/g_{m1} + (\beta_1 + 1)R_{e1} + \beta_2/g_{m2} + (\beta_2 + 1)R_{e2}} = 1 \tag{3-12}$$

where the transconductances $g_{m1} = 40I_{C1}$ and $g_{m2} = 40I_{C2}$ Note that $I_{C1} = I_{C2}$ implies that $g_{m1} = g_{m2}$ and also $R_{c1} = R_{c2}$ and $R_{e1} = R_{e2}$ and previous numerical results, we obtain

$$R_{e1} = \frac{\beta_1 + \beta_2}{\beta_1 + \beta_2 + 2}[R_{c1} - 1/g_{m1}] = 2.05\ k\Omega \tag{3-13}$$

An expression for the dc current in the input stage for equal collector currents is given by[11]

$$I_{EE} = [(\beta_1 + 1)/\beta_1 + (\beta_2 + 1)/\beta_2]I_{C1} \tag{3-14}$$

The resistor R_E is added to provide a finite common-mode (CM) input resistance. Because the current source I_{EE} is often realized with an npn transistor, the resistance of R_E is taken as its output resistance. The expression for R_E is given by[11]

$$R_E \approx V_A/I_C = V_A/I_{EE} = 11.2\ M\Omega \tag{3-15}$$

where V_A is the Early voltage of the device. For a small npn transistor, the voltage V_A is typically 180 V. (A value V_A = 180 V was used.)

To introduce excess phase effects in the differential-mode amplifier response, another capacitor C_1 is added in the input stage. The following expressions for the voltage gain function and its phase were developed to fill in gaps in the Boyle et al. paper:[11]

$$a_V(\omega) = a_{VD}/(1 + j\omega/\omega_1)(1 + j\omega/\omega_2) \tag{3-16a}$$

$$\angle a_V(\omega) = -\tan^{-1}(\omega/\omega_1) - \tan^{-1}(\omega/\omega_2) \tag{3-16b}$$

where ω_1 and ω_2 are angular frequencies corresponding to the dominant pole and second pole respectively, and the frequency ω_2 is given by $1/2R_{c1}C_1$. The excess phase at $f = f_{0dB}$ caused by the presence of the non-dominant pole is given by[11]

$$\Delta\Phi = \tan^{-1}(\omega/\omega_2) = \tan^{-1}[(2\pi f_{0dB})(2R_{c1}C_1)] = \tan^{-1}(2C_1/C_2) \tag{3-17}$$

Rearranging this expression and using the data in Table 3-1, the value of C_1 required to produce the excess phase is

$$C_1 = (C_2/2)\tan\Delta\phi = 2.38\ pF \tag{3-18}$$

From Eq. (3-9), the product of (G_aR_2) and (G_bR_{02}) is determined by the differential voltage gain. The gain G_a was previously chosen equal to $1/R_{c1}$ = 189 $\mu\mho$ for convenience. We have some degree of freedom in the value of R_2 or G_b. A reasonable, but arbitrary, value of 100 kΩ

is therefore assigned to R_2; i.e. R_2 = 100 kΩ.

The common-mode voltage gain in the input stage from v_{in} to v_e is approximately unity since R_E is large. The common-mode voltage gain from the input to v_b is then approximately given by[11]

$$v_{bCM}/v_{inCM} \approx G_{cm}R_2 \tag{3-19}$$

The differential voltage gain from input to v_b is given by[11]

$$v_{bDM}/v_{inDM} = G_aR_2 = R_2/R_{c1} \tag{3-20}$$

The common-mode rejection ratio (CMRR) is the ratio of the two gains.[26] Dividing Eqs.(3-19) by (3-20), we obtain the CMRR expression

$$CMRR = 1/R_{c1}G_{cm} \tag{3-21}$$

Rearranging and using data given in Table 3-1 and results calculated previously, we obtain

$$G_{cm} = 1/(CMRR)R_{c1} = 5.97\ n\mho \tag{3-22}$$

In the output stage, the output resistance at very low frequencies is[11]

$$R_{Odc} = R_{O1} + R_{O2} \tag{3-23}$$

At high frequencies, the resistor R_{O2} is shorted by the Miller-effect shunt capacitance[20,21] caused by C_2, and the output resistance becomes $R_{Oac} = R_{O1}$. The values of R_{Odc} and R_{Oac} were obtained experimentally to be 75 Ω and 10 Ω, respectively. See Table 3-1. Values for R_{O1} and R_{O2} were calculated as follows:

$$R_{O1} = R_{Oac} = 10\ \Omega, \qquad R_{O2} = R_{Odc} - R_{O1} = 65\ \Omega \tag{3-24}$$

It also follows that G_b can be calculated from Eq. (3-9).

$$G_b = (a_{VD}R_{c1})/(R_2R_{O2}) = 163\ \mho \tag{3-25}$$

The calculated values of the macromodel parameters for the 741 type op amp are summarized in Table 3-2. These values will be used in NCAP simulations of demodulation RFI in 741 op amp circuits.

3.3 Macromodel Parameters for the LF355, LM10, and CA081 Op Amps

The LF355 op amp is a JFET-bipolar type with a JFET differential input stage. Its general purpose macromodel, as shown in Figure 3-4a, has been reported by Krajewska and Holmes,[14] who extended the macromodel procedures developed by Boyle et al.[11] In this section, we simplify the general purpose macromodel to the incremental macromodel for RFI simulation as shown in Fig. 3-4b. The calculations of the LF355 macromodel parameter values are basically similar to those of the 741 macromodel parameter values except for the calculations of values of the source resistors R_{s1} and R_{s2}. The calculation of values for R_{s1} and R_{s2} will be described next.

The input stage of the macromodel is assumed to have a differential voltage gain a_{vDM} of unity, i.e. $a_{vDM} = 1$. The following expressions are obtained:[14]

$$a_{vDM} = g_mR_{d1}/(1 + g_mR_{s1}) = 1 \tag{3-26a}$$

$$R_{s1} = R_{d1} - 1/g_m \tag{3-26b}$$

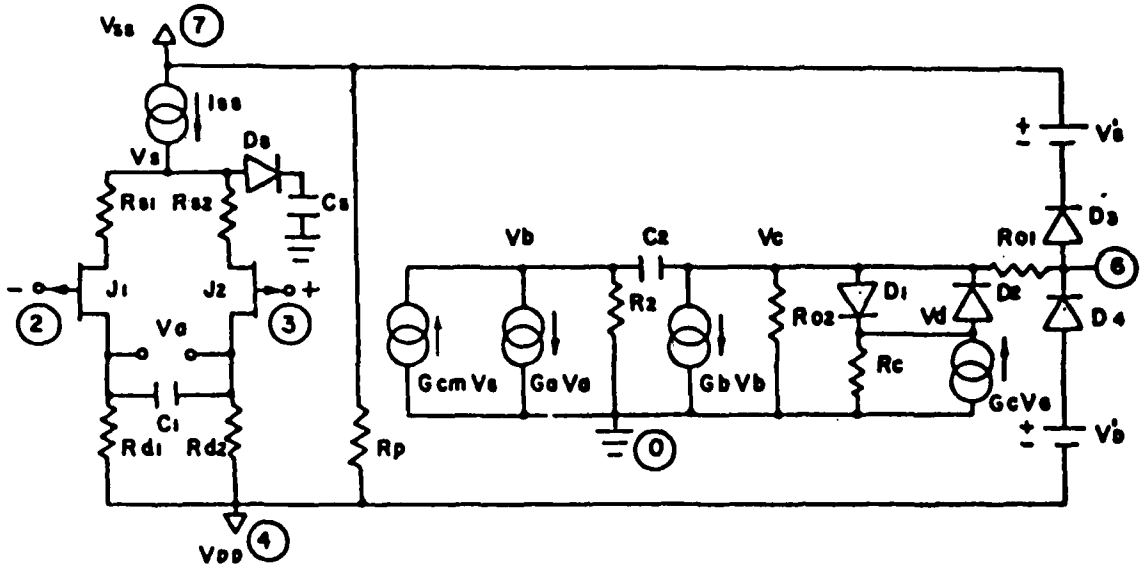

(a) Macromodel for LF355 JFET–Bipolar Op Amp

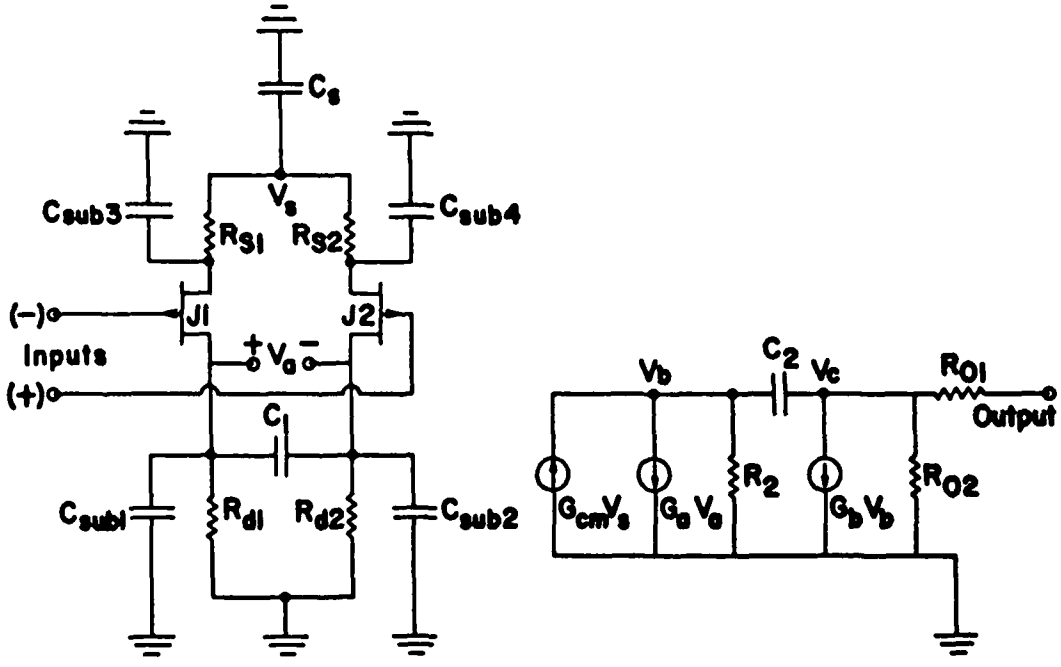

(b) Incremental Macromodel for LF355 JFET–Bipolar Op Amp

Fig. 3-4. Macromodel[14] and incremental macromodel[12] circuit for LF355 JFET-Bipolar op amp. Note reversal of $G_{cm}V_s$ from [14].

TABLE 3-3

SUMMARY OF RELAVANT CHARACTERISTICS OF THE LF355 OP AMP

Symbols	Characteristics	Typical Values[a]	Units
S_R^+	Positive going slew rate	5.6	V/μs
S_R^-	Negative going slew rate	11.5	V/μs
C_2	Compensation capacitor	10	pF
I_B	Input bias current	30	pA
I_{os}	Input offset current	3	pA
f_{0dB}	Zero dB frequency	2.4	MHz
β	$2I_{DSS}/V_T^2$	0.23[b]	mA/V^2
$\|p_2\|$	Non-dominant pole	$\geq 10\pi$[c]	Mrad/s
CMRR	Common-mode rejection ratio	100	dB
a_{VD}	Open-loop voltage gain	100,000	
R_{0ac}	AC output resistance (1kHz)	0.1	Ω
R_{0dc}	DC output resistance	100[b]	Ω

[a] All values are from National Semiconductor Linear Databook, 1980, except for R_{0dc}.

[b] After Krajewska and Holmes, Table I of Ref. [14].

[c] Assume $|p_2| = 10\pi$ Mrad/s.

TABLE 3-4

SUMMARY OF LF355 OP AMP MACROMODEL PARAMETERS[a]

Parameter	Value
I_{d1}, I_{d2} (μA)	57.5
C_s (pF)	10.5
R_{d1}, R_{d2} (kΩ)	6.63
R_{s1}, R_{s2} (kΩ)	0.481
C_1 (pF)	2.4
G_a (m℧)	0.151
R_2 (kΩ)	100
G_{cm} (n℧)	1.51
R_{O1} (Ω)	0.1
R_{O2} (Ω)	100
G_b (℧)	66.3
C_2 (pF)	10

[a] All parameters except I_{d1} and I_{d2} are linear macromodel parameters.

where g_m is the transconductance of the JFETs of the input stage. The value of g_m has to be known before the resistance value for R_{s1} can be computed. Since the drain current I_D for a JFET in the saturation region can be approximated by[18]

$$I_D = I_{DSS}(V_{GS}/V_T - 1)^2 \qquad (3\text{-}27)$$

where I_{DSS} is the drain current for $V_{GS} = 0$, V_{GS} the gate-source voltage, and V_T the threshold voltage for the JFET. The small-signal transconductance g_m is obtained from Eq. (3-27) using the definition for g_m which is

$$g_m = \partial I_D/\partial V_{GS} = \beta(V_{GS} - V_T) , \quad \text{where} \quad \beta = 2I_{DSS}/V_T^2 \qquad (3\text{-}28)$$

Combining Eqs. (3-27) and (3-28), the transconductance g_m can be expressed as

$$g_m = \sqrt{2\beta I_D} \qquad (3\text{-}29)$$

With the information from Table 3-3, a value for I_D may be obtained using the expression

$$I_D = S_R^- C_c/2 = 57.5\ \mu A \quad \text{for} \quad S_R^- > S_R^+$$

The value for β is obtained from Table I of Ref. [14]. Substituting I_D and β into Eqs. (3-29) and (3-26b), we obtain $g_m = 0.163$ m℧ and $R_{s1} = R_{s2} = 481\ \Omega$.

The relevant LF355 op amp characteristics and the derived macromodel parameters are listed in Tables 3-3 and 3-4, respectively. Macromodel parameters of the LM10 and the CA081 op amps are also available.

Interested readers should consult Refs. [12], [4], and [39,40]. The macromodel parameters in Table 3-4 will be used in NCAP simulations for demodulation RFI in LF355 op amp circuits.

Up to now, we have been discussing the linear parameters in the op amp macromodels. In the next sections, we will review the nonlinear device models for the two transistors in the input stage of the macromodel.

3.4 NCAP Nonlinear BJT Model[3]

The NCAP model for the BJT is referred to as the nonlinear T model. It is a modified Ebers-Moll model which was developed by Narayanan.[22,23] It has been shown to be accurate for frequencies up to 100 MHz.[15,24] It also was shown to be satisfactory for frequencies less than f_T, the BJT curoff frequency.[10] The nonlinear T model is illustrated in Figure 3-5.[2,3,15] This model represents the npn BJT in the amplification region. The inherent nonlinearities of the BJT are accounted for by four elements in Figure 3-5, i.e. R_{je}, C_d, C_s and $\alpha(i_C)Mi_{JE}$. The resistors r_b and r_c represent the base bulk resistance and the collector-base junction leakage resistance respectively. The capacitor C_{je} is the base-emitter junction space-charge capacitance. The resistor R_{je} is the nonlinear emitter-base junction resistor. Its current voltage relationship is given by[3,15]

$$i_{JE} = I_s[\exp(qv_{JE}/nkT) - 1] \qquad (3\text{-}30)$$

The capacitor C_d is the nonlinear emitter-base junction diffusion capacitance and is given by[3,15]

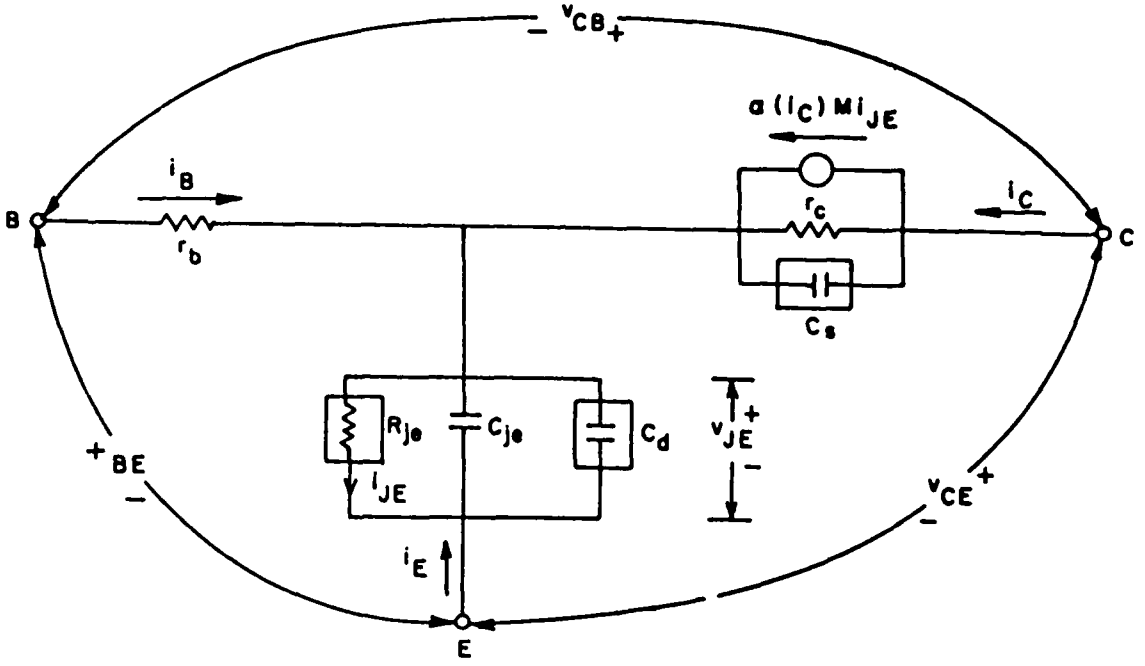

Fig. 3-5. Global model for the npn bipolar junction transistor in the amplification region.

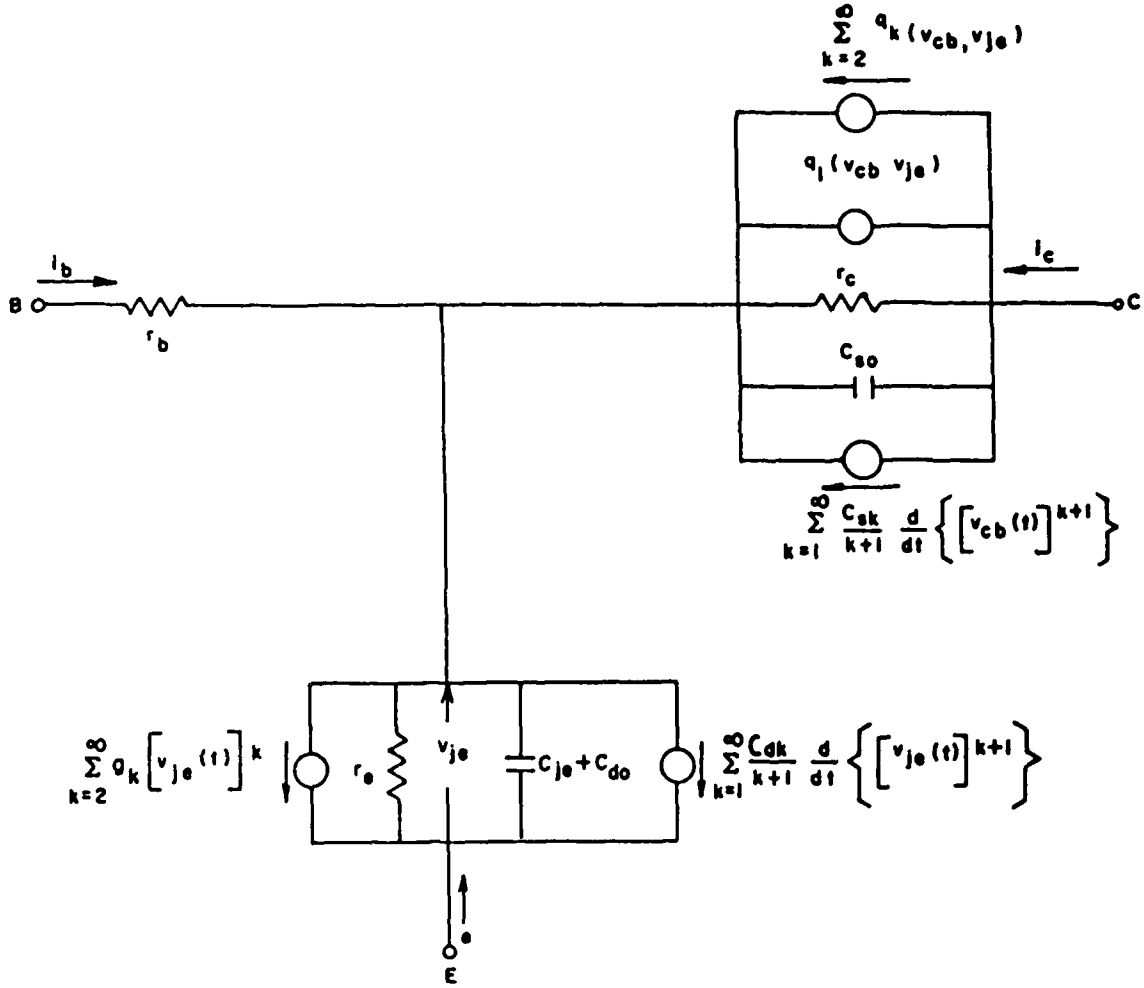

Fig. 3-6. Nonlinear incremental equivalent circuit for npn bipolar junction transistor in the amplification region.

TABLE 3-5

NCAP BJT MODEL PARAMETERS IN 741 OP AMP MACROMODEL

Parameter	Q1	Q2	Description
η	4.34	4.34	Avalanche exponent
V_{CB} (V)	14.57	14.57	Collector-base bias voltage
V_{CBO} (V)	20	20	Avalanche voltage
μ	0.165	0.165	Collector capacitance exponent
I_C (A)	7.95×10^{-6}	7.95×10^{-6}	Collector bias current
I_{Cmax} (A)	500×10^{-6}	500×10^{-6}	Collector current at maximum dc current gain
a	1.09	0.779	h_{FE} (β) nonlinearity coefficient
h_{FEmax}	400	400	Maximum dc current gain
K ($F\text{-}V^{\frac{1}{2}}$)	1.23×10^{-12}	1.23×10^{-12}	Collector capacitance scale factor
n	1.091	1.091	Diode nonideality factor
C_{je} (F)	1.23×10^{-12}	1.23×10^{-12}	Base-emitter junction space charge capacitance
C_2' (F/A)	9.09×10^{-9}	9.09×10^{-9}	Derivative of base-emitter diffusion capacitance
r_b (Ω)	830	830	Base resistance
r_c (Ω)	5.33×10^{6}	5.33×10^{6}	Collector resistance
C_1 (F)	0.1×10^{-12}	0.1×10^{-12}	Base-emitter capacitance
C_3 (F)	0.1×10^{-12}	0.1×10^{-12}	Base-collector and overlap capacitance

$$C_d = C_2' i_{je} \tag{3-31}$$

The capacitor C_s is the nonlinear collector-base junction space-charge layer capacitance and is given by[3,15]

$$C_s = KV_{CB}^{-\mu}, \quad V_{CB} > 0 \tag{3-32}$$

The parameter $\alpha(i_C)$ is the common-base, normal-mode, dc current gain ($\alpha(i_C) = I_C/I_E$). Its dependence on collector current is given by an empirical formula:[3,15]

$$\alpha(i_C) = \frac{h_{FEmax}}{1 + h_{FEmax} + a \cdot \log_{10}^2(\frac{i_C}{I_{Cmax}})} \tag{3-33}$$

The parameter M is the avalanche multiplication factor and is given by [3,15]

$$M = [1 - (\frac{V_{CB}}{V_{CBO}})^{\eta}]^{-1} \tag{3-34}$$

The parameters which appear in Eqs. (3-30) to (3-34) are described in Table 3-5.

To obtain the nonlinear incremental equivalent circuit for the BJT, it is necessary to expand the incremental currents through the nonlinear elements R_{je}, C_d, C_s, and $\alpha(i_C)Mi_{JE}$ in a power series. Since NCAP is based upon nodal analysis, all of these expansions must be given in terms of incremental voltages. For example, the incremental current through R_{je} may be written as[3]

$$i_{je}(t) = \sum_{k=1}^{\infty} g_k [v_{je}(t)]^k \qquad (3\text{-}35)$$

where the linear incremental emitter resistance of the transistor is defined to be

$$r_e = 1/g_1 = nkT/q(-I_E) \qquad (3\text{-}36)$$

and higher order coefficients may be obtained recursively in terms of lower order coefficients.

$$g_k = g_1 g_{k-1}/k(-I_E) \qquad \text{for } k \geq 2 \qquad (3\text{-}37)$$

Other expansions may be found in Refs. [2-3]. The nonlinear incremental equivalent circuit is shown in Figure 3-6.

In order for NCAP to generate the power series coefficients of the nonlinear elements of the BJT, values of 16 BJT parameters are required. Listed in Table 3-5 are the parameter values for the two small npn transistors in the input stage of the 741 op amp. All parameter values were measured by Fang.[6] See Table 4-3 in Ref. [6]. There were two exceptions. The values used for I_{C1} and I_{C2} were obtained from Table 3-2. The values for a_1 and a_2 were calculated using Eq. (3-33) with $i_C = I_C$ and $\alpha = \beta/(1 + \beta)$ with values for I_C and β taken from Table 3-2. The subscripts "1" and "2" denote parameter values for transistors Q1 and Q2 respectively.

3.5 NCAP Nonlinear JFET Model[3]

When used as an amplifier, the JFET is biased to operate in a region of its static characteristics known as the saturation region. This is

a region where weakly nonlinear effects are of considerable interest. A global model for the n-channel JFET in the saturation region is shown in Figure 3-7. The inherent nonlinearities of the JFET are accounted for by the nonlinear current source $i(v_{GJ})$ and nonlinear capacitor C_{GS}. The resistor R_S is the source bulk resistance. The capacitor C_{GD} is the gate-to-drain capacitance. The parameter $i(v_{GJ})$ is a nonlinear voltage-controlled current source described by analytical expressions based upon Fair's field-dependent mobility model.[25] These expressions are

$$i(v_{GJ}) = 3I_{Dmax}(\rho/2)[-\rho + \sqrt{\rho^2 + 4(1/3 - B + (2/3)B^{1.5})}] \qquad (3\text{-}38)$$

$$\rho = \frac{1 - e^{-\Gamma}}{\Gamma^2} \quad \text{with} \quad \Gamma = V_p/E_c L_g \qquad (3\text{-}39)$$

$$B = (v_{GJ} + \psi)/(V_p + \psi) \qquad (3\text{-}40)$$

The parameters which appear in Eqs. (3-38) to (3-40) are defined as follows:

I_{Dmax} = drain current parameter,

V_p = pinch-off voltage

ψ = JFET barrier potential,

E_c = critical field value associated with the mobility,

L_g = gate length.

Note that the parameters I_{Dmax}, ρ, ψ, and V_p are sufficient to determine the current $i(v_{GJ})$. Finally, the nonlinear gate-to-source capacitance C_{GS} for an n-type JFET is given by

$$C_{GS} = K(-V_o - v_{GJ})^{-m}, \quad v_{GJ} < 0 \qquad (3\text{-}41)$$

where V_o = gate-to-source capacitance built-in voltage,

K = gate-to-source capacitance for $-V_o - v_{GJ} = 1$ V,

m = gate-to-source capacitance exponent.

For p-type JFETs, the minus signs preceding V_o and v_{GJ} are changed to + signs.

To obtain the nonlinear incremental equivalent circuit for the JFET, it is necessary to expand in power series the incremental currents through the nonlinear elements $i(v_{GJ})$ and C_{GS}. Interested readers should consult Refs. [2] and [3] for the expressions of the power series coefficients. The nonlinear incremental equivalent circuit is shown in Fig. 3-8.

In order to calculate values for the power series coefficients of the nonlinear elements of the JFET, NCAP requires values for the 10 parameters listed in Table 3-6. Shown in that table are the parameter values for the two JFETs in the input stage of the LF355 op amp macromodel. The parameter values given in Table 3-6 are identical to those given by K.N. Chen et al. in Ref. [13] except for the I_{Dmax} and V_{GS} values. K.N. Chen used the parameter values given by J. J. Whalen et al. in Ref. [17]. Thus the p-JFET model in the LF355 op amp macromodel is actually the same as the n-JFET model in Ref. [17] with the exceptions noted. The values for ψ, K, m, V_o, C_{GD}, and R_S are taken directly from Table AV of Ref. [17]. The value for ρ is calculated using Eq. (3-39) with

Γ = 1.13 given in Table AV of Ref. [17]. The value for V_p is identical to V_{TH} (1.0 V) in Table I of Ref. [14]. Using Eqs. (3-28) and (3-29) with β = 0.23 mA/V^2 and $V_T = V_{TH}$ = 1.0 V from Table I of Ref. [14], and I_D = 57.5 μA from Table 3-4 of this dissertation, the numerical values for g_m and V_{GS} can be computed as follows:

$$g_m = \sqrt{2\beta I_D} = 0.163 \text{ m℧}$$

$$V_{GS} = g_m/\beta + V_T = -0.293 \text{ V}$$

The value for I_{Dmax} is obtained by applying Eq. (3-38) with $i(v_{GJ}) = I_D$ = 57.5 μA and values for the other parameters taken from Table 3-6.

This completes our discussion of the macromodels for 741 and LF355 op amps. These macromodels will be used in the NCAP simulations for demodulation RFI in circuits involving 741 or LF355 op amps.

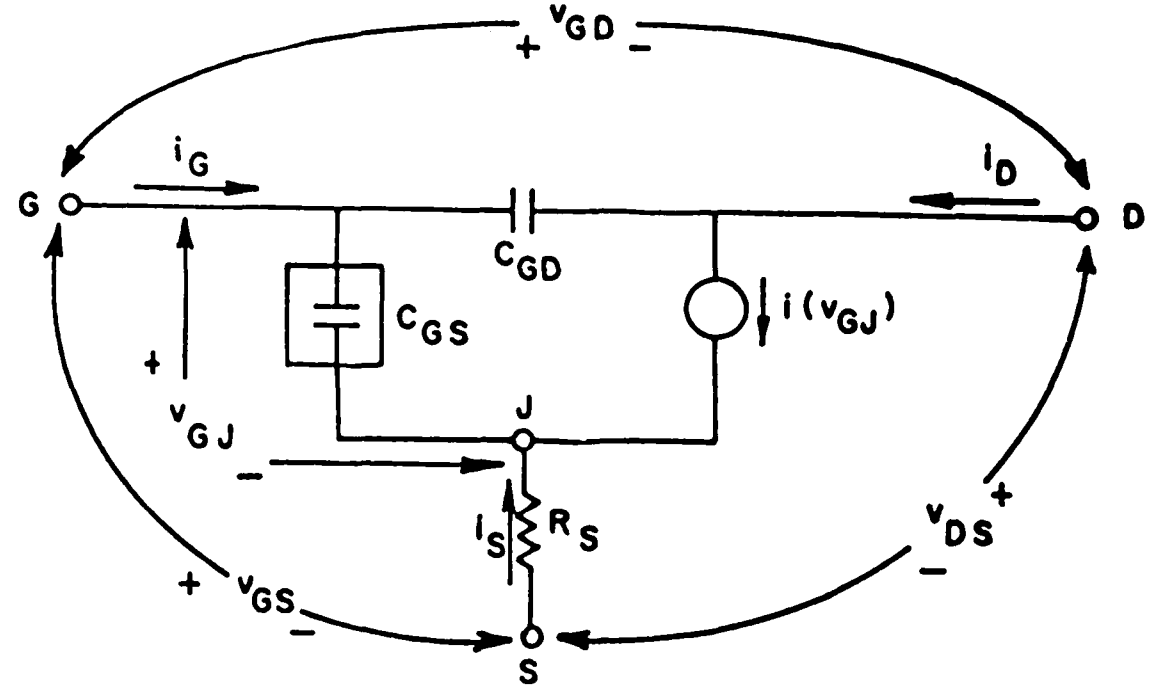

Fig. 3-7. Global model for the n-channel junction field-effect transistor in the saturation region.

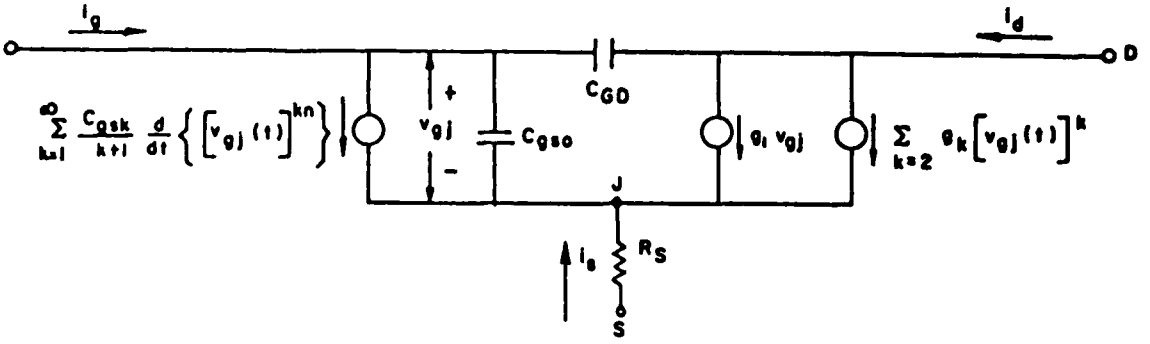

Fig. 3-8. Nonlinear incremental equivalent circuit for the n-channel junction field-effect transistor in the saturation region.

TABLE 3-6

NCAP JFET MODEL PARAMETERS IN LF355 OP AMP MACROMODEL

Parameter	J1	J2	Description
C_{GD} (F)[a]	0.87×10^{-12}	0.87×10^{-12}	Gate-drain capacitance
R_S (Ω)[a]	27	27	Source bulk resistance
I_{Dmax}(A)[b]	371.5×10^{-6}	371.5×10^{-6}	Drain current parameter
ρ[c]	0.53	0.53	Saturated drain current parameter
V_p (V)[d]	-1.0	-1.0	Pinch-off voltage
ψ (V)[a]	-0.5	-0.5	JFET barrier potential
V_{GS} (V)[b]	-0.293	-0.293	External gate-source voltage
K (F $V^{\frac{1}{2}}$)[a]	2.2×10^{-12}	2.2×10^{-12}	Gate-source capacitance for $-V_o - v_{GJ} = 1V$
m[a]	0.5	0.5	Asymptotic slope of $C(V'_{GS})$ on logarithmic plot
V_o (V)[a]	-0.5	-0.5	Gate-source built-in potential

[a] Values taken from Table AV of [17].

[b] Values calculated in this report

[c] Value calculated using Γ value from Table AV of [17].

[d] Value taken from [14].

CHAPTER FOUR

STATISTICS OF MEASURED DEMODULATION RFI RESPONSES OF THE UNITY GAIN BUFFER

The specific RFI effect investigated is how amplitude-modulated (AM) RF signals are demodulated in operational amplifiers (op amps) to produce undesired low frequency responses at the AM-modulation frequency. The undesired demodulated response may then be processed as a desired low frequency signal by the low frequency components that follow the op amp. In this chapter, the investigation of the op amp unity gain buffer configuration which was chosen initially by Fang[6] is discussed. In subsequent chapters of this dissertation, the investigation of another popular op amp configuration will be discussed. The op amp types chosen are the widely used 741 bipolar op amps which have conventional npn input transistors, the newer LM10 bipolar op amps which have less conventional pnp input transistors, the LF355 JFET-bipolar op amps which have junction field-effect-transistor (JFET) input transistors, and the CA081 MOS-bipolar op amps which have metal-oxide-semiconductor field-effect transistor (MOSFET) input transistors. Information on the units tested is summarized in Table 4-1. The second-order transfer function $H_2(f_1,-f_2)$, which characterizes the RFI demodulation response, was

TABLE 4-1

Operational Amplifiers Tested

Desig.	741	LM10	CA081	LF355
Type	Bipolar	Bipolar	Bi-MOS	Bi-FET
Input	npn	pnp	MOSFET	JFET
Interior	bipolar	bipolar	bipolar	bipolar
Units	30	25	30	30
Codes[a]	5	4	2	4
Manu.	2	1	1	1

[a] Date Codes

determined from the measured data. The scatter plot and statistics such as mean and standard deviation of $H_2(f_1,-f_2)$ for 25 to 30 units of each op amp type will be presented.

4.1 Measurement of Linear Response

The linear response of an amplifier is also called its first-order transfer function. Before starting measurements of the second-order transfer function of a nonlinear circuit, measurement of the linear response is usually performed to check the normal operation of the amplifier circuit. Figure 4-1 shows the experimental set-up for measuring the linear response of an op amp unity gain buffer. In this measurement, the input voltage amplitude V_i was held constant at 50 mV while the output voltages V_{01} and V_{02} were measured corresponding to $R_x = 0$ and $R_x = 50\ \Omega$, respectively. Then the linear response V_o/V_i corresponding to $R_x = \infty$ can be derived from the expression

$$\frac{V_o}{V_i} = \left(\frac{100}{V_{02}(mV)} - \frac{50}{V_{01}(mV)}\right)^{-1}, \quad R_x = \infty \qquad (4\text{-}1)$$

The reason for using this scheme is that the linear response of an op amp unity gain buffer is a function of load resistance at RF frequencies where the loop-gain is small. The coaxial cable which connects the output node V_o to the input of an RF voltmeter has to be terminated by a 50 Ω resistor, which loads the amplifier output. Therefore the linear response corresponding to $R_x = \infty$ which

corresponds to not connecting the RF voltmeter, has to be derived indirectly from Eq. (4-1). Figures 4-2 to 4-5 show the linear responses of the unity gain configuration of the 741, LM10, CA081, and LF355 op amps, respectively.

Examining the data shown in Figures 4-2 to 4-5, we observe that the unity gain buffer stage linear frequency response is down 3 dB at 0.03 MHz for the LM10, is down 3 dB at 0.7 MHz for the 741, is down 3 dB at 4 MHz for the CA081, and is down 3 dB at 7 MHz for the LF355. These results indicate that the gain-bandwidth product for the unity gain buffer amplifier configuration is lowest for the LM10 and highest for the LF355. However, we should note that the linear responses were measured for only one unit of each op amp type.

4.2 Measurement of Demodulation RFI Response

From the previous section, we have just shown that all four op amps are best operated at frequencies less than 10 MHz in the unity gain buffer configuration. Now, we are going to demonstrate how amplitude-modulated (AM) RF signals are demodulated to produce undesired audio frequency signals which fall into the normal frequency range of the op amp circuit.

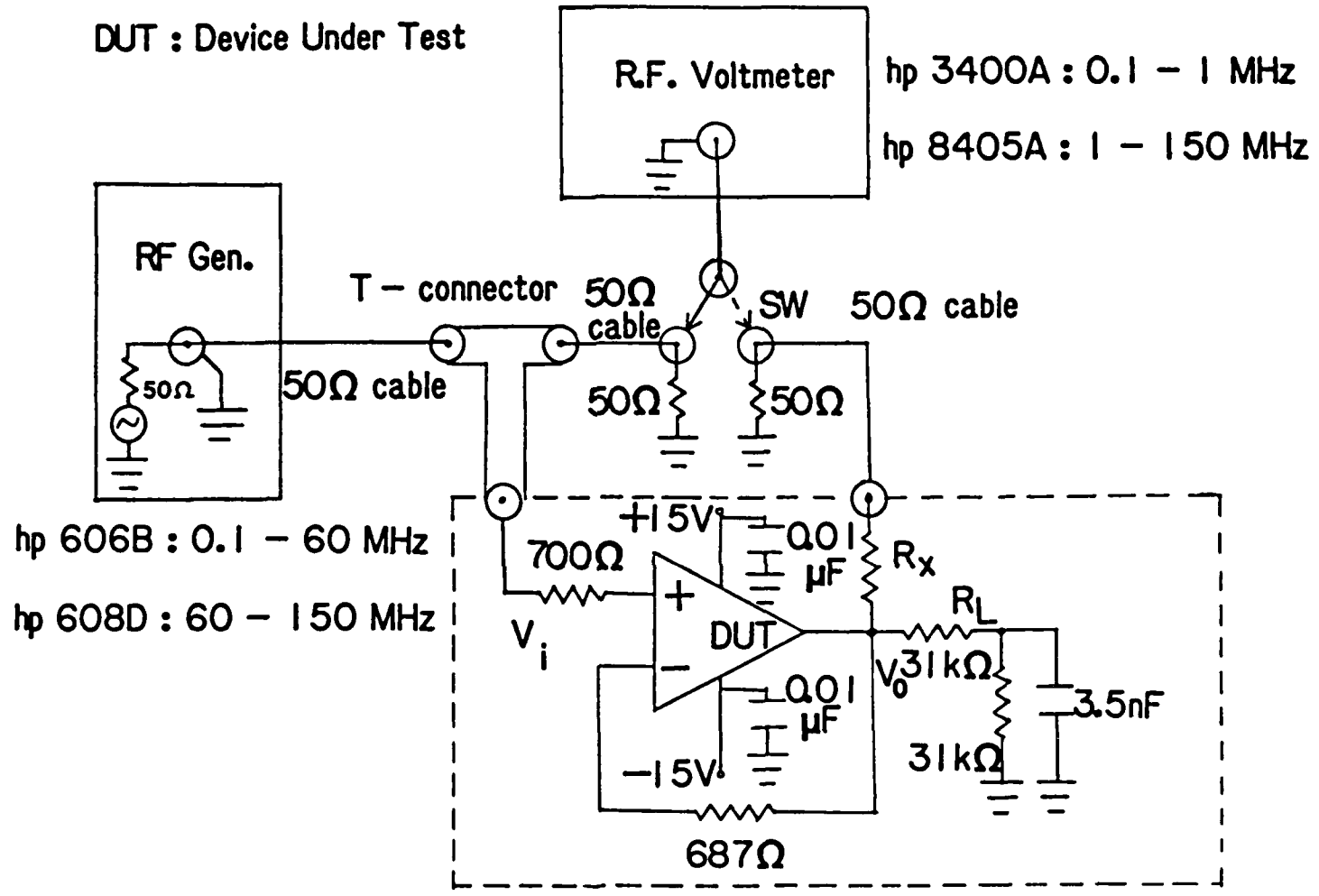

Fig. 4-1. Experimental set-up for linear response measurement V_o/V_i for the 10 kHz to 200 MHz frequency range. Data are taken with $R_x = 0$ and $R_x = 50$ ohm in order to calculate the response with $R_x = \infty$ With $R_x = \infty$, the op amp is loaded only by $R_L = 31$ kohm because the 3.5 nF capacitor is an ac short-circuit above 1.5 kHz.

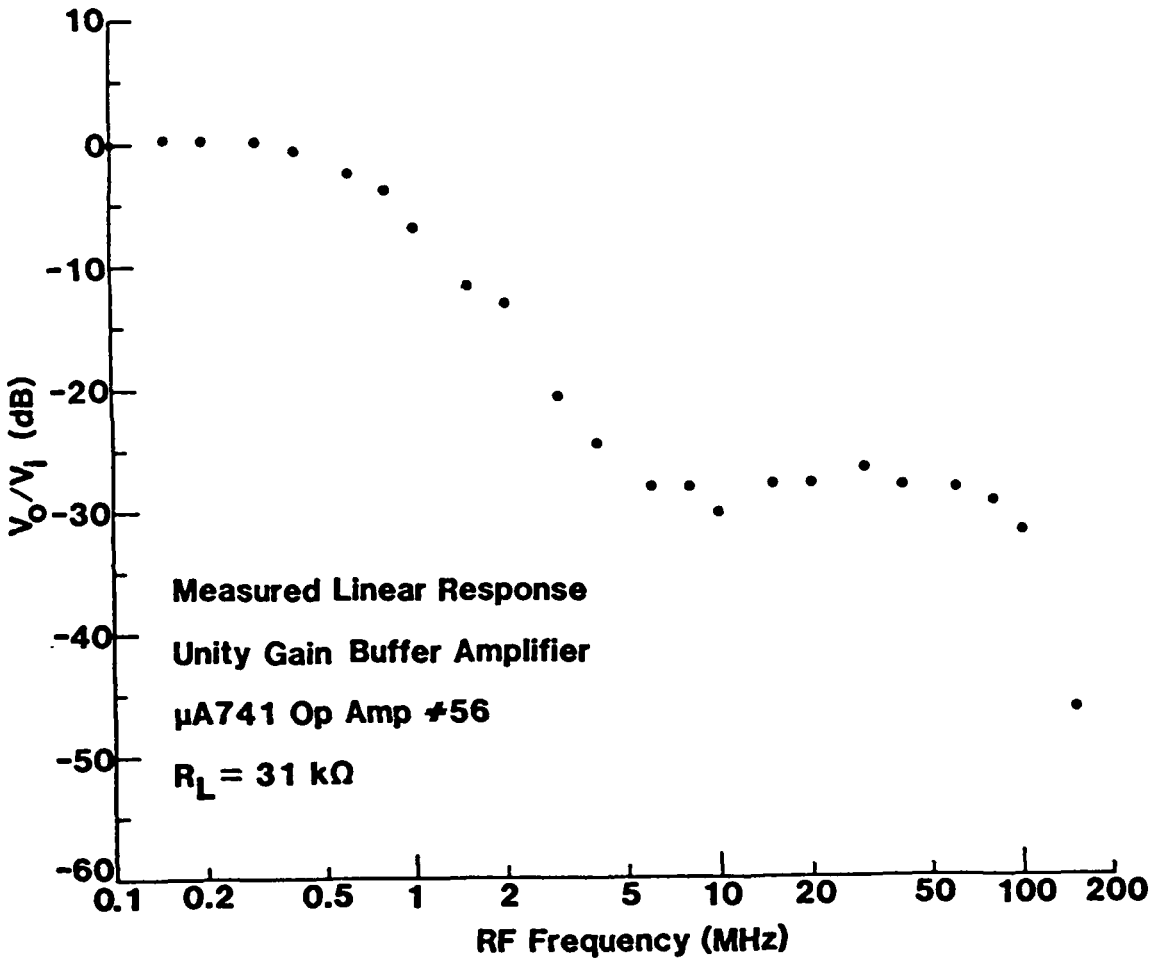

Fig. 4-2. Linear response V_o/V_i vs frequency for μA741 op amp #56 in unity gain buffer amplifier circuit.

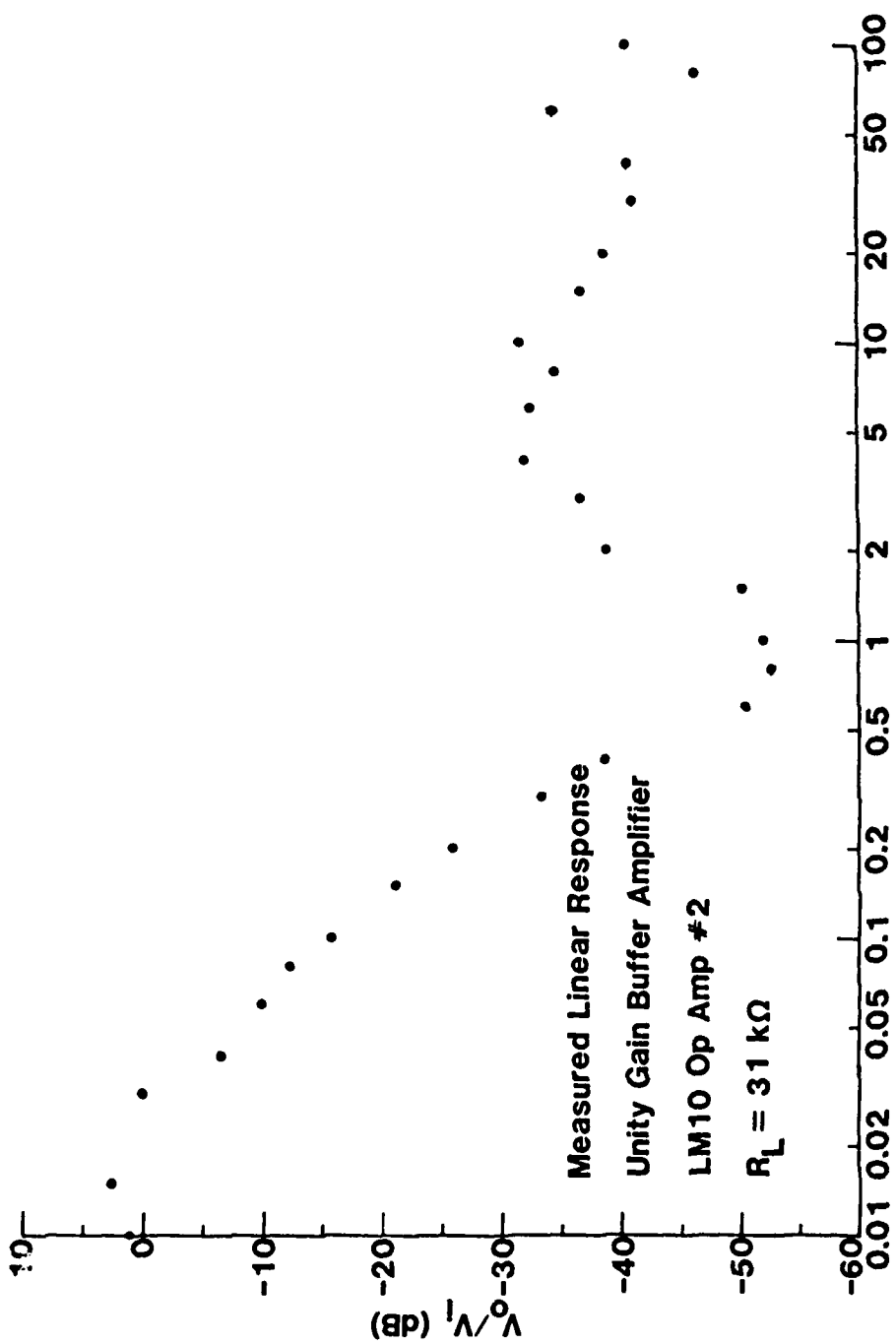

Fig. 4-3. Linear response V_o/V_1 vs frequency for LM10 op amp #2 in unity gain buffer amplifier circuit.

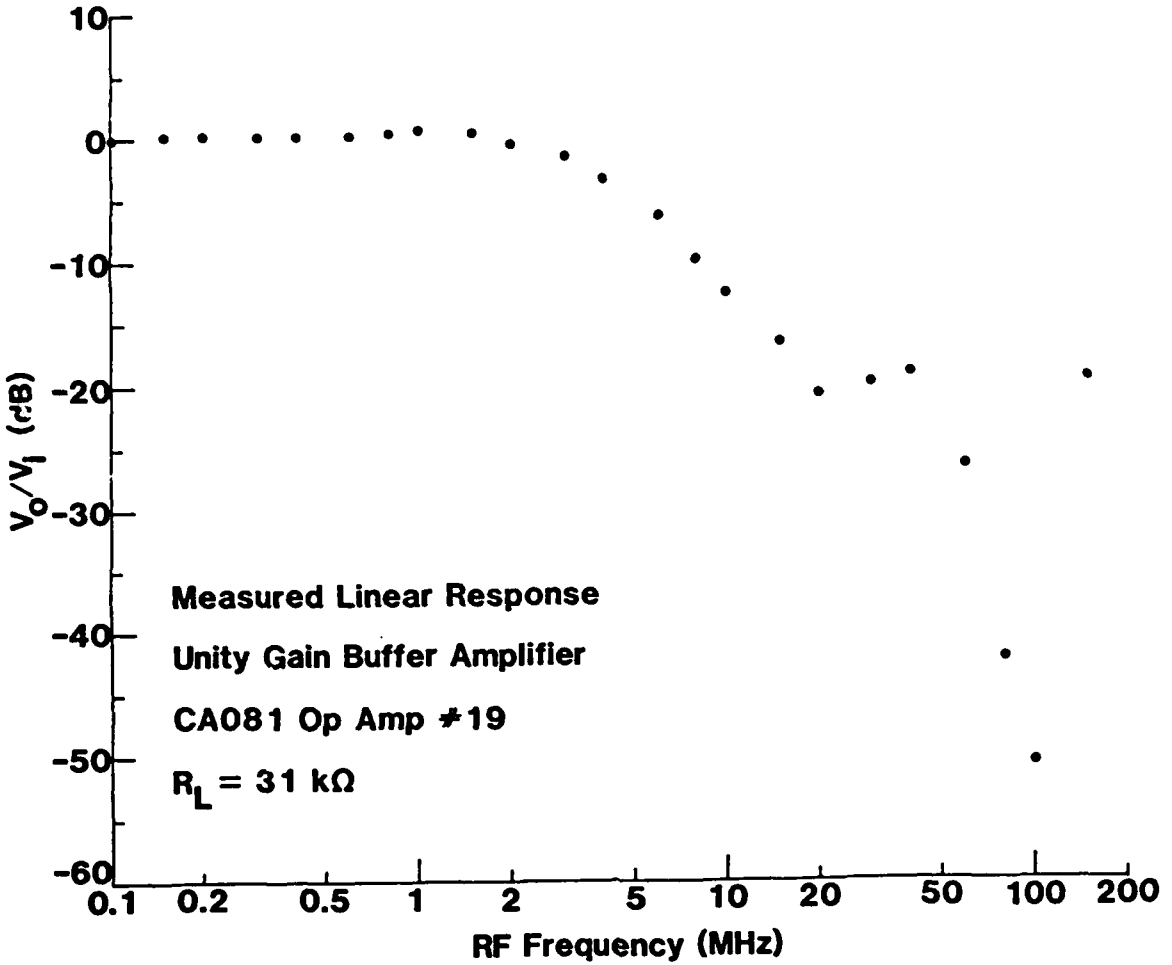

Fig. 4-4. Linear response V_o/V_i vs frequency for CA081 op amp #19 in unity gain buffer amplifier circuit.

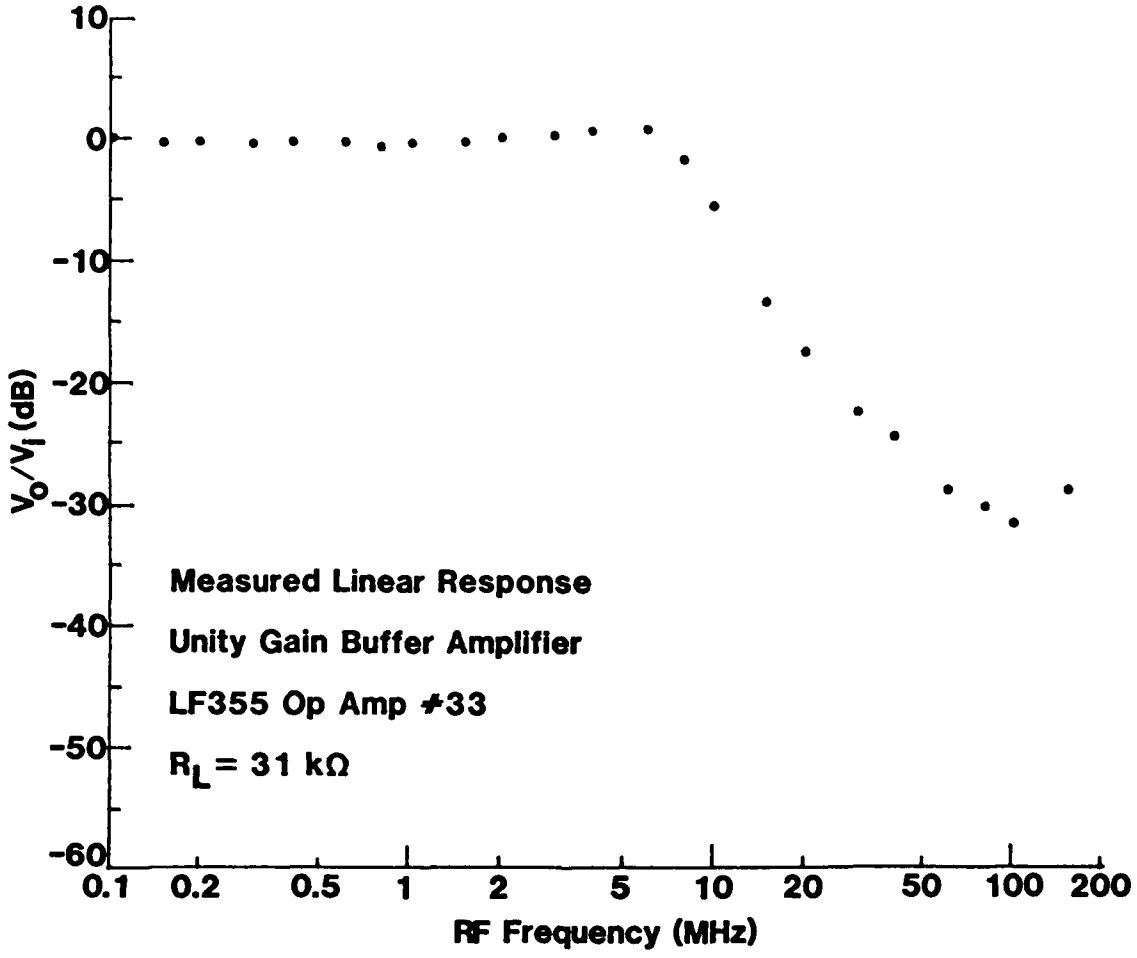

Fig. 4-5. Linear response V_o/V_i vs frequency for LF355 op amp #33 in unity gain buffer amplifier circuit.

4.2.1 Experimental Set-up

The block diagram of the experimental system for measuring the demodulation RFI response is shown in Figure 4-6. The RF signal generator injects into the non-inverting input of the op amp circuit an amplitude-modulated RF signal, V_g, which may be expressed as

$$V_g(t) = A(1 + m\cos 2\pi f_{AF} t)\cos 2\pi f_{RF} t \qquad (4\text{-}2)$$

where A is the amplitude of the RF signal without modulation ($m = 0$), m is the modulation index, f_{AF} is the frequency of modulation, and f_{RF} is the RF signal frequency. The low pass filter is inserted between the amplifier output and the tuned AF voltmeter in order to reduce the RF signals entering the AF voltmeter input. This is done to eliminate the possibility that an amplitude-modulated RF signal entering the AF voltmeter would generate audio frequency responses in the tuned AF voltmeter. Figure 4-7 shows a more detailed circuit diagram for the measurement system. Notice that the 50 Ω coaxial cable from the RF source to the circuit has been terminated with a 50 Ω resistor to eliminate the reflection of the RF signal at the receiving end of the cable.

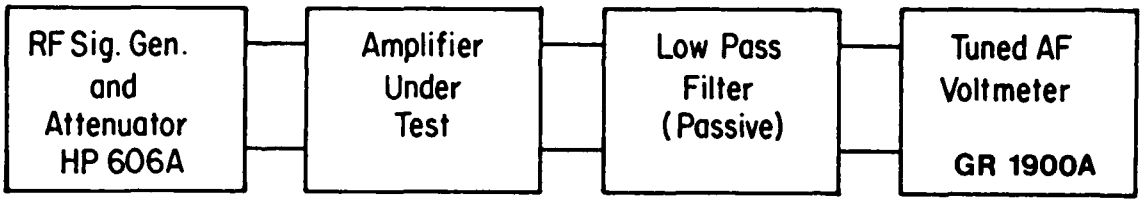

$f_1 = f_{RF}$ f_{RF} = RF frequency

$f_2 = f_{RF} - f_{AF}$ f_{AF} = AF frequency

Modulation: 50% AM at f_{AF}

Fig. 4-6. Block diagram of experimental system for measuring the demodulation RFI response.

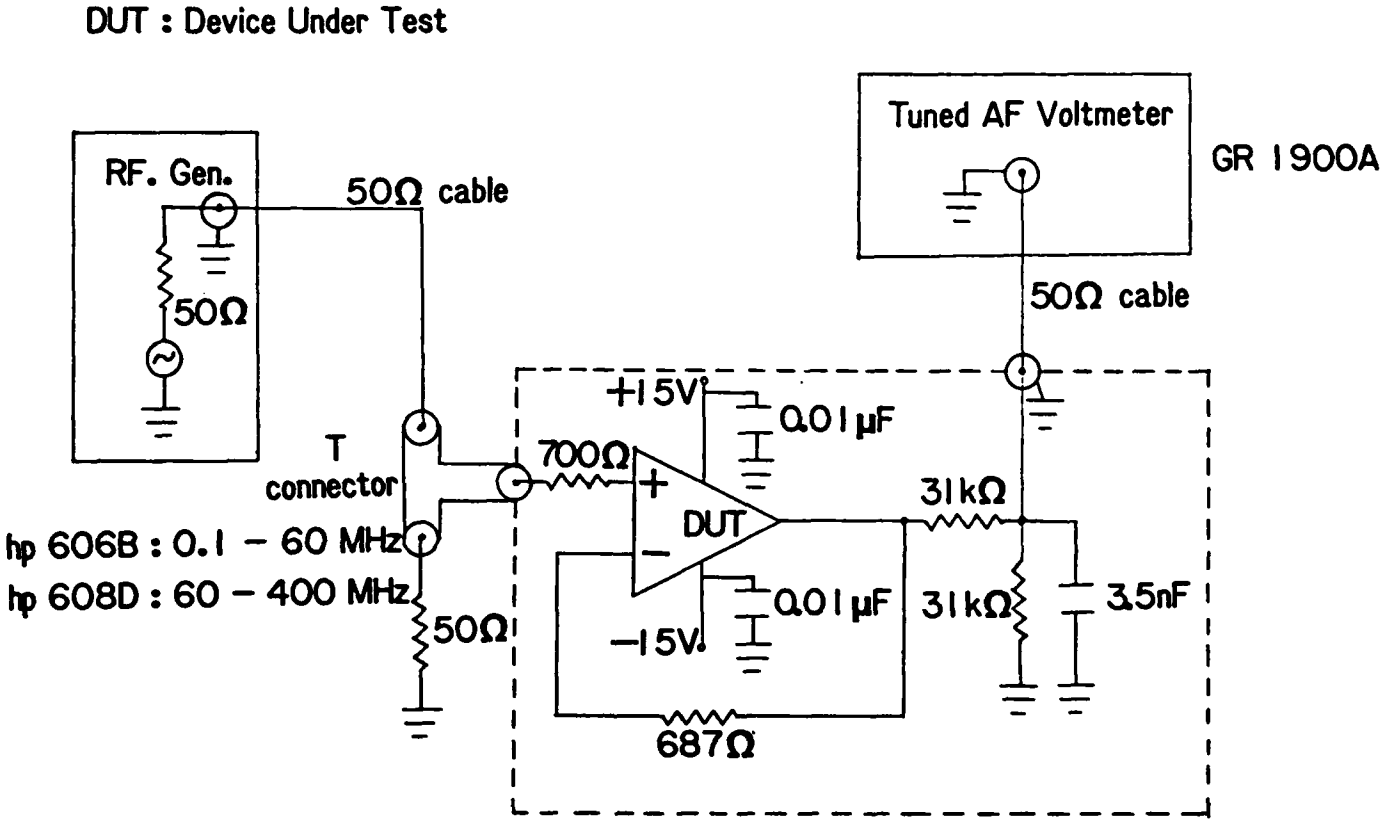

Fig. 4-7. Experimental set-up for demodulation RFI response measurement (after Fang[6]). The 687 ohm resistor is often replaced by a short-circuit in voltage follower circuits of this type.

4.2.2 Measurement Procedure

The voltage reading at the tuned AF voltmeter is a direct measure of the demodulation RFI response which can be characterized by the second-order-transfer function $H_2(f_1,-f_2)$ of the circuit under consideration. We shall derive an expression from which $H_2(f_1,-f_2)$ values can be determined from the tuned AF voltmeter readings.

By applying a trigonometry identity for the product of two cosine functions, we can express $V_g(t)$ in Eq. (4-2) as

$$V_g(t) = A\cos 2\pi f_{RF}t + \frac{mA}{2}\cos 2\pi(f_{RF} - f_{AF})t + \frac{mA}{2}\cos 2\pi(f_{RF} + f_{AF})t \quad (4-3)$$

Because of the second-order nonlinearities of the op amp circuit, the RF carrier and the lower sideband of Eq. (4-3) will generate an intermodulation signal at f_{AF}. Similarly, interaction of the RF carrier and the upper sideband will also generate an intermodulation signal at frequency f_{AF}.

From Table 2-1, the amplitude of the intermodulation signal generated by the RF carrier and the lower sideband is given by

$$V_{m1} = \frac{mA^2}{2} |H_2(f_1,-f_2)| \quad (4-4)$$

where $f_1 = f_{RF}$ and $f_2 = f_{RF} - f_{AF}$. Similarly, the amplitude of

the intermodulation signal generated by the RF carrier and the upper sideband is given by

$$V_{m2} = \frac{mA^2}{2} \left| H_2(-f_1, f_3) \right| \tag{4-5}$$

where $f_3 = f_{RF} + f_{AF}$,

We assume that the carrier frequency $f_1 = f_{RF}$, the lower sideband frequency $f_2 = f_{RF} - f_{AF}$, and the upper sideband frequency $f_3 = f_{RF} + f_{AF}$ are sufficiently close together so that $H_1^k(f_1) = H_1^k(f_2) = H_1^k(f_3)$ at each node k in the circuit where $H_1^k(f)$ is the first-order transfer function at node k evaluated at frequency f. Then it follows that $H_2(f_1, -f_2) = H_2(-f_1, f_3)$. Thus, the total amplitude of the intermodulation signal at frequency f_{AF} is given by[6]

$$V_m = V_{m1} + V_{m2} = mA^2 \left| H_2(f_1, -f_2) \right| \tag{4-6}$$

The AF voltmeter indicates the rms voltage of the AF signal. If we denote this rms voltage by V_M, then

$$V_M = 0.707mA^2 \left| H_2(f_1, -f_2) \right| \tag{4-7}$$

Equation (4-7) can be expressed in dB with respect to a 1 mV reference level:

$$20\cdot\log_{10}|V_M/1mV| = 20\cdot\log_{10}[0.707mA^2|H_2(f_1,-f_2)|] - 20\cdot\log_{10}(10^{-3})$$

$$= 57 + 20\cdot\log_{10}(m) + 40\cdot\log_{10}(A)$$

$$+ 20\cdot\log_{10}|H_2(f_1,-f_2)| \qquad (4\text{-}8)$$

The amplitude of the RF carrier voltage A can be given in terms of the generator available power P_{gen} which by definition is the power the generator would deliver to a load $R_i = R_g$ where R_g is the generator internal impedance. Using the equivalent circuit of Figure 4-8 with $R_i = R_g$, we obtain the relationship

$$P_{gen} = \frac{V_i^2}{R_i} = \frac{A^2}{8R_g} \qquad (4\text{-}9)$$

Note that V_i is an rms voltage, but that A is an amplitude. If $R_i = R_g = 50\ \Omega$, Equation (4-8) can be expressed in terms of dBm as

$$P_{gen}(dBm) = 10\cdot\log_{10}((A^2/400)/10^{-3}) = 4 + 20\cdot\log_{10}(A) \qquad (4\text{-}10)$$

With m = 0.5, Equation (4-7) can be written as

$$20\cdot\log_{10}|V_M/1mV| = 2P_{gen}(dBm) + 43 + 20\cdot\log_{10}|H_2(f_1,-f_2)| \qquad (4\text{-}11)$$

Thus, we have an expression relating $H_2(f_1,-f_2)$ values and the tuned AF voltmeter readings. Besides, Equation (4-11) also suggests a convenient way of checking whether the AF voltmeter readings are caused by the second-order nonlinearities of the

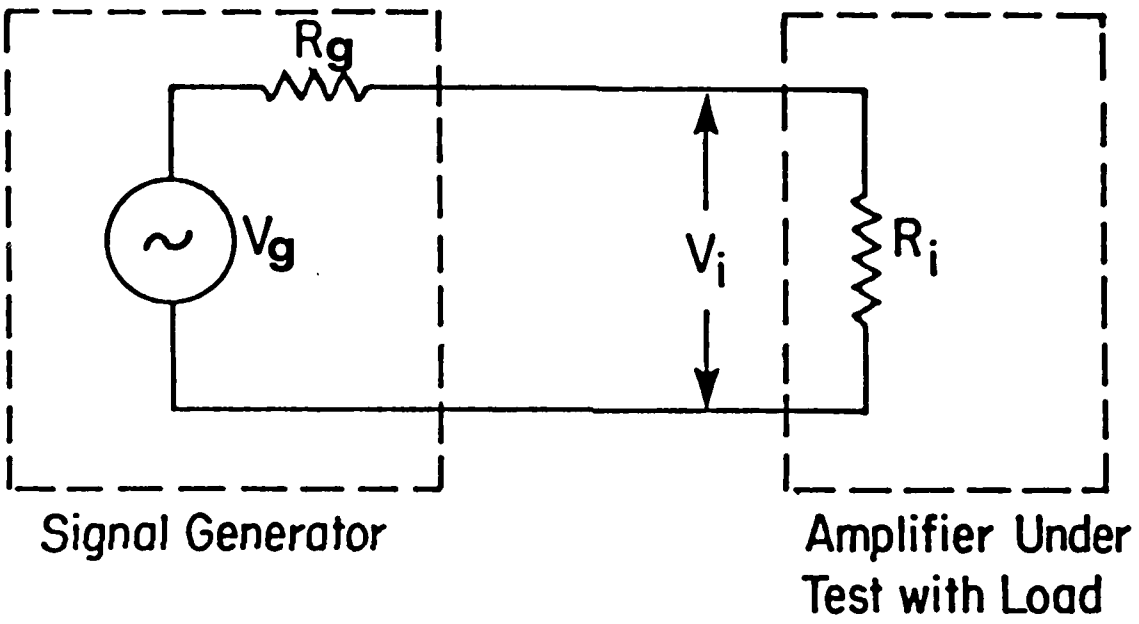

Fig. 4-8. Circuit used to relate the available power P_{gen} that the signal generator can deliver to a matched load $R_i = R_g$ to the signal generator voltage amplitude V_g. See Eq. (4-9).

amplifier circuit under test. For every 1 dBm variation in P_{gen}, a corresponding 2 dB variation should be observed in the measured V_M value. We assure this condition when we use Equation (4-11) to calculate $H_2(f_1,-f_2)$. Figure 4-9 shows values of the measured AF voltmeter reading V_M in dBV versus the generator available power P_{gen} for four types of op amps at f_{RF} = 10 MHz. It is seen that for P_{gen} < 0 dBm, all four op amps have data plots that are straight lines with slopes equal to two in agreement with Equation (4-11). The region in which this behavior is observed is often called the square-law response region. For P_{gen} > 0 dBm, the slopes of the data curves start to deviate from two because of nonlinear terms of order higher than two. Whereas we cannot set P_{gen} to values too large, it is also not appropriate to set it to values too low. We must not let the AF signal produced by second-order nonlinearities of the amplifier fall below the ambient noise level and become difficult to measure. Each curve shown in Figure 4-9 is used to obtain a $H_2(f_1,-f_2)$ value at one RF frequency. Values of $H_2(f_1,-f_2)$ at other RF frequencies may be obtained from plots similar to that shown in Figure 4-9. It is not necessary to measure as many data points as shown in Figure 4-9. Often, measurements were made at two values of P_{gen} such as -10 dBm and -20 dBm to verify the square-law response. Then the value of V_M(rms) at P_{gen} = -10 dBm was used to determine $H_2(f_1,-f_2)$.

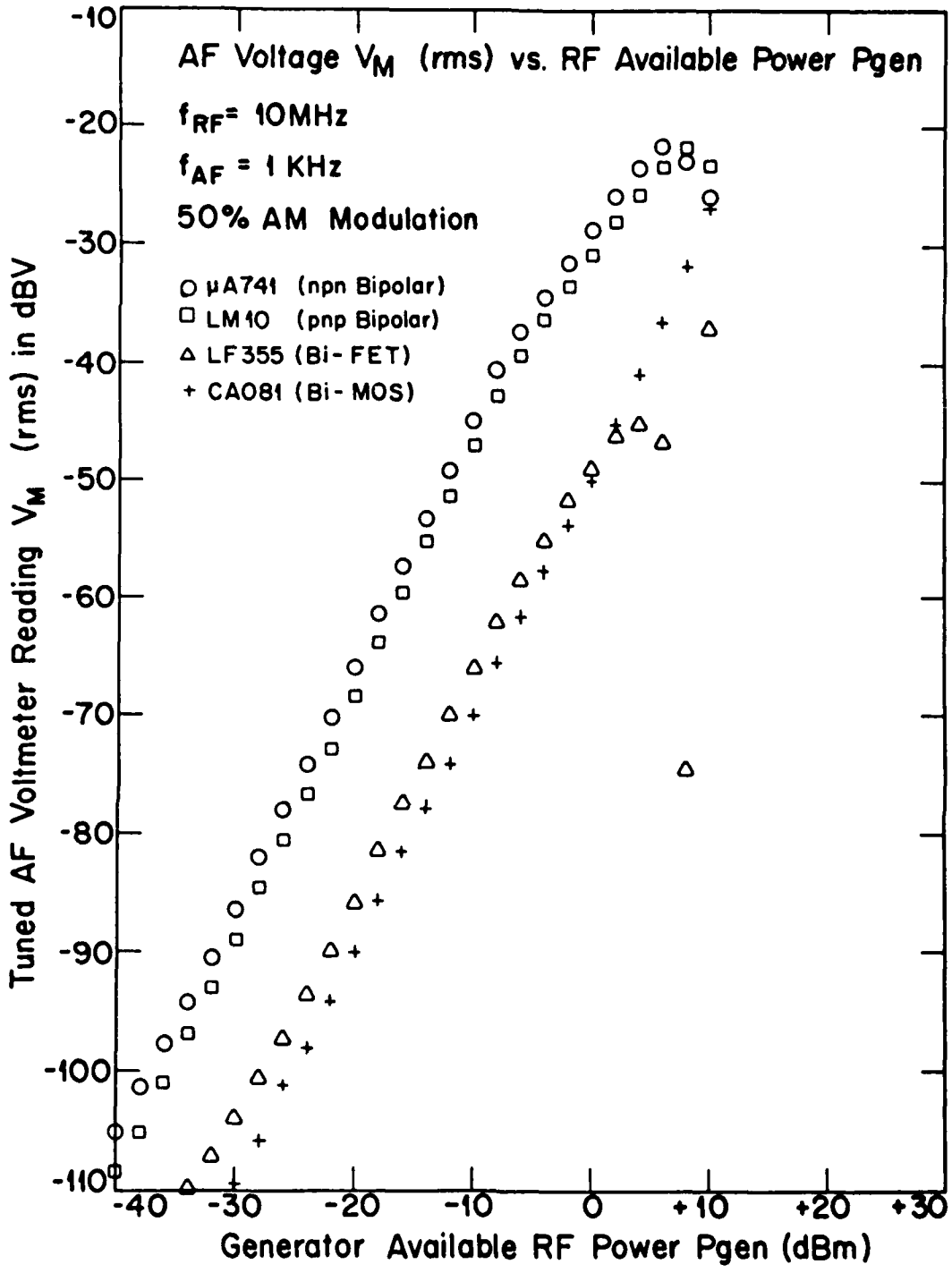

Fig. 4-9. Measured values of AF voltage V_M(rms) at the tuned AF voltmeter vs the generator available power P_{gen} for the unity gain buffer circuit for four types of op amps at one RF frequency.

4.2.3 Measurement Results

Shown in Figures 4-10 to 4-13 are values for the second-order transfer function $H_2(f_1,-f_2)$ vs RF frequency for the four op amp types for three values of dc power supply voltage V_{DC}. The $H_2(f_1,-f_2)$ values for the one 741 op amp shown in Figure 4-10 decrease 2 to 4 dB when V_{DC} is changed from $\pm$ 10 V to $\pm$ 18 V. The $H_2(f_1,-f_2)$ values for the one LM10 op amp shown in Figure 4-11 increase 1 to 5 dB as V_{DC} is changed from $\pm$ 10 V to $\pm$ 30 V. The $H_2(f_1,-f_2)$ values for the one CA081 op amp shown in Figure 4-12 decrease 0 to 3 dB as V_{DC} is changed from $\pm$ 10 V to $\pm$18 V. The $H_2(f_1,-f_2)$ values for the one LF355 op amp shown in Figure 4-13 vary less than 2 dB as V_{DC} is changed from $\pm$ 10 V to $\pm$ 18 V except in the resonance region where changes as large as 25 dB are observed. A value $V_{DC} = \pm$ 15 V was selected as the normal value for all op amps tested subsequently.

As discussed previously, the demodulation RFI in the square-law response region can be characterized by the one parameter $H_2(f_1,-f_2)$. Shown in Figures 4-14 to 4-17 are values of $H_2(f_1,-f_2)$ for RF frequencies ranging from 0.1 to 400 MHz for the 115 op amps tested. In Figure 4-14 data for 30 741 op amps are presented. Among these 741 op amps, five were made by RCA in 1981 and the others were made by Fairchild during 1976 to 1982. The detailed

information is listed in Table 4-2. The $H_2(f_1,-f_2)$ values at a specific RF frequency vary $\pm$ 1.5 to $\pm$ 11.5 dB. In Figure 4-15 data for 25 LM10 op amps are presented. All 25 op amps were made during 1981 and 1982 by National Semiconductor. The most interesting aspect of the LM10 data is that two LM10 units (called mavericks) have $H_2(f_1,-f_2)$ values very different from the other LM10 units. It should be noted that one maverick LM10 op amp has a normal linear response as shown in Figure 4-18. Its voltage gain vs frequency response appeared to be similar to the other 23 LM10 op amps. Recall from Chapter 2 that second-order nonlinear transfer functions such as $H_2(f_1,-f_2)$ are functions of first-order linear transfer functions such as $H_1(f_1)$, $H_1(-f_2)$, $H_1(f_1 - f_2)$ and the power series coefficients of the second-order nonlinear sources. Since the maverick LM10 has a normal linear response, a simple explanation for its unusual H_2 values is that the power series coefficients of its nonlinearities differ significantly from other normal LM10 op amps. However, other explanations cannot be ruled out. The 23 similar LM10 op amps have $H_2(f_1,-f_2)$ values varying $\pm$ 3 to $\pm$ 12 dB at any one RF frequency. In Figure 4-16, data for 30 CA081 op amps are presented. All 30 units were made by RCA during 1980. The $H_2(f_1,-f_2)$ values vary $\pm$ 1 to $\pm$ 5 dB at any one RF frequency. In Figure 4-17 data for 30 LF355 op amps are presented. All 30 units were made by

National Semiconductor during 1980 to 1982. The most interesting aspects of the LF355 data are the resonances near 4.5 MHz and 12 MHz where the $H_2(f_1,-f_2)$ values decrease as much as 25 dB and 15 dB, respectively. The cause of the resonances has been investigated by computer-aided analysis of the circuit with the LF355 op amp replaced by its macromodel as described in Chapter 3. The result of the analysis will be discussed later in Chapter 6. The $H_2(f_1,-f_2)$ values outside the resonance regions vary from $\pm$ 3 dB to $\pm$ 8 dB at any one RF frequency.

4.3 Statistical Results

Shown in Figures 4-19 and 4-20 are the mean values for $H_2(f_1,-f_2)$ which are denoted by $\overline{H}_2$ and the standard deviation σ for the four types of op amps tested. Values for $\overline{H}_2$ and σ were calculated using the data for all the op amps given in Figures 4-14 to 4-17.

The mean values for $H_2(f_1,-f_2)$ indicate clearly that demodulation RFI effects are greater in op amps with bipolar input transistors (741 and LM10) than they are in op amps with FET input transistors (CA081 and LF355). This is a most important observation. In Section 4.4 this phenomenon will be shown to be related to the unity gain bandwidths of the four types of op amps.

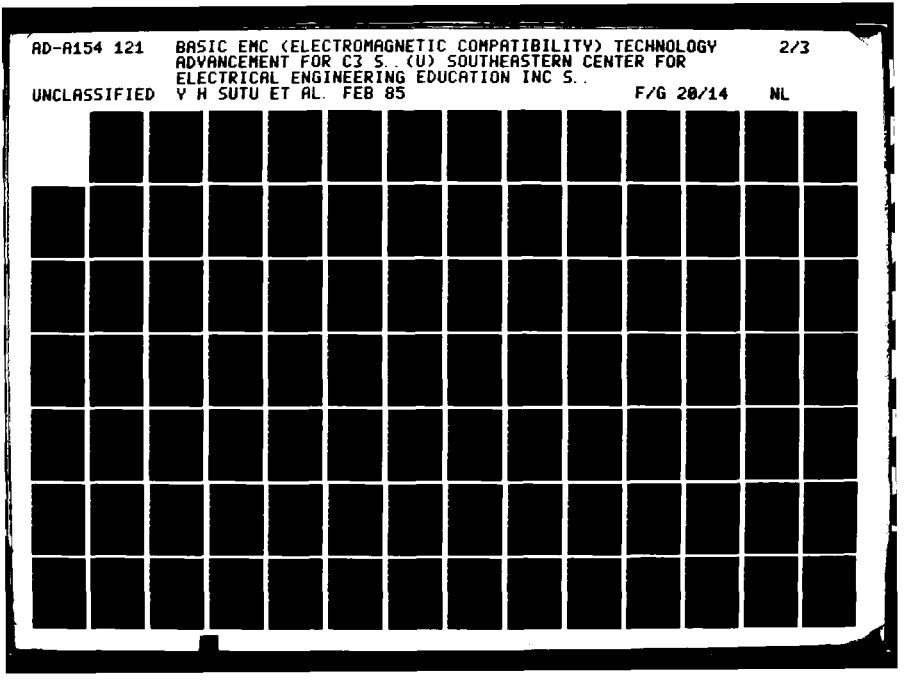
AD-A154 121 BASIC EMC (ELECTROMAGNETIC COMPATIBILITY) TECHNOLOGY ADVANCEMENT FOR C3 S..(U) SOUTHEASTERN CENTER FOR ELECTRICAL ENGINEERING EDUCATION INC S..
2/3
UNCLASSIFIED Y H SUTU ET AL. FEB 85
F/G 20/14
NL

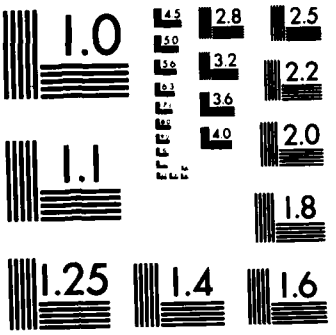

At RF frequencies above 10 MHz, demodulation RFI effects in the 741 op amp are significantly greater than in the LM10 op amp. It is believed that this is a result of the cutoff frequency of the npn bipolar input transistors in the 741 op amp being higher than the cutoff frequency of the pnp bipolar input transistors in the LM10 op amp. It is also noted that the mean value $\overline{H}_2$ for the LF355 op amp shows much less resonant excursion than do individual units. This is a result of the spread in values for the resonant frequencies which causes a smoothing effect for $\overline{H}_2$. For RF frequencies less than 10 MHz, the mean value $\overline{H}_2$ is lowest for the CA081 op amps (MOSFET input transistors). For RF frequencies greater than 10 MHz, the mean value $\overline{H}_2$ is lowest for the LF355 op amps (JFET input transistors).

The values for the standard deviation σ[a] vs RF frequency are shown in Figure 4-20. It is noted that for the CA081 op amps, the σ values are less than 2 dB except at 0.1 MHz where $\overline{H}_2$ is very small. For the LM10 op amps, the σ values could be calculated both for all op amps and also for the normal op amps only.

[a]Standard Deviation = $\sigma = [(\Sigma(x - \mu)^2) \div n]^{.5}$

where n = total number of items,

x = item value,

μ = mean value of all items.

Omitting the $H_2(f_1,-f_2)$ values for the two maverick LM10 op amps would decrease σ by approximately 2 to 4 dB below 2 MHz and by approximately 1 dB or less above 2 MHz.[27] The σ values shown in Figure 4-20 are the values calculated for all 25 op amps. For the LF355 op amps, the σ values are large especially in resonant regions near 4.5 MHz and 12 MHz. The σ values are also large above 200 MHz where the $H_2(f_1,-f_2)$ values are small.

The mean and standard deviation of $H_2(f_1,-f_2)$ values of the 741 op amps presented in Figures 4-19 and 4-20 included all 30 units. The means and standard deviations are shown in Figures 4-21 and 4-22 for each individual group of 741 op amps described in Table 4-2. It is interesting to note that 741 op amps that were made by different companies (Group 1 and Group 5) have $\overline{H}_2$ values that differ by as much as 11 dB at 1 MHz. Even 741 op amps made by one company in different years (Group 2 and Group 5) have $\overline{H}_2$ values that differ by as much as 12.5 dB at 1 MHz. Among the 5 groups, the standard deviation σ of Group 5 is the largest and is nearly 5 dB at f_1 = 1 MHz. (It is not known why the variations in H_2 for the five groups are largest at 1 MHz.)

The measured mean values of $H_2(f_1,-f_2)$ for the 741 op amps in the unity gain buffer circuit will be compared to the measured mean values of $H_2(f_1,-f_2)$ for the 741 op amps in the inverting amplifier circuit in Chapter 5.

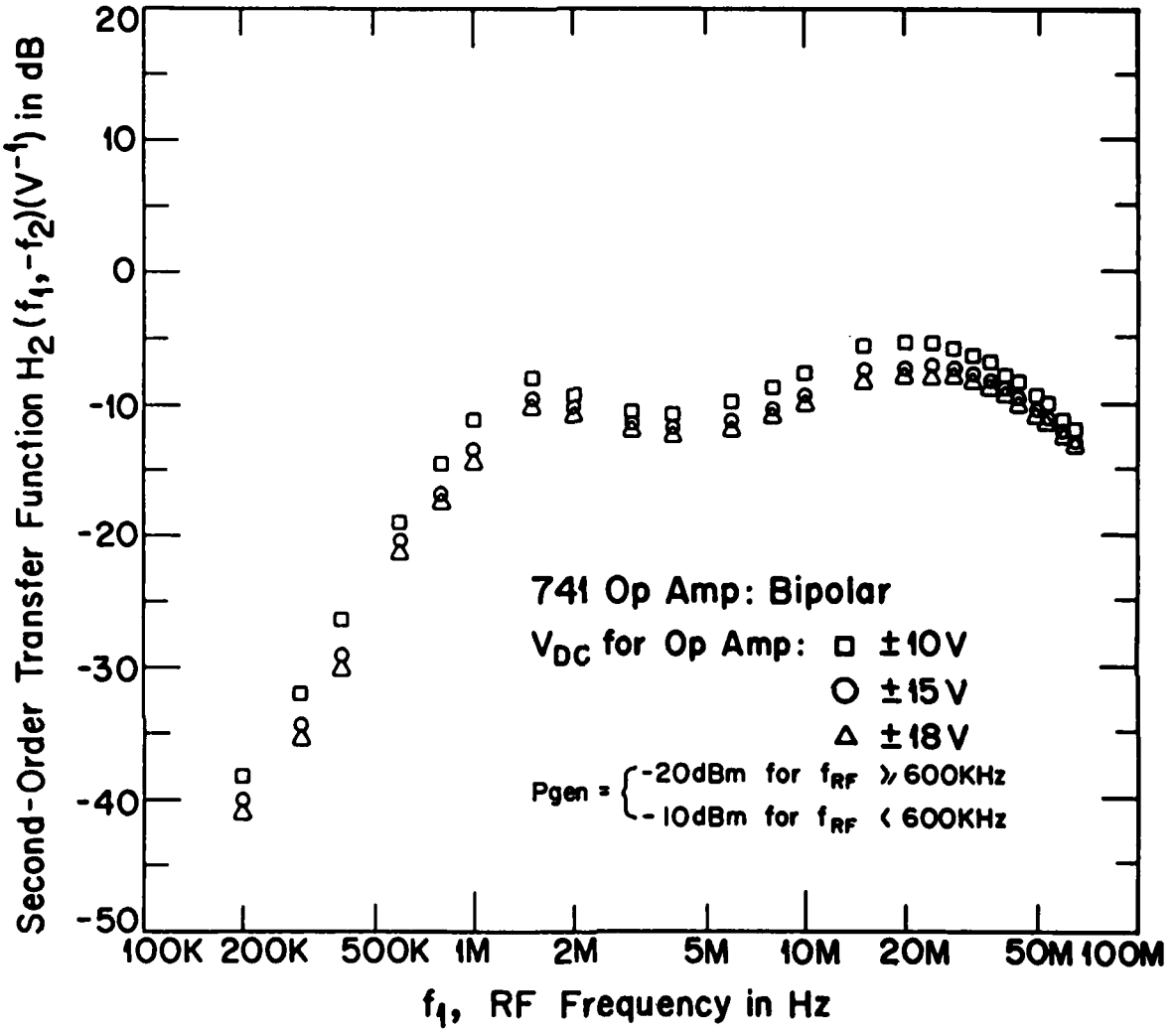

Fig. 4-10. Measured values of the second-order transfer function $H_2(f_1,-f_2)$ vs RF frequency for a 741 op amp at three dc power supply voltages.

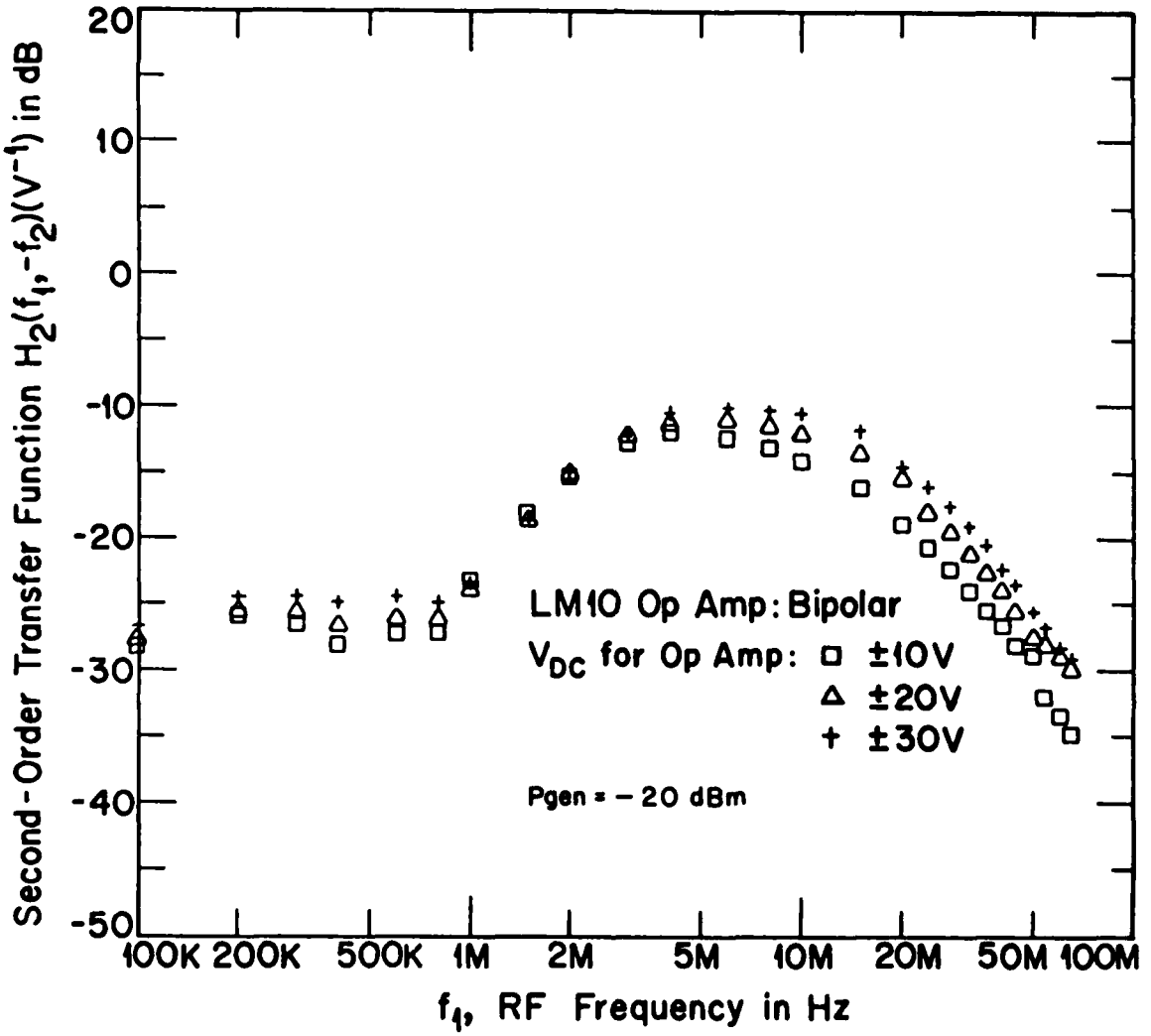

Fig. 4-11. Measured values of the second-order transfer function $H_2(f_1,-f_2)$ vs RF frequency for a LM10 op amp at three dc power supply voltages.

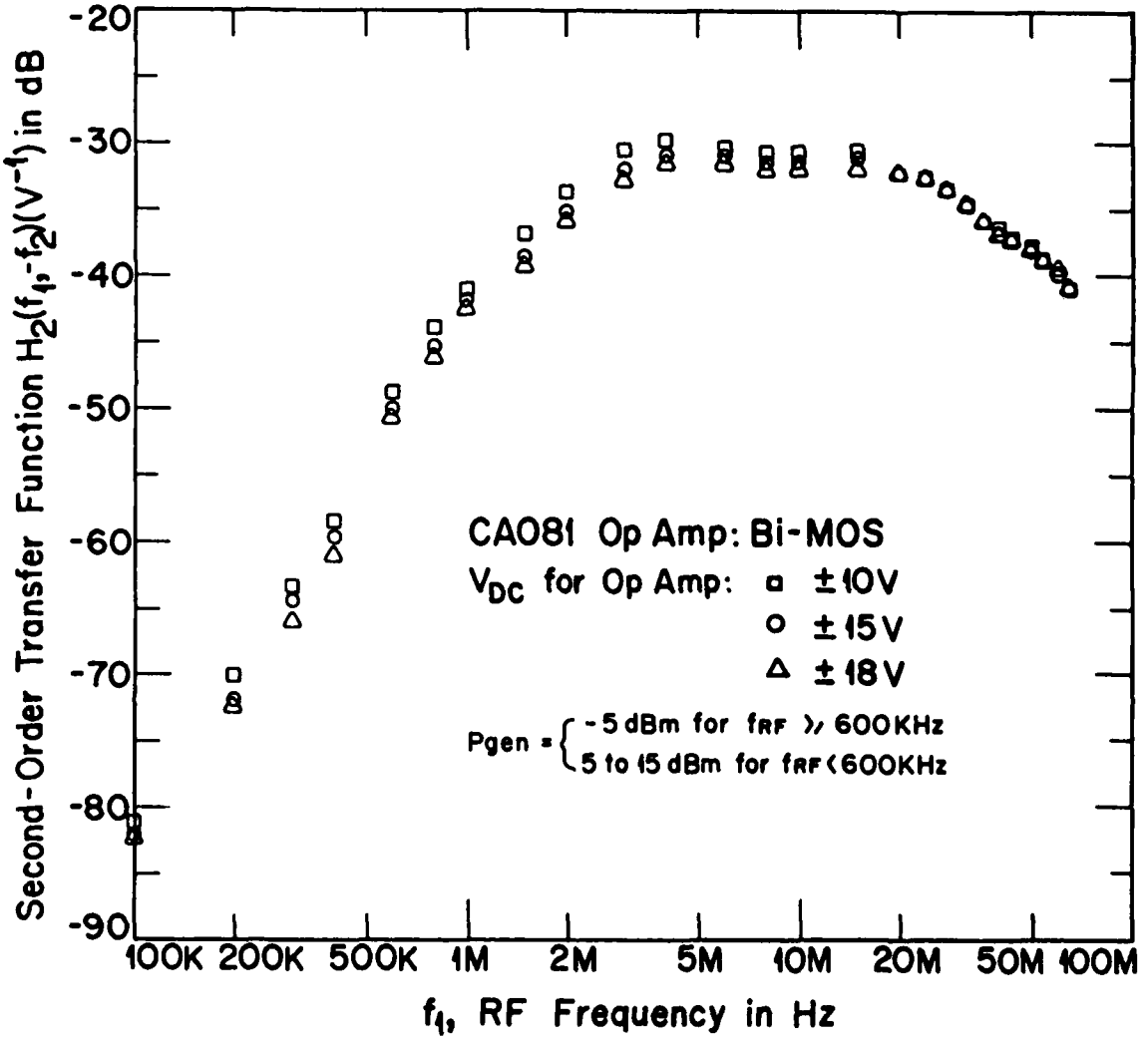

Fig. 4-12. Measured values of the second-order transfer function $H_2(f_1,-f_2)$ vs RF frequency for a CA081 op amp at three dc power supply voltages.

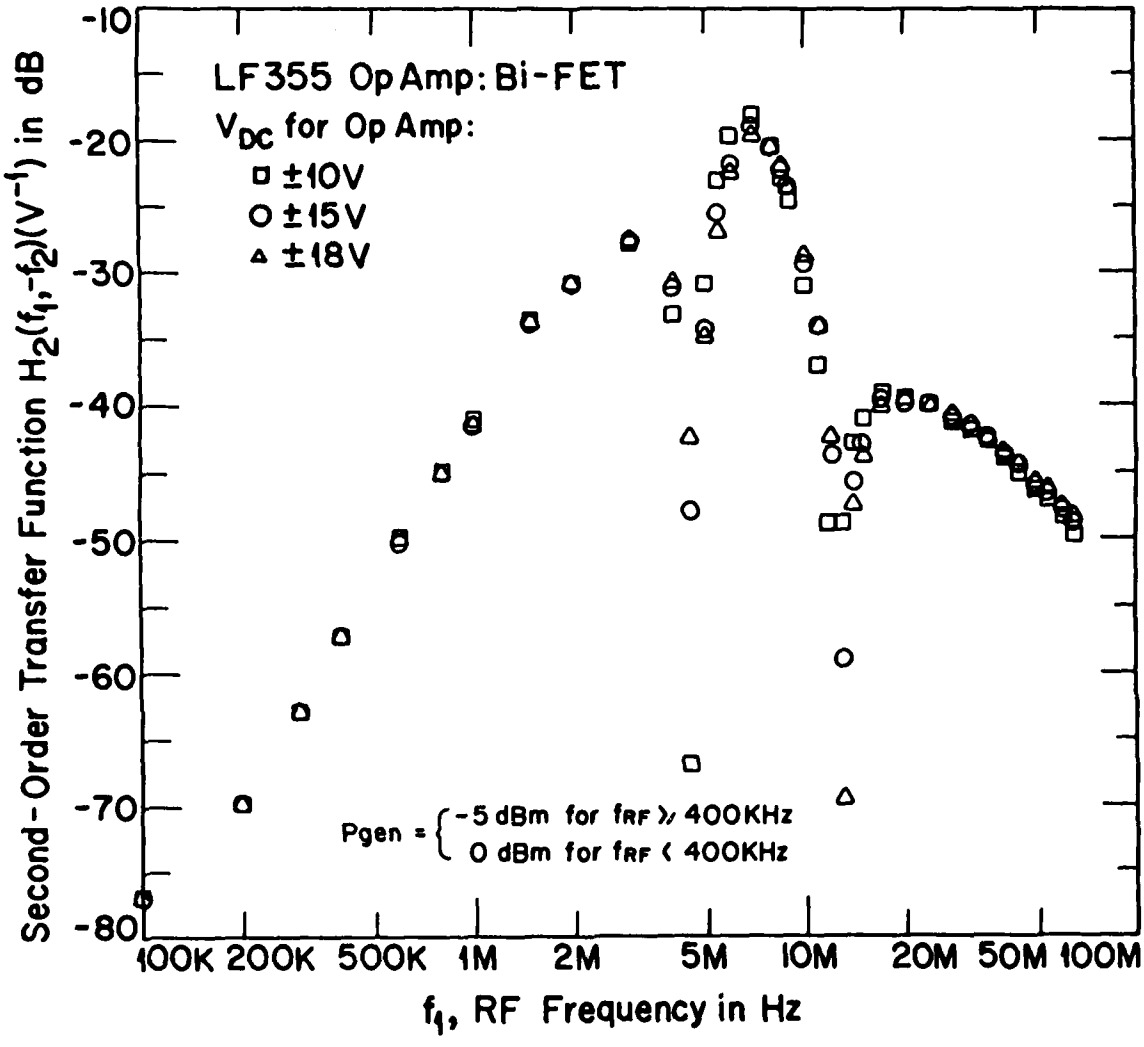

Fig. 4-13. Measured values of the second-order transfer function $H_2(f_1,-f_2)$ vs RF frequency for a LF355 op amp at three dc power supply voltages.

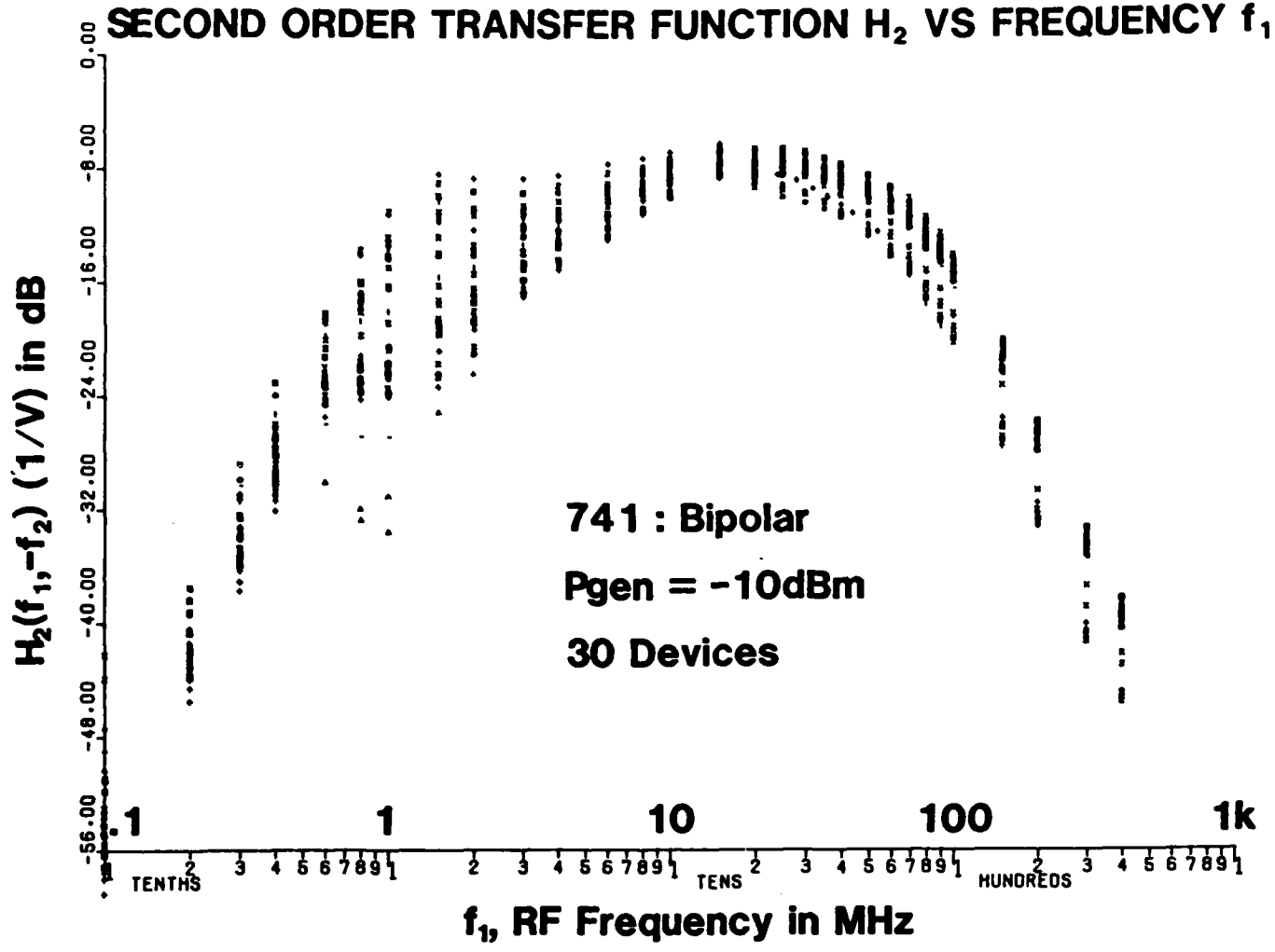

Fig. 4-14. Measured values of the second-order transfer function $H_2(f_1,-f_2)$ of the unity gain buffer circuit vs RF frequency for thirty 741 (bipolar) op amps.

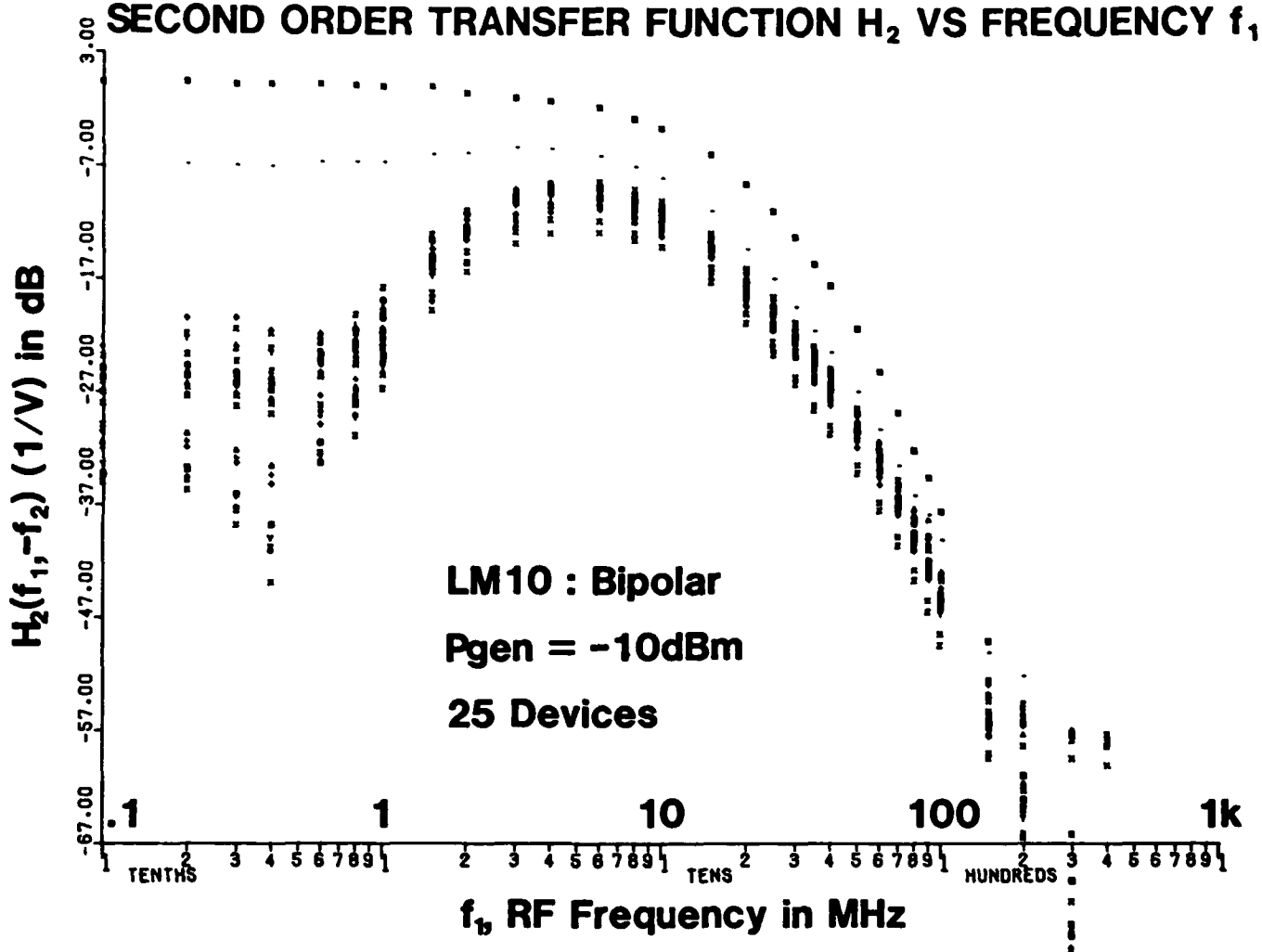

Fig. 4-15. Measured values of the second-order transfer function $H_2(f_1,-f_2)$ of the unity gain buffer circuit vs RF frequency for twenty-five LM10 (bipolar) op amps.

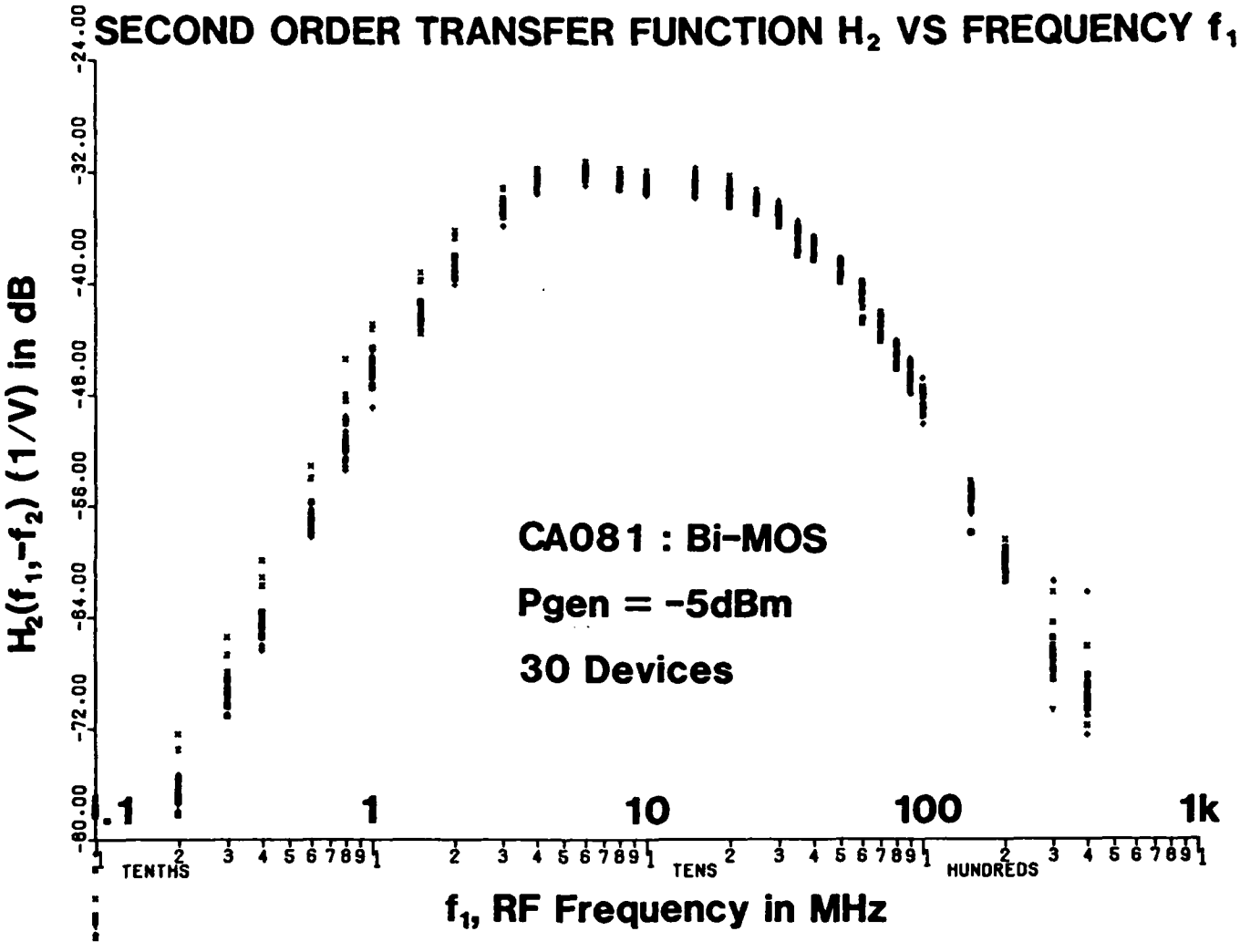

Fig. 4-16. Measured values of the second-order transfer function $H_2(f_1,-f_2)$ of the unity gain buffer circuit vs RF frequency for thirty CA081 (Bi-MOS) op amps.

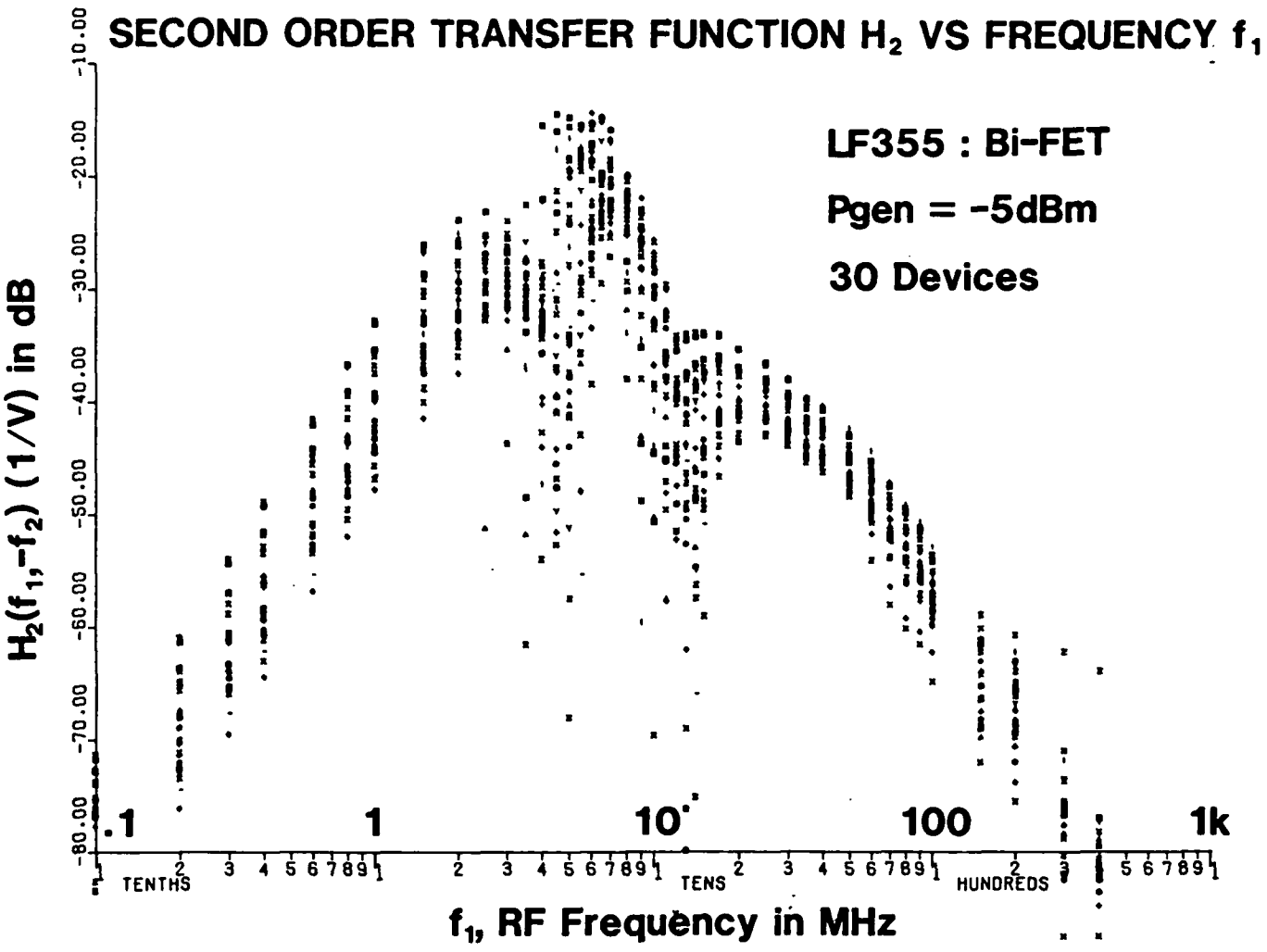

Fig. 4-17. Measured values of the second-order transfer function $H_2(f_1,-f_2)$ of the unity gain buffer circuit vs RF frequency for thirty LF355 (Bi-FET) op amps.

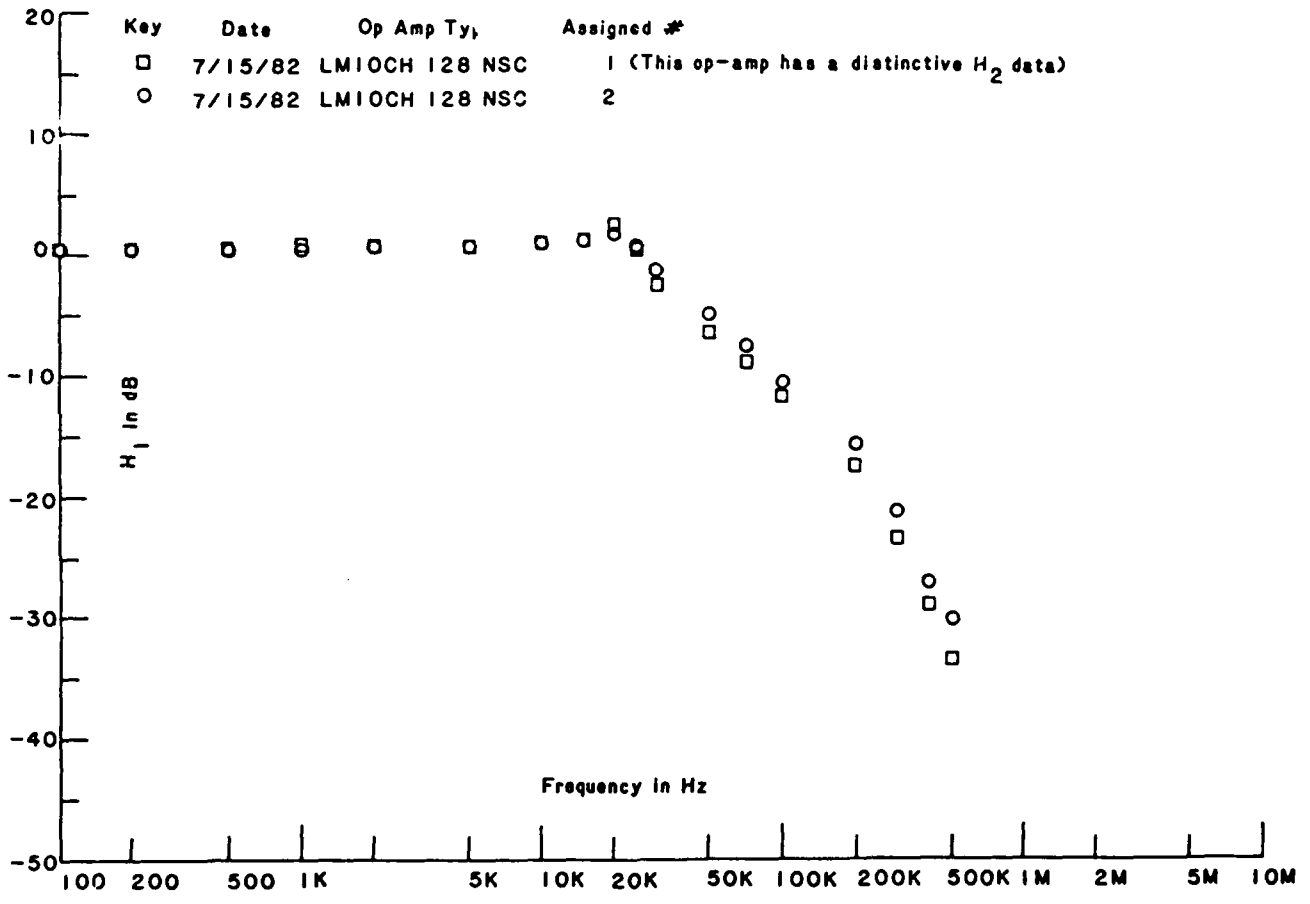

Fig. 4-18. Measured linear responses of the maverick LM10 and a normal LM10.

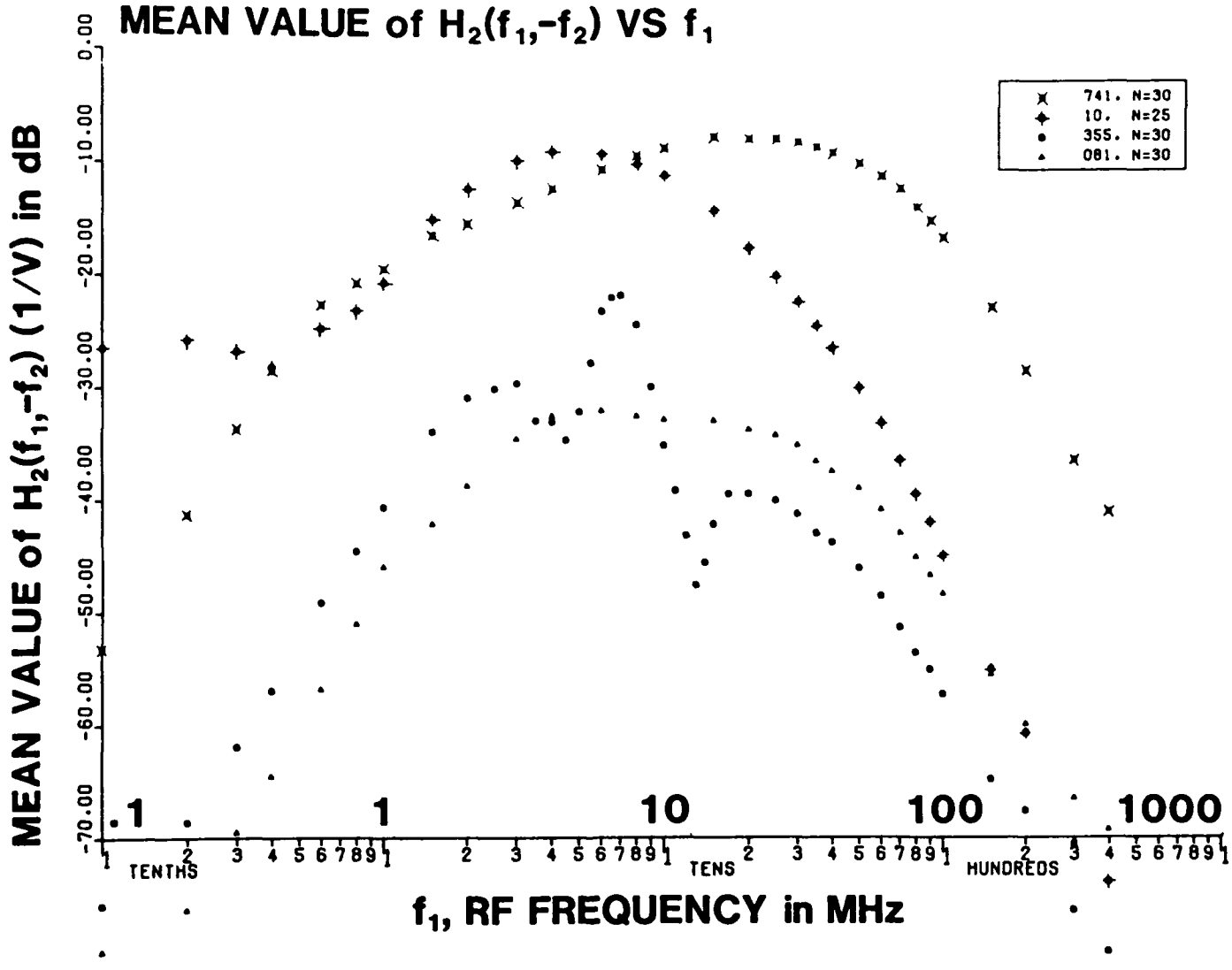

Fig. 4-19. Experimental mean value of the second-order transfer function $H_2(f_1,-f_2)$ of the unity gain buffer circuit vs RF frequency for four types of op amps.

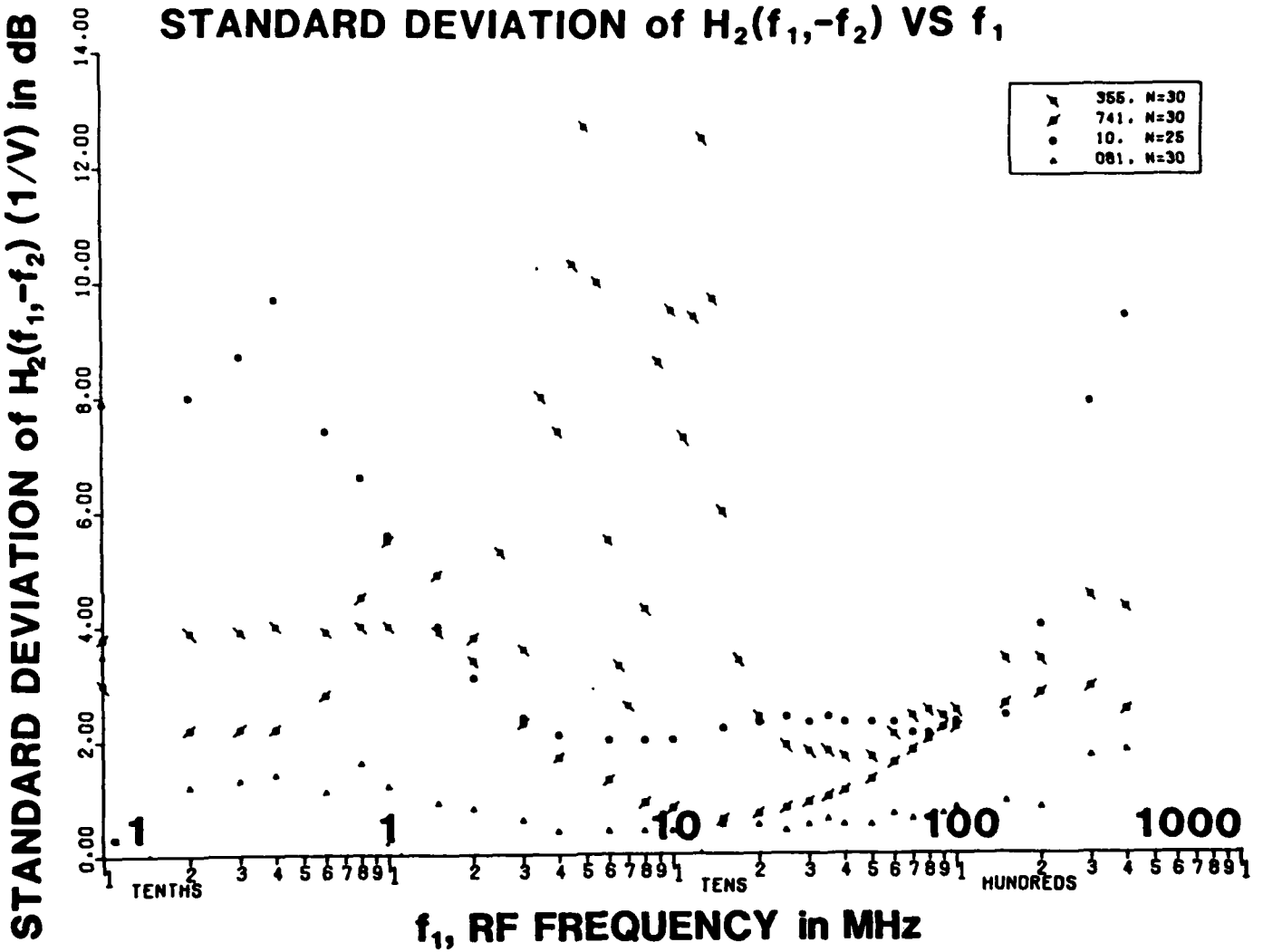

Fig. 4-20. Experimental standard deviation, σ, of the second-order transfer function $H_2(f_1,-f_2)$ of the unity gain buffer circuit vs RF frequency for four types of op amps.

TABLE 4-2

MAKER AND PRODUCTION DATE INFORMATION OF THE 30 741 OP AMPS

Group	Units	Maker	Year	Week
1	5	RCA	1981	27
2	5	Fairchild	1976	36
3	10	Fairchild[a]	1981	38
4	5	Fairchild[a]	1981	35
5	5	Fairchild[b]	1982	49

[a] Manufactured in Hong Kong.

[b] Manufactured in Korea.

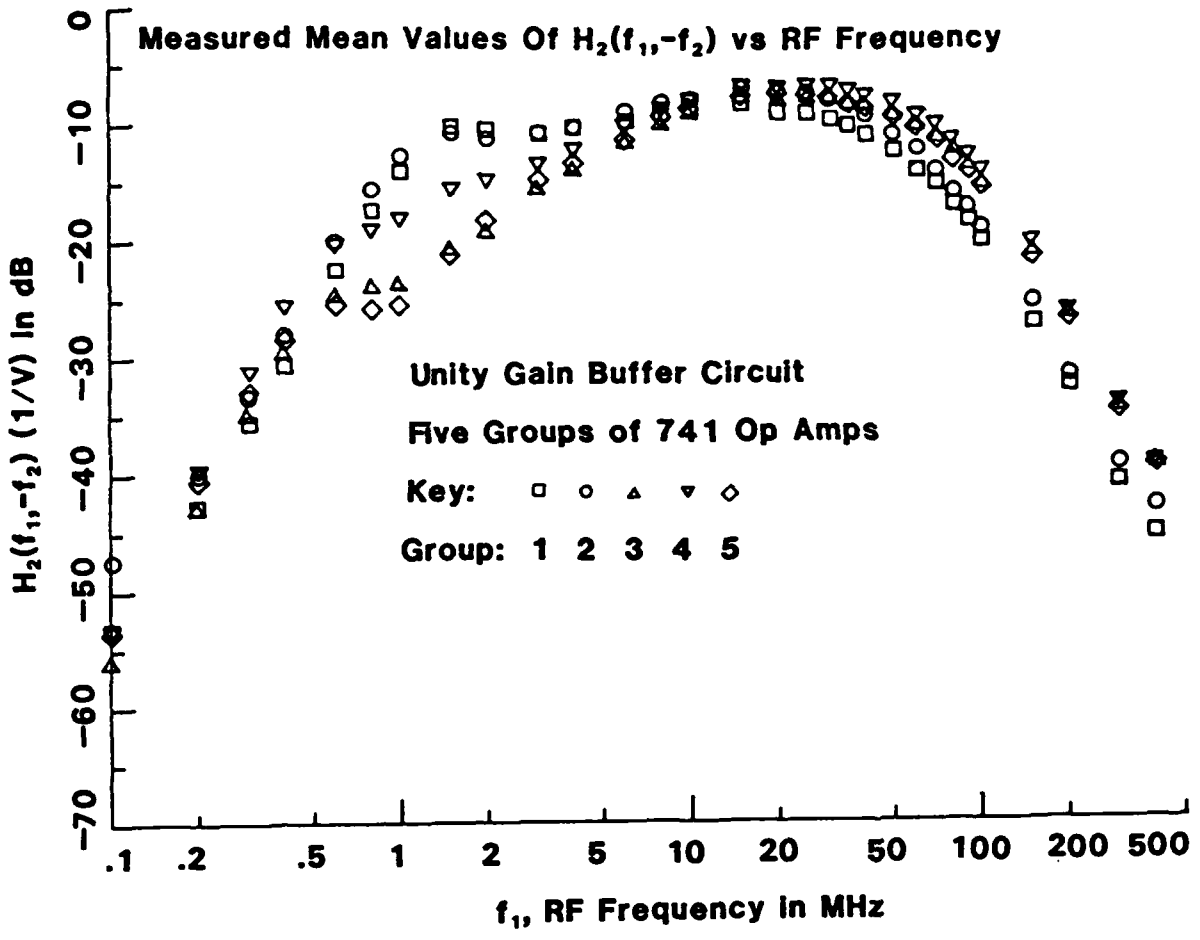

Fig. 4-21. Mean values of measured $H_2(f_1,-f_2)$ for five groups of 741 op amps differed by makers or production dates. See Table 4-2.

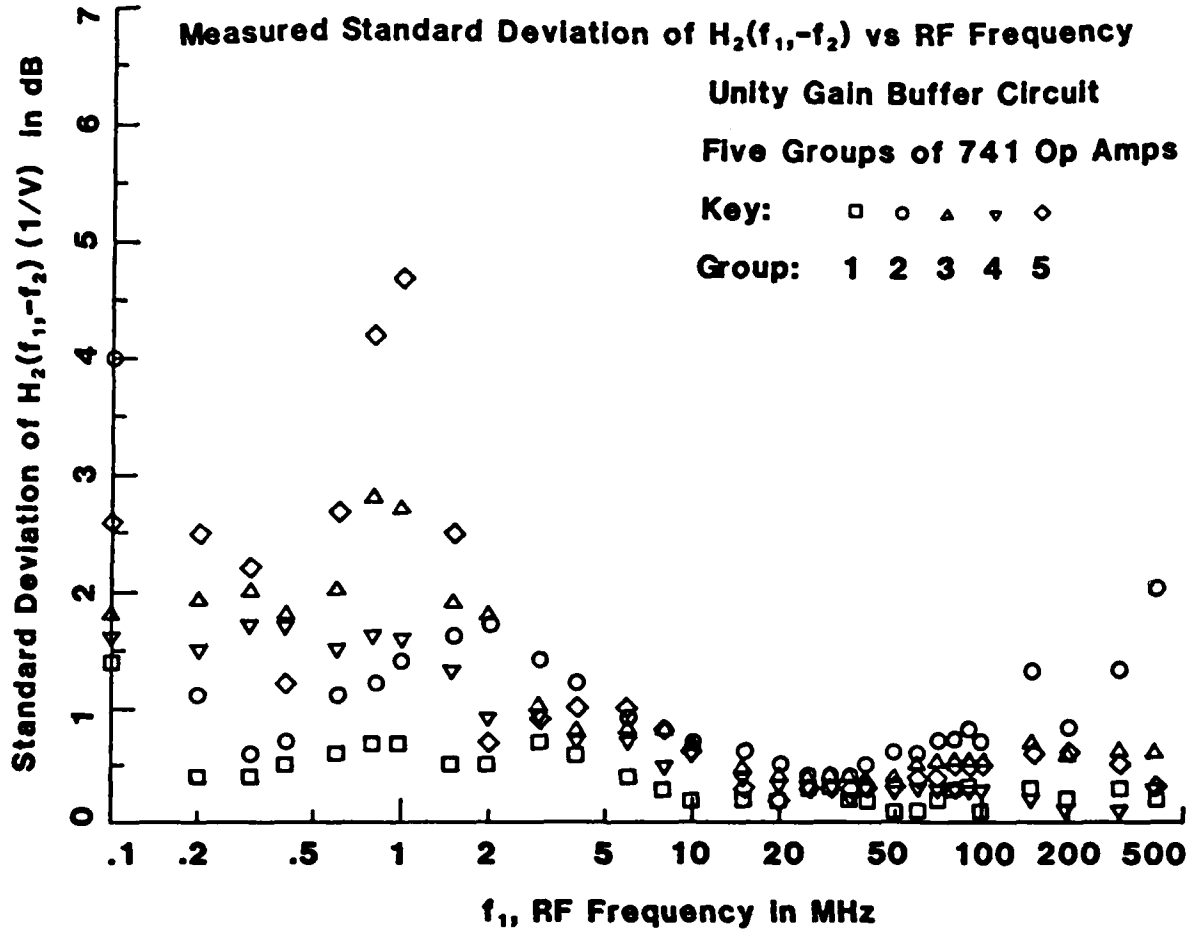

Fig. 4-22. Standard deviations of measured $H_2(f_1,-f_2)$ for five groups of 741 op amps differed by makers or production dates. See Table 4-2.

4.4 Discussion: Transfer Function Representation of Op Amp Unity Gain Buffer.

The op amp unity gain buffer is represented by a unilateral open-loop op amp in the forward path and a unilateral linear feedback path $\beta(f) = 1$. The open-loop op amp is characterized by an open-loop first-order transfer function $A_1(f)$ and an open-loop second-order transfer function $A_2(f_1,f_2)$. Higher order transfer functions have been omitted. Figure 4-23 shows the transfer function representation of the op amp unity gain buffer described above. Expressions for the closed-loop transfer functions $H_1(f)$ and $H_2(f_1,f_2)$ in terms of the open-loop transfer functions and the feedback network transfer function $\beta(f)$ have been given by Narayanan:[23]

$$H_1(f) = \frac{A_1(f)}{1 + \beta(f)A_1(f)} \qquad (4\text{-}12)$$

$$H_2(f_1,f_2) = \frac{A_2(f_1,f_2)}{[1 + A_1(f_1)\beta(f_1)][1 + A_1(f_2)\beta(f_2)][1 + A_1(f_1+f_2)\beta(f_1+f_2)]} \qquad (4\text{-}13)$$

For the op amp unity gain buffer, we have $\beta(f) = 1$. Therefore, Equation (4-13) can be written as

$$H_2(f_1,f_2) = \frac{A_2(f_1,f_2)}{[1 + A_1(f_1)][1 + A_1(f_2)][1 + A_1(f_1+f_2)]} \qquad (4\text{-}14)$$

Note that Equation (4-14) relates the RFI demodulation response in the op amp unity gain buffer to the open-loop first-order transfer function $A_1(f)$ at frequencies f_1, f_2, and $f_1 + f_2$. Note that in

our case $f_1 = f_{RF}$, $f_2 = -f_{RF} + f_{AF} = -f_{RF} + 1$ kHz and $f_1 + f_2 = f_{AF}$. According to Eq. (4-14), op amps with large $A_2(f_1,f_2)$ and small $A_1(f_1)$, $A_1(f_2)$ and $A_1(f_1 + f_2)$ would have large $H_2(f_1,f_2)$. It is believed that op amps with bipolar input transistors should have larger $A_2(f_1,f_2)$ values than op amps with FET input transistors because the bipolar exponential nonlinearity is stronger than any FET nonlinearity. It would be possible to check this belief by using NCAP to calculate $H_2(f_1,f_2)$ with the feedback resistor omitted. Then we could have $\beta(f) = 0$ and $H_2(f_1,f_2) = A_2(f_1,f_2)$. Unfortunately, this has not been done up to now. However, we do have information on the values for $A_1(f_1)$, $A_1(f_2)$, and $A_1(f_1 + f_2)$. Shown in Figure 4-24 are typical values for the magnitude of op amp open-loop voltage gain vs frequency for the four op amp types tested. The data are taken from manufacturers' data sheets. Recall that in our experiment $f_1 = f_{RF} \geq 100$ kHz, $-f_2 = f_{RF} - 1$ kHz ≥ 99 kHz, and $f_1 + f_2 = 1$ kHz. Thus the frequencies f_1, $-f_2$, and $f_1 + f_2$ are all greater than the 3-dB corner frequency for all four op amp types. Using the typical data given in Figure 4-24, we can rank the magnitudes of the denominator of Eq. (4-14) for the four op amp types in the unity gain buffer circuit. Let $|D|$ denote the magnitude of the denominator in Eq. (4-14). Then we must have $|D(CA081)| > |D(LF355)| > |D(741)| > |D(LM10)|$ because the $A_1(f)$ vs f curve for the CA081 lies above the $A_1(f)$ vs f curve for the LF355 which in turn lies above the $A_1(f)$ vs f curve for the 741,

which in turn lies above the $A_1(f)$ vs f curve for the LM10 at the three frequencies f_1, $-f_2$, and $f_1 + f_2$ for all $f_1 \geq 100$ kHz. It is worthwhile to note that for $f_1 > 10$ MHz that $|A_1(f_1)|$ and $|A_1(f_2)|$ are less than one and the denominator of Eq. (4-14) reduces to $1 + A_1(f_1 + f_2) = 1 + A_1(1\ \text{kHz})$. Our comments on the magnitude of the numerator and denominator of Eq. (4-14) are consistent with the experimental results shown in Figure 4-19 for the mean values of $H_2(f_1,-f_2)$ vs f_1. The op amps with FET-input transistors have the lower H_2 values because they have lower A_2 values and higher A_1 values at the frequencies of interest. The op amp with bipolar input transistors have higher H_2 values because they have higher A_2 values and lower A_1 values at the frequencies of interest.

Transfer Function Model Of The Op Amp Unity Gain Buffer

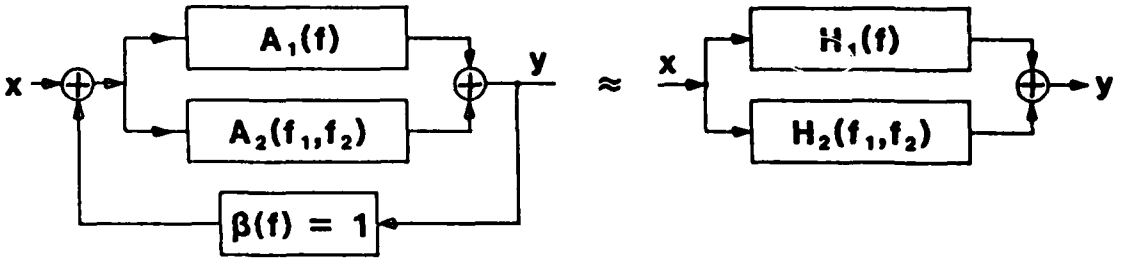

$$H_2(f_1,f_2) = \frac{A_2(f_1,f_2)}{[1+A_1(f_1)\beta(f_1)][1+A_1(f_2)\beta(f_2)][1+A_1(f_1+f_2)\beta(f_1+f_2)]}$$

A_I : Open Loop ith-Order Transfer Function

H_I : Closed Loop ith-Order Transfer Function

Fig. 4-23. Transfer function model of the op amp unity gain buffer.

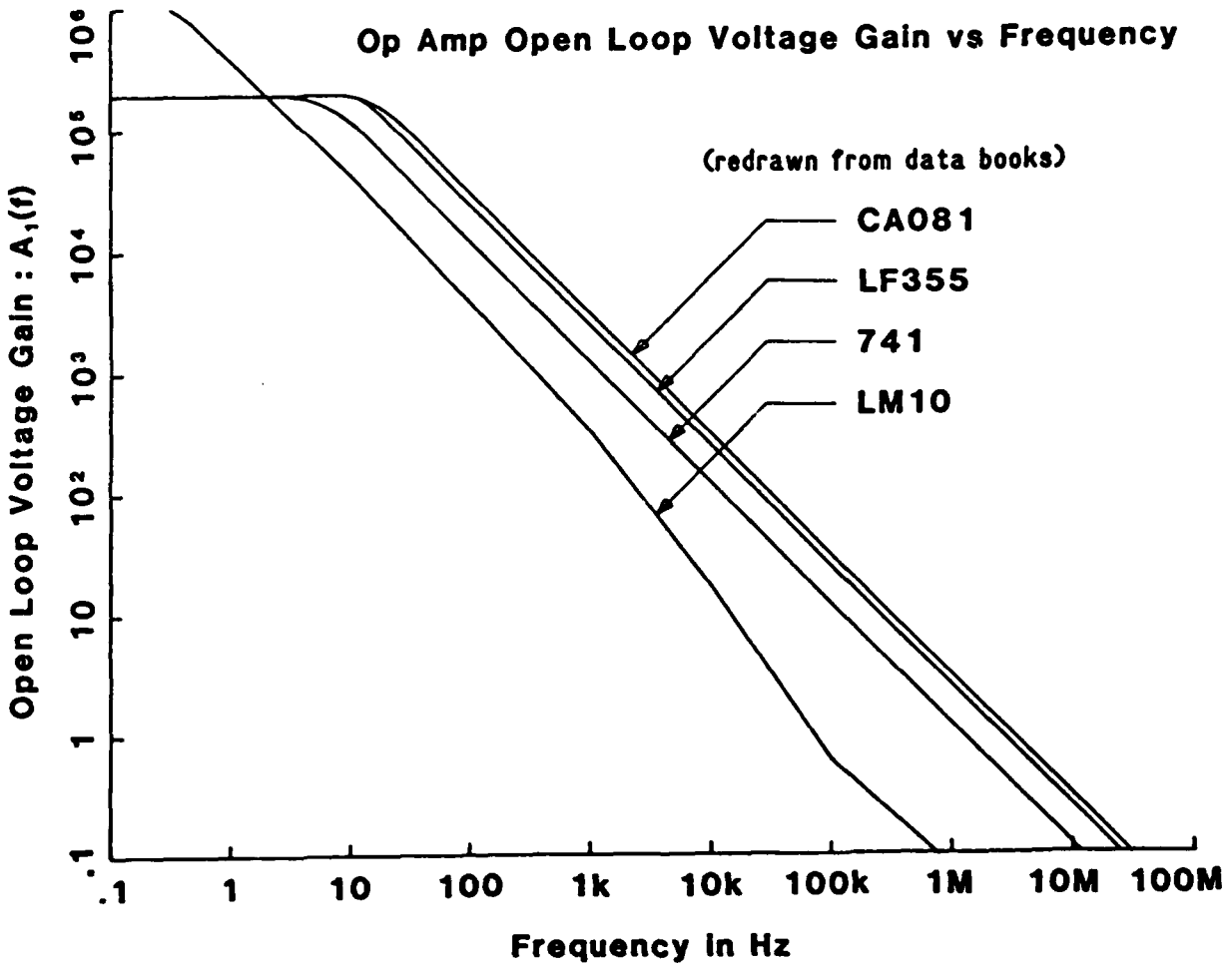

Fig. 4-24. Open-loop voltage gain vs frequency for four types of op amps.[19,39,40,44]

CHAPTER FIVE

STATISTICS OF MEASURED DEMODULATION RFI RESPONSES OF THE INVERTING AMPLIFIER

In our previous investigations the op amp circuit configuration was kept constant.[4,6-9,13,27-30] The specific op amp circuit used was the unity voltage gain buffer amplifier circuit called a voltage follower. That circuit configuration is also called noninverting because the intended signal is injected into the noninverting input denoted by (+). The RFI signal was also injected into the noninverting input. In this chapter, we report the results of an investigation of the inverting op amp configuration shown in Figure 5-1. The intended signal voltage gain is $A_v = V_{OUT}/V_{IN} = -R2/R1$ and the intended signal input impedance is R1. The capacitance C4 in the feedback path, when included, provides RFI suppression.[31] An experimental configuration similar to that shown in Figure 4-6 was used to measure demodulation RFI for RF frequencies in the range 100 kHz to 400 MHz. Measurement results will be presented for some of the combinations of R1, R2 and C4 listed in Table 5-1 for 35 units of 741 op amps. Thirty units are identical to those reported in Chapter 4; the five additional 741 op amps used in this experiment were made by National Semiconductor in 1982.

5.1 Measurement Set-up

The actual circuit used in the measurement of demodulation RFI effects in inverting op amp circuits is shown in Figure 5-2. This circuit will be referred to as the 3-stage op amp LED circuit hereafter. The 3-stage op amp LED circuit was designed by a team of investigators from the Rome Air Development Center (RADC), the University of

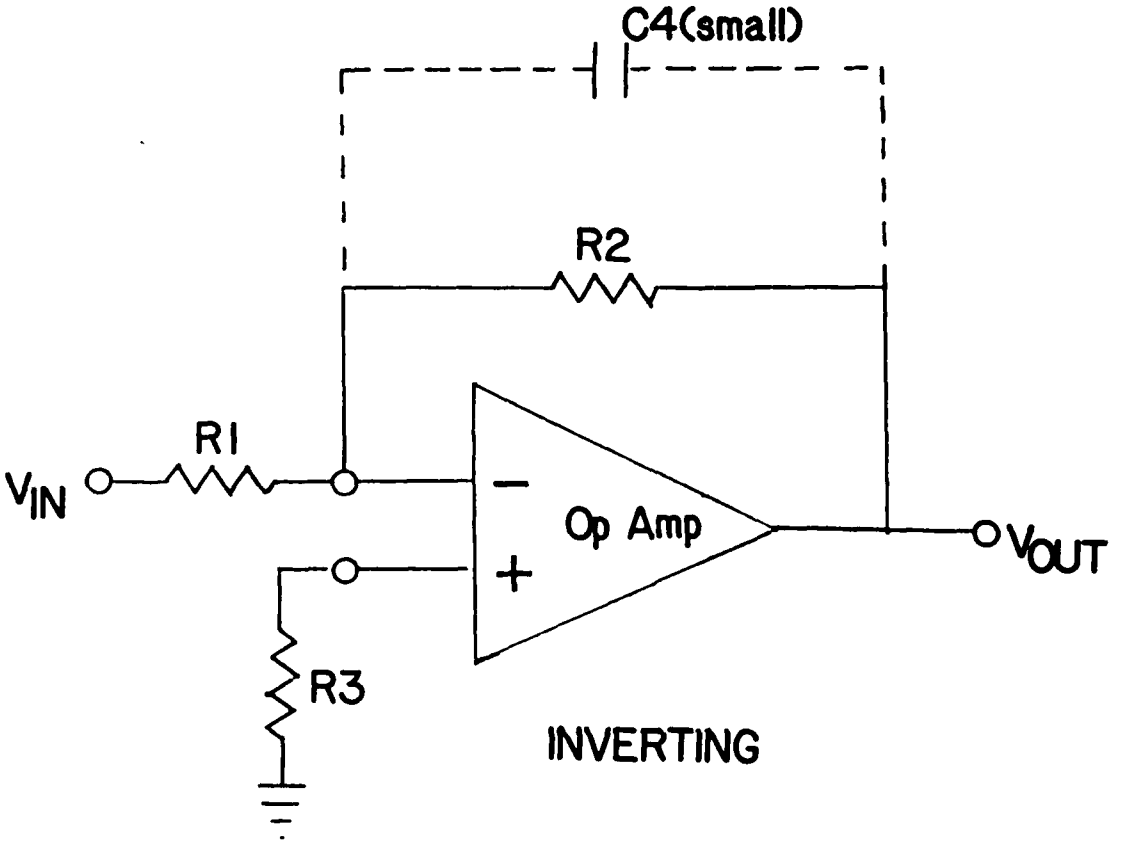

Fig. 5-1. Inverting op amp circuit with voltage gain A_v = -R2/R1. The capacitor C4, when included, provides RFI suppression.[31]

TABLE 5-1

COMBINATIONS OF R1, R2 AND C4
FOR INVERTING OP AMP CIRCUIT CONFIGURATION

Input Resistor R1 (Ω)	Feedback Resistor/ Voltage Gain R2 (Ω)/A_v	RFI Suppression Capacitor C4 (F)
10 k	100 k/-10	0
10 k	100 k/-10	27 p
10 k	1 M/-100	0
10 k	1 M/-100	27 p
100 k	1 M/-10	0
100 k	1 M/-10	27 p

Kentucky (UK), Syracuse University (SU), the University of South Florida (USF), and the State University of New York at Buffalo (SUNYAB). The RFI signal produced in the 1st stage is amplified by the 2nd stage and by the third stage which drives the Light-Emitting Diode (LED). The amplified RFI signal can light the LED to produce a visual display of the existence of RFI. The EMI experiment was designed to demonstrate how two sets of statistics from two independent experiments can be combined to predict the statistics of a combined experiment.[41] One experiment undertaken at UK provided statistics on cable coupling for wires terminated in 1 kΩ loads.[42,43] Another experiment undertaken at SUNYAB provided second-order transfer function statistics for the 3-stage op amp LED circuit. Two sets of independent statistics were combined and compared with the statistics of a combined experiment. The second-order transfer function of the inverting op amp configuration of Figure 5-1 can be related to the second-order transfer function of the 3-stage op amp LED circuit by accounting for the linear voltage gains of the second and third stage and the attenuation of the circuit between the RF generator and input of the 1st stage.

This paragraph will describe the function of each element in the circuit of Figure 5-2. The RF signal generator produces an RF voltage with an RF carrier frequency f_{RF} in the range 0.1 to 400 MHz. The RF voltage is AM-modulated with modulation index m = 0.5 and AM-modulation frequency f_{AF} = 1 kHz. The capacitors C6, C7, and C1 and resistors R10, R11, and the 50 Ω input resistor of the RF voltmeter form a high-pass RC filter which blocks dc and any spurious 1 kHz components from the RF generator. The first stage is the op amp under test; it has an

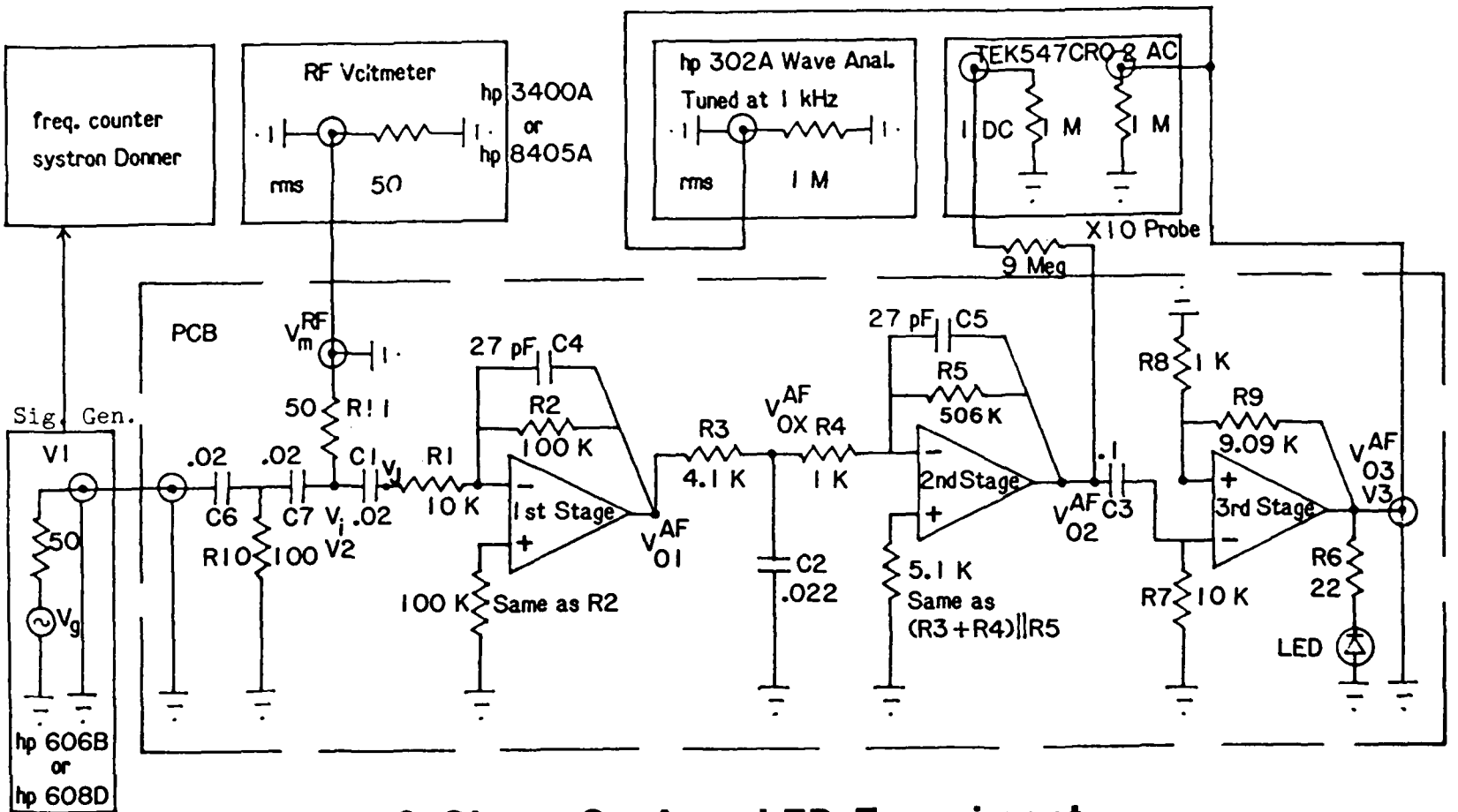

3-Stage Op Amp LED Experiment

Fig. 5-2. Three-stage op amp LED experiment. Resistor values are in Ω. Capacitor values are in μF unless otherwise specified.

inverting configuration. Its second-order nonlinearities cause an undesired demodulation of the amplitude-modulated RF signal to produce an undesired audio modulation frequency component V_{01}^{AF} at the output of the first stage. The ratio of the feedback resistor R2 to the input resistor R1 provides the intended linear voltage gain A_{v1} of the first stage at low frequencies. The capacitor C4, when included, serves as an RFI suppression capacitor.[31] The RF voltmeter reads the rms RF voltage V_m^{RF} which is one-half the rms RF voltage V_i at the input of the first stage. Note that a 50 Ω resistor is used to terminate the 50 Ω coaxial cable connecting the circuit and the RF voltmeter. Furthermore, the resistor combination of R10 in parallel with the series combination R11 + the 50 Ω termination resistor at the RF voltmeter input provides at high frequencies a 50 Ω terminating resistance to the 50 Ω coaxial cable connecting the RF generator and the circuit. Between the first and second stages there is a low-pass filter formed by R3, R4, and C2. It attenuates any RF components from the first stage, but it allows the audio frequency component V_{01}^{AF} to pass through. The second and third stages provide linear voltage amplification of the audio-frequency component V_{01}^{AF}. The second stage is an inverting amplifier with a voltage gain of 100 determined by the ratio R5/(R3 + R4). It is critical to include a resistor equal in value to the feedback resistor R2 from the noninverting input of the first stage to ground. That resistor reduces the dc offset voltage[32,33] at the output of the first stage so as to avoid saturation at the output of the second stage. The resistor connecting the noninverting input of the second stage to ground serves a similar purpose, but it is less critical. The capacitor C3 and resistor R7 form a high-pass filter with a 160 Hz cutoff frequency

to block any remaining dc offsets at the output of the second stage from entering the 3rd stage. The third stage is a noninverting amplifier with a voltage gain of 10 determined by the ratio (R8 + R9)/R8. The LED goes on when the rms voltage of the amplified demodulated audio frequency components V_{03}^{AF} at the output of the 3rd stage exceeds a threshold value. The threshold value for a purely 1 kHz signal was typically 1.1 V (rms) which corresponds to a peak voltage of 1.5 V. There were occasions when the LED went on and the 1 kHz voltage component was much less than 1.1 V (rms). In these cases a strong 2 kHz voltage component was observed. A 2 kHz voltage component can also be a second-order demodulation RFI component. It results from a beating or mixing (intermodulation) of the upper and lower sidebands of the AM-modulated RF input signal in the 1st op amp stage. Usually, the 2 kHz RFI component was in the range 0.15 ± 0.05 V (rms) when the 1 kHz RFI component was 1.0 V (rms). However, when a resonant effect was observed which caused the 1 kHz voltage component to be suppressed, the RF voltage had to be increased to an unusually high level in order to turn on the LED. Then a strong 2 kHz voltage component was observed. The 2 kHz voltage component might be as large as the 1 kHz voltage component. Occasionally, the 2 kHz voltage component exceeded the 1 kHz voltage component. We suspect that these circumstances indicate that a 4th-order nonlinear effect may have manifested itself.

A frequency counter was used to measure accurately the RF frequency. A CRO was used to monitor the dc offset voltage and the AF voltage waveform at the output of the second stage.

5.2 Measurement Procedure

Prior to the measurement of demodulation RFI responses, the linear voltage gain at audio frequency 1 kHz of the entire 3-stage op amp LED assembly and of each section was measured to verify the circuit connections. An Audio Frequency (AF) oscillator (hp651B) was connected in place of the RF voltmeter to apply an AF signal to the circuit while the RF generator was turned off. The AF voltages V_{03}^{AF}, V_{02}^{AF}, V_{0X}^{AF}, V_{01}^{AF}, V_{j}^{AF}, and V_{i}^{AF} which are shown in Figure 5-2 were read with a tuned AF wave analyzer (hp302A). The superscript AF denotes Audio Frequency component. The AF voltage V_{03}^{AF} at the output of the 3rd stage was set at 1.0 V (rms) while readings of other AF voltages were taken. The results are given in Table 5-2. The V_{0X}^{AF} reading drew our attention. When the op amp used in the 2nd stage was a 741 op amp, the voltage V_{0X}^{AF} was 0.25 mV instead of the expected 0.2 mV. When the 741 op amp was replaced with a LF355 op amp, the voltage V_{0X}^{AF} was 0.2 mV in agreement with what we expected. We believe that the discrepancy in the V_{0X}^{AF} value when a 741 op amp was used in the second stage is related to the low input impedance of the 741 op amp. Other AF voltages in Table 5-2 have values in satisfactory agreement with calculated values.

In all measurements of demodulation RFI responses, the op amps for the 2nd and 3rd stage of the 3-stage op amp LED circuit were the same (741-#20 and 741-#12 respectively). The 1st stage op amp was changed. Each of the 30 units of 741 op amps used in Chapter 4 and the five additional 741 op amps made by National Semiconductor was used in the 1st stage. The signal from the RF generator was a 50% amplitude-modulated (1 kHz) RF signal as before. The input RF signal

TABLE 5-2

LINEAR AF NODE VOLTAGES AT 1 KHZ
OF THE 3-STAGE OP AMP LED CIRCUIT

AF Voltage	hp 302A Reading[a]	Expected Value
V_{O3}^{AF} (V)	1.0	1.0
V_{O2}^{AF} (mA)	102	100
V_{OX}^{AF} (mA)	0.25[b]	0.20
V_{O1}^{AF} (mA)	0.98	1.0
V_{j}^{AF} (μV)	98	100
V_{i}^{AF} (μV)	115	≥ 100

[a] All readings are in rms values. The 741 op amps were used in all 3 stages (1st: 741-#1, 2nd: 741-#20, 3rd: 741-#12).

[b] When a LF355 was used in 2nd stage, reading was 0.2 mV.

at a specific RF frequency was adjusted so that the demodulated 1 kHz AF component at output V3 of the 3rd stage reached rms values of V_{03}^{AF} = 1.0 V and 0.4 V sequentially. At the same time, the meter readings of the RF generator and RF voltmeter were recorded. This procedure was used to verify the square-law response region described in Chapter 4. To understand this, note that the two AF voltages (1.0 V and 0.4 V) at output V3 corresponds to a ratio of -8 dB. Therefore, the two corresponding meter readings of the RF voltmeter or RF generator should give a ratio of approximately -4 dB. If otherwise, the data taken do not reflect the characteristics of second-order nonlinearities and should be rejected for use in determining H_2. If the data correspond to the square-law response region, the second-order transfer function can be determined from the data.

The 1 kHz AF rms voltage V_{03}^{AF} at the output is related to the RF rms voltage V_g^{RF} from the RF generator by the second-order transfer function $H_2(f_1,-f_2)$.

$$\sqrt{2}V_{03}^{AF} = m(\sqrt{2}V_g^{RF})^2|H_2(f_1,-f_2)| \qquad (5\text{-}1)$$

where m is the modulation index. The factor $\sqrt{2}$ arise because amplitudes are used in nonlinear transfer function expressions. From Figure 5-2, we note the voltage relationship given by

$$V_g^{RF} = 4V_m^{RF} \qquad (5\text{-}2)$$

Substitute Eq. (5-2) into Eq. (5-1) and solve for $H_2(f_1,-f_2)$ with m = 0.5. The result is

$$|H_2(f_1,-f_2)| = \sqrt{2}V_{03}^{AF}/(4V_m^{RF})^2 \qquad (5\text{-}3)$$

where V_{03}^{AF} and V_m^{RF} are in rms volts. Equation (5-3) can be expressed in dB as

$$20\log_{10}|H_2(f_1,-f_2)| = 20\log_{10}V_{03}^{AF} - 40\log_{10}V_m^{RF} - 21.0 \qquad (5\text{-}4)$$

The second-order transfer function H_2' of the 1st stage alone, i.e. between the output node of the 1st stage and the node connecting C1 and R1, can be related to the second-order transfer function H_2 of the complete circuit. Accounting for the linear gains of the 2nd stage (100) and the 3rd stage (10) and the attenuation factor (0.5) of the input attenuator, we obtain the results

$$|H_2'(f_1,-f_2)| = |H_2(f_1,-f_2)|(2)^2/(100\cdot10) = |H_2(f_1,-f_2)|/250 \qquad (5\text{-}5)$$

or $$20\log_{10}|H_2'(f_1,-f_2)| = 20\log_{10}|H_2(f_1,-f_2)| - 48.0 \qquad (5\text{-}6)$$

5.3 Measurement Results

As discussed previously, the demodulation RFI at 1 kHz in the square-law response region can be characterized by the one parameter $H_2(f_1,-f_2)$. Shown in Figures 5-3 and 5-4 are measured values of $H_2(f_1,-f_2)$ of the 3-stage op amp LED circuit for RF frequencies in the range of 0.1 to 150 MHz for 35 units of 741 op amps tested. In Figure 5-3, the resistor and capacitor combinations are R1 = 10 kΩ, R2 = 100 kΩ, and C4 = C5 = 0. The $H_2(f_1,-f_2)$ values at a specific RF frequency vary $\pm$ 3 to $\pm$ 11 dB. In Fig. 5-4, the resistor and capacitor combinations are R1 = 10 kΩ, R2 = 100 kΩ, and C4 = C5 = 27 pF. The $H_2(f_1,-f_2)$ values at a specific RF frequency vary $\pm$ 4 to $\pm$ 15 dB. Whereas H_2 values in Figures 5-3 and 5-4 are for the complete 3-stage op amp LED

circuit, the H_2' values for the 1st stage alone can be obtained easily by subtracting 48 dB from H_2 values for the complete circuit. See Eq. (5-6). The value of the ordinate in Figures 5-3 and 5-4 is reduced by 48 dB. The variations of H_2' values in dB at a specific frequency are identical to those of H_2 values.

5.4 Statistical Results

Shown in Figures 5-5 and 5-6 are the mean values for $H_2(f_1,-f_2)$ which are denoted by $\bar{H}_2$ and the standard deviation, σ, for 35 units of 741 op amps tested in the 3-stage op amp LED circuit. One of the two sets of data in each figure corresponds to R1 = 10 kΩ, R2 = 100 kΩ, and C4 = C5 = 0. Another set corresponds to R1 = 10 kΩ, R2 = 100 kΩ, and C4 = C5 = 27 pF. The mean values for $H_2(f_1,-f_2)$ indicate clearly the effect of the RFI suppression capacitor C4 when it is connected in the feedback path of the 1st stage. The suppression of demodulation RFI effects caused by a 27 pF capacitor result in a reduction in $\bar{H}_2$ from 3.5 dB to as much as 36.5 dB at a specific RF frequency. Another effect of the RFI suppression capacitor C4 is indicated by the two sets of standard deviation data in Figure 5-6. That plot shows that the spreading of H_2 values is wider in general by including C4 = 27 pF. An increase as much as 5 dB in standard deviation is observed at certain RF frequencies.

In Figure 5-7, RFI demodulation responses in two 741 op amp circuits are shown. One set of data are mean values of measured H_2 for the 741 unity gain buffer. Another set of data are mean values of measured H_2 for the 741 inverting amplifier with a voltage gain of 10 and no RFI suppression capacitor (C4 = 0). For comparison purposes, the H_2 values

for the 741 unity gain buffer from Figure 4-19 have to be adjusted. We want an H_2' for the unity gain buffer that relates the audio-frequency voltage at the op amp output to the RF voltage at the non-inverting input terminal. We must account for the voltage division at the output which contributes a factor of (2) and the voltage division at the input which contributes a factor of $(2)^2$. See Figure 4-7 in Chapter 4. Therefore, the relationships between H_2' and H_2 are given by

$$|H_2'(f_1,-f_2)| = 8|H_2(f_1,-f_2)| \tag{5-7}$$

$$20\log_{10}|H_2'(f_1,-f_2)| = 20\log_{10}|H_2(f_1,-f_2)| + 18.1 \tag{5-8}$$

The result is an increase of 18 dB in the H_2 values plotted in Figure 4-19 in Chapter 4. Also H_2 values for the 741 inverting amplifier from Figure 5-5 have been adjusted using Eq.(5-6). The result is a decrease of 48 dB in the values plotted in Figure 5-5. The adjusted H_2 values in Figure 5-7 therefore exclude the linear amplification and attenuation stages in the experimental setups. The adjusted mean values for H_2' are surprisingly similar in that both sets of data points have a peak value near 10 dB. The comparison shows that the 741 unity gain buffer has an average lower RFI response for RF frequencies below 8 MHz. Above 8 MHz, the average RFI demodulation response in the 741 inverting amplifier is lower.

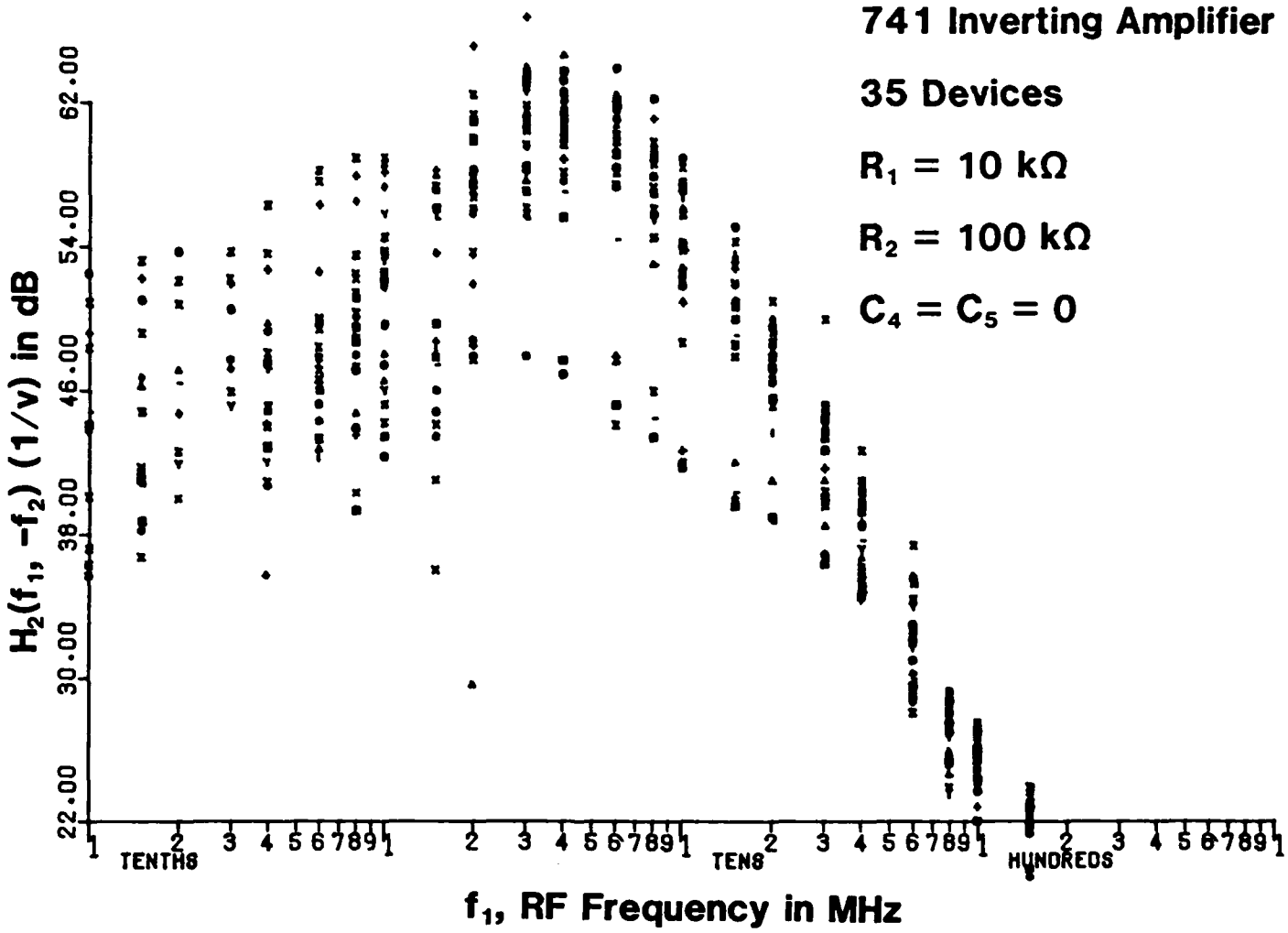

Fig. 5-3. Measured values of the second-order transfer function $H_2(f_1,-f_2)$ of the 3-stage op amp LED circuit vs RF frequency for 35 741 op amps. RFI suppression capacitor omitted.

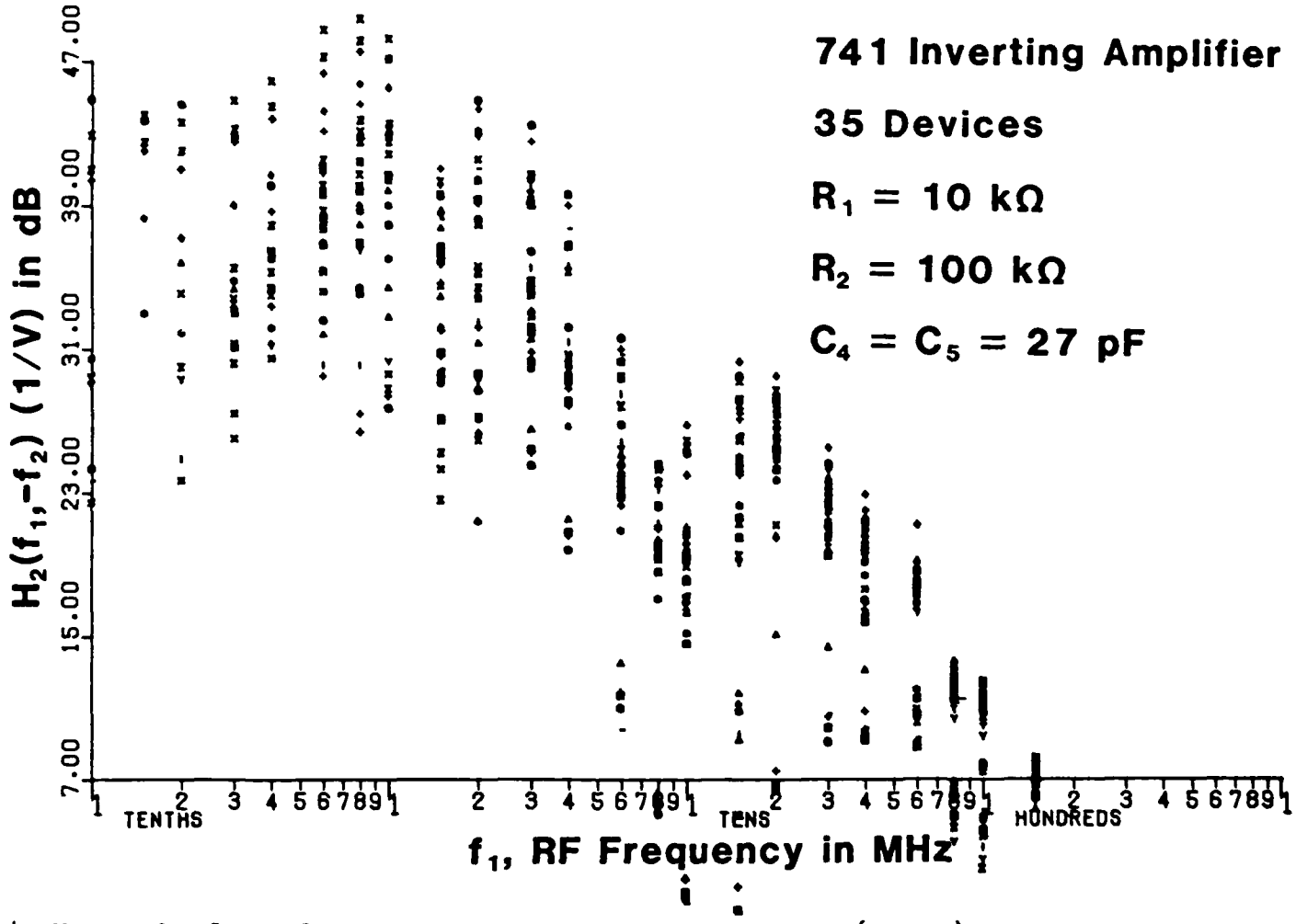

Fig. 5-4. Measured values of the second-order transfer function $H_2(f_1,-f_2)$ of the 3-stage op amp LED circuit vs RF frequency for 35 741 op amps. RFI suppression capacitor included.

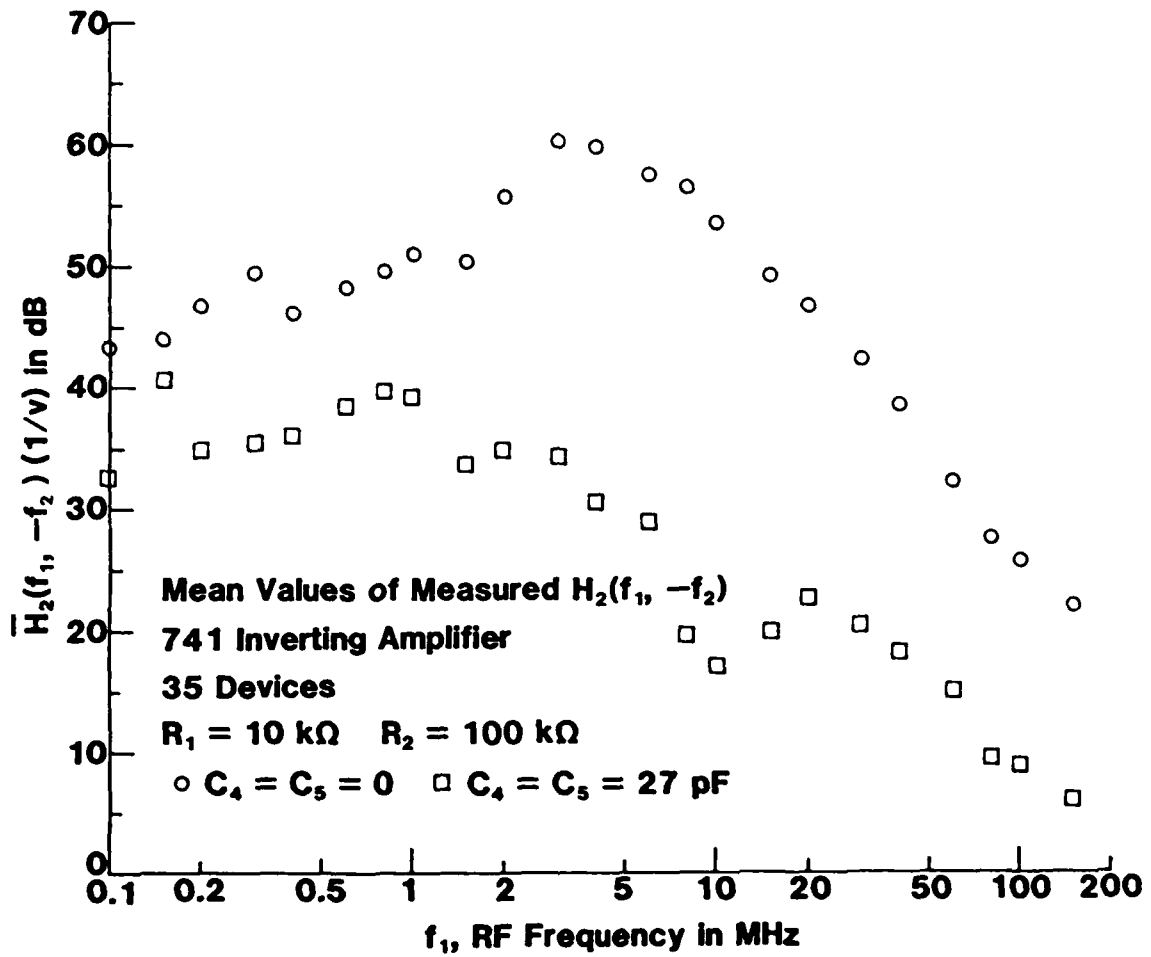

Fig. 5-5. Mean values of measured $H_2(f_1,-f_2)$ of the 3-stage op amp LED circuit for two feedback capacitor values, C4 = 0 and C4 = 27 pF. This plot shows the suppression of the demodulation RFI effects by the feedback capacitor.

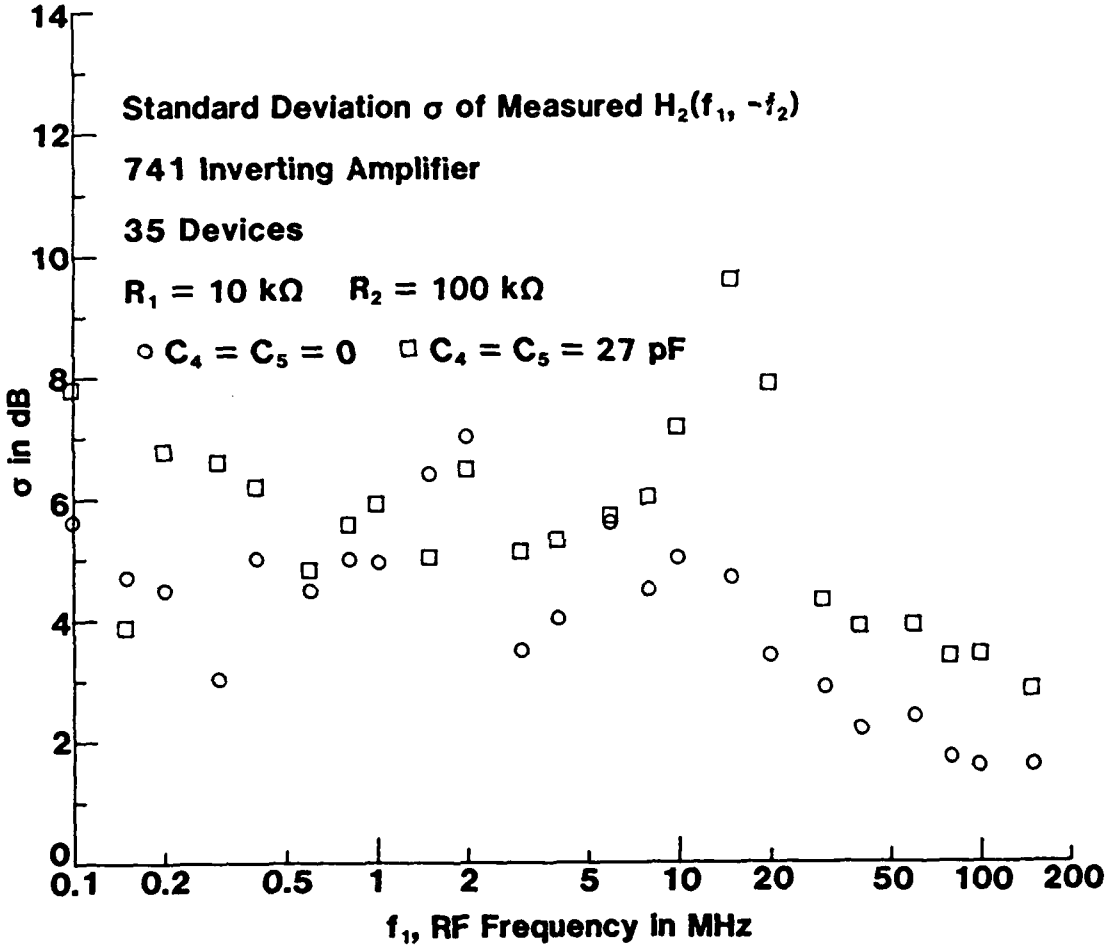

Fig. 5-6. Standard deviation, σ, of the measured $H_2(f_1,-f_2)$ of the 3-stage op amp LED circuit for two feedback capacitor values, C4 = 0 and C4 = 27 pF. This plot shows the spreading of H_2 values is wider in general for C4 = 27 pF than for C4 = 0.

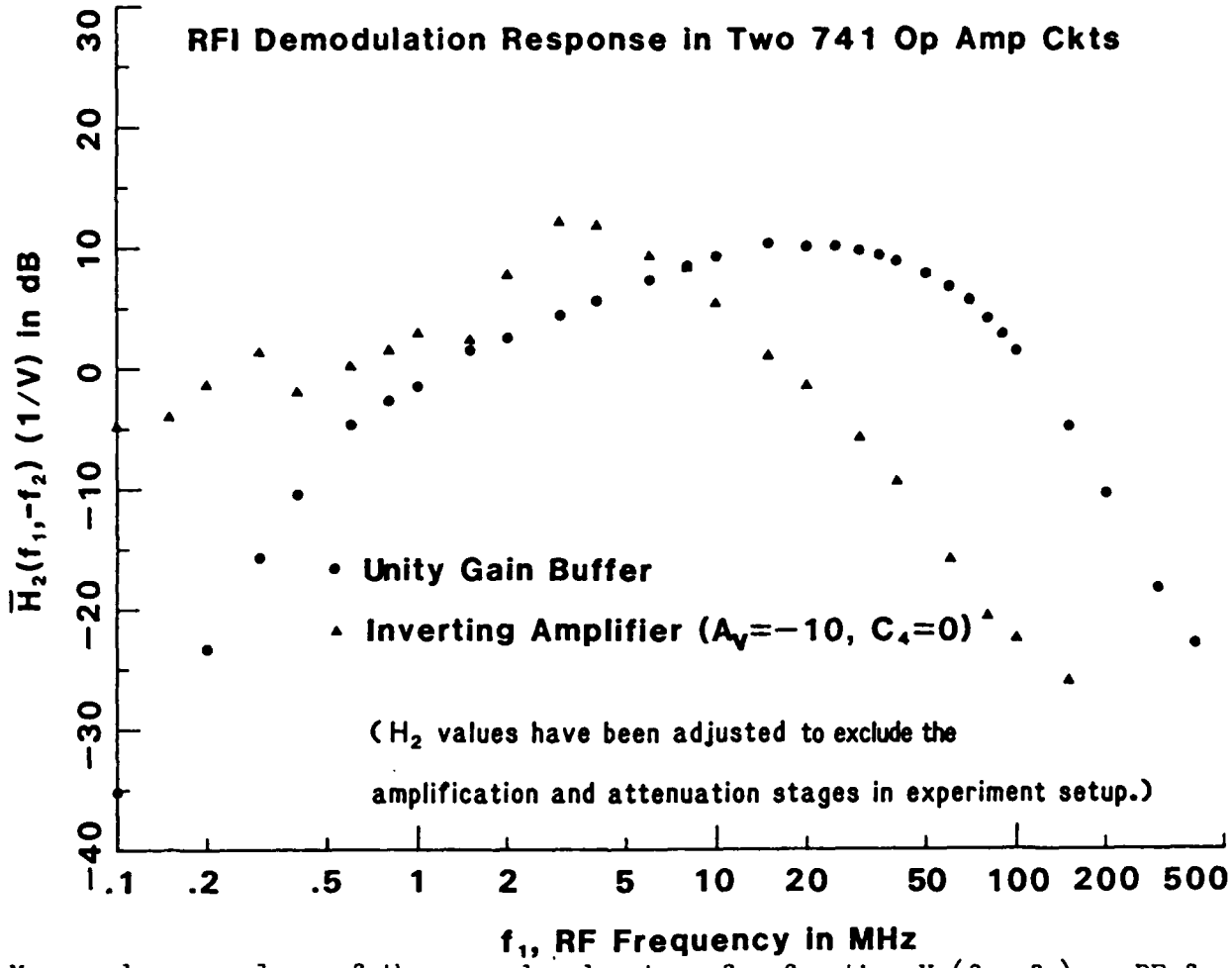

Fig. 5-7. Measured mean values of the second-order transfer function $H_2(f_1,-f_2)$ vs RF frequency for two 741 op amp circuits. The H_2 values for the unity gain buffer were obtained by adding 18 dB to the H_2 values shown in Fig. 4-19. The H_2 values for the inverting amplifier were obtained by subtracting 48 dB from the H_2 values shown in Fig. 5-5.

CHAPTER SIX

NCAP SIMULATIONS OF DEMODULATION RFI IN OP AMP CIRCUITS

In Chapter 2, we have described the NCAP procedure for determining the nonlinear transfer functions which characterize many nonlinear effects including demodulation in weakly nonlinear circuits. We have also described the macromodeling procedures for a 741 (bipolar) op amp and a LF355 (JFET-bipolar) op amp in Chapter 3. Now in this chapter, we shall present NCAP simulations of demodulation RFI effects in op amp circuits used in our experiments. The NCAP predictions are compared with measurements. The NCAP values for the second-order transfer function, $H_2(f_1,-f_2)$ will be compared to the mean measured values of $H_2(f_1,-f_2)$ since most NCAP parameter values were determined from typical values given by manufacturers. These typical values are believed to correspond to mean values. Also, using the op amp buffer circuit, we performed a sensitivity analysis of NCAP parameters. The sensitivity analysis provides information on the most critical parameters in the op amp macromodel in causing demodulation RFI effects in op amp circuits.

6.1 The 741 Unity Gain Buffer

Shown in Figure 6-1 is the incremental equivalent circuit of the the 741 unity gain buffer used in NCAP simulations. The 741 op amp has been replaced by its incremental macromodel. The values of the 14 linear macromodel elements shown in Figure 6-1 were determined from the typical values of op amp characteristics provided by manufacturers. See Table 3-2. The values of the 16 nonlinear BJT model parameters for the two transistors in the input stage are listed in Table 3-5. The

NCAP input data for the circuit shown in Figure 6-1 are listed in Appendix A. Note that in Figure 6-1, four capacitors have been included from the collectors and emitters of both input transistors to ground to account for parasitic substrate capacitances. The four capacitors were added so that their values could be adjusted to fit simulation results to experimental results.[12] Shown in Figure 6-2 are the NCAP simulation results for the second-order transfer function $H_2(f_1,-f_2)$ which characterizes the demodulation RFI response of the 741 unity gain buffer to an RF signal, 50% amplitude-modulated at 1 kHz. Also shown are the experimental mean values for $H_2(f_1,-f_2)$ for 30 741 op amp units. The mean values are taken from Figure 4-19 in Chapter 4. The simulation and the measured mean values agree within 6 dB over the RF frequency range 0.1 to 400 MHz. The NCAP simulation was performed with all four parasitic substrate capacitances set to zero, i.e. $C_{sub1} = 0$, etc. The effects of BJT parasitic substrate capacitances C_{sub1}, C_{sub2}, C_{sub3}, and C_{sub4} are illustrated in Figures 6-3 and 6-4. In Figure 6-3, NCAP simulations of BJT collector-substrate capacitance effects are shown for four values of C_{sub1} and C_{sub2} with $C_{sub3} = C_{sub4} = 0$. The effects of collector-substrate capacitances are minor except around 3 MHz and above 100 MHz. In Figure 6-4, NCAP simulations of BJT emitter-substrate capacitance effects are shown for four values of C_{sub3} and C_{sub4} with $C_{sub1} = C_{sub2} = 0$. Simulation results indicate that the RFI demodulation response in the 741 unity gain buffer is very sensitive to the value of the BJT emitter-substrate capacitance in the input stage. Comparing Figure 6-3 and Figure 6-4, we observe that the emitter-substrate capacitance effects are far more significant than collector-substrate capacitance effects. In an eariler investigation the values of C_{sub1}

= C_{sub2} = C_{sub3} = C_{sub4} = 4 pF were assigned in order to fit the NCAP simulation results to the experimental results.[12] We set C_{sub1} = C_{sub2} = C_{sub3} = C_{sub4} = 0 and obtain very good agreement between NCAP results and experimental results as shown in Figure 6-2. Our experimental results are for the mean value of $H_2(f_1,-f_2)$ for 30 op amps and they differ from the experimental results reported upon previously for 1 to 3 op amps.[12] Our measured mean values are lower than the experimental results reported by G.K.C. Chen.[12] That our experimental mean values for $H_2(f_1,-f_2)$ agree better with the NCAP simulation results without the capacitors C_{sub1}, etc. indicates the importance of having a data base large enough to yield a reliable mean value. This is especially true when a macromodel is used for the NCAP simulation and values for the macromodel parameters are determined from "typical values" given in manufacturers' data sheets. Finally, it might be possible to improve the agreement shown in Figure 6-2 between experimental and simulation by using values C_{sub1} = C_{sub2} = 0 and C_{sub3} = C_{sub4} = 0.5 pF, but this has not been done.

6.2 The LF355 Unity Gain Buffer

Shown in Figure 6-5 is the incremental equivalent circuit of the LF355 unity gain buffer used in NCAP simulations. The LF355 op amp has been replaced by its incremental macromodel. The values of the 13 linear macromodel elements are listed in Table 3-4. The values of the 10 nonlinear JFET model parameters for the two JFETs in the input stage are given in Table 3-6. The NCAP input data for the circuit shown in Figure 6-5 are listed in Appendix A. Shown in Figure 6-6 are two sets of $H_2(f_1,-f_2)$ data for the LF355 unity gain buffer amplifier plotted

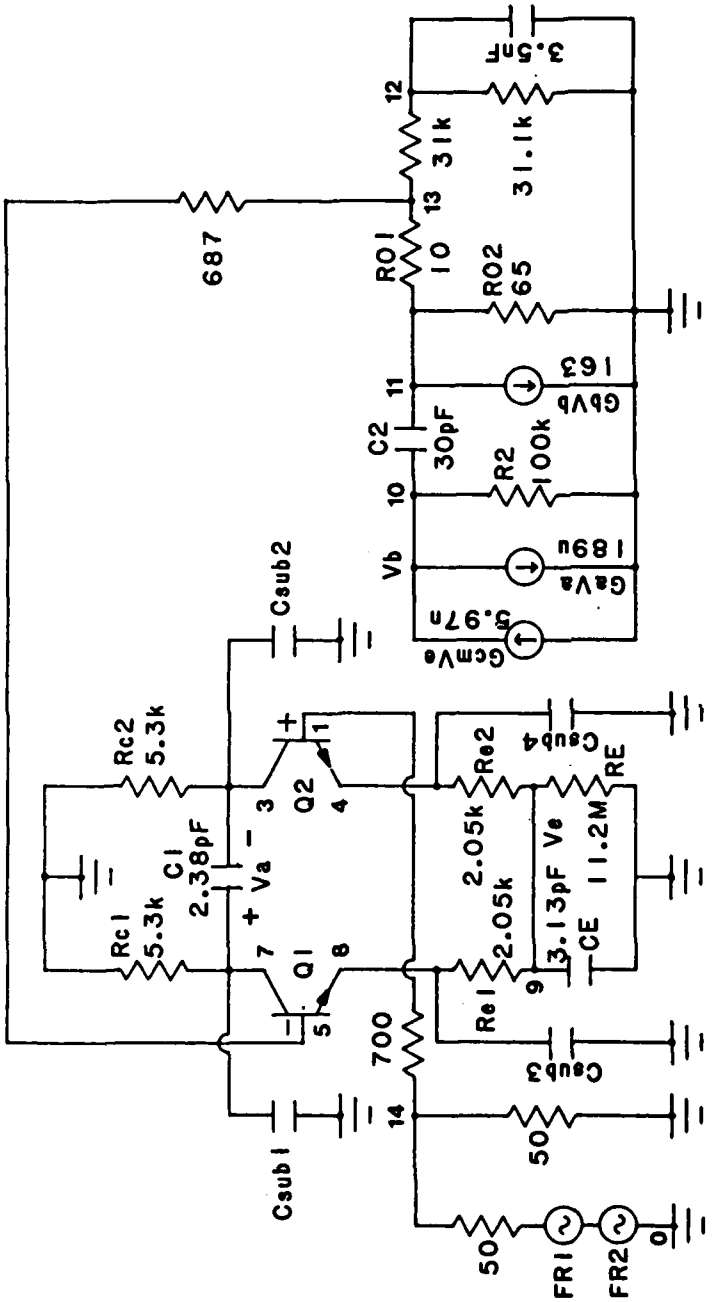

Fig. 6.1 Incremental Macromodel Of The 741 Unity Gain Buffer Amplifier

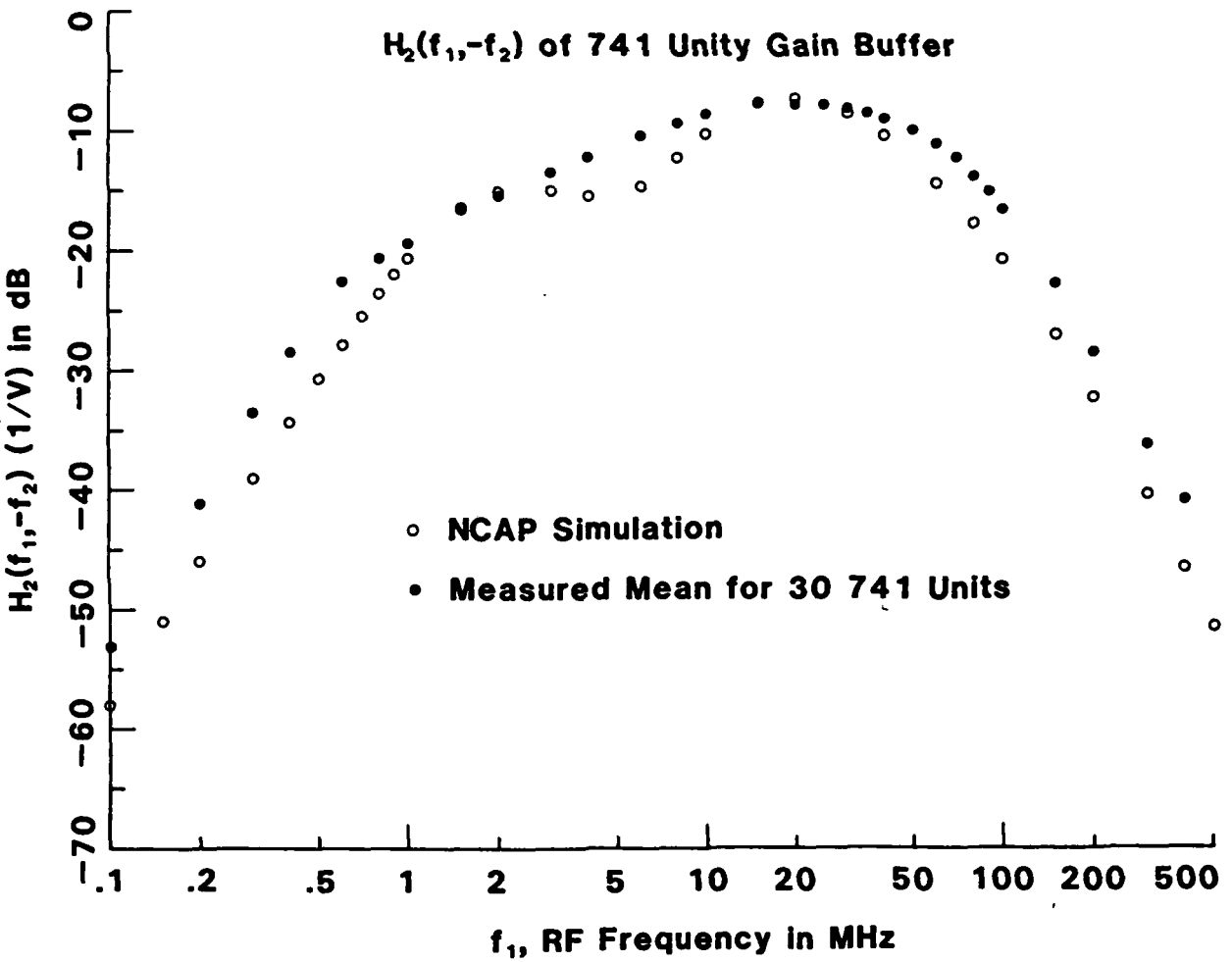

Fig. 6-2 NCAP simulation and measured mean values of the second-order transfer function $H_2(f_1,-f_2)$ for the 741 unity gain buffer amplifier.

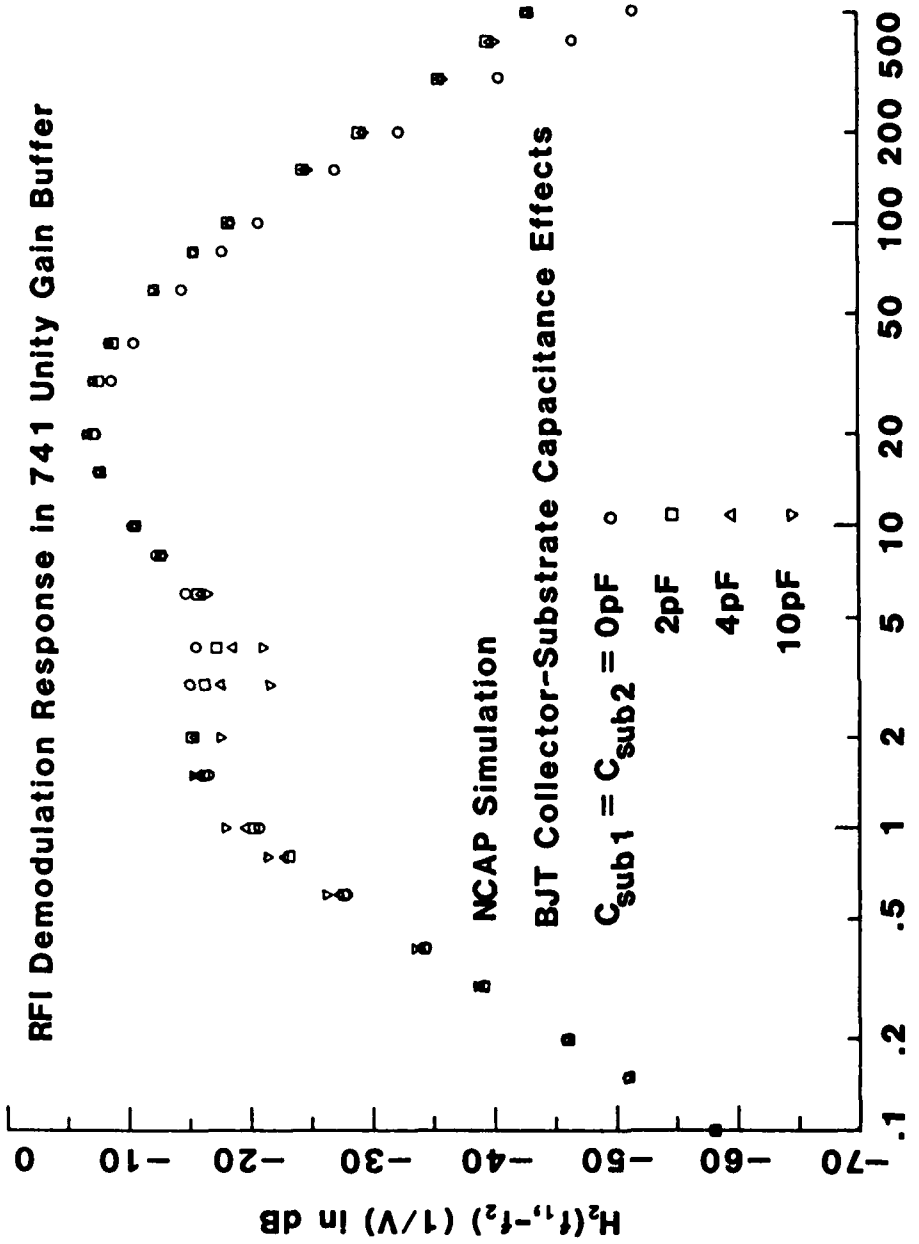

Fig. 6-3 NCAP values of $H_2(f_1,-f_2)$ vs RF frequency for unity gain buffer for several values of parasitic capacitances C_{sub1} and C_{sub2} with $C_{sub3} = C_{sub4} = 0$.

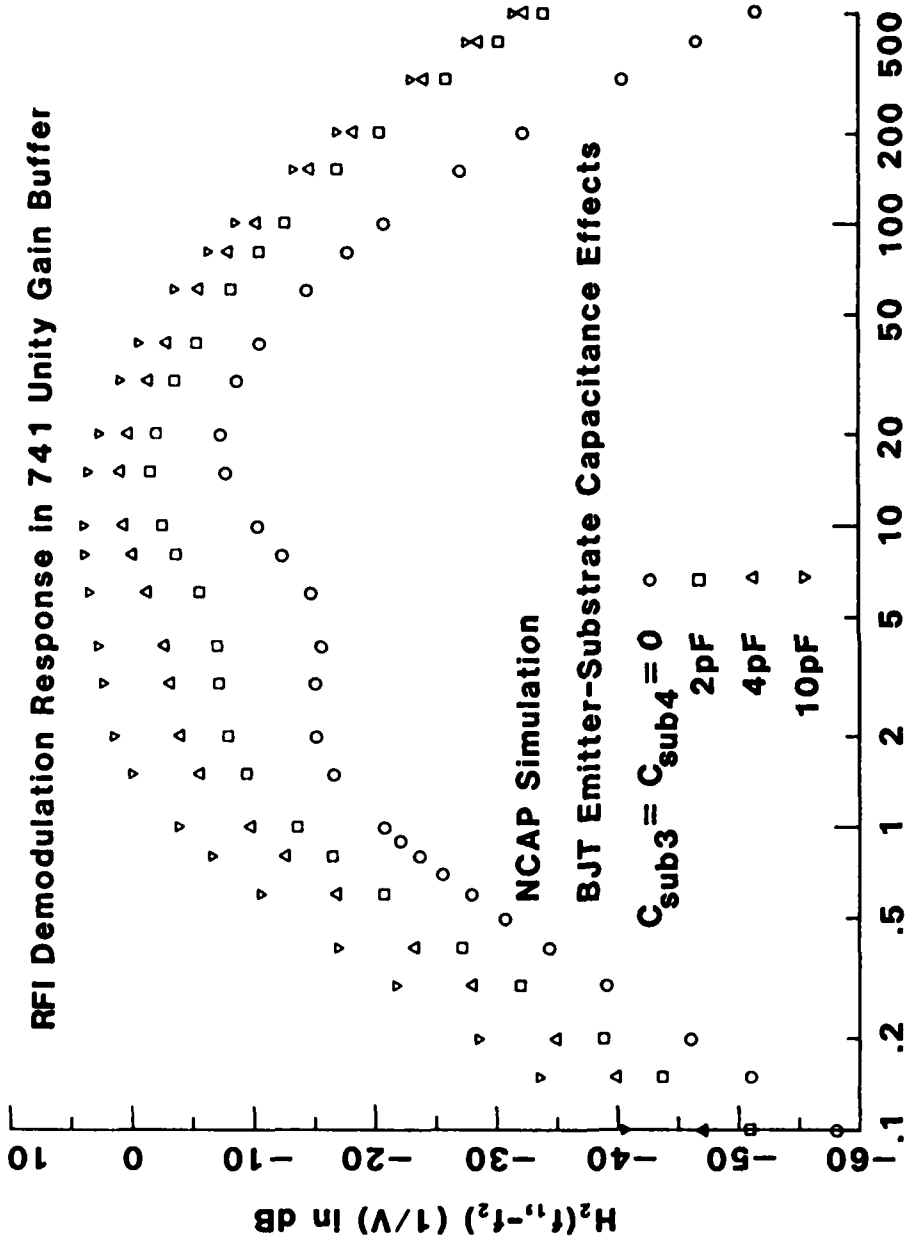

Fig. 6-4 NCAP values of $H_2(f_1,-f_2)$ vs RF frequency for 741 unity gain buffer for several values of parasitic capacitances C_{sub3} and C_{sub4} with $C_{sub1} = C_{sub2} = 0$.

vs RF frequency from 0.1 to 400 MHz. One set of H_2 data are NCAP simulation results. Another set of H_2 data are mean values of the measured H_2 for 30 LF355 op amp units which are from Figure 4-19. In the NCAP simulations, the effects of parasitic capacitances are not included, i.e, $C_{sub1} = 0$, etc. For RF frequencies below 3 MHz, the NCAP H_2 values and measured mean H_2 values agree within 1 to 3 dB. For RF frequencies above 3 MHz, the discrepancies are large because the resonances observed in the experiment are not observed in the simulation.

In order to determine the cause of the resonances observed, additional NCAP simulations were performed. In Figure 6-7 are shown NCAP values for H_2 calculated with $C_{sub3} = C_{sub4} = 0$ and with $C_{sub1} = C_{sub2}$ = 2 pF, 4 pF or 8 pF. In Figure 6-8 are shown NCAP values for H_2 calculated with $C_{sub1} = C_{sub2} = 0$ and $C_{sub3} = C_{sub4} = 0$ pF, 1 pF or 4 pF. Resonant effects, if present, are minor and are less than 3 dB. Thus we concluded that the parasitic capacitors C_{sub1}, etc. are not the cause of the resonant effects observed in Figure 6-6.

An additional effort was then made to investigate the cause for the resonances by including the effects of other parasitic capacitances. Additional NCAP analysis indicate that the resonances could be related to the interelectrode parasitic capacitances of the JFETs in the input stage of the LF355 op amp. Shown in Figure 6-9 is the nonlinear device circuit model for a JFET. The intrinsic device model is shown enclosed within dotted lines. The capacitances C_{p1}, C_{p2} and C_{p3} are extrinsic interelectrode parasitic elements which have values in the 0.1 to 5 pF range. The effects of C_{p1}, C_{p2} and C_{p3} upon the second-order transfer

function values calculated by NCAP are illustrated in Figure 6-10. Three different values (1 pF, 2 pF and 4 pF) were assigned to them equally in three separate NCAP runs. When $C_{p1} = C_{p2} = C_{p3} = 1$ pF, no obvious resonances can be identified in the H_2 vs RF frequency plot. When $C_{p1} = C_{p2} = C_{p3} = 2$ pF, one resonance is clearly distinguishable at approximately 3 MHz. When $C_{p1} = C_{p2} = C_{p3} = 4$ pF, two resonances can be clearly identified at approximately 1.5 MHz and 3.5 MHz respectively. However, note that the NCAP simulation resonances occur at frequencies lower than those resonant frequencies actually observed in the experiment (approximately 4 MHz and 12 MHz respectively). The NCAP results in Figure 6-10 do suggest an explanation. The resonances seem related to small parasitic capacitance effects caused by capacitance values of the order 1 to 5 pF. There are two possible physical locations for parasitic capacitors of this size. One location is inside the op amp itself, i.e. interelectrode capacitance. The other location is the external circuit, i.e. the external circuit wiring to ground capacitance. It is our belief that capacitance effects internal to the LF355 op amp are responsible for the resonances because similar resonances are not observed when the other op amp types (741, LM10, and CA081) are inserted in the same circuit. However, a more complicated situation may exist which is caused by an external circuit and op amp interaction which is sensitive to the impedance values inside the LF355 op amp. It would be desirable to model more completely the external circuit wiring and external circuit component parasitics in order to investigate these resonances further.

Shown in Figure 6-11 is an NCAP simulation which assumed inter-electrode parasitic capacitances $C_{p1} = 5$ pF, $C_{p2} = 3$ pF, and $C_{p3} =$

4 pF. Also shown is the measured mean for 30 LF355 op amp units. The capacitance values have been adjusted to obtain a better fit between experiment and simulation.

The discrepancy above 15 MHz has been reduced from 10 to 15 dB to 1 to 4 dB but the discrepancy below 1 MHz has increased from 1 to 3 dB to 4 to 7 dB. Larger discrepancies continue to exist in the vicinity of the resonant frequencies.

6.3 Three-Stage Op Amp LED Circuit

The incremental circuit of the 3-stage op amp LED circuit for NCAP simulations is shown in Figure 6-12. All three 741 op amps have been replaced by an equivalent 741 macromodel. The 14 linear macromodel elements and the 16 nonlinear BJT parameters are indentical to those used for the 741 unity gain buffer amplifier described in Section 6.1. See Tables 3-2 and 3-5. Recall that the values for the 14 linear macromodel elements were determined from typical values of the 741 op amp characteristics (Table 3-1) using the procedures developed by Boyle et al.[11] Most of the 16 nonlinear BJT parameters were obtained from Fang's [6] measurements of the 741 input stage. The NCAP input data for the circuit shown in Figure 6-12 are listed in Appendix A. First we verified that the second and third stages of the 3-stage op amp LED circuit indeed did provide linear gain for the demodulation AF component produced by the first stage. Using NCAP we calculated values for the magnitudes of $H_2(f_1,-f_2)$ at nodes 17 and 42 of the circuit shown in Figure 6-12. Throughout the RF frequency region of interest, the ratio of the two H_2 magnitudes at nodes 17 and 42 is 72.95 ± 0.05 dB, which corresponds to a linear gain of about 4440. The experimental value for

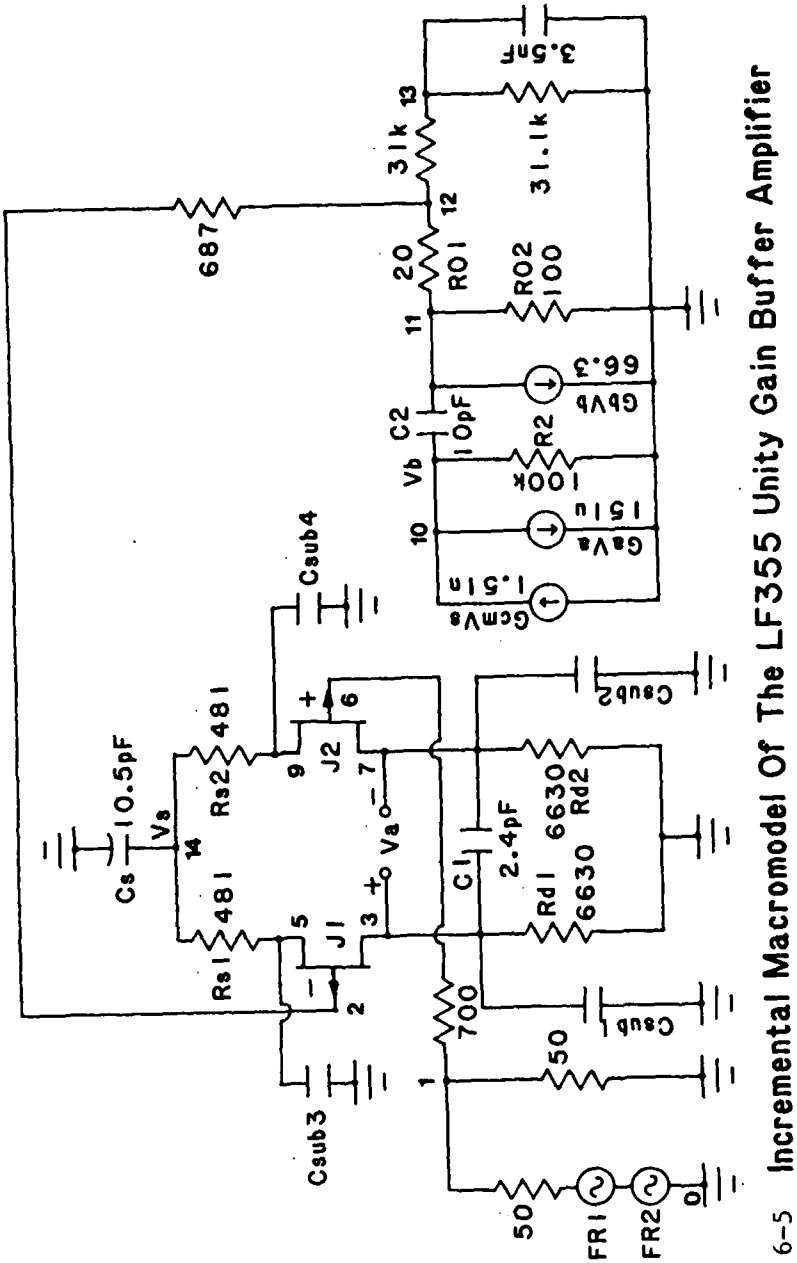

Fig. 6-5 Incremental Macromodel Of The LF355 Unity Gain Buffer Amplifier

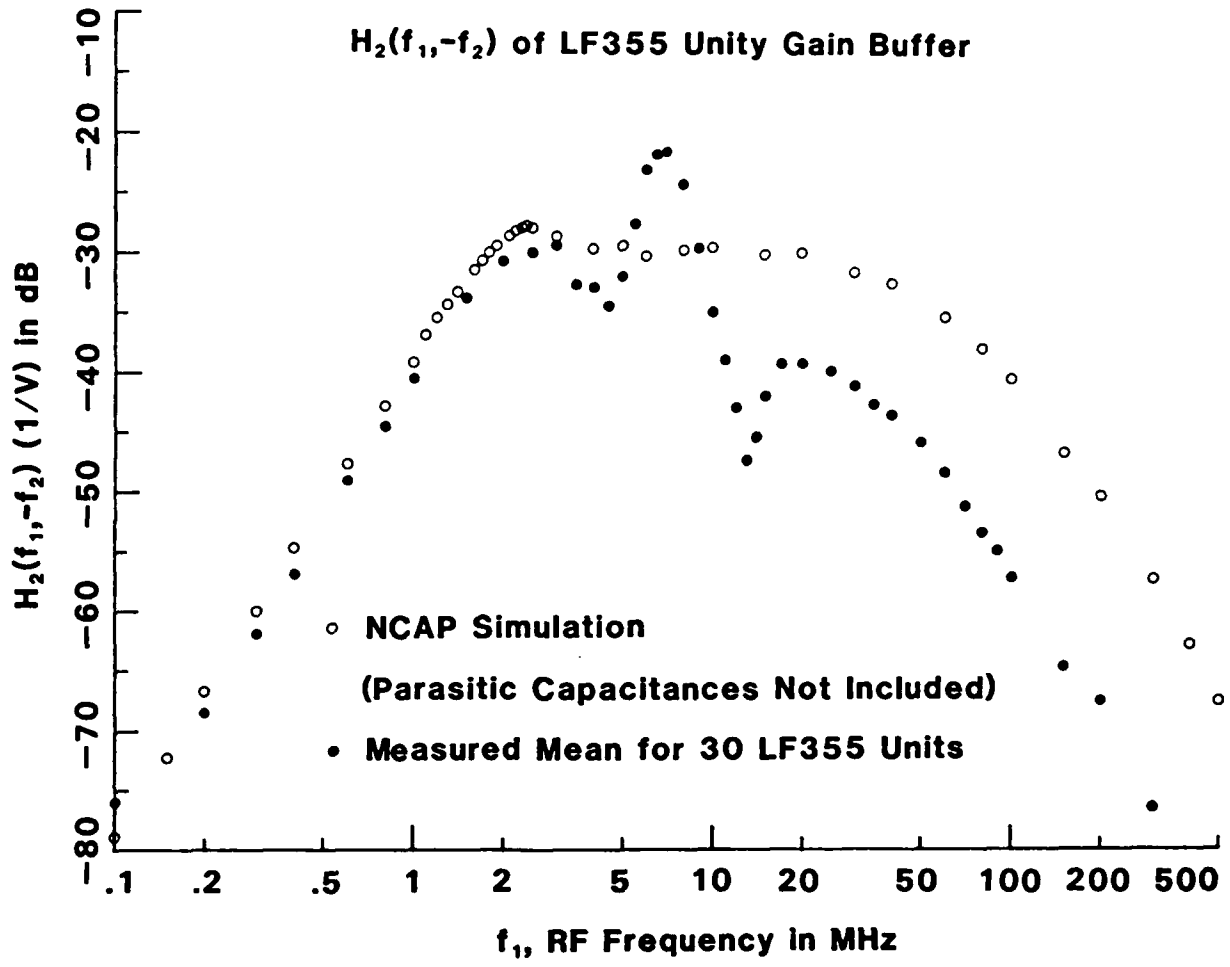

Fig. 6-6 NCAP simulation and measured mean values of the second-order transfer function $H_2(f_1,-f_2)$ for the LF355 unity gain buffer amplifier.

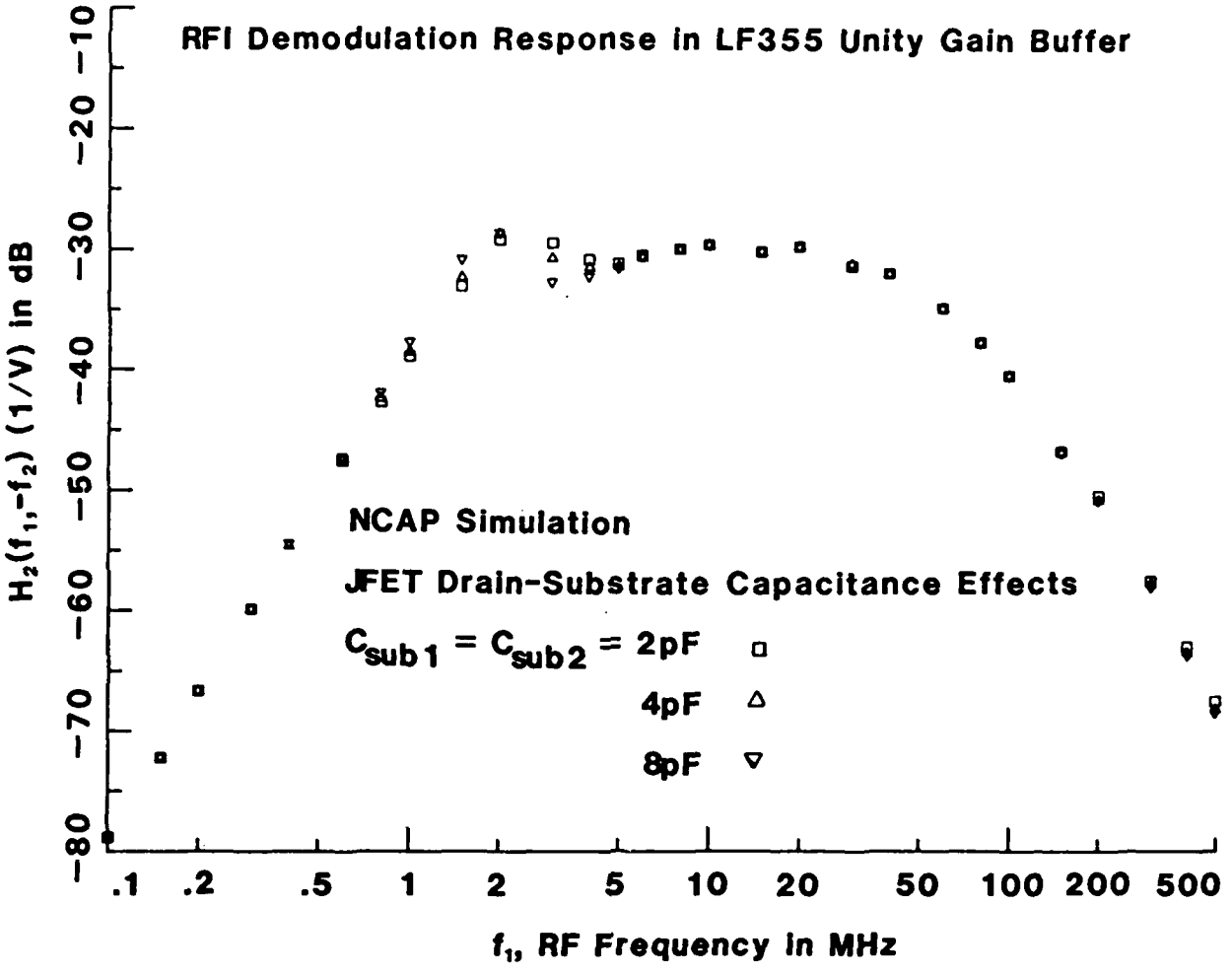

Fig. 6-7 NCAP values of $H_2(f_1,-f_2)$ vs RF frequency for LF355 unity gain buffer for several values of parasitic capacitances C_{sub1} and C_{sub2} with C_{sub3} and C_{sub4} = 0.

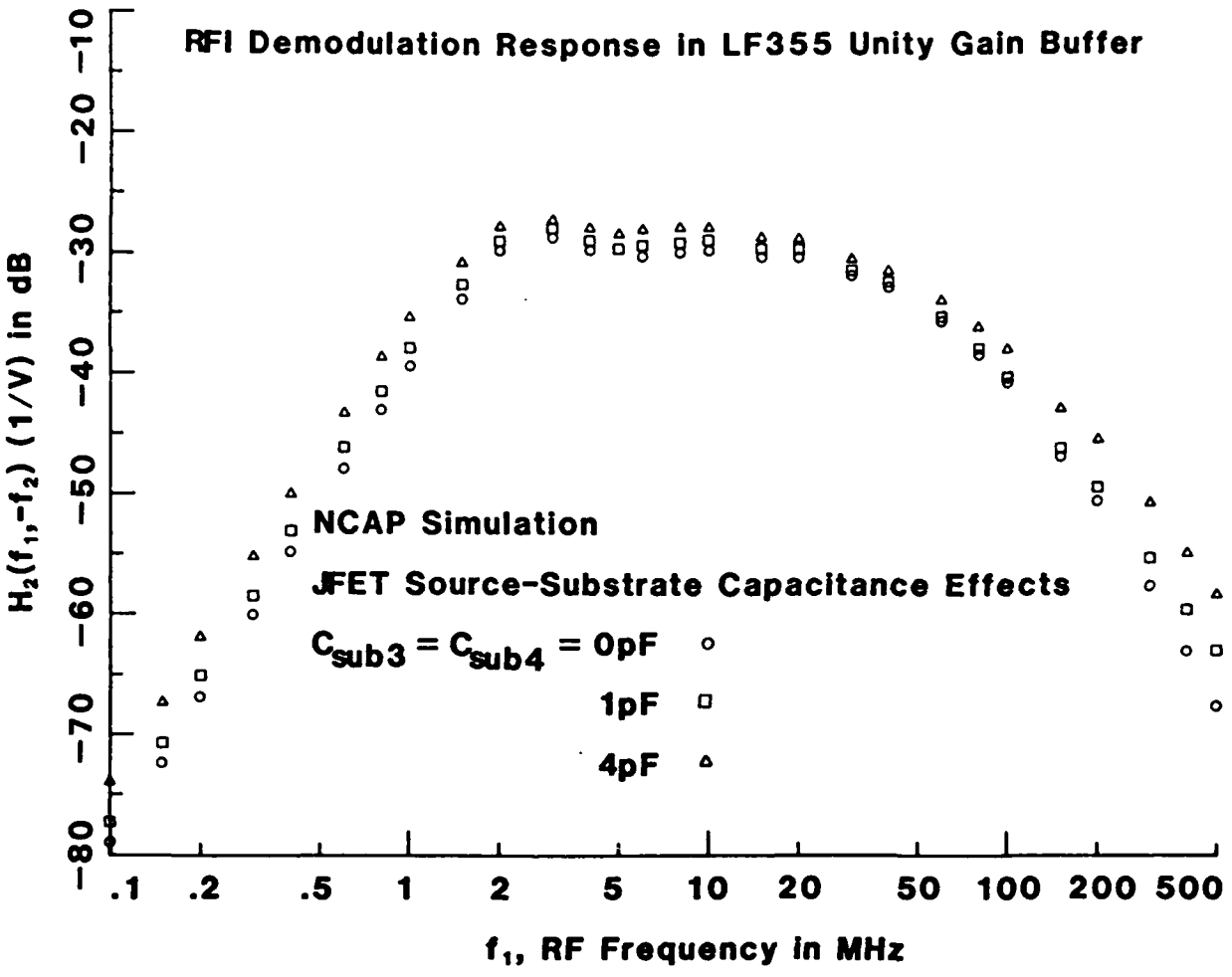

Fig. 6-8 NCAP values of $H_2(f_1,-f_2)$ vs RF frequency for the LF355 unity gain buffer for several values of parasitic capacitances C_{sub3} and C_{sub4} with $C_{sub1} = C_{sub2} = 0$.

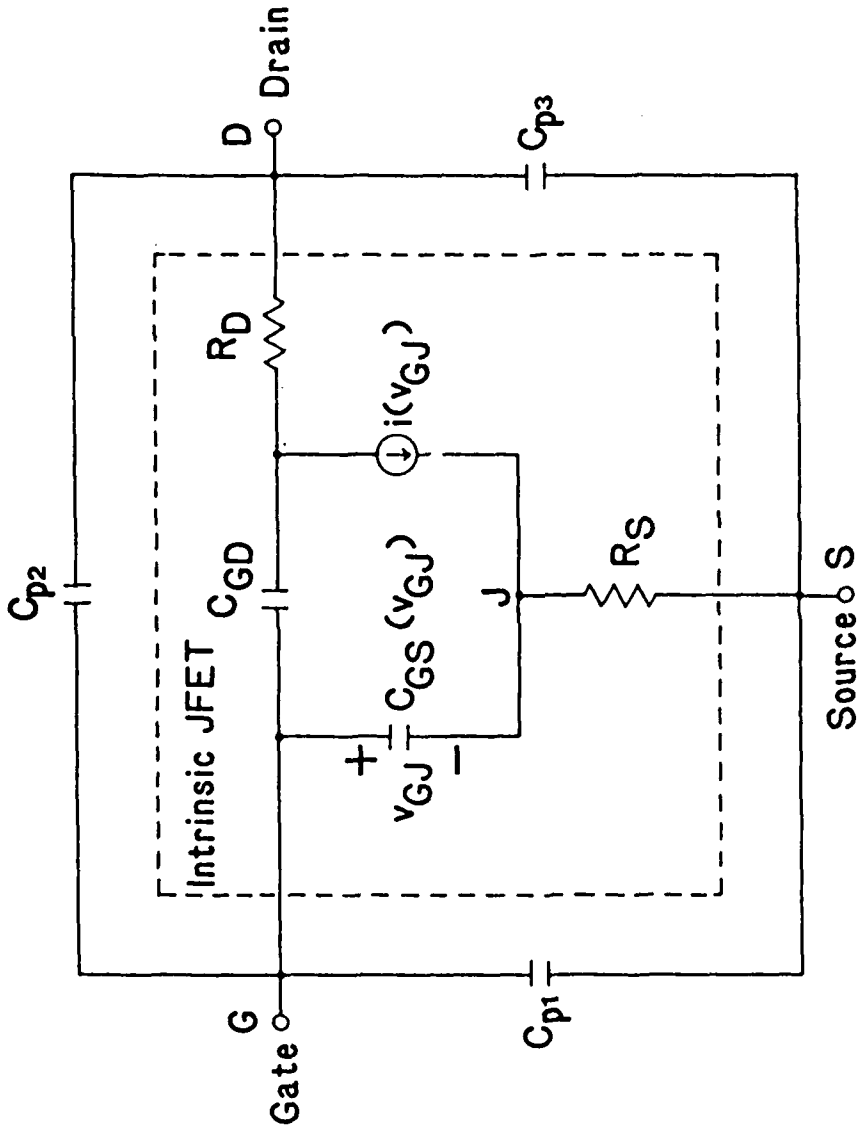

Fig. 6-9 Interelectrode Parasitic Capacitances (C_{p1}, C_{p2}, C_{p3}) in The JFET Model

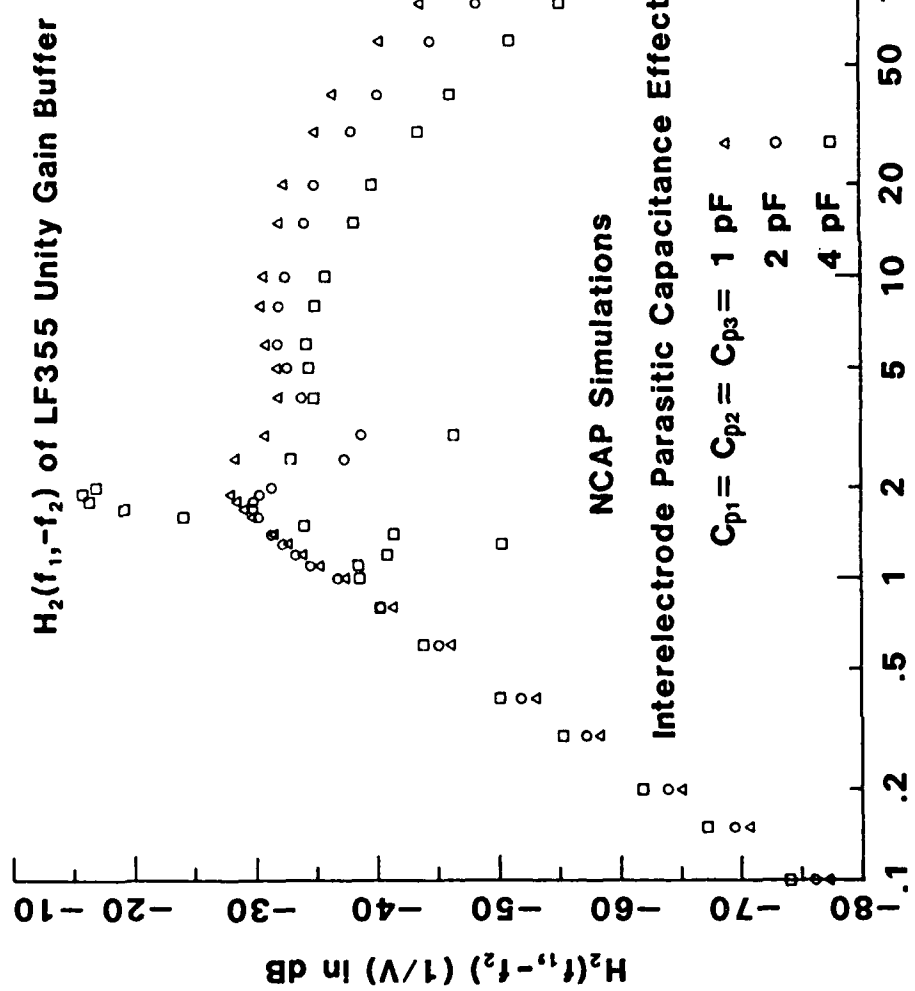

Fig. 6-10 NCAP values of $H_2(f_1,-f_2)$ vs RF frequency for LF355 unity gain buffer for several values of interelectrode parasitic capacitances C_{p1}, C_{p2} and C_{p3}.

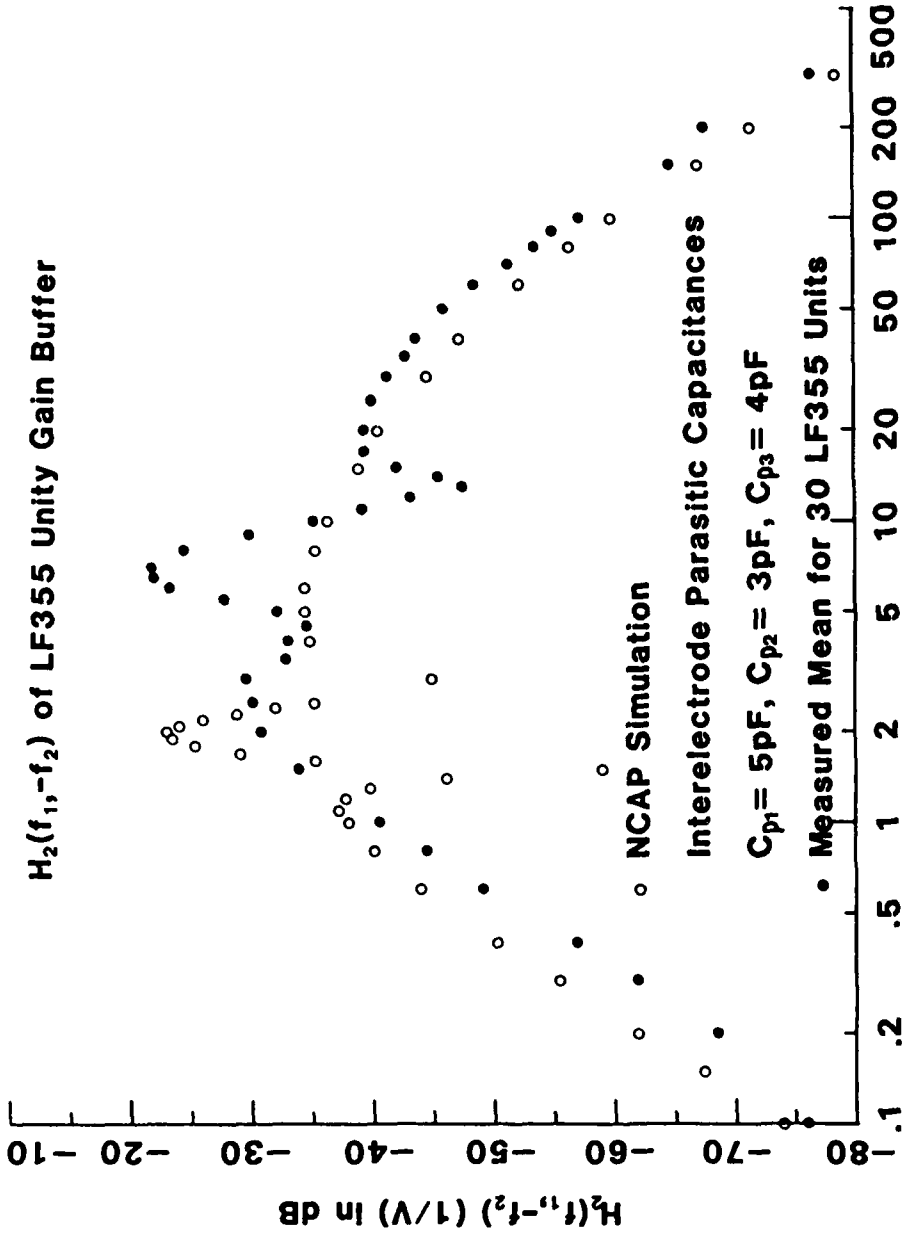

Fig. 6-11 NCAP simulation and measured mean values of the second-order transfer function $H_2(f_1,-f_2)$ for the LF355 unity gain buffer amplifier with non-zero interelectrode parasitic capacitances.

the linear voltage gain at 1 kHz is $V_{03}^{AF} \div V_{0X}^{AF} = 4000$. See Table 5-2.

Shown in Figure 6-13 are NCAP simulations of H_2 of the 3-stage op amp LED circuit with R_1 = 10 kΩ and R_2 = 100 kΩ for two values of the RFI supperssion capacitor C_4 (0 and 27 pF). The corresponding measured mean values are also shown. Let us first discuss the two sets of experimental results obtained with $C_4 = C_5 = 0$ and $C_4 = C_5 = 27$ pF. Note that the RFI suppression capacitors reduce $H_2(f_1,-f_2)$ at every RF frequency. The reduction in H_2 varies from a low of 3 dB at .15 MHz to a high of 36 dB at 10 MHz and exceeds 15 dB at all RF frequencies above 10 MHz. Now let us compare NCAP simulation results to experimental results with the RFI suppression capacitors omitted ($C_4 = C_5 = 0$). Below 1.0 MHz the NCAP simulation values exceed the measured values by 10 to 17 dB. From 1.0 to 6.0 MHz the NCAP values and the measured values agree within 1 to 4 dB. Above 6 MHz the NCAP values exceed the measured values by 6 to 15 dB. Finally let us compare NCAP simulation results and experimental results with the RFI suppression capacitor included ($C_4 = C_5 =$ 27 pF). Below 1.0 MHz the NCAP simulation values exceed the measured values by 23 to 42 dB. Note that below 1 MHz NCAP predicts an increase in H_2 when the RFI suppression capacitors are added and that this is contradictory to what is observed experimentally. Above 1 MHz NCAP predicts a decrease in H_2 when the RFI suppression capacitors are added; this is in agreement to what is observed experimentally. From 2 MHz to 20 MHz the NCAP values and measured values agree quite well with differences in the range 0 to 7 dB. Above 20 MHz the NCAP values decrease much more rapidly than the experimental values and exceed the NCAP values by 20 to 40 dB. The NCAP predictions leave

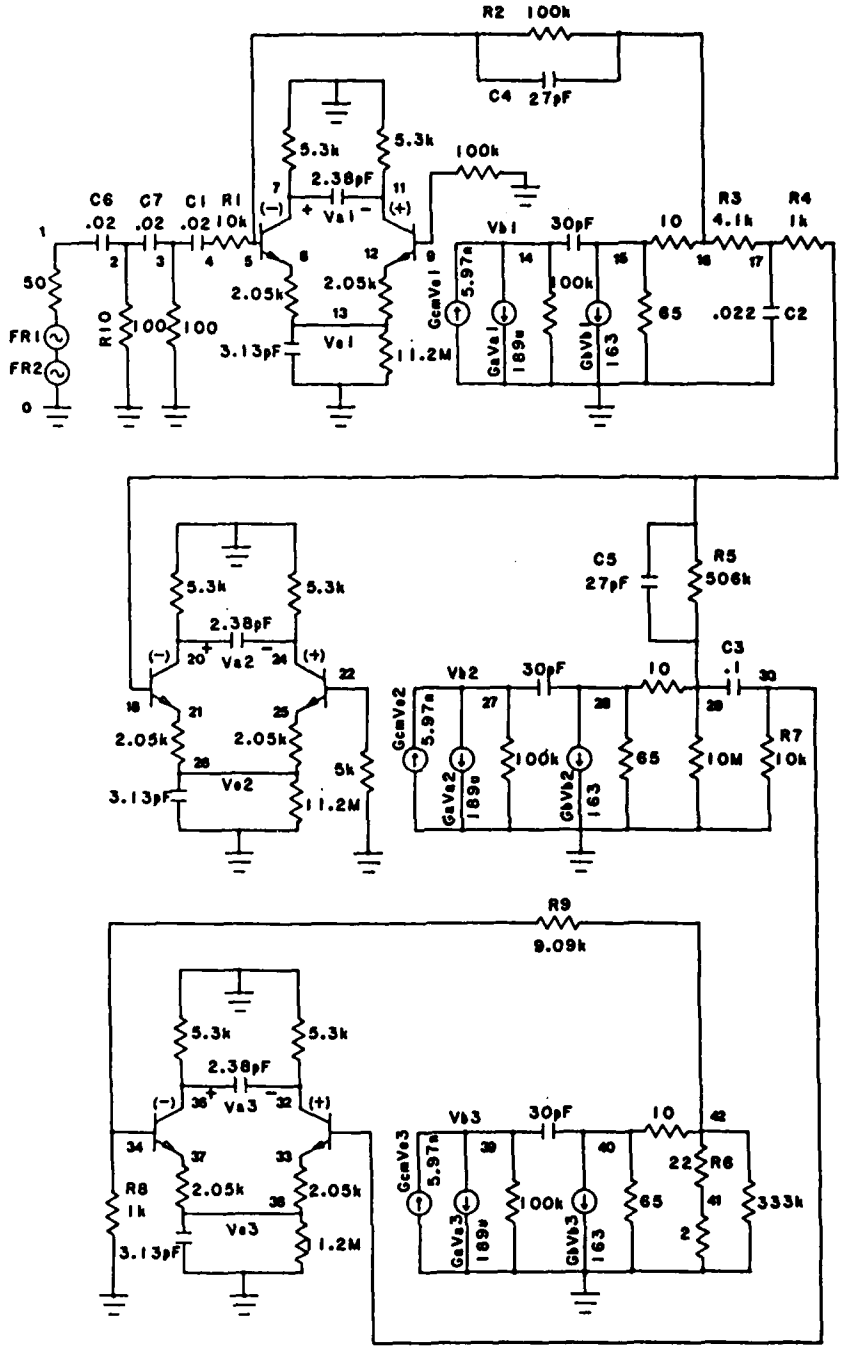

Fig. 6-12 Incremental macromodel of the 3-stage op amp LED circuit for NCAP simulation

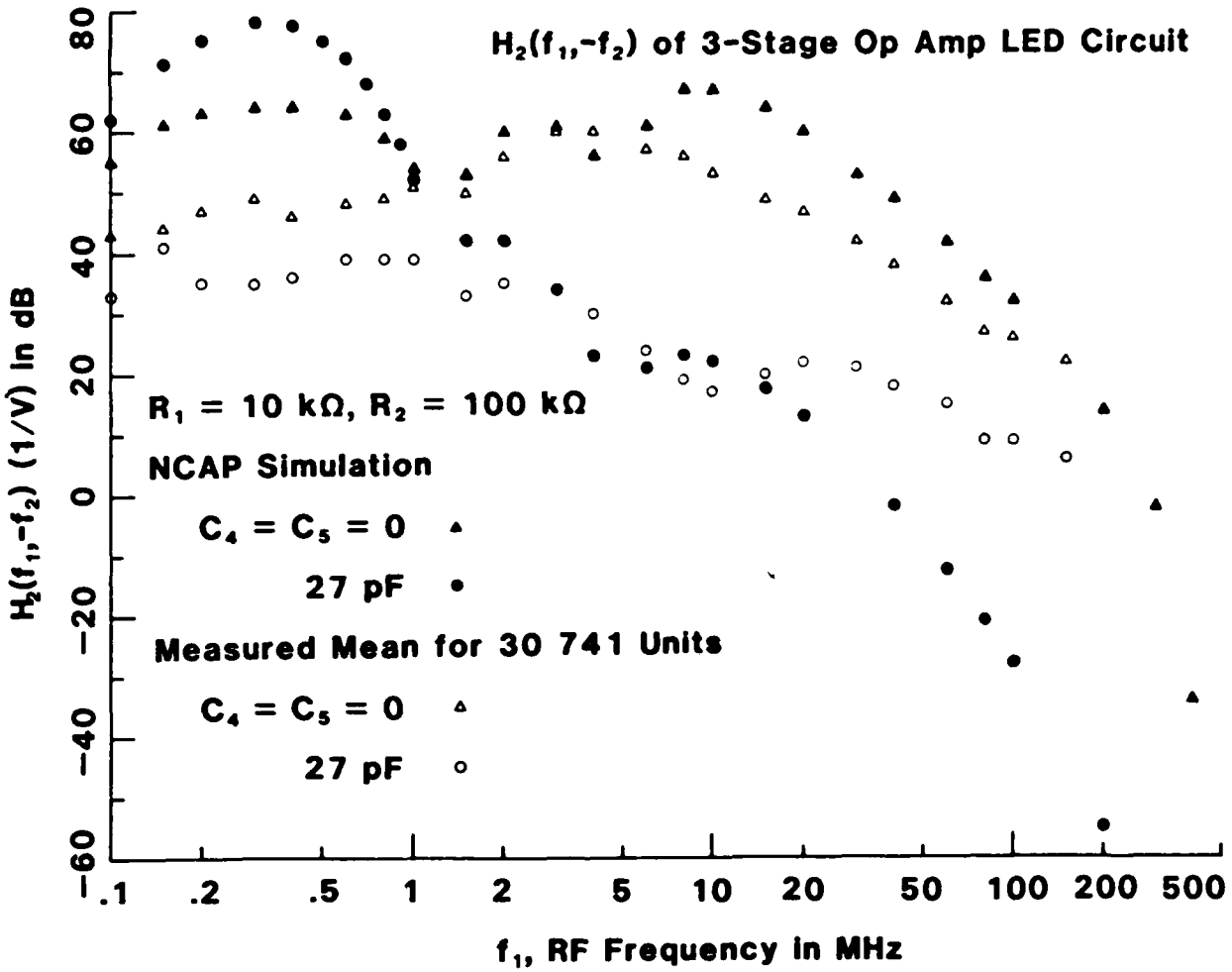

Fig. 6-13 NCAP simulation and measured mean values of the second-order transfer function $H_2(f_1,-f_2)$ for the 3-stage op amp LED circuit without and with RFI suppression capacitors.

something to be desired and this may indicate that additional modeling effort is required. It would be worthwhile to include in the NCAP simulations the appropriate parasitic elements associated with all the passive components,[34] but especially R1, R2, and C4 in the first stage and the capacitance associated with the Printed Circuit Board wiring.

6.4 Sensitivity Analysis of NCAP Parameters

In Chapter 4, we presented the scatter plots of measured $H_2(f_1,-f_2)$ for the op amp unity gain buffer. Large variations in H_2 values were observed at certain frequencies. It is the objective of this section to present results of a sensitivity analysis of NCAP parameters. The sensitivity analysis indicates which transistor model parameters and op amp macromodel linear parameters cause the largest H_2 variations. The sensitivity analysis was performed by varying the NCAP parameters of the 741 and LF355 unity gain buffer amplifiers. In the analysis, $H_2(f_1,-f_2)$ values were calculated using NCAP for the RF frequency range 0.1 to 400 MHz. Recall from Section 6.1 that the model for the 741 unity gain buffer has 14 linear macromodel elements and 16 nonlinear BJT model parameters for each transistor. Their values are listed in Tables 3-2 and 3-5. Also recall from Section 6.2 that the model for the LF355 unity gain buffer has 13 linear macromodel parameters and 10 nonlinear JFET model parameters for each transistor. Their values are listed in Tables 3-4 and 3-6. In each computer run, one NCAP parameter was varied 10% from its original value. While one NCAP parameter was varied, all other parameters were kept at their

original values. A complete set of NCAP results are given in tabular form in Appendix D.

Let us first discuss the results of the sensitivity analysis for the 741 op amp buffer circuit. We examined the variations in $H_2(f_1,-f_2)$ at each RF frequency. At each RF frequency we determined which NCAP BJT model parameter variation yielded the largest variation in H_2 values. That NCAP BJT model parameter was labeled the critical NCAP parameter at that RF frequency. When all RF frequencies were considered, there were only four critical NCAP BJT model parameters: the avalanche voltage V_{CBO}; the dc bias collector current I_C; the dc bias collector junction voltage V_{CB}; and the base emitter space charge capacitance C_{je}. Shown in Figures 6-14 to 6-17 are plots of $H_2(f_1,-f_2)$ vs RF frequencies for ± 10% variations of the four BJT model critical parameters. Shown in Figure 6-18 is a composite plot which indicates the critical BJT model parameters at each RF frequency. For example, the critical BJT parameter at f_1 = 0.1 MHz is the dc bias collector current I_C; at f_1 = 1 MHz, the avalanche voltage V_{CBO} is the critical BJT parameter; at f_1 = 0.6 MHz, both I_C and V_{CBO} are equally critical. The value of the ordinate is equal to the difference in H_2 values divided by 2 corresponding to a ± 10% variation in value of the critical parameter. Also shown in Figure 6-18 are experimental values for the spread in H_2 obtained from Figure 4-14 by subtracting the lowest H_2 value from the highest H_2 value and dividing the difference by 2. The spread in H_2 values indicates that the variations in NCAP model parameters would have to be much greater than ± 10% to account for the

experimental spread in H_2. Unfortunately, we do not know which parameter values vary the most experimentally because the sensitivity analysis does not provide that information. At each RF frequency we also determined which linear macromodel parameter variation yielded the largest variation in H_2 values. That linear macromodel parameter was labeled the critical linear macromodel parameter at that RF frequency. When all RF frequencies were considered, there were only four critical linear macromodel parameters: the capacitor C_E which implements the difference in positive and negative slew rate related to charge-storage effects[18] in the input stage of the op amp; the resistance for R_{e1} and R_{e2} which model emitter degeneration for slew rate enhancement[18]; the compensation capacitor C_2; and the parameter G_a for differential voltage gain. Shown in Figures 6-19 to 6-22 are plots of $H_2(f_1,-f_2)$ vs RF frequencies for ± 10% variations* of the four critical linear macromodel parameters. Shown in Figure 6-23 is a composite plot which indicates the critical linear macromodel parameters at each RF frequency. Also shown are experimental values for the spread in H_2 previously shown in Figure 6-18. Let us compare Figure 6-18 to Figure 6-23. The plots indicate that the H_2 values are more sensitive to variations in the values of the BJT model parameters than to the variations in the values of the linear macromodel parameters.

Next we discuss the results of the sensitivity analysis for the LF355 op amp buffer circuit. We examined the variations in $H_2(f_1,-f_2)$ at each RF frequency. At each RF frequency we determined which NCAP JFET model parameter variation yielded the largest variation in H_2

* In Figure 6-21 the plot for a -10% variation is not shown because the appropriate NCAP simulation was not performed.

values. That NCAP JFET model parameter was labeled the critical NCAP parameter at that RF frequency. When all RF frequencies were considered, there were only four critical NCAP JFET model parameters: the pinch-off voltage V_p; the drain current parameter I_{Dmax}; the parameter ρ which is related to the critical field associated with carrier mobility and to the gate length; and the barrier potential ψ. Shown in Figures 6-24 to 6-27 are plots of $H_2(f_1,-f_2)$ vs RF frequencies for -10% variations* of the four critical JFET model parameters. Shown in Figure 6-28 is a composite plot which indicates the critical JFET model parameters at each RF frequency. Also shown in Figure 6-28 are experimental values for the spread in H_2 obtained from Figure 4-17 by subtracting the lowest H_2 value from the highest H_2 value and dividing the difference by 2. The spread in H_2 values indicates that the variations in NCAP model parameters would have to be much greater than ± 10% to account for the experimental spread in H_2 values. Unfortunately, we do not know which parameter values vary the most experimentally because the sensitivity analysis does not provide that information. At each RF frequency, we also determined which linear macromodel parameter variation yielded the largest variation in H_2 values. That linear macromodel parameter was labeled the critical linear macromodel parameter at that RF frequency. When all RF frequencies were considered, there were only five critical linear macromodel parameters: the resistances R_{d1} and R_{d2}; the parameter G_a for differential voltage gain; the resistances R_{s1} and R_{s2}; the compensation capacitor C_2; and the capacitor C_s which models the difference in positive and negative slew rates of the LF355 op amp. Shown in Figures 6-29 to 6-33 are plots of $H_2(f_1,-f_2)$ vs RF frequencies

* In Figure 6-25, the plot for a + 10% variation is also shown.

for ± 10% variations of the five critical linear macromodel parameters. Shown in Figure 6-34 is a composite plot which indicates the critical linear macromodel parameters at each RF frequency. Also shown are experimental values for the spread in H_2 previously shown in Figure 6-28. Let us compare Figure 6-28 to Figure 6-34. The plots indicate that the H_2 values are more sensitive to variations in the values of the JFET model parameters than to the variations in the values of the linear macromodel parameters.

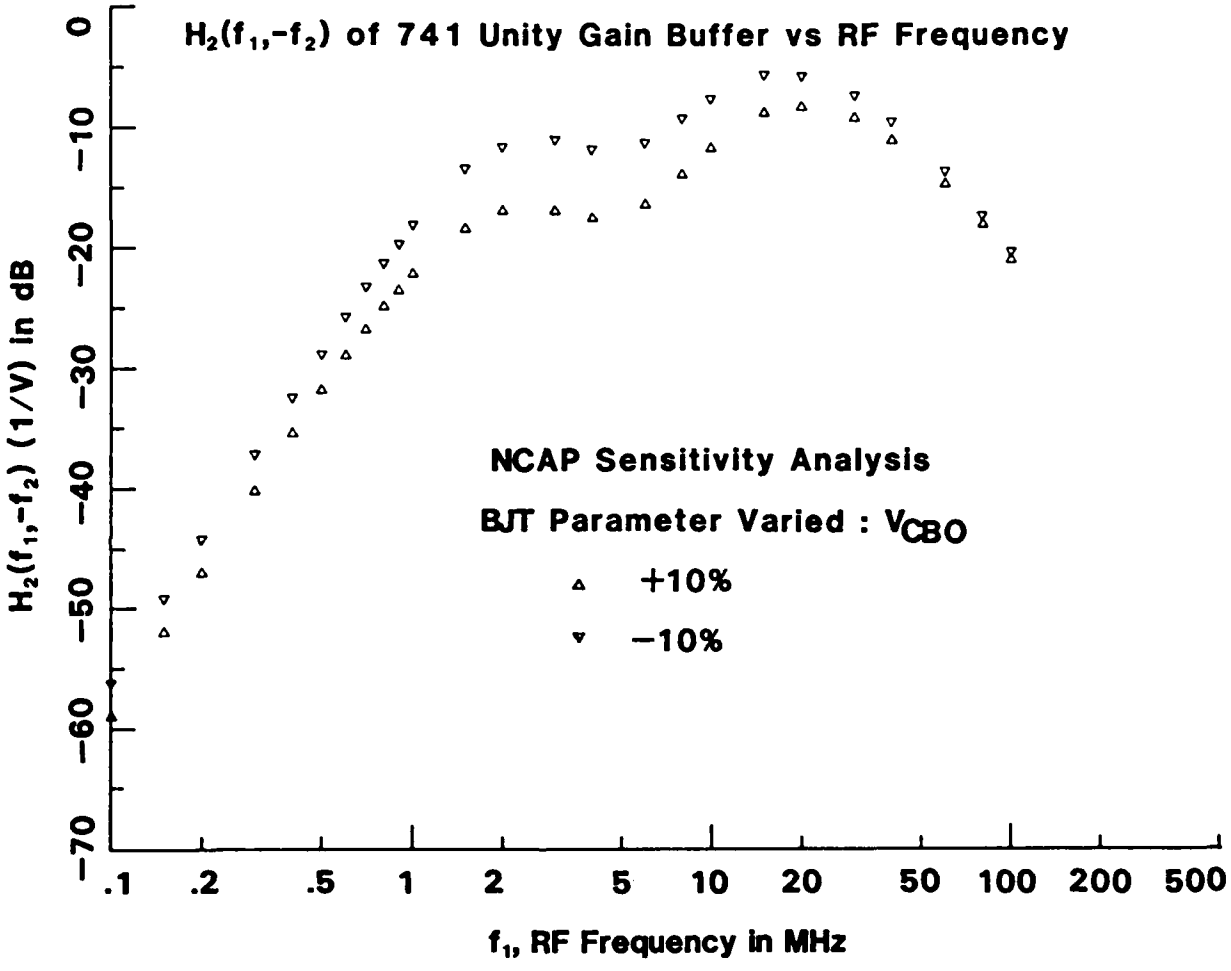

Fig. 6-14 V_{CBO} NCAP sensitivity analysis of 741 unity gain buffer: $H_2(f_1,-f_2)$ vs RF frequency.

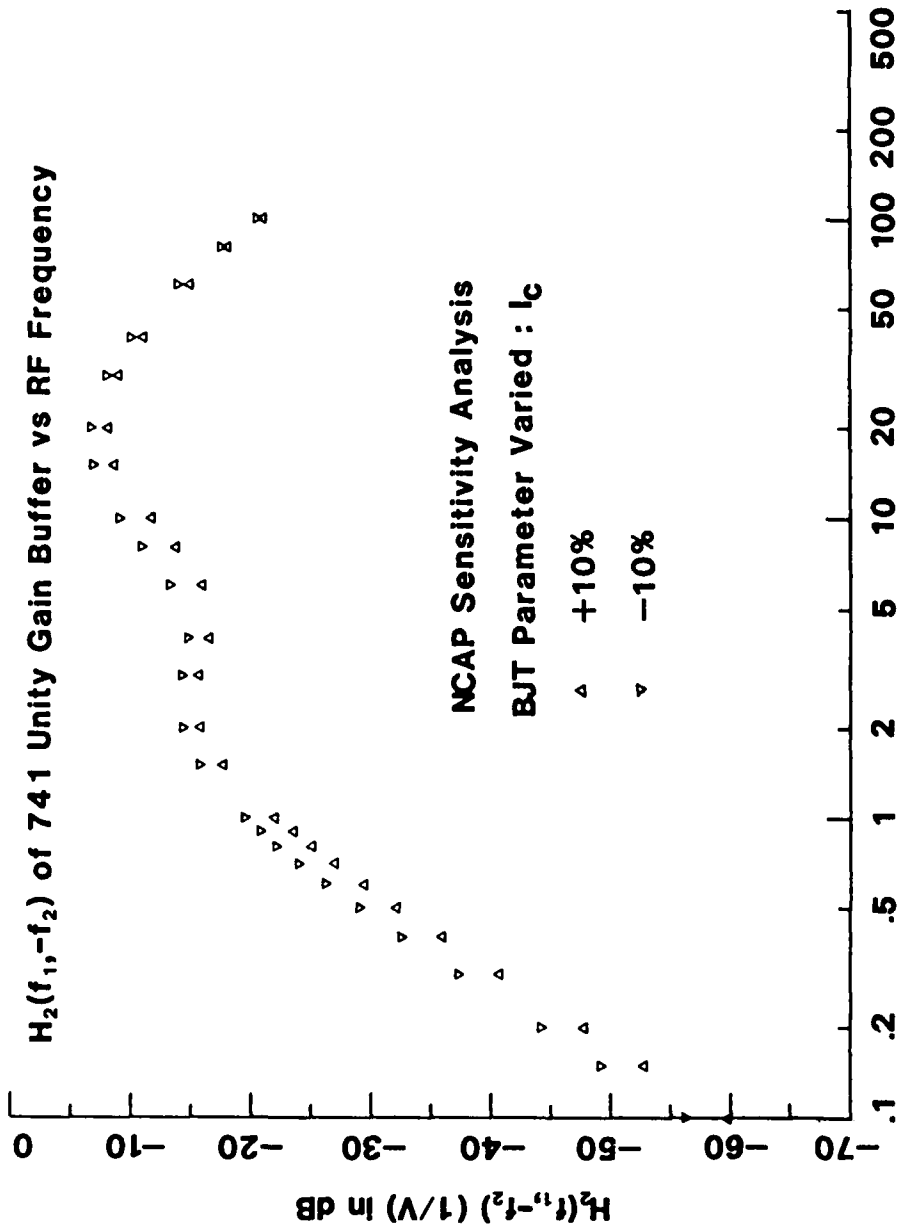

Fig. 6-15 I_C NCAP sensitivity analysis of 741 unity gain buffer: $H_2(f_1,-f_2)$ vs RF frequency.

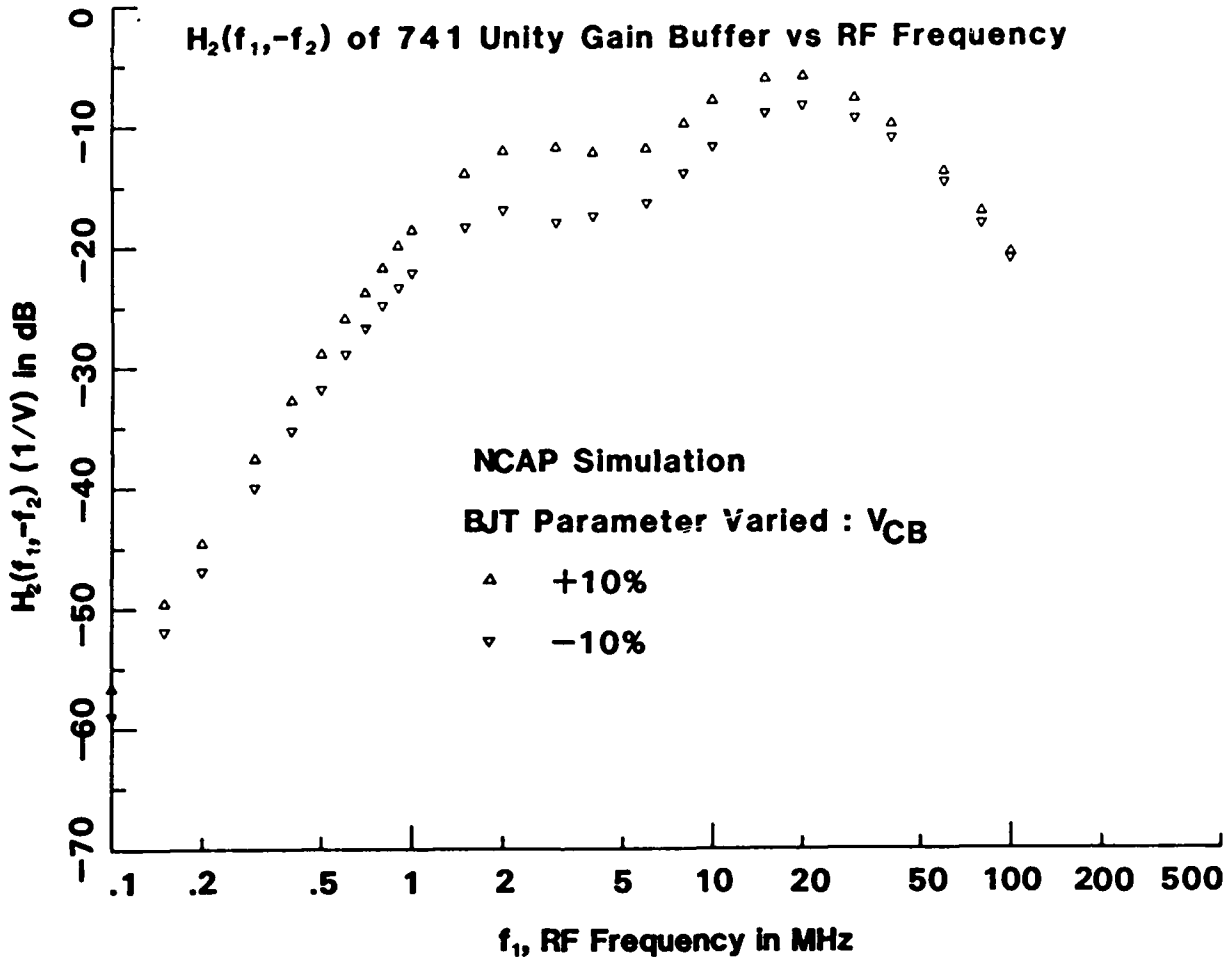

Fig. 6-16 V_{CB} NCAP sensitivity analysis of 741 unity gain buffer: $H_2(f_1,-f_2)$ vs RF frequency.

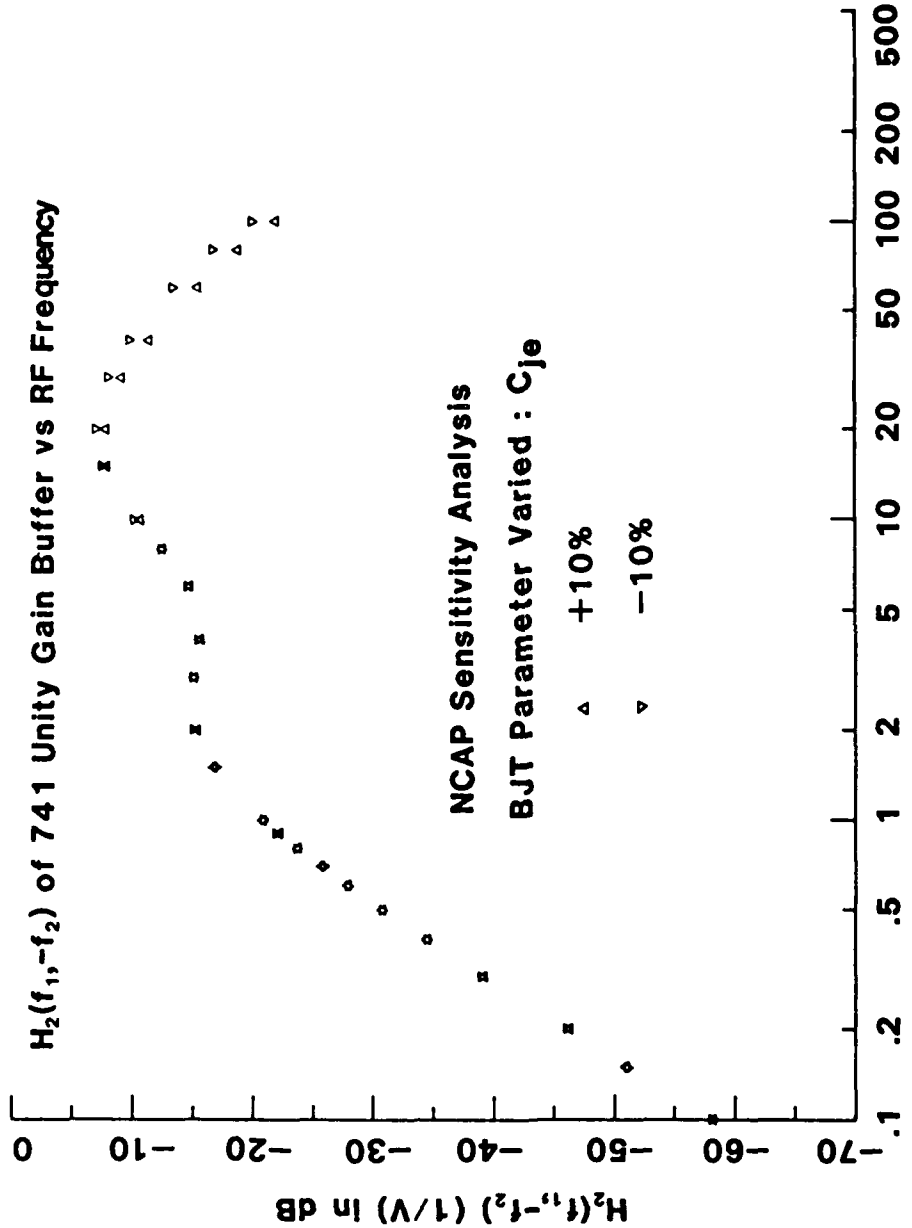

Fig. 6-17 C_{je} NCAP sensitivity analysis of 741 unity gain buffer: $H_2(f_1,-f_2)$ vs RF frequency.

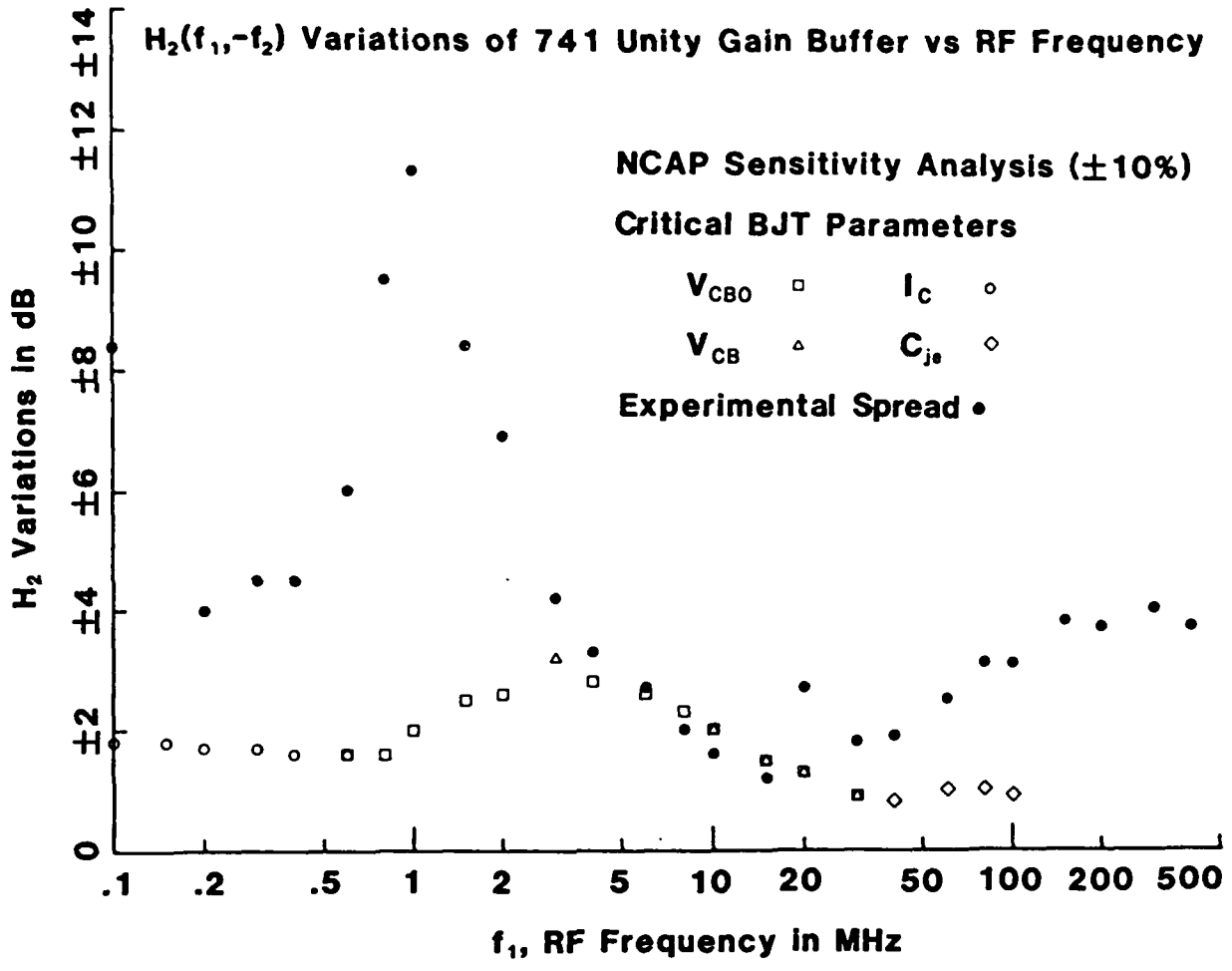

Fig. 6-18 Composite plot showing *critcal BJT parameters* at each RF frequency: H_2 variations vs RF frequency for 741 unity gain buffer. Also shown is the experimental spread in H_2.

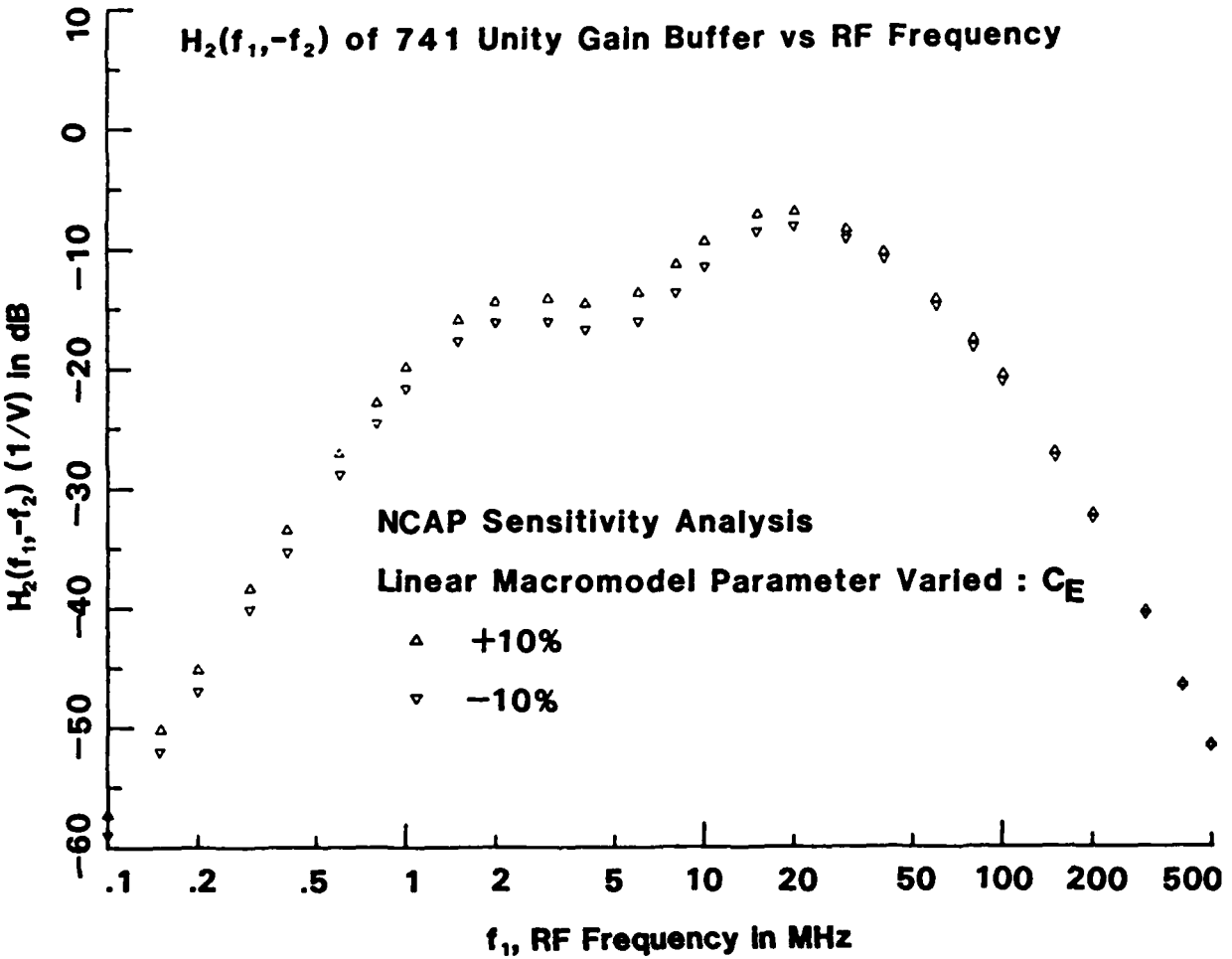

Fig. 6-19 C_E NCAP sensitivity analysis of 741 unity gain buffer: $H_2(f_1,-f_2)$ vs RF frequency.

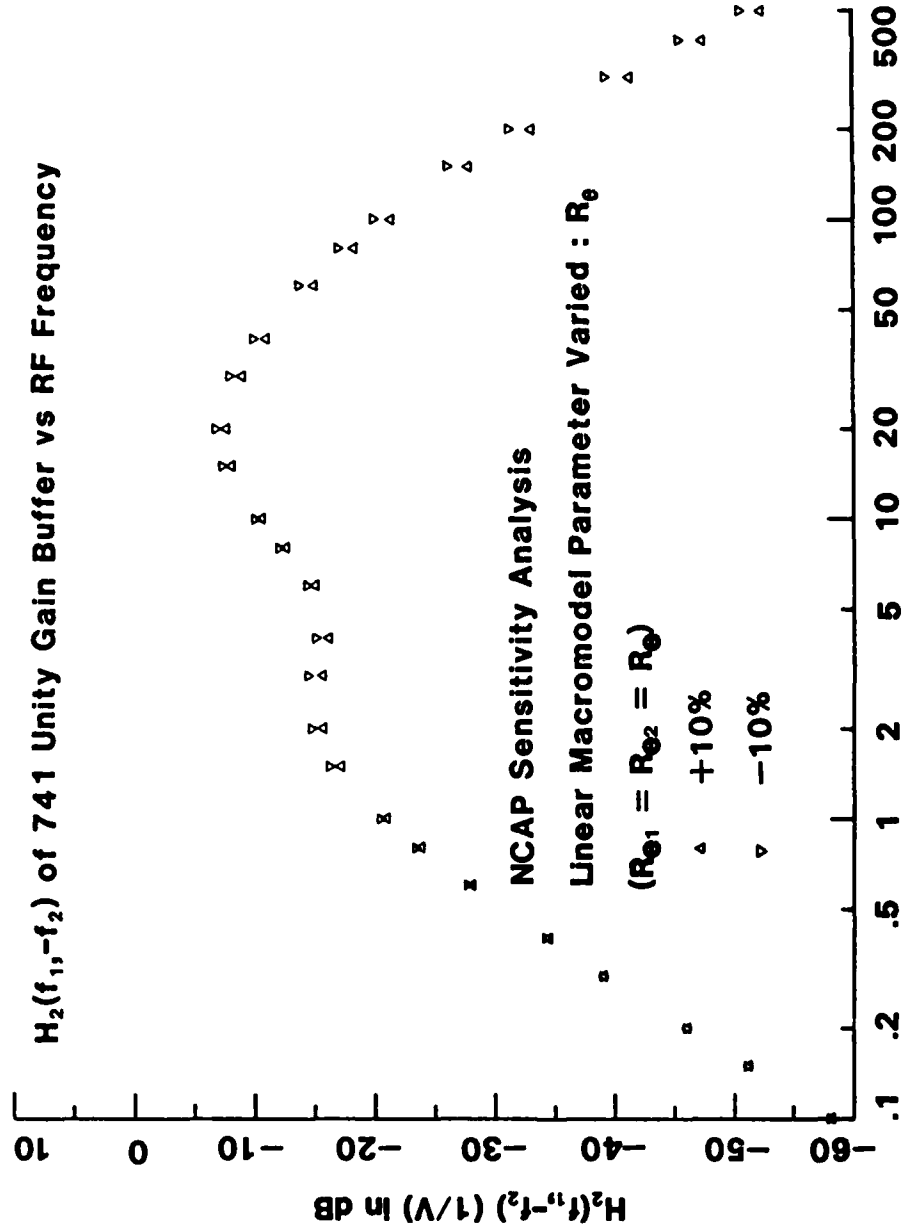

Fig. 6-20 R_e NCAP sensitivity analysis of 741 unity gain buffer: $H_2(f_1,-f_2)$ vs RF frequency.

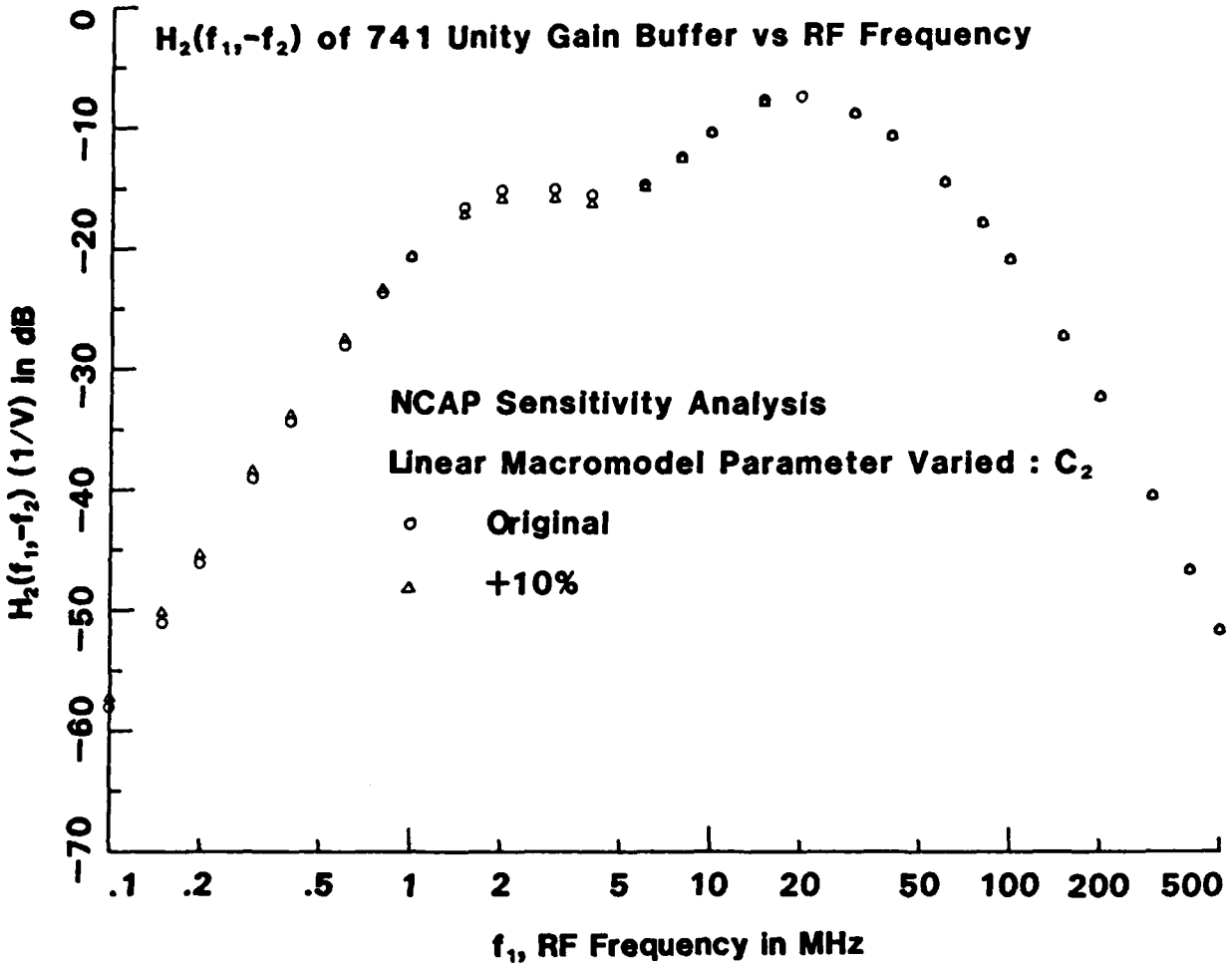

Fig. 6-21 C_2 NCAP sensitivity analysis of 741 unity gain buffer: $H_2(f_1,-f_2)$ vs RF frequency.

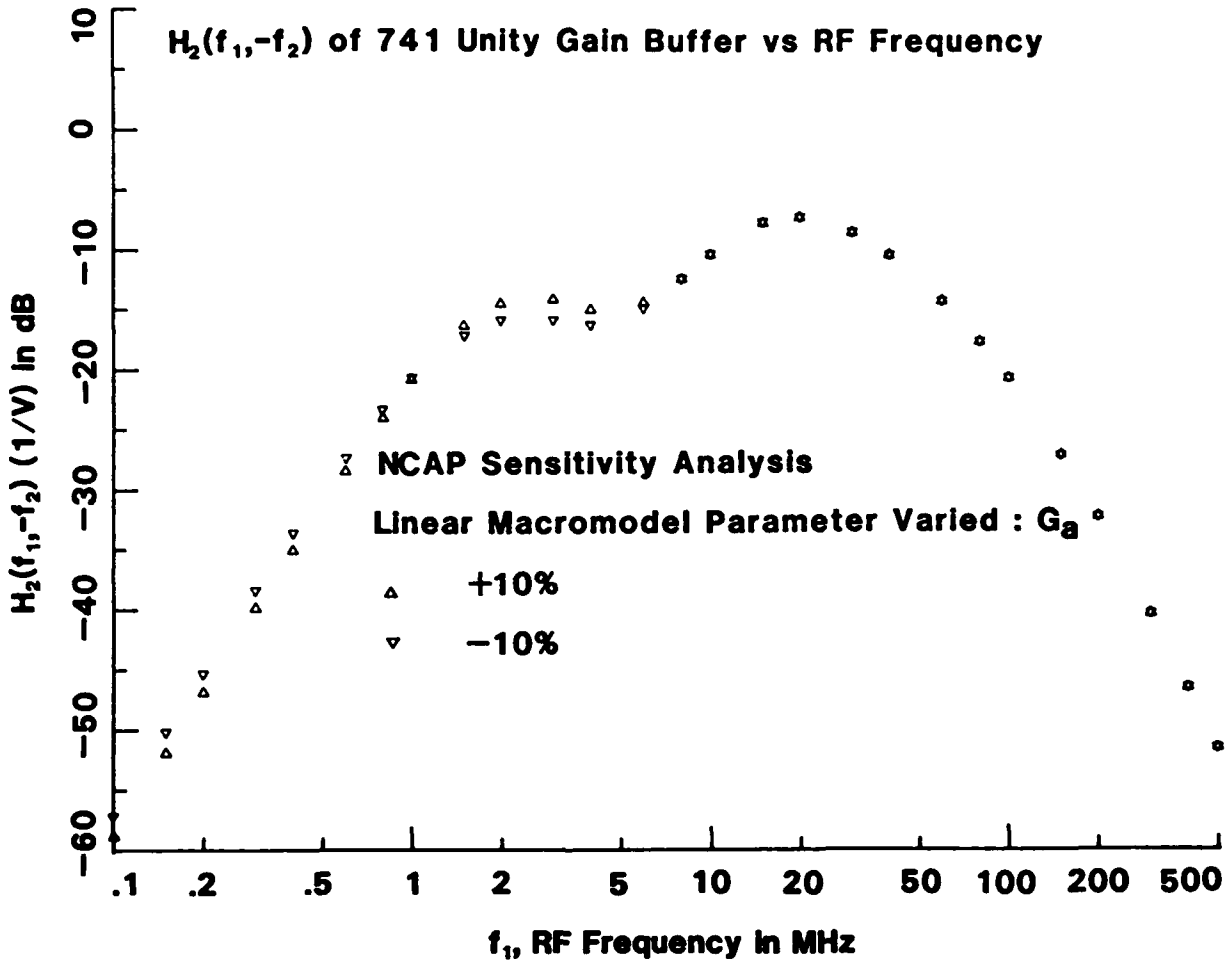

Fig. 6-22 G_a NCAP sensitivity analysis of 741 unity gain buffer: $H_2(f_1,-f_2)$ vs RF frequency.

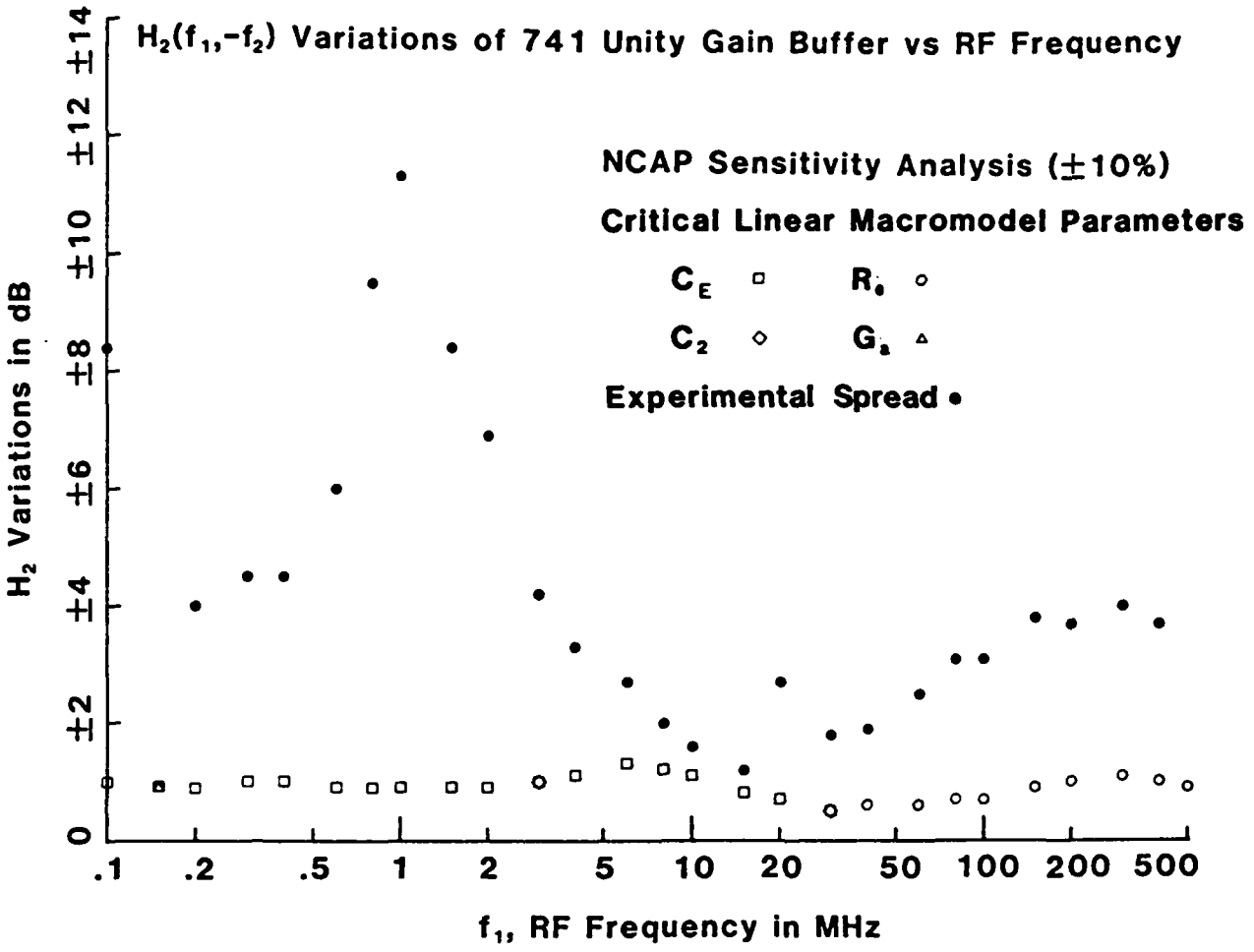

Fig. 6-23 Composite plot showing *critical linear macromodel parameters* at each RF frequency: H_2 variations vs RF frequency for 741 unity gain buffer. Also shown is the experimental spread in H_2.

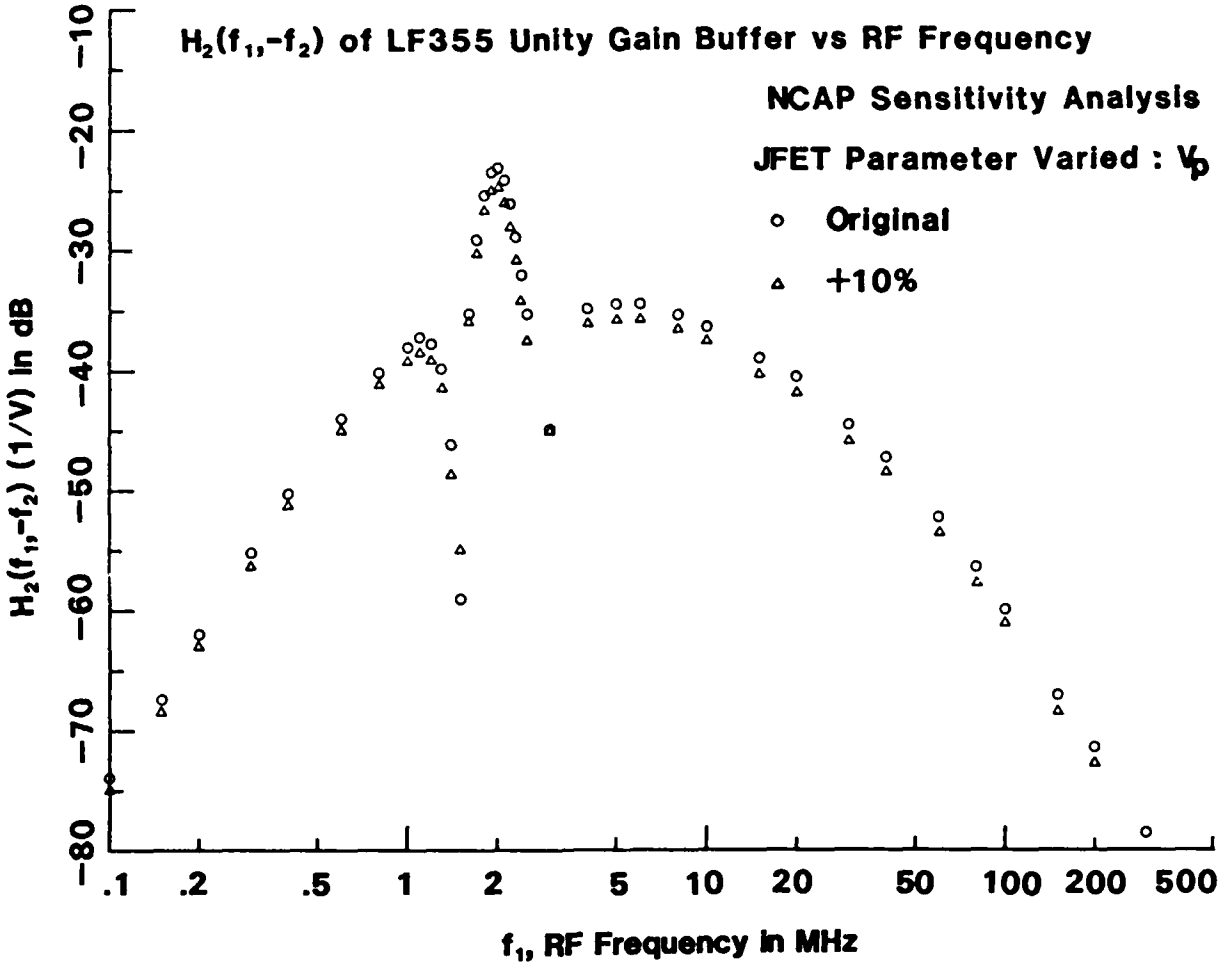

Fig. 6-24 V_p NCAP sensitivity analysis of LF355 unity gain buffer: $H_2(f_1,-f_2)$ vs RF frequency.

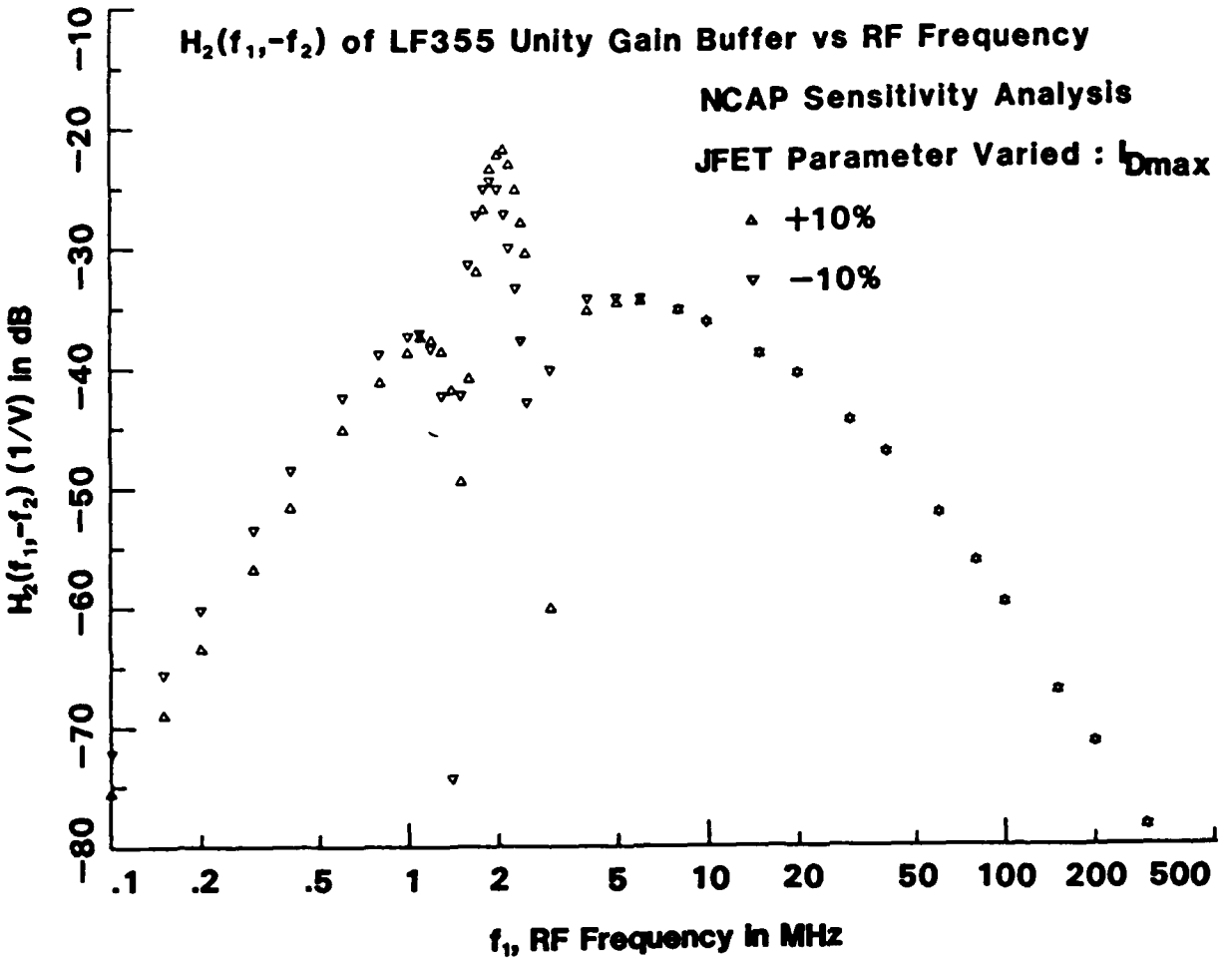

Fig. 6-25 I_{Dmax} NCAP sensitivity analysis of LF355 unity gain buffer: $H_2(f_1,-f_2)$ vs RF frequency.

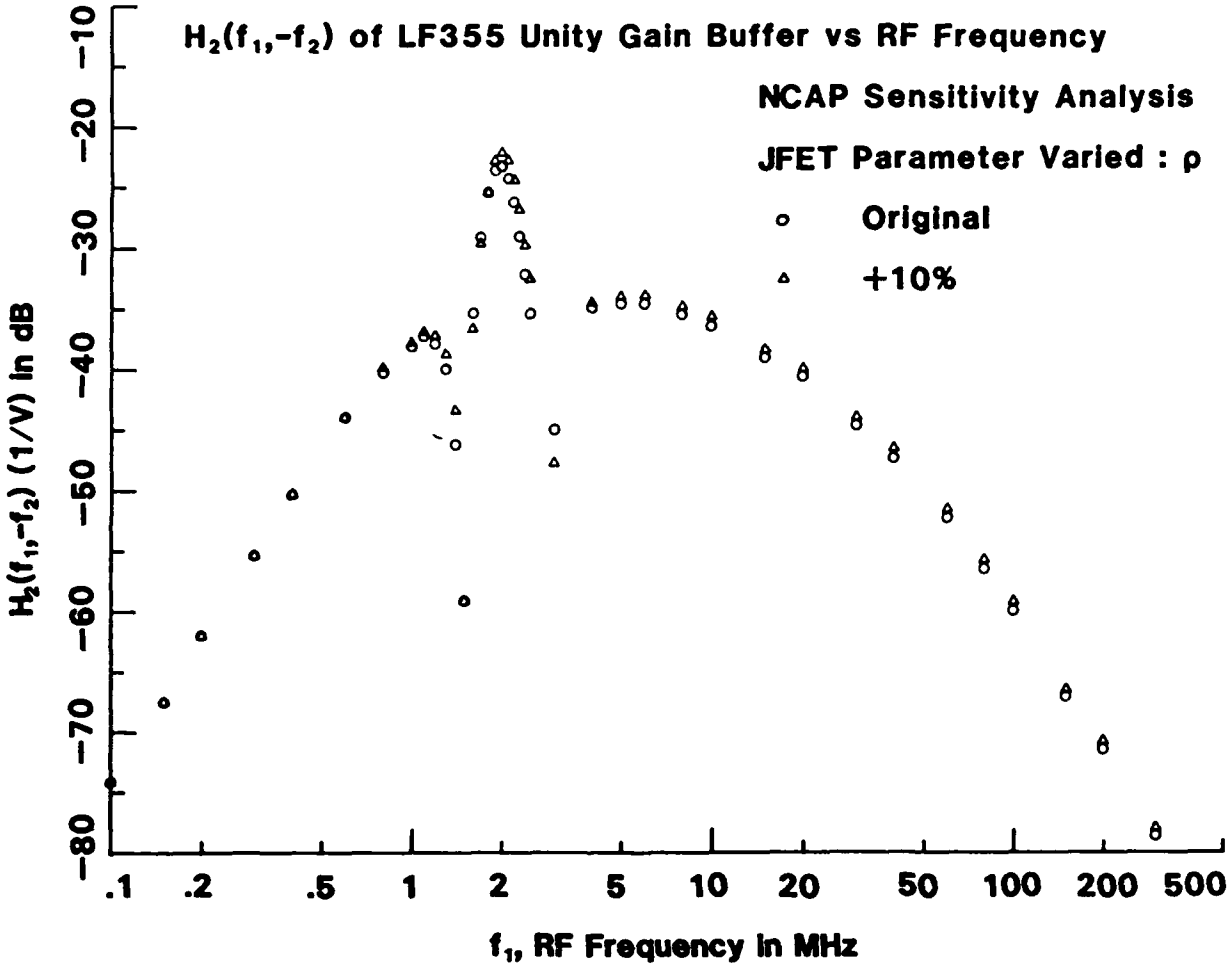

Fig. 6-26 ρ NCAP sensitivity analysis of LF355 unity gain buffer: $H_2(f_1,-f_2)$ vs RF frequency.

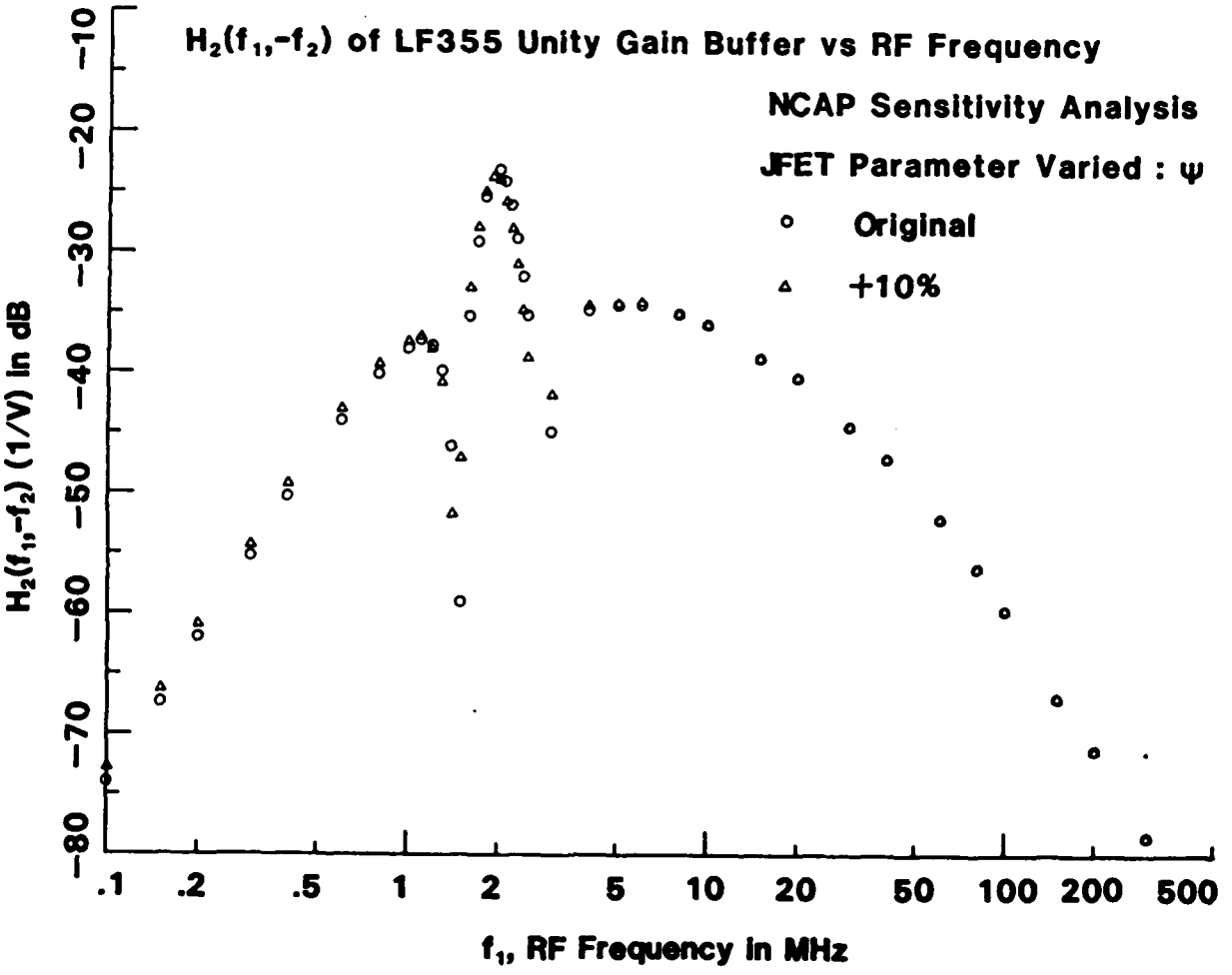

Fig. 6-27 ψ NCAP sensitivity analysis of LF355 unity gain buffer: $H_2(f_1,-f_2)$ vs RF frequency.

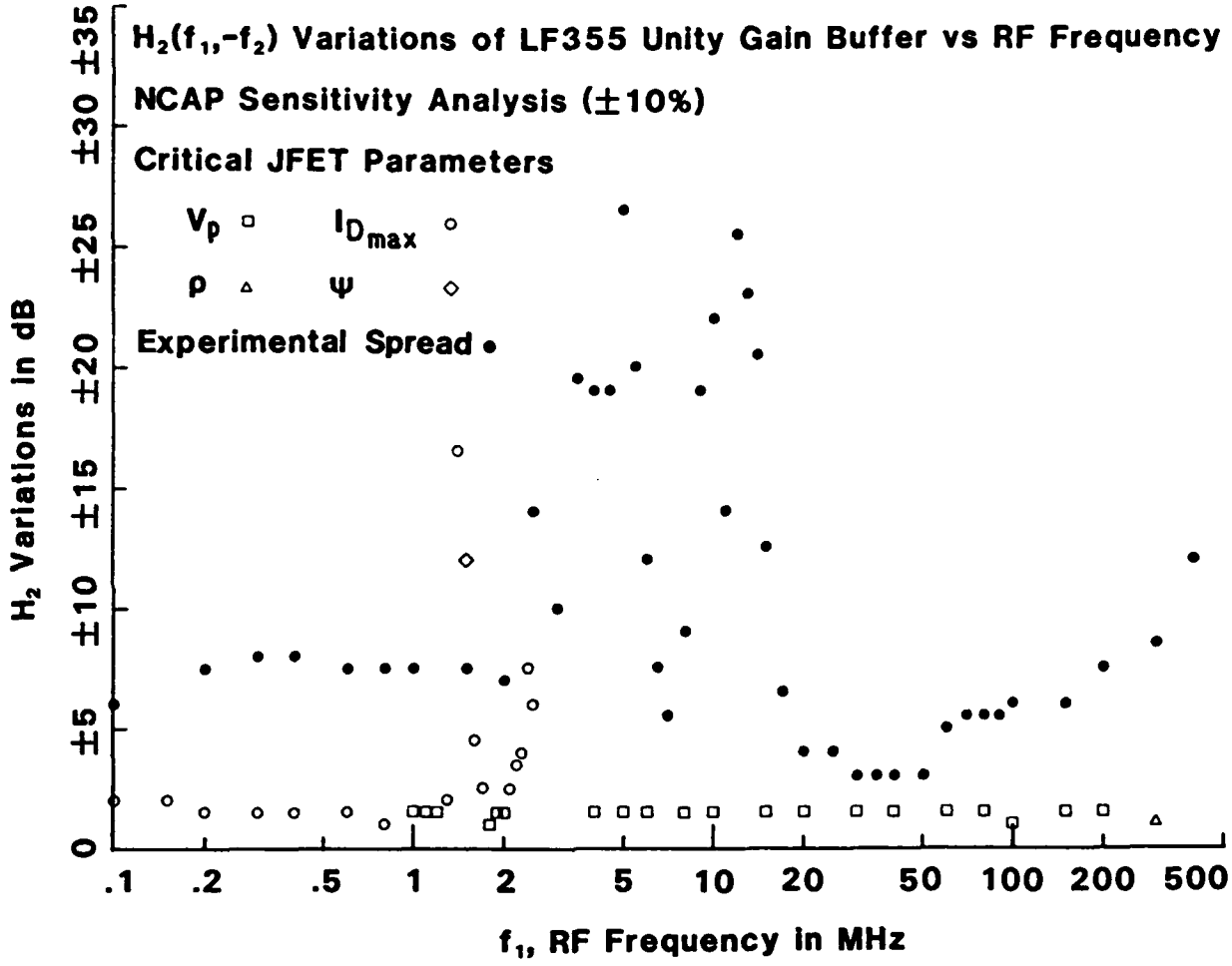

Fig. 6-28 Composite plot showing *critical JFET parameters* at each RF frequency: H_2 variations vs RF frequency for LF355 unity gain buffer. Also shown is the experimental spread in H_2.

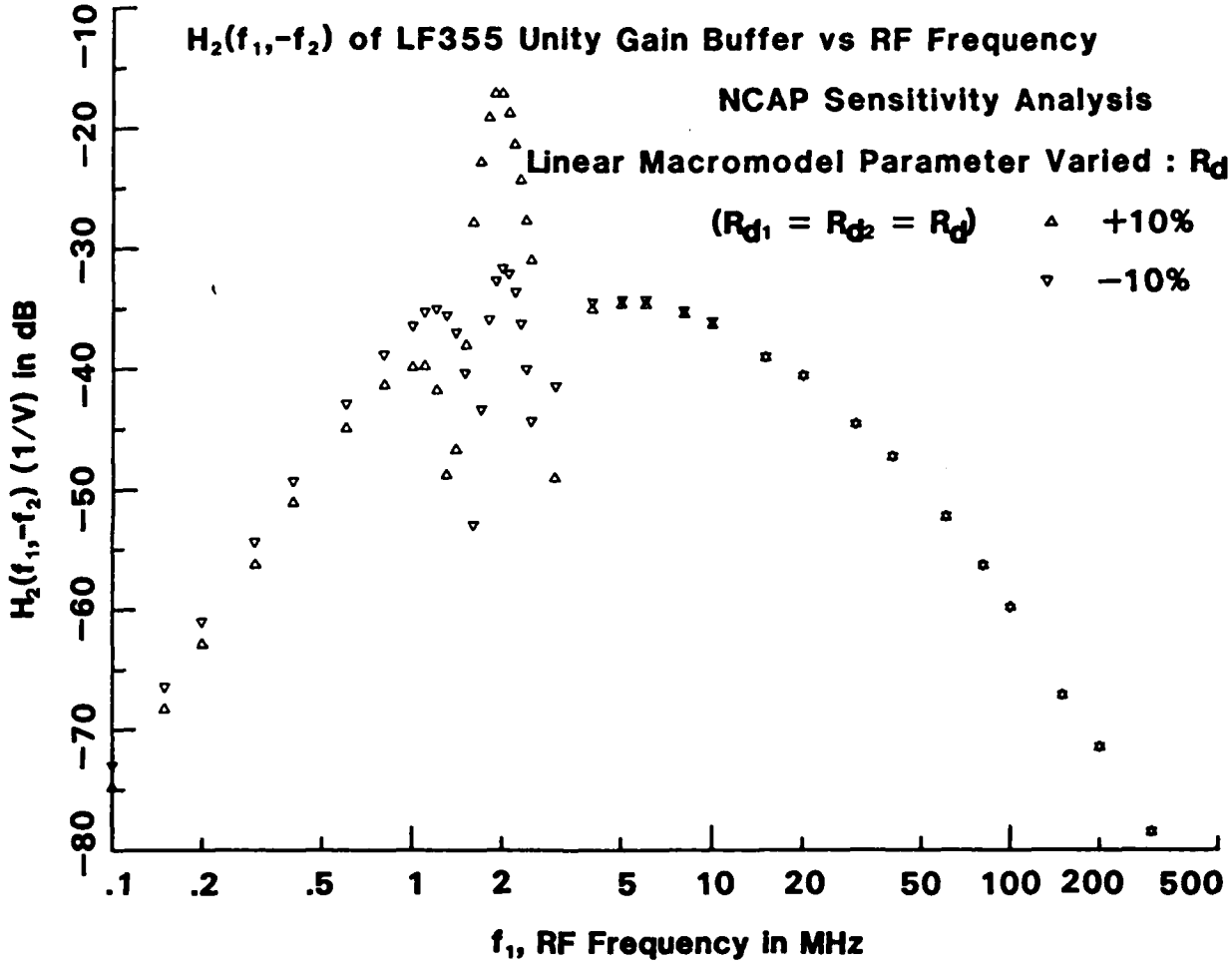

Fig. 6-29 R_d NCAP sensitivity analysis of LF355 unity gain buffer: $H_2(f_1,-f_2)$ vs RF frequency.

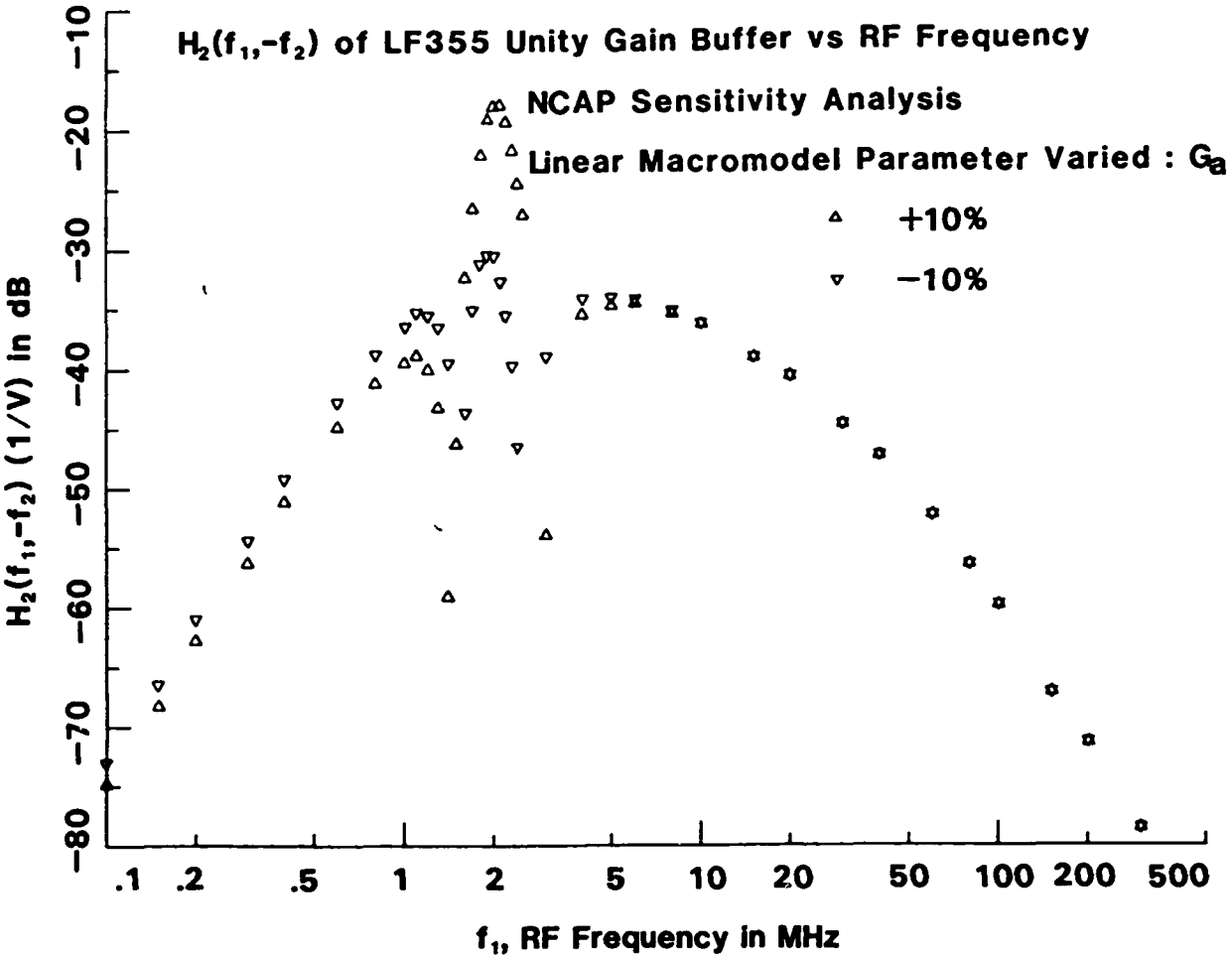

Fig. 6-30 G_a NCAP sensitivity analysis of LF355 unity gain buffer: $H_2(f_1,-f_2)$ vs RF frequency.

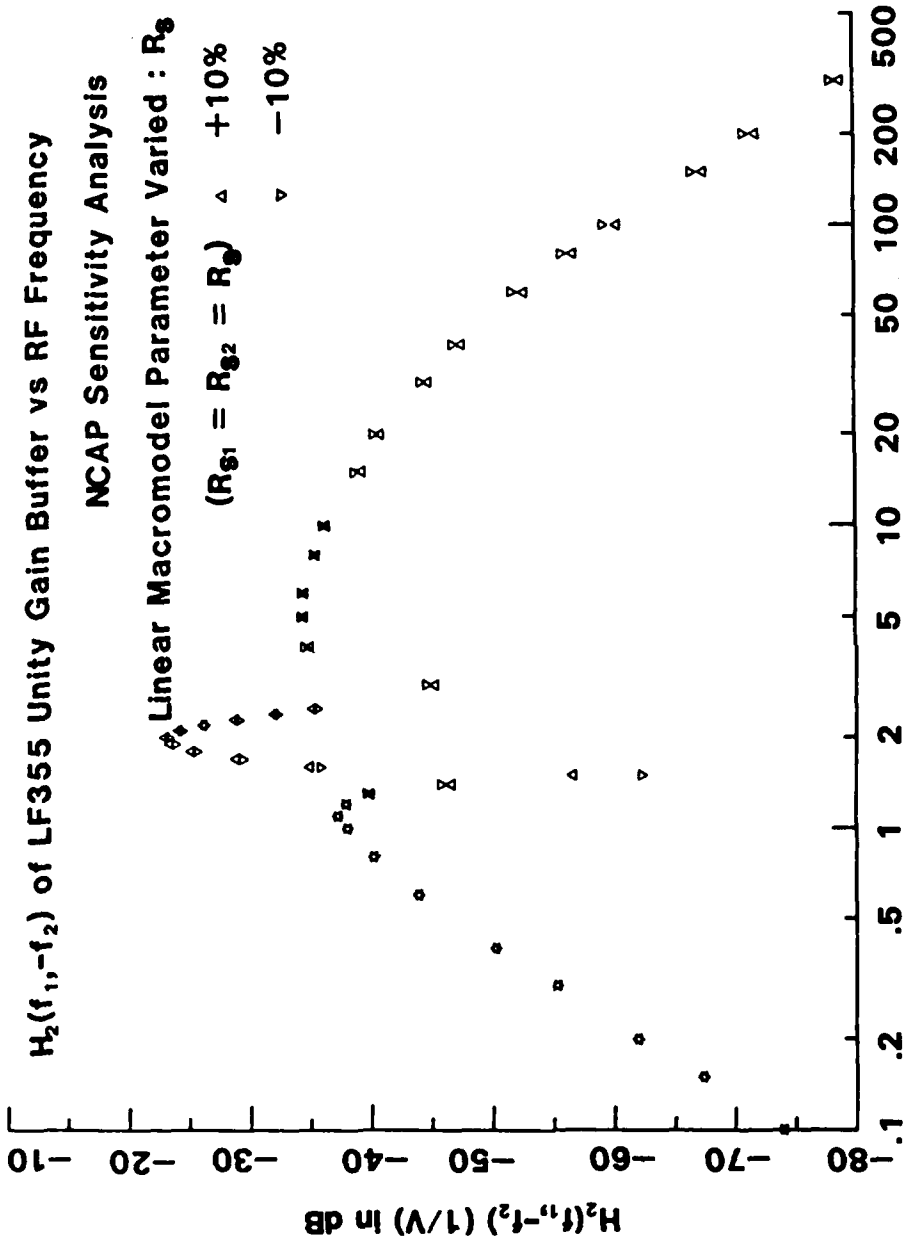

Fig. 6-31 R_s NCAP sensitivity analysis of LF355 unity gain buffer: $H_2(f_1,-f_2)$ vs RF frequency.

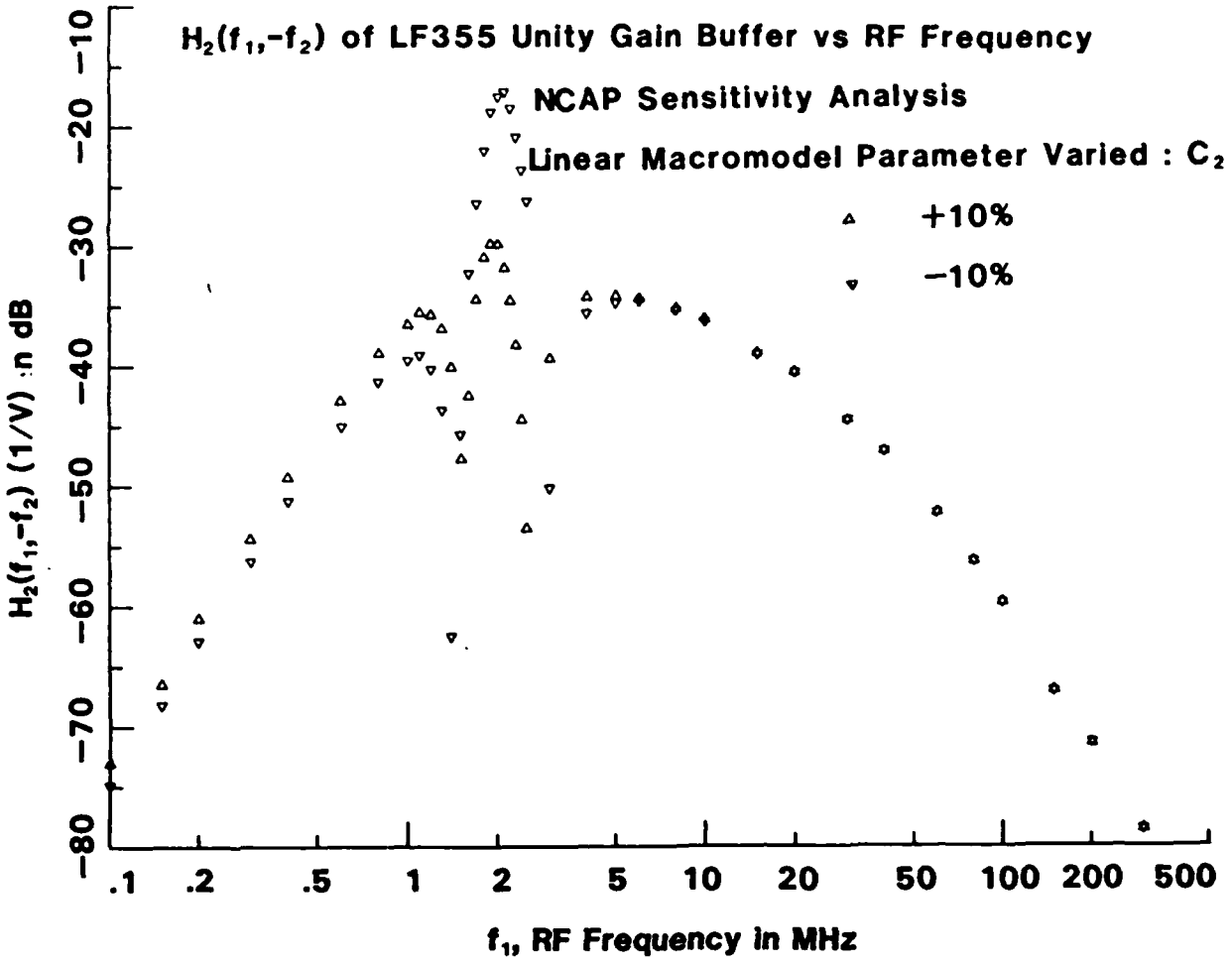

Fig. 6-32 C_2 NCAP sensitivity analysis of LF355 unity gain buffer: $H_2(f_1,-f_2)$ vs RF frequency.

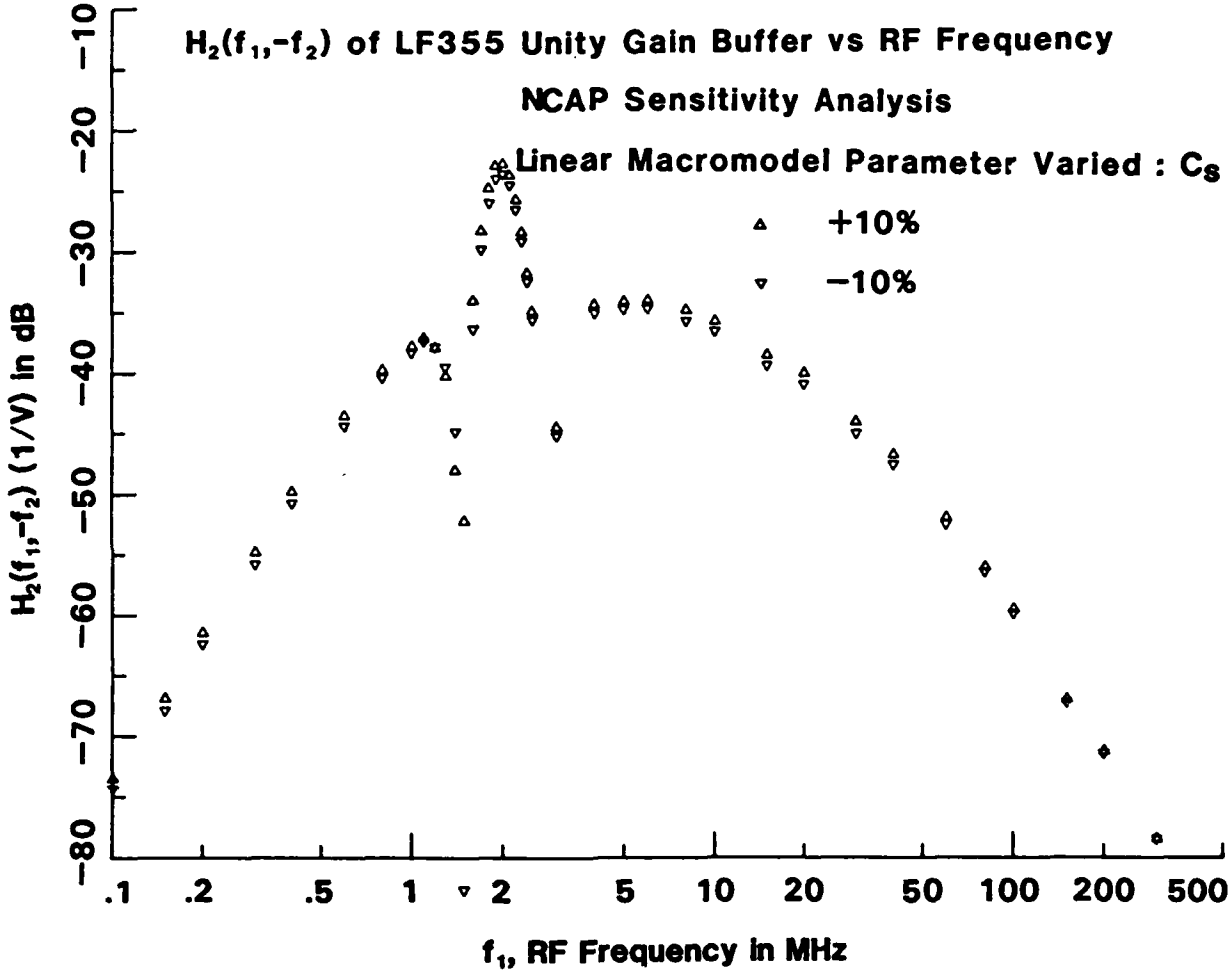

Fig 6-33 C_s NCAP sensitivity analysis of LF355 unity gain buffer: $H_2(f_1,-f_2)$ vs RF frequency.

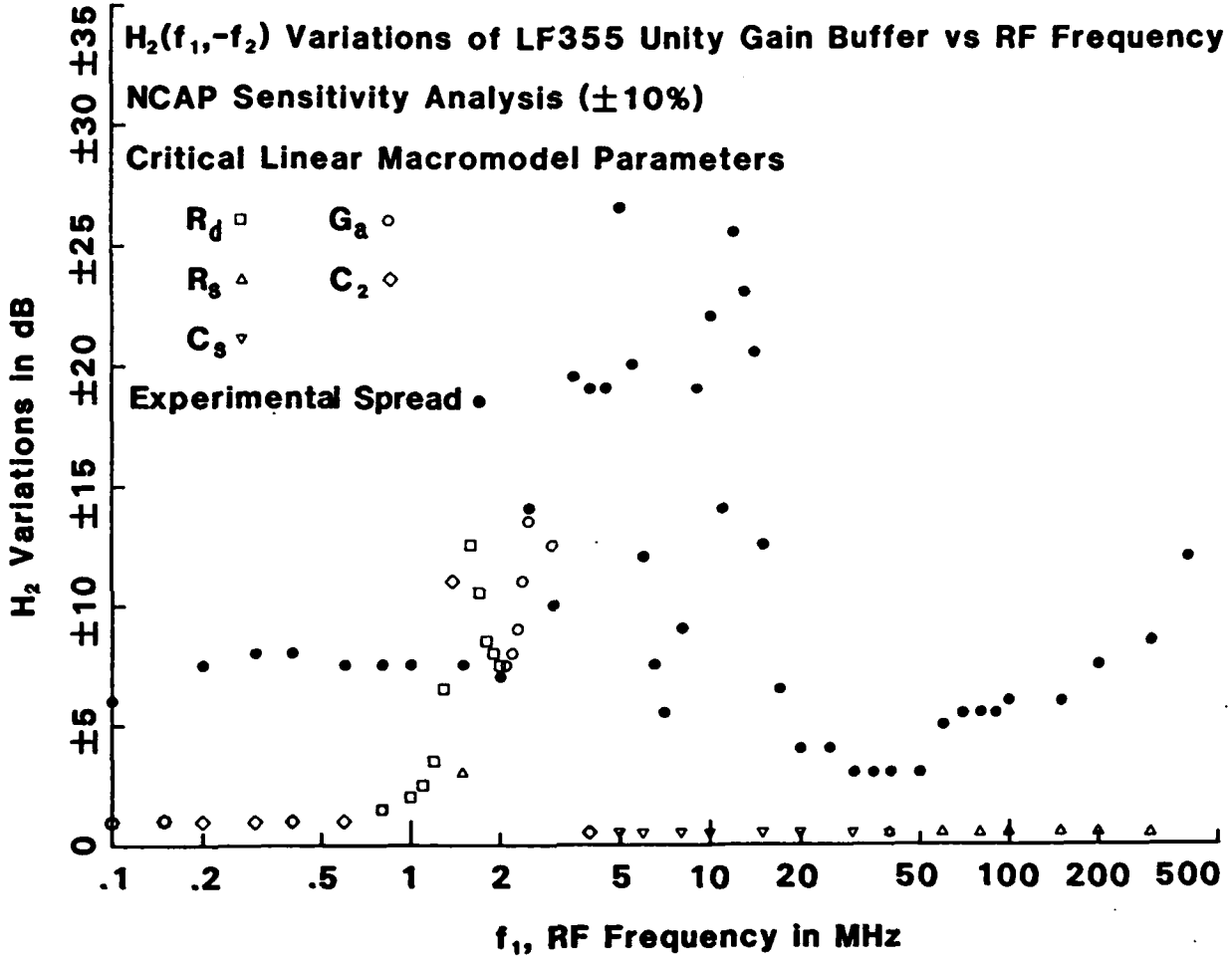

Fig. 6-34 Composite plot showing *critical linear macromodel parameters* at each RF frequency: H_2 variations vs RF frequency for LF355 unity gain buffer. Also shown is the experimental spread in H_2.

CHAPTER SEVEN

SUMMARY, CONCLUSIONS AND RECOMMENDATIONS

An experimental investigation has been conducted to determine the statistical variations of RFI demodulation effects in operational amplifiers (op amps). Amplitude-modulated (AM) RF signals were injected into the non-inverting input of an op amp unity gain voltage follower circuit called a buffer amplifier circuit or into the inverting input of an op amp inverting voltage amplifier circuit with a voltage gain of ten. The undesired demodulated responses at the AM-modulation frequency (1 kHz) were measured as the RF frequency was varied over the range 0.1 to 400 MHz. The op amps investigated were the 741 bipolar op amp which has conventional npn input transitors, the LM10 bipolar op amp which has less conventional pnp input transistors, the CA081 MOS-bipolar op amp which has MOSFET input transistors, and the LF355 JFET-bipolar op amp which has JFET input transistors. Approximately 30 of each op amp type were tested in the non-inverting unity gain buffer amplifier circuit. Thirty 741 op amps have been tested in the inverting voltage amplifier circuit. Mean values and standard deviations have been determined for demodulation RFI. The computer program NCAP has been used to calculate mean values for demodulation RFI. Macromodels were

used for the op amps in the computer simulations. Calculated and experimental values for demodulation RFI are compared and discussed. A sensitivity analysis was also performed using NCAP to determine the critical macromodel and transistor parameters. In Section 7.1 the results will be summarized and conclusions will be given. In Section 7.2 recommendations for future work will be made.

7.1 Summary and Conclusions

This dissertation begins with a review of the nonlinear transfer function approach for analyzing a weakly nonlinear circuit excited by sinusoidal signals with different frequencies. The RFI signals used in the experiments described in this dissertation can be written as a sum of sinusoids. The Nonlinear Circuit Analysis Program NCAP was developed specifically to calculate first and higher order transfer functions of weakly nonlinear circuits excited by a sum of sinusoids. The procedure used by NCAP is described in this dissertation. A simple circuit consisting of a nonlinear resistor was used as an example to illustrate the iterative NCAP calculation procedure.

In Chapter 3, macromodels are reviewed for the bipolar op amp and for the JFET-bipolar op amp. Values are given for the macromodel linear parameters of the 741 bipolar op amp and LF355

JFET-bipolar op amp. Manufacturers' typical data were used. The NCAP BJT parameter values used for the bipolar input transistors of the 741 op amp macromodel are the same as the values given by Fang et al.[6,8] for the small npn transistors in an actual 741 op amp except for the adjustments described in Chapter 3. The adjustments are related to quiescent point differences. The NCAP JFET parameter values for the JFET input transistors of the LF355 op amp are the same as the values given by Whalen et al.[17] for discrete n-type JFETs except for the adjustments described in Chapter 3. Again, the adjustments are related to quiescent point differences.

This dissertation next describes experimental investigations to determine the statistical variations of RFI demodulation responses in two op amp circuit configurations. In Chapter 4 results for the unity gain buffer amplifier configuration are given. Four different types of op amps were tested: the 741 bipolar op amp with a npn transistor input stage; the LM10 bipolar op amp with a pnp transistor input stage; the CA081 Bi-MOS op amp with a MOSFET input stage; and the LF355 Bi-FET op amp with a JFET input stage. Approximately 30 units of each op amp type have been tested in the unity gain buffer amplifier. The op amps tested were purchased five at a time over an extended time duration in order to obtain units with different manufacturing date codes. A 50% amplitude-modulated RF signal with a 1 kHz modulation fre-

quency, f_{AF}, was injected into the non-inverting input of the op amp under test. The RF frequency, f_{RF}, was varied over the frequency range 0.1 to 400 MHz. Because of the second-order nonlinearities of the op amp, intermodulation interference signal components at f_{AF} = 1 kHz were produced at the output. The phenomenon is called the RFI demodulation effects. The strength of the interference signal at f_{AF} as a function of the RF carrier frequency at the input is termed the RFI demodulation response. Throughout the dissertation, the nonlinear second-order transfer function, $H_2(f_1,-f_2)$ where $f_1 = f_{RF}$ and $f_2 = f_{RF} - f_{AF}$, has been used as the parameter which characterizes the RFI demodulation response because the response was kept in the square-law response region. The experimental $H_2(f_1,-f_2)$ values for approximately 30 units of each type of op amp were plotted vs RF frequency. The experimental mean values of $H_2(f_1,-f_2)$ for the four types of op amps were plotted and compared. The results showed that RFI demodulation effects are 10 to 20 dB lower in CA081 and LF355 FET-bipolar op amps than in 741 and LM10 bipolar op amps except above 40 MHz where the LM10 RFI response begins to approach that of the CA081. Analysis using the transfer function model of the op amp unity gain buffer indicates that the result is related to two factors. One factor is the open-loop, second-order transfer function of the op amp. It is believed that the second-order transfer functions of FET-bipolar op amps are smaller than those of bipolar op amps. The other factor is the open-loop linear transfer function vs frequency of the op

amp. The linear gain-bandwidth products of the CA081 and LF355 op amps are larger than those of 741 and LM10 op amps. As a result, the demodulation RFI of CA081 and LF355 op amps is lower than that of 741 and LM10 op amps. One interesting phenomenon in the RFI demodulation response of the unity gain buffer was observed only for LF355 op amps. The experimental results indicated two resonances at RF frequencies near 4 MHz and 12 MHz. The standard deviation of $H_2(f_1,-f_2)$ values for the four types of op amps were also plotted and compared. The CA081 op amps have the smallest standard deviation. The LF355 op amps have the largest standard deviation near their two resonance frequencies, and the LM10 op amps have the largest standard deviation at low and high RF frequencies.

In Chapter 5 experimental results are given for the second op amp circuit configuration which is an inverting amplifier with voltage gain equal to ten. In the inverting amplifier experiment, the amplitude-modulated RF signal was applied to the inverting input of the op amp under test. To date, only 741 op amp units have been tested in the inverting op amp circuits. Values for the second-order transfer function which characterizes the RFI demodulation response were derived from the tuned AF voltmeter readings at the output and RF voltmeter readings at the input. Two sets of experimental $H_2(f_1,-f_2)$ values were plotted. One set of data corresponds to the 741 inverting amplifier with no RFI suppression capacitor. Another set of data corresponds to the

inverting apmplifier with a 27 pF RFI suppression capacitor in the feedback path. The mean values of the two sets of H_2 data were compared for 741 op amps. The experimental mean values for 741 op amps showed that RFI demodulation responses in the inverting amplifier with the 27 pF capacitor were suppressed from 10 to 35 dB over the RF frequency range 0.1 to 150 MHz except at 0.15 MHz where only 3.5 dB suppression was observed. Adding the 27 pF RFI suppression capacitor to the feedback path also caused an increase in the values of the standard deviation for H_2. The theory for the effect of an RFI suppression capacitor in the feedback path of an inverting amplifier was reviewed.[31] The difference between our experimental mean values for H_2 without and with the 27 pF RFI suppression capacitor are in reasonable agreement with the theory. See Appendix E for the details.

In Chapter 6 computer simulation results are given. In NCAP simulations, op amps were replaced by their macromodels. The 741 incremental macromodel has 12 linear parameters and 16 nonlinear BJT parameters. Chen[12] added four capacitors to model the parasitic substrate capacitances of the two BJTs in the input stage. He set the four parasitic substrate capacitors equal to 4 pF in order to fit the NCAP simulation results to his experimental results.[12] We set the four parasitic substrate capacitors equal to 0 pF. The NCAP predictions and our experimental mean values for the measured RFI demodulation response in the 741 op amp unity

gain buffer amplifier agreed within 6 dB over the RF frequency range 0.1 to 400 MHz. Our experimental results for the mean value of $H_2(f_1,-f_2)$ for 30 op amps differ from the experimental results reported upon previously for 1 to 3 op amps.[12] Our measured mean values are lower than the experimental results reported by G. K. C. Chen.[12] That our experimental mean values for $H_2(f_1,-f_2)$ agree better with the NCAP simulation results without the four additional parasitic substrate capacitors indicates the importance of having a data base large enough to yield a reliable mean value. This is especially true when a macromodel is used for the NCAP simulation and values for the macromodel parameters are determined from "typical values" given in manufacturers' data sheets.

In Chapter 6 NCAP simulations for the LF355 op amp unity gain buffer amplifier are also given. The LF355 incremental macromodel has 11 linear parameters and 10 nonlinear JFET parameters. Three capacitors C_{p1}, C_{p2}, and C_{p3} were added to the intrinsic JFET model to account for the interelectrode parasitic capacitors. When $C_{p1} = C_{p2} = C_{p3} = 1$ pF, no obvious resonances could be identified. When $C_{p1} = C_{p2} = C_{p3} = 2$ pF, one resonance is clearly distinguishable at approximately 3 MHz. When $C_{p1} = C_{p2} = C_{p3} = 4$ pF, two resonances can be clearly identified at approximately 1.5 MHz and 3.5 MHz. However, the NCAP simulation resonances occur at frequencies lower than the 4 MHz and 12 MHz resonant frequencies observed

in the experiment. The NCAP results suggest that the resonances are related to small parasitic capacitance values of the order 1 to 5 pF. There are two possible physical locations for parasitic capacitors of this size. One location is inside the op amp itself, i.e., inter-electrode capacitance. The other location is the external circuit, i.e., the external circuit wiring to ground capacitance. Our current thinking is that capacitance effects internal to the LF355 op amp are responsible for the resonances because similar resonances are not observed when the other op amp types (741, LM10, and CA081) are inserted in the same unity gain buffer circuit. However, a more complicated situation may exist which is caused by an external circuit and op amp interaction which is sensitive to the impedance values inside the LF355 op amp. It would be desirable to model more completely the external circuit wiring and external circuit component parasitics in order to investigate these resonances further. With the interelectrode parasitic capacitances C_{p1} = 5 pF, C_{p2} = 3 pF, and C_{p3} = 4 pF, the discrepancy between experimental and NCAP results above 15 MHz has been reduced from 10 to 15 dB to 1 to 4 dB but the discrepancy below 1 MHz has increased from 1 to 3 dB to 4 to 7 dB. Larger discrepancies continue to exist in the vicinity of the resonant frequencies.

Also given in Chapter 6 are NCAP simulation results for the 3-stage op amp LED circuit. The three 741 op amps were replaced by 741 op amp macromodels. Recall that the input stage had an input resistor R_1 = 10 kΩ, a feedback resistor R_2 = 100 kΩ, and a desired signal linear voltage gain of -10. Recall, also, that measurements were made without and with an RFI suppression capacitor C_4 in parallel with the feedback resistor R_2. The RFI suppression capacitors reduce $H_2(f_1,-f_2)$ at every RF frequency. The reduction in H_2 varies from a low of 3 dB at .15 MHz to a high of 36 dB at 10 MHz and exceeds 15 dB at all RF frequencies above 10 MHz. First, we compared NCAP simulation results to experimental results with the RFI suppression capacitors omitted (C_4 = 0). Below 1.0 MHz the NCAP simulation values exceed the measured values by 10 to 17 dB. From 1.0 to 6.0 MHz the NCAP values and the measured values agree within 1 to 4 dB. Above 6 MHz the NCAP values exceed the measured values by 6 to 15 dB. Finally, we compared NCAP simulation results and experimental results with the RFI suppression capacitor included (C_4 = 27 pF). Below 1.0 MHz the NCAP simulation values exceed the measured values by 23 to 42 dB. Below 1 MHz NCAP predicts an increase in H_2 when the RFI suppression capacitor is added; this is contradictory to what is observed experimentally. Above 1 MHz NCAP predicts a decrease in H_2 when the RFI suppression capacitor is added; this is in agreement with

what is observed experimentally. From 2 MHz to 20 MHz the NCAP values and measured values agree quite well with differences in the range 0 to 7 dB. Above 20 MHz the NCAP values decrease much more rapidly than the experimental values and the experimental values exceed the NCAP values by 20 to 40 dB. The NCAP predictions leave something to be desired and this may indicate that additional modeling effort is required. It would be worthwhile to include in the NCAP simulations the appropriate parasitic elements associated with all the passive components,[34] but especially R_1, R_2, and C_4 in the first stage and the capacitance associated with the printed circuit board wiring.

The last set of NCAP simulations described in Chapter 6 yielded data for a sensitivity analysis. The sensitivity analysis has been performed to determine the linear macromodel parameters and nonlinear device model parameters whose variations cause the largest variations in the RFI demodulation response of the op amp unity gain buffer circuit. Macromodels for the 741 bipolar op amp and for the LF355 JFET-bipolar op amp were used. More than 100 NCAP simulations for the RF range 0.1 to 400 MHz were carried out. In each NCAP simulation, all macromodel parameters were assigned their standard values except for one macromodel parameter which was varied either by +10% or by -10% from its standard value. The parameter which caused the largest variation at each RF frequency was defined as the critical parameter at that RF frequency.

At one or more RF frequencies in the range 0.1 to 400 MHz, four of the 16 nonlinear BJT model parameters are critical parameters. They are: the avalanche voltage V_{CBO}; the dc bias collector current I_C; the dc bias collector junction voltage V_{CB}; and the base-emitter space charge capacitance C_{je}. Among the 12 linear macromodel parameters, four are critical parameters. They are: the capacitor C_E which implements the difference in positive and negative slew rates, the resistors R_{e1} and R_{e2} which model the emitter degeneration for slew rate enhancement; the compensation capacitor C_2, and the parameter G_a for differential voltage gain. The RFI calculations are more sensitive to variations in the values of BJT model parameters than to variations in values of linear macromodel parameters. In the LF355 unity gain buffer, four among the 10 nonlinear JFET model parameters are critical parameters. They are: the pinch-off voltage V_p; the drain current parameter I_{Dmax}; the parameter ρ which is related to the critical field associated with carrier mobility and to the gate length; and the barrier potential ψ. Five among the 11 linear macromodel parameters are critical. They are: the drain resistances R_{d1} and R_{d2}; the parameter G_a for differential voltage gain; the source resistances R_{s1} and R_{s2}, the compensation capacitor C_2; and the capacitor C_s which models the difference in positive and negative slew rates of the LF355 op amp. The RFI calculations are more sensitive to variations in the values of JFET model parameter values than to variations in values of the linear macromodel parameters.

AD-A154 121 BASIC EMC (ELECTROMAGNETIC COMPATIBILITY) TECHNOLOGY ADVANCEMENT FOR C3 S..(U) SOUTHEASTERN CENTER FOR ELECTRICAL ENGINEERING EDUCATION INC S.. 3/3

UNCLASSIFIED Y H SUTU ET AL. FEB 85 F/G 20/14 NL

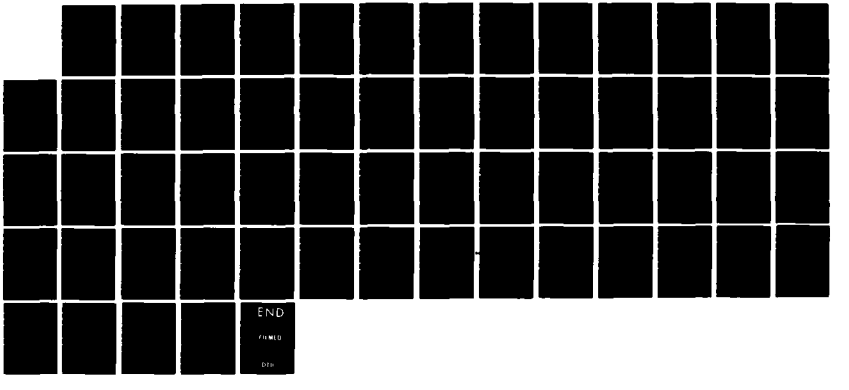

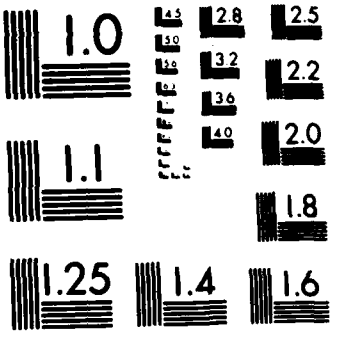

7.2 Recommendations for Future Work

Based upon the results obtained in this dissertation there are six recommendations for future investigations. Each recommendation will now be presented.

(1) Additional Measurements of Demodulation RFI in Inverting Amplifiers

Additional measurements of demodulation RFI in inverting operational amplifier circuits are needed. The sets of values for the input resistor R1 and the feedback resistor R2 listed in Table 7-1 are suggested. Data should be obtained for the four op amp types: the bipolar 741; the bipolar LM10; the Bi-MOS CA081; the JFET-bipolar LF355. The measurements should be made without and with RFI suppression capacitors in the locations suggested by Goedblood et al.[31]

TABLE 7-1

RESISTOR COMBINATIONS FOR INVERTING OP AMP CIRCUIT CONFIGURATION

Input Resistor	Resistor Combinations for Inverting Op Amp Circuit Configuration		
R1	R2:A_v	R2:A_v	R2:A_v
10 k	10 k:-1	100 k:-10	1 M:-100
100 k	100 k:-1	1 M:-10	10 M:-100
1 M	1 M:-1	10 M:-10	-------

(2) Automatic Measurement System

The data generated for this dissertation was obtained with a manual measurement system. The volume of data was large and almost unmanageable. The volume of data that would be generated by implementing the first recommendation requires an automatic measurement system. The automatic measurement system would need to set the RF frequency and amplitude, turn on the 1 kHz AM-modulation, measure RF and AF voltages, store the data, compute second-order transfer functions such as $H_2(f_1,-f_2)$, and plot the results for each op amp tested in each circuit configuration. The data stored for all op amps of one type could then be used to calculate mean values, standard deviations, etc. which also would be plotted.

(3) Additional NCAP Simulations To Improve Understanding of Demodulation RFI in Feedback Amplifiers

The computer program NCAP should be used to calculate the second-order transfer functions $H_2(f_1,-f_2)$ that characterize demodulation RFI in open-loop op amp circuits. The NCAP calculations would yield interesting information, as a function of RF frequency, on the magnitude of $H_2(f_1,-f_2)$ produced by the fast npn input transistors in the 741 vis'-$\bar{a}$-vis' that produced by the slow pnp input transistors in the LM10 vis'-$\bar{a}$-vis' that produced by the MOSFET input transistors in the CA081 vis'-$\bar{a}$-vis'

that produced by the JFET input transistors in the LF355. This information, which can be obtained quite easily, and manufacturers' data on the typical gain-bandwidth product for the linear voltage gain might be sufficient to explain the relative magnitudes of the demodulation RFI observed in the four different op amp types and other experimental observations.

(4) Additional NCAP Simulations In Which Parasitic Effects Are Accounted For More Thoroughly

It would be desirable to model more completely the external circuit wiring on the printed circuit board to account for small capacitances from wire to wire and wire to ground. It would also be desirable to model the external circuit component parasitics. Of particular importance are parasitic effects in the op amp input resitor R1, the feedback resistor R2, and the RFI suppression capacitors. The results obtained in this dissertation suggest that parasitic effects caused by the capacitance of reverse-biased isolation junctions inside the op amp may not require the addition of extra capacitors to the standard op amp macromodel. Additional investigation of this topic is suggested.

(5) Additional Sensitivity Analysis

Sensitivity analyses have been performed for the 741 bipolar op amp and LF355 JFET-bipolar op amp. A similar sensitivity analysis for the CA081 MOS-bipolar op amp is recommended. The sensitivity analysis will indicate the linear macromodel parameters and the MOSFET input transistor model parameters whose variations cause the largest variations in the RFI demodulation response in an op amp circuit such as the unity gain buffer circuit. The MOSFET model developed for NCAP by K. N. Chen[4,5,30] should be used.

(6) Experimental Investigation On Variations Of Transistor And Integrated Circuit Parameters

The sensitivity analysis described in this dissertation provides interesting information on the critical parameters in op amp macromodels for producing RFI demodulation effects in op amp circuits. What is needed are experimental results on variations of transistor and integrated circuit parameters observed in practice. Possibly manufacturers of integrated circuits would be willing to provide some information on the mean value and standard deviation of selected parameters which they routinely monitor. Other transistor and integrated circuit parameters required to predict RFI would have to be measured to determine mean values and standard deviations. This would be a worthwhile investigation to initiate.

APPENDIX A

NCAP INPUT DATA

This appendix contains three listings of NCAP input data. Table A1 is a listing of input data for a μA741 op amp unity gain buffer amplifier. The listing in Table A1 corresponds to the circuit shown in Fig. 6-1. The RF frequency f_1 was varied over the frequency range 1.0E5 to 500E6 (0.1 to 500 MHz) by using the MODIFY command. The frequency f_2 was set at $f_2 = -(f_1 - 1E3)$. The responses at nodes 12 and 13 in Fig. 6-1 were printed.

Table A2 is a listing of input data for a LF355 op amp unity gain buffer. The listing in Table A2 corresponds to the circuit shown in Fig. 6-5. The RF frequencies f_1 and f_2 were varied in the manner described for Table A1. The responses at nodes 12 and 13 in Fig. 6-5 were printed.

Table A3 is a listing of input data for the 3-stage μA741 op amp LED circuit. The listing in Table A3 corresponds to the circuit shown in Fig. 6-12. The RF frequencies f_1 and f_2 were varied in the manner described for Table A1. The responses at nodes 17 and 42 in Fig. 6-12 were printed.

TABLE A1

NCAP INPUT DATA LISTING FOR A 741 UNITY GAIN BUFFER

```
** FILE NAME: S741A
** UA741C UNITY GAIN AMPLIFIER
** RECALCULATED PARAMETERS BASED ON UA741
** DATE: OCT. 31 1983
* START CIRCUIT
* GENERATOR
NODE 14 0
FR 1 0.15E6
AMP 1.0 0.0
FR 2 -0.149E6
AMP 1.0 0.0
IMP 50 0
* MODIFY
FR 1 1.5E6
FR 2 -1.499E6
* MODIFY
FR 1 15E6
FR 2 -14.999E6
* MODIFY
FR 1 150E6
FR 2 -149.999E6
* MODIFY
FR 1 0.3E6
FR 2 -0.299E6
* MODIFY
FR 1 3E6
FR 2 -2.999E6
* MODIFY
FR 1 30E6
FR 2 -29.999E6
* MODIFY
FR 1 0.1E6
FR 2 -0.099E6
* MODIFY
FR 1 0.2E6 1E6 5 LIN
FR 2 -0.199E6 -0.999E6 5 LIN
* MODIFY
FR 1 2E6 10E6 5 LIN
FR 2 -1.999E6 -9.999E6 5 LIN
* MODIFY
FR 1 20E6 100E6 5 LIN
FR 2 -19.999E6 -99.999E6 5 LIN
* MODIFY
FR 1 200E6 500E6 4 LIN
FR 2 -199.999E6 -499.999E6 4 LIN
* LINEAR COMPONENTS
R 14 0 50
```

TABLE A1
PART 2 OF 2

```
R 14 1 700
R 7 0 5.3E3
R 3 0 5.3E3
R 8 9 2.05E3
R 4 9 2.05E3
R 9 0 11.2E6
R 10 0 100E3
R 11 0 65
R 11 13 10
R 13 12 31E3
R 5 13 687
R 12 0 31.1E3
C 7 3 2.38E-12
C 9 0 3.13E-12
C 10 11 30E-12
C 12 0 3500E-12
* TRANSISTOR
NODE 5
4.34 14.57 20.0 0.165 7.95E-6 500E-6
1.09 400.0 1.23E-12 1.091 1.23E-12 9.09E-9
830. 5.33E6 0.1E-12 0.1E-12
* TRANSISTOR
NODE 1
4.34 14.57 20.0 0.165 7.95E-6 500E-6
0.779 400.0 1.23E-12 1.091 1.23E-12 8.09E-9
830. 5.33E6 0.1E-12 0.1E-12
* LINEAR DEPENDENT SOURCE
NODE 7 3 0 10
VC 189E-6 0.0
* LINEAR DEPENDENT SOURCE
NODE 9 0 10 0
VC 5.97E-9 0.0
* LINEAR DEPENDENT SOURCE
NODE 10 0 0 11
VC 163.0 0.0
* PRINT SELECT
NODE 12 13
* END CIRCUIT
* END
```

TABLE A2

NCAP INPUT DATA LISTING FOR A LF355 UNITY GAIN BUFFER

```
** FILE NAME: LF355
** MACROMODEL OF LF355 BIFET OP AMP
** ANALYSED BY NCAP FOR H2
** SUBMITTED AT SUNYAB
* START CIRCUIT
* GENERATOR
NODE 1 0
FR 1 0.15E6
AMP 1.0 0.0
FR 2 -0.149E6
AMP 1.0 0.0
IMP 50 0
* MODIFY
FR 1 1.5E6
FR 2 -1.499E6
* MODIFY
FR 1 15E6
FR 2 -14.999E6
* MODIFY
FR 1 150E6
FR 2 -149.999E6
* MODIFY
FR 1 0.3E6
FR 2 -0.299E6
* MODIFY
FR 1 3E6
FR 2 -2.999E6
* MODIFY
FR 1 30E6
FR 2 -29.999E6
* MODIFY
FR 1 0.1E6
FR 2 -0.099E6
* MODIFY
FR 1 0.2E6 1E6 5 LIN
FR 2 -0.199E6 -0.999E6 5 LIN
* MODIFY
FR 1 2E6 10E6 5 LIN
FR 2 -1.999E6 -9.999E6 5 LIN
* MODIFY
FR 1 20E6 100E6 5 LIN
FR 2 -19.999E6 -99.999E6 5 LIN
* MODIFY
FR 1 200E6 500E6 4 LIN
FR 2 -199.999E6 -499.999E6 4 LIN
* MODIFY
FR 1 2.5E6
FR 2 -2.499E6
```

TABLE A2
PART 2 OF 2

```
* MODIFY
FR 1 1.1E6 1.4E6 4 LIN
FR 2 -1.099E6 -1.399E6 4 LIN
* MODIFY
FR 1 1.6E6 1.9E6 4 LIN
FR 2 -1.599E6 -1.899E6 4 LIN
* MODIFY
FR 1 2.1E6 2.4E6 4 LIN
FR 2 -2.099E6 -2.399E6 4 LIN
* LINEAR COMPONENTS
R 1 6 700.0
R 1 0 50.0
R 3 0 6630.0
R 5 14 481.0
R 7 0 6630.0
R 9 14 481.0
R 10 0 1.0E5
R 11 0 100.0
R 11 12 20.0
R 12 13 31.0E3
R 13 0 31.1E3
R 12 2 687.0
C 3 7 2.4E-12
C 14 0 10.5E-12
C 10 11 10.0E-12
C 13 0 3.5E-9
** INTERELECTRODE PARASITIC CAPACITANCES
C 2 5 5E-12
C 6 9 5E-12
C 2 3 3E-12
C 6 7 3E-12
C 5 3 4E-12
C 9 7 4E-12
* JFET
NODE 2
CONSTANTS 0.87E-12 27.0
AC 371.5E-6 0.53 -1.0 -0.5 -0.293 2.2E-12 0.5 -0.5
* JFET
NODE 6
CONSTANTS 0.87E-12 27.0
AC 371.5E-6 0.53 -1.0 -0.5 -0.293 2.2E-12 0.5 -0.5
* LINEAR DEPENDENT SOURCE
NODE 3 7 0 10
VC 1.51E-4 0.0
* LINEAR DEPENDENT SOURCE
NODE 14 0 10 0
VC 1.51E-9 0.0
* LINEAR DEPENDENT SOURCE
NODE 10 0 0 11
VC 66.3 0.0
* PRINT SELECT
NODE 12 13
* END CIRCUIT
* END
```

TABLE A3

NCAP INPUT DATA LISTING FOR 3-STAGE OP AMP LED CIRCUIT

```
** FILE NAME S741B IN F02WHALEN
** THREE STAGE UA741C OP AMP LED CIRCUIT
** DATE APRIL 10, 1984
* START CIRCUIT
* GENERATOR
NODE 1 0
FR 1 0.15E6
AMP 1.0 0.0
FR 2 -0.149E6
AMP 1.0 0.0
IMP 50 0
* MODIFY
FR 1 1.5E6
FR 2 -1.499E6
* MODIFY
FR 1 15E6
FR 2 -14.999E6
* MODIFY
FR 1 3E6
FR 2 -2.999E6
* MODIFY
FR 1 30E6
FR 2 -29.999E6
* MODIFY
FR 1 0.1E6 1E6 10 LIN
FR 2 -0.099E6 -0.999E6 10 LIN
* MODIFY
FR 1 2E6 10E6 5 LIN
FR 2 -1.999E6 -9.999E6 5 LIN
* MODIFY
FR 1 20E6 100E6 5 LIN
FR 2 -19.999E6 -99.999E6 5 LIN
* MODIFY
FR 1 200E6 400E6 3 LIN
FR 2 -199.999E6 -399.999E6 3 LIN
* LINEAR COMPONENTS
R 2 0 100.0
R 3 0 100.0
R 4 5 10E3
R 5 16 100E3
R 7 0 5.3E3
R 11 0 5.3E3
R 8 13 2.712E3
R 12 13 2.712E3
R 13 0 9.872E6
R 9 0 100E3
R 14 0 100E3
```

TABLE A3
PART 2 OF 3

```
R 15 0 65.0
R 15 16 10.0
R 16 17 4.1E3
R 17 18 1E3
R 20 0 5.3E3
R 24 0 5.3E3
R 21 26 2.712E3
R 25 26 2.712E3
R 26 0 9.872E6
R 22 0 5E3
R 27 0 100E3
R 28 0 65.0
R 28 29 10.0
* LINEAR COMPONENTS
R 18 29 506E3
R 29 0 10E6
R 30 0 10E3
R 36 0 5.3E3
R 32 0 5.3E3
R 37 38 2.712E3
R 33 38 2.712E3
R 38 0 9.872E6
R 39 0 100E3
R 40 0 65.0
R 40 42 10.0
R 42 41 22.0
R 41 0 2.0
R 42 0 333E3
R 34 0 1E3
R 42 34 9.09E3
C 1 2 0.02E-6
C 2 3 0.02E-6
C 3 4 0.02E-6
C 7 11 5.46E-12
C 13 0 2.41E-12
C 14 15 30E-12
C 17 0 0.022E-6
C 20 24 5.46E-12
C 26 0 2.41E-12
C 27 28 30E-12
C 29 30 0.1E-6
C 36 32 5.46E-12
C 38 0 2.41E-12
C 39 40 30E-12
C 5 16 27E-12
C 18 29 27E-12
* TRANSISTOR
NODE 5
4.34 14.57 20.0 0.165 7.95E-6 500E-6
1.09 400. 1.23E-12 1.091 1.23E-12 9.09E-9
830 5.33E6 0.1E-12 0.1E-12
* TRANSISTOR
NODE 9
4.34 14.57 20.0 0.165 7.95E-6 500E-6
```

TABLE A3
PART 3 OF 3

```
0.779 400. 1.23E-12 1.091 1.23E-12 9.09E-9
830. 5.33E6 0.1E-12 0.1E-12
* TRANSISTOR
NODE 18
4.34 14.57 20.0 0.165 7.95E-6 500E-6
1.09 400. 1.23E-12 1.091 1.23E-12 9.09E-9
830. 5.33E6 0.1E-12 0.1E-12
* TRANSISTOR
NODE 22
4.34 14.57 20.0 0.165 7.95E-6 500E-6
0.779 400. 1.23E-12 1.091 1.23E-12 9.09E-9
830. 5.33E6 0.1E-12 0.1E-12
* TRANSISTOR
NODE 34
4.34 14.57 20.0 0.165 7.95E-6 500E-6
1.09 400. 1.23E-12 1.091 1.23E-12 9.09E-9
830. 5.33E6 0.1E-12 0.1E-12
* TRANSISTOR
NODE 30
4.34 14.57 20.0 0.165 7.95E-6 500E-6
0.779 400. 1.23E-12 1.091 1.23E-12 9.09E-9
830. 5.33E6 0.1E-12 0.1E-12
* LINEAR DEPENDENT SOURCE
NODE 7 11 0 14
VC 189E-6 0.0
* LINEAR DEPENDENT SOURCE
NODE 13 0 14 0
VC 5.97E-9 0.0
* LINEAR DEPENDENT SOURCE
NODE 14 0 0 15
VC 163.0 0.0
* LINEAR DEPENDENT SOURCE
NODE 20 24 0 27
VC 189E-6 0.0
* LINEAR DEPENDENT SOURCE
NODE 26 0 27 0
VC 5.97E-9 0.0
* LINEAR DEPENDENT SOURCE
NODE 27 0 0 28
VC 163.0 0.0
* LINEAR DEPENDENT SOURCE
NODE 36 32 0 39
VC 189E-6 0.0
* LINEAR DEPENDENT SOURCE
NODE 38 0 39 0
VC 5.97E-9 0.0
* LINEAR DEPENDENT SOURCE
NODE 39 0 0 40
VC 163.0 0.0
* PRINT SELECT
NODE 17 42
* END CIRCUIT
* END
```

APPENDIX B

MEASURED VALUES OF DEMODULATION RFI RESPONSES OF THE UNITY GAIN BUFFER

Appendix B contains four tables, each with three parts, of experimental results for the unity gain buffer amplifier circuit shown in Fig. 4-7. The four tables contain values for $20\log[H_2(f_1,-f_2)$ in $V^{-1}]$ which were calculated using Eq. (4-11). The values for P_{gen}(dBm) are indicated in each table. Note that H_2 values, when alternate P_{gen} values were used, were indicated by underlining of the H_2 values, enclosing the H_2 values in parenthesis, or enclosing the H_2 values in brackets. Table B1 lists 30 values for H_2 for 741 op amps which are plotted in Fig. 4-14. Table B2 lists 25 values for H_2 for LM10 op amps which are plotted in Fig. 4-15. Table B3 lists 30 values for CA081 op amps which are plotted in Fig. 4-16. Table B4 lists values for 30 LF355 op amps which are plotted in Fig. 4-17. The values for H_2 listed in Tables B1 to B4 were used to calculate the mean values for H_2 plotted in Fig. 4-19 and the standard deviation of H_2 plotted in Fig. 4-20.

TABLE B1 (1 of 3)

EXPERIMENTAL VALUES OF $H_2(f_1,-f_2)$ VS RF FREQUENCY f_1

FOR 30 741 OP AMPS IN UNITY GAIN BUFFER CIRCUIT

f_1	$20\log_{10}[H_2(f_1,-f_2)$ in $V^{-1}]$									
MHZ	#1	#2	#3	#4	#5	#6	#7	#8	#9	#10
0.1	-57.1	-56.3	-55.9	-59.0	-53.0	-55.9	-58.0	-56.3	-56.3	-53.0
0.2	-43.8	-43.1	-41.8	-45.5	-39.3	-43.5	-44.6	-42.8	-43.3	-39.3
0.3	-35.9	-35.3	-33.9	-37.7	-31.1	-35.2	-37.1	-34.8	-35.3	-31.4
0.4	-30.1	-29.9	-30.1	-32.1	-26.0	-29.3	-31.4	-29.4	-29.5	-26.3
0.6	-23.4	-24.6	-30.1	-25.5	-22.8	-24.2	-24.3	-24.0	-23.2	-22.9
0.8	-22.1	-23.8	-32.0	-24.3	-22.0	-23.5	-22.8	-25.3	-22.2	-22.9
1.0	-21.7	-23.8	-31.1	-24.1	-20.8	-22.8	-22.5	-23.5	-21.8	-22.2
1.5	-19.7	-22.5	-22.8	-23.4	-17.3	-19.0	-20.9	-21.8	-19.6	-18.6
2.0	-18.8	-21.1	-19.0	-22.5	-16.7	-18.3	-19.4	-20.6	-18.1	-16.5
3.0	-15.9	-16.8	-15.2	-17.1	-15.1	-16.4	-15.1	-16.9	-15.1	-14.0
4.0	-14.5	-14.7	-12.9	-14.7	-13.6	-14.9	-13.4	-15.0	-13.6	-12.6
6.0	-12.2	-12.8	-10.3	-12.8	-11.3	-12.2	-11.8	-12.5	-11.5	-10.7
8.0	-10.9	-11.1	- 8.8	-11.1	- 9.5	-10.3	-10.3	-10.9	-10.1	- 9.3
10	- 9.7	-10.1	- 7.9	- 9.9	- 9.0	- 9.1	- 9.2	- 9.7	- 9.0	- 8.3
15	- 8.3	- 8.6	- 6.9	- 8.6	- 8.0	- 7.9	- 8.0	- 8.3	- 7.8	- 7.6
20	- 8.3	- 8.6	- 7.1	- 8.6	- 8.0	- 8.0	- 8.1	- 8.1	- 7.6	- 7.7
25	- 8.2	- 8.5	- 7.3	- 8.6	- 8.2	- 7.9	- 8.0	- 8.0	- 7.4	- 7.6
30	- 8.3	- 8.5	- 7.4	- 8.5	- 8.3	- 8.0	- 8.0	- 8.1	- 7.4	- 7.9
35	- 8.6	- 8.8	- 7.9	- 8.8	- 8.8	- 8.0	- 8.3	- 8.5	- 7.7	- 8.3
40	- 9.0	- 9.3	- 8.3	- 9.1	- 9.3	- 8.5	- 8.6	- 8.8	- 8.0	- 8.6
50	- 9.9	-10.1	- 9.0	- 9.9	-10.1	- 9.2	- 9.3	- 9.7	- 8.8	- 9.7
60	-10.9	-11.0	-10.1	-10.7	-11.1	- 9.9	-10.2	-10.6	- 9.7	-10.7
70	-12.0	-12.2	-10.9	-11.3	-11.8	-11.0	-11.0	-11.3	-11.0	-11.9
80	-13.3	-13.7	-12.2	-12.8	-13.3	-12.3	-12.3	-12.8	-12.2	-13.2
90	-14.3	-14.6	-13.3	-13.7	-14.4	-13.3	-13.5	-13.8	-13.2	-14.3
100	-15.9	-16.0	-14.8	-15.2	-15.9	-14.9	-14.9	-15.2	-14.6	-15.7
150	-20.3	-22.3	-21.0	-21.3	-22.1	-20.7	-21.0	-21.3	-20.4	-22.1
200	-25.9	-27.9	-26.7	-26.9	-27.4	-26.3	-26.3	-26.9	-25.8	-27.3
300	-33.3	-35.2	-34.8	-34.6	-34.7	-33.9	-34.6	-34.3	-33.7	-34.9
400	-38.3	-40.4	-40.0	-40.0	-39.6	-39.0	-39.7	-39.5	-38.7	-39.7

Note: All H_2 values were measured at P_{gen} = -10 dBm.

TABLE B1 (2 of 3)

EXPERIMENTAL VALUES OF $H_2(f_1,-f_2)$ VS RF FREQUENCY f_1
FOR 30 741 OP AMPS IN UNITY GAIN BUFFER CIRCUIT

f_1	$20\log_{10}[H_2(f_1,-f_2)$ in $V^{-1}]$									
MHz	#31	#32	#33	#34	#35	#41	#42	#43	#44	#45
0.1	-53.9	-51.8	-54.9	-53.0	-51.1	-53.5	-47.4	-49.0	-42.2	-43.9
0.2	-43.0	-42.5	-41.9	-43.0	-42.6	-40.7	-41.4	-40.4	-38.4	-39.2
0.3	-35.4	-35.8	-34.7	-35.8	-35.4	-33.5	-34.1	-33.2	-32.4	-32.5
0.4	-30.5	-30.5	-29.6	-31.0	-31.0	-28.5	-29.0	-27.7	-27.4	-27.0
0.6	-22.0	-22.8	-21.3	-22.2	-23.0	-20.7	-21.3	-19.0	-20.1	-18.4
0.8	-17.0	-18.2	-16.1	-17.2	-17.9	-16.0	-16.8	-14.2	-16.2	-13.8
1.0	-13.6	-15.0	-12.9	-13.8	-14.4	-13.3	-14.2	-11.3	-14.2	-11.1
1.5	-10.3	-11.4	-10.0	-10.4	-10.1	-11.1	-11.8	- 8.5	-12.9	- 9.1
2.0	-11.1	-10.9	-10.9	-11.1	- 9.7	-11.4	-12.4	- 8.8	-13.5	- 9.7
3.0	-11.6	-10.7	-11.3	-11.5	- 9.8	-11.1	-12.0	- 8.8	-12.6	- 9.8
4.0	-11.3	-10.4	-11.0	-11.2	- 9.8	-10.4	-11.5	- 8.6	-11.5	- 9.3
6.0	-10.4	- 9.7	-10.1	-10.3	- 9.4	- 9.1	-10.1	- 7.8	-10.0	- 8.4
8.0	- 9.8	- 9.3	- 9.5	- 9.6	- 9.0	- 8.3	- 9.4	- 7.4	- 9.3	- 8.0
10	- 9.4	- 8.9	- 9.1	- 9.0	- 8.8	- 7.8	- 9.0	- 7.0	- 8.8	- 7.7
15	- 8.8	- 8.5	- 8.6	- 8.4	- 8.3	- 7.1	- 8.1	- 6.4	- 7.5	- 6.9
20	- 9.3	- 9.4	- 9.0	- 9.1	- 9.0	- 7.1	- 8.4	- 6.9	- 7.8	- 7.4
25	- 9.5	- 9.6	- 9.3	- 9.2	-10.1	- 7.4	-	- 7.2	- 8.2	- 7.8
30	- 9.9	- 9.9	- 9.8	- 9.7	-10.5	- 7.9	-	- 7.8	- 8.7	- 8.4
35	-10.5	-10.4	-10.4	-10.3	-10.9	- 8.5	-	- 8.4	- 9.3	- 9.0
40	-11.3	-11.1	-11.2	-11.0	-11.5	- 9.1	-10.4	- 9.2	-10.0	- 9.8
50	-12.6	-12.4	-12.6	-12.4	-12.8	-10.4	-12.0	-10.5	-11.4	-11.2
60	-14.1	-13.9	-14.2	-13.9	-14.2	-11.8	-13.5	-12.0	-12.9	-12.6
70	-15.1	-15.0	-15.4	-15.6	-15.2	-13.6	-15.4	-13.6	-14.6	-14.2
80	-16.9	-16.9	-17.2	-17.6	-17.2	-15.2	-17.1	-15.4	-16.4	-16.2
90	-18.5	-18.4	-18.8	-19.2	-18.7	-16.5	-18.7	-16.6	-17.8	-17.5
100	-20.0	-20.0	-20.3	-20.0	-20.1	-18.2	-20.1	-18.5	-19.5	-19.2
150	-26.9	-26.9	-27.4	-27.6	-27.2	-23.3	-27.0	-25.6	-26.3	-26.1
200	-33.0	-32.4	-32.9	-32.9	-32.8	-30.7	-33.2	-31.6	-32.1	-32.5
300	-40.9	-41.2	-41.3	-41.2	-40.6	-37.4	-41.1	-40.1	-38.9	-40.7
400	-45.4	-45.0	-45.6	-45.0	-45.4	-39.8	-45.5	-44.9	-42.2	-43.0

Note: All H_2 values were measured at P_{gen} = - 10 dBm except that underlined H_2 values were measured at P_{gen} = -5 dBm.

TABLE B1 (3 of 3)

EXPERIMENTAL VALUES OF $H_2(f_1,-f_2)$ VS RF FREQUENCY f_1
FOR 30 741 OP AMPS IN UNITY GAIN BUFFER CIRCUIT

f_1	$20\log_{10}[H_2(f_1,-f_2)$ in $V^{-1}]$									
MHZ	#51	#52	#53	#54	#55	#56	#57	#58	#59	#60
0.1	-55.5	-54.2	-53.0	-50.9	-51.8	-51.1	-54.8	-54.2	-50.3	-57.5
0.2	-41.7	-40.6	-39.4	-37.5	-38.3	-37.7	-42.0	-40.7	-37.5	-44.0
0.3	-33.5	-32.4	-31.1	-28.8	-29.9	-30.3	-33.9	-32.6	-30.9	-36.3
0.4	-27.7	-26.5	-25.3	-23.1	-24.0	-26.9	-28.2	-27.1	-28.6	-30.1
0.6	-22.4	-20.7	-19.8	-18.2	-18.7	-26.0	-23.2	-23.2	-30.1	-22.9
0.8	-21.6	-19.8	-18.8	-17.1	-17.5	-26.9	-22.9	-23.1	-32.8	-21.2
1.0	-20.6	-18.9	-18.1	-16.3	-16.5	-26.9	-22.4	-22.5	-33.6	-20.5
1.5	-17.6	-16.3	-15.7	-14.0	-14.2	-22.6	-19.1	-18.8	-25.2	-19.1
2.0	-16.5	-15.5	-15.0	-13.9	-14.2	-18.5	-17.5	-17.0	-18.8	-18.8
3.0	-14.7	-13.9	-13.4	-12.2	-12.9	-14.2	-15.0	-14.7	-14.1	-16.7
4.0	-13.3	-12.5	-12.0	-11.1	-11.7	-12.4	-13.5	-13.3	-12.4	-15.2
6.0	-11.2	-10.7	-10.3	- 9.3	- 9.7	-10.5	-11.3	-11.3	-10.3	-13.1
8.0	- 9.7	- 9.3	- 9.0	- 8.2	- 8.5	- 9.0	- 9.8	- 9.9	- 9.1	-11.3
10	- 9.0	- 8.5	- 8.0	- 7.4	- 7.7	- 8.6	- 8.7	- 9.0	- 8.3	-10.1
15	- 7.9	- 7.1	- 7.4	- 6.6	- 6.9	- 7.8	- 7.6	- 7.9	- 7.7	- 8.5
20	- 7.7	- 7.3	- 7.3	- 6.7	- 6.9	- 8.0	- 7.6	- 7.7	- 7.7	- 8.2
25	- 7.7	- 7.3	- 7.1	- 6.7	- 6.9	- 8.1	- 7.5	- 7.6	- 8.0	- 8.1
30	- 7.9	- 7.3	- 7.4	- 6.9	- 7.1	- 8.5	- 7.7	- 7.9	- 8.2	- 7.7
35	- 8.0	- 7.6	- 7.7	- 7.3	- 7.4	- 8.9	- 8.0	- 8.2	- 8.6	- 8.3
40	- 8.5	- 7.9	- 8.2	- 7.7	- 7.9	- 9.2	- 8.5	- 8.6	- 9.1	- 8.6
50	- 9.3	- 8.6	- 9.0	- 8.5	- 8.6	-10.1	- 9.3	- 9.5	-10.1	- 9.5
60	-10.1	- 9.5	- 9.9	- 9.3	- 9.5	-11.2	-10.3	-10.3	-11.2	-10.5
70	-10.9	-10.1	-10.8	-10.5	-10.5	-12.3	-11.4	-11.4	-12.0	-11.2
80	-12.2	-11.5	-12.1	-11.7	-11.8	-13.9	-12.7	-12.9	-13.5	-12.6
90	-13.4	-12.6	-13.3	-12.9	-12.9	-15.0	-13.9	-13.9	-14.7	-13.6
100	-14.8	-14.1	-14.7	-14.3	-14.3	-16.5	-15.4	-15.4	-16.0	-15.0
150	-20.7	-20.1	-20.8	-20.4	-20.4	-22.6	-21.5	-21.3	-22.0	-21.0
200	-26.2	-26.1	-26.2	-26.1	-25.9	-27.6	-26.6	-26.6	-27.4	-26.1
300	-33.9	-33.9	-34.2	-34.2	-34.2	-35.5	-34.8	-34.5	-35.2	-34.2
400	-39.0	-39.0	-39.6	-39.8	-39.9	-40.0	-39.4	-39.3	-39.6	-39.0

Note: All H_2 values were measured at P_{gen} = -10 dBm.

TABLE B2 (1 of 3)

EXPERIMENTAL VALUES OF $H_2(f_1,-f_2)$ VS RF FREQUENCY f_1
FOR 25 LM10 OP AMPS IN UNITY GAIN BUFFER CIRCUIT

f_1	$20\log_{10}[H_2(f_1,-f_2)$ in $V^{-1}]$									
MHZ	#1	#2	#3	#4	#5	#6	#7	#8	#9	#10
0.1	- 7.1	-25.7	-25.0	-26.9	-31.6	-34.3	-24.8	-31.4	-32.0	0.4
0.2	- 6.9	-25.6	-24.7	-26.3	-31.4	-33.9	-24.7	-30.7	-31.9	0.4
0.3	- 7.0	-26.3	-25.3	-27.2	-32.9	-36.1	-25.6	-32.2	-33.3	0.2
0.4	- 7.1	-26.9	-25.9	-27.7	-34.4	-38.8	-26.3	-33.6	-35.2	0.2
0.6	- 6.7	-24.2	-23.7	-25.3	-29.2	-31.5	-23.5	-28.7	-29.9	0.2
0.8	- 6.7	-22.7	-22.6	-23.9	-25.9	-28.0	-21.5	-26.6	-26.9	0.1
1.0	- 6.7	-20.4	-20.5	-21.5	-22.0	-23.8	-18.9	-23.4	-22.9	0.0
1.5	- 6.0	-15.0	-15.4	-15.5	-15.4	-16.0	-13.6	-16.1	-15.9	0.0
2.0	- 5.9	-12.5	-12.6	-12.6	-12.4	-12.6	-11.2	-12.9	-12.9	- 0.6
3.0	- 5.4	-10.2	- 9.8	- 9.7	- 9.8	- 9.9	- 9.2	- 9.9	-10.1	- 1.0
4.0	- 5.5	- 9.4	- 8.9	- 8.6	- 9.0	- 9.0	- 8.6	- 8.9	- 9.2	- 1.3
6.0	- 6.2	- 9.8	- 9.1	- 8.6	- 8.8	- 9.1	- 9.0	- 8.8	- 9.6	- 1.9
8.0	- 7.1	-10.5	- 9.9	- 9.4	- 9.7	- 9.9	-10.0	- 9.6	-10.2	- 2.9
10	- 8.1	-11.6	-11.0	-10.3	-10.6	-11.0	-11.1	-10.5	-11.3	- 3.7
15	-11.0	-14.4	-13.8	-13.2	-13.5	-14.1	-14.2	-13.3	-15.0	- 6.0
20	-14.4	-17.8	-17.1	-17.1	-17.0	-17.3	-17.4	-16.5	-18.6	- 8.6
25	-17.0	-20.1	-19.4	-19.6	-19.2	-19.6	-19.9	-18.8	-21.4	-11.0
30	-19.5	-22.2	-21.6	-21.9	-21.6	-22.0	-22.4	-21.3	-23.9	-13.3
35	-21.6	-24.2	-23.6	-24.1	-23.6	-24.1	-24.5	-23.4	-26.2	-15.7
40	-23.5	-26.4	-25.6	-26.1	-25.7	-26.2	-26.7	-25.4	-28.2	-17.6
50	-27.0	-29.9	-29.0	-29.6	-29.2	-29.9	-30.5	-28.8	-31.9	-21.4
60	-30.3	-33.0	-32.1	-32.9	-32.1	-33.9	-33.9	-32.2	-35.2	-25.2
70	-33.5	-37.2	-36.4	-35.0	-35.8	-36.3	-36.9	-35.1	-37.9	-28.8
80	-36.2	-39.8	-38.7	-37.4	-38.4	-39.5	-40.0	-38.1	-41.1	-32.2
90	-37.9	-43.4	-39.8	-38.4	-40.1	-42.0	-42.7	-40.6	-43.6	-34.6
100	-40.1	-46.1	-44.9	-43.0	-43.0	-45.3	-45.7	-43.6	-46.3	-37.6
150	-50.1	-56.1	-55.5	-53.9	-53.0	-56.3	-56.8	-53.9	-57.5	-49.1
200	-52.2	-61.0	-	-57.4	-56.1	-63.1	-63.7	-61.7	-64.2	-56.4
300	-	-	-		-	-70.3	-75.2	-74.2	-76.7	-66.2
400	-	-	-	-	-	-77.5	-79.6	-78.0	-79.6	-

Note: All H_2 values were measured at P_{gen} = - 10 dBm except that underlined H_2 values were measured at P_{gen} = - 5 dBm.

TABLE B2 (2 of 3)

EXPERIMENTAL VALUES OF $H_2(f_1,-f_2)$ VS RF FREQUENCY f_1
FOR 25 LM10 OP AMPS IN UNITY GAIN BUFFER CIRCUIT

f_1	$20\log_{10}[H_2(f_1,-f_2)$ in $V^{-1}]$									
MHz	#11	#12	#13	#14	#15	#16	#17	#18	#19	#21
0.1	(-29.9)	(-30.5)	(-23.0)	(-24.9)	(-26.1)	-27.0	-25.9	-25.5	-28.0	-23.8
0.2	(-27.4)	(-27.3)	(-20.5)	(-21.9)	(-23.7)	-26.6	-25.6	-25.3	-27.4	-23.7
0.3	(-27.4)	(-27.2)	(-20.5)	(-21.5)	(-23.2)	-27.4	-26.5	-26.0	-28.3	-24.3
0.4	(-29.0)	(-27.7)	(-21.6)	(-21.9)	(-23.2)	-28.1	-26.9	-26.7	-29.0	-25.2
0.6	(-28.2)	(-27.4)	(-22.0)	(-22.6)	(-22.7)	-25.5	-24.6	-23.8	-25.7	-22.1
0.8	(-28.2)	(-27.4)	(-21.6)	(-23.0)	(-23.2)	-24.2	-23.5	-22.0	-24.6	-20.2
1.0	(-25.5)	(-25.3)	(-20.0)	(-22.0)	(-22.7)	-22.0	-21.4	-19.7	-22.6	-17.8
1.5	(-19.8)	(-19.0)	(-16.0)	(-18.3)	(-18.8)	-15.9	-15.8	-14.4	-16.4	-13.1
2.0	(-16.4)	(-15.6)	(-13.6)	(-15.6)	(-15.6)	-12.8	-12.8	-11.8	-13.3	-11.0
3.0	(-13.9)	(-12.4)	(-11.3)	(-12.9)	(-12.2)	- 9.9	-10.1	- 9.5	-10.3	- 9.3
4.0	(-13.0)	(-11.1)	(-10-4)	(-11.8)	(-10.9)	- 8.6	- 9.3	- 8.8	- 9.3	- 9.0
6.0	(-13.0)	(-10.9)	(-10.9)	(-12.0)	(-10.4)	- 8.5	- 9.3	- 9.0	- 9.0	-10.3
8.0	(-13.6)	(-11.6)	(-12.0)	(-13.0)	(-11.2)	- 9.1	-10.1	- 9.9	- 9.7	-11.3
10	(-14.2)	(-12.8)	(-13.3)	(-14.2)	(-12.2)	-10.1	-11.3	-11.1	-10.5	-12.8
15	(-16.0)	(-15.2)	(-16.2)	(-16.8)	(-14.9)	-13.0	-14.7	-14.5	-13.3	-17.3
20	(-18.7)	(-18.4)	(-19.5)	(-20.1)	(-18.5)	-16.1	-18.1	-17.7	-16.3	-20.9
25	(-21.1)	(-20.7)	(-21.6)	(-22.6)	(-20.9)	-18.6	-20.8	-20.4	-18.7	-23.7
30	(-23.0)	(-22.6)	(-23.9)	(-23.9)	(-23.1)	-20.9	-23.2	-22.7	-20.9	-26.3
35	(-24.9)	(-24.4)	(-25.9)	(-26.1)	(-25.0)	-23.2	-25.5	-25.0	-23.0	-28.6
40	(-26.7)	(-26.7)	(-27.7)	(-27.7)	(-27.0)	-25.2	-27.5	-27.0	-25.0	-30.7
50	(-29.9)	(-29.0)	(-31.0)	(-30.5)	(-30.3)	-28.8	-31.1	-30.5	-28.5	-34.2
60	(-33.5)	(-31.4)	(-33.5)	(-32.4)	(-32.9)	-32.2	-34.4	-33.9	-31.8	-37.5
70	-36.4	-35.6	-37.2	-37.5	-36.8	-35.2	-37.3	-36.8	-34.8	-40.6
80	-39.5	-38.7	-40.4	-40.5	-39.7	-38.3	-40.4	-39.8	-37.8	-43.7
90	-42.6	-41.9	-43.0	-43.2	-42.7	-41.0	-43.1	-42.6	-40.3	-46.5
100	-45.0	-44.4	-45.5	-45.7	-45.3	-43.7	-45.9	-45.5	-43.5	-49.5
150	-54.4	-52.9	-52.6	-54.1	-52.6	-55.3	-56.7	-55.9	-53.9	-59.4
200	-58.4	-55.8	-56.6	-55.4	-54.7	-62.3	-64.2	-63.1	-61.0	66.2
300	-59.5	-57.0	-57.4	-57.4	-57.9	-74.2	-76.3	-74.8	-72.2	79.6
400	-60.1	-58.4	-57.9	-57.4	-58.4	-77.5	-80.2	-78.5	-77.5	-79.6

Note: H_2 values in parenthesis were measured at P_{gen} = - 20 dBm. All other values were measured at P_{gen} = - 10 dBm.

TABLE B2 (3 of 3)

EXPERIMENTAL VALUES OF $H_2(f_1,-f_2)$ VS RF FREQUENCY f_1
FOR 25 LM10 OP AMPS IN UNITY GAIN BUFFER CIRCUIT

f_1	$20\log_{10}[H_2(f_1,-f_2)$ in $V^{-1}]$				
MHz	#26	#27	#28	#29	#30
0.1	-33.4	-35.0	-35.0	-22.2	-34.1
0.2	-33.7	-35.7	-34.8	-22.3	-34.6
0.3	-36.3	-38.8	-37.5	-22.9	-37.3
0.4	-40.0	-43.9	-40.8	-23.6	-41.1
0.6	-32.8	-32.4	-33.3	-21.8	-33.3
0.8	-29.3	-27.4	-30.9	-21.1	-29.1
1.0	-24.8	-23.0	-26.7	-19.3	-24.3
1.5	-16.8	-15.4	-18.3	-14.3	-16.2
2.0	-13.4	-12.4	-14.6	-11.6	-12.7
3.0	-10.5	- 9.8	-11.5	- 9.1	- 9.8
4.0	- 9.8	- 9.1	-10.5	- 8.5	- 8.8
6.0	-10.3	- 9.5	-10.7	- 9.0	- 9.1
8.0	-11.2	-10.7	-11.9	- 9.5	- 9.9
10	-12.4	-12.1	-13.0	-10.7	-11.2
15	-16.1	-16.1	-16.0	-14.6	-14.8
20	-19.1	-20.1	19.1	-17.8	-18.4
25	-21.6	-23.1	-21.5	-20.8	-21.1
30	-23.9	-25.7	-23.5	-23.0	-23.4
35	-26.0	-28.2	-25.4	-25.4	-25.9
40	-28.0	-30.0	-27.4	-27.3	-27.7
50	-31.4	-33.5	-30.9	-30.9	-31.3
60	-34.7	-36.8	-34.2	-33.9	-34.5
70	-37.8	-39.8	-37.2	-36.8	-37.4
80	-41.1	-42.8	-40.3	-40.0	-40.4
90	-43.5	-45.5	-43.0	-42.6	-42.8
100	-46.7	-48.5	-45.9	-45.6	-46.1
150	-57.5	-59.0	-56.7	-55.9	-56.7
200	-64.8	-66.5	-64.4	-63.5	-63.8
300	-77.1	-77.1	-78.5	-77.1	-77.1
400	-83.1	-81.5	-80.2	-79.6	-80.2

Note: All H_2 values were measured at P_{gen} = - 10 dBm.

TABLE B3 (1 of 3)

EXPERIMENTAL VALUES OF $H_2(f_1,-f_2)$ VS RF FREQUENCY f_1
FOR 30 CA081 OP AMPS IN UNITY GAIN BUFFER CIRCUIT

f_1	$20\log_{10}[H_2(f_1,-f_2)$ in $V^{-1}]$									
MHz	#1	#2	#3	#4	#5	#6	#7	#8	#9	#10
0.1	-77.9	-77.6	-78.2	-77.9	[-84.2]	-78.2	-78.2	-78.2	-78.3	-77.3
0.2	-76.7	-75.5	-77.3	-75.7	[-72.4]	-77.9	-76.7	-76.7	-78.2	-76.0
0.3	-70.3	-68.5	-70.4	-68.9	(-65.4)	-71.1	-70.0	-70.2	-71.0	-69.3
0.4	-65.3	-63.6	-65.3	-63.9	(-61.1)	-66.2	-65.0	-65.0	-66.0	-64.5
0.6	-57.6	-55.7	-57.9	-56.2	(-53.1)	-58.2	-57.0	-57.0	-58.2	-56.7
0.8	-51.8	-49.8	-51.8	-50.8	-45.4	-52.5	-50.8	-51.3	-52.5	-51.3
1.0	-46.4	-44.6	-45.6	-45.7	-42.9	-46.4	-45.4	-45.4	-46.3	-46.4
1.5	-42.5	-41.3	-42.8	-41.4	-39.2	-43.4	-42.6	-42.4	-43.3	-41.5
2.0	-39.3	-38.0	-39.5	-38.0	-36.2	-40.1	-39.3	-39.0	-39.8	-38.0
3.0	-35.1	-34.0	-35.0	-34.1	-33.2	-35.3	-34.8	-34.3	-35.1	-34.1
4.0	-33.3	-32.4	-32.9	-32.4	-32.0	-32.9	-32.7	-32.4	-32.7	-32.2
6.0	-32.6	-32.1	-31.9	-32.2	-32.0	-33.0	-32.1	-31.9	-31.7	-31.8
8.0	-33.2	-32.7	-32.4	-32.9	-32.5	-32.7	-32.5	-32.6	-31.9	-32.4
10	-33.4	-33.0	-32.7	-33.1	-32.5	-32.3	-32.8	-32.9	-32.8	-32.7
15	-33.7	-33.2	-33.1	-33.3	-32.4	-31.7	-32.9	-33.0	-33.1	-32.9
20	-34.4	-33.9	-33.6	-34.0	-32.3	-33.7	-33.5	-33.8	-33.8	-33.4
25	-35.0	-34.3	-33.9	-34.6	-34.1	-34.0	-33.8	-34.2	-34.0	-34.0
30	-35.9	-35.7	-34.7	-35.6	-35.3	-34.7	-34.7	-35.2	-34.7	-34.8
35	-38.0	-37.7	-36.2	-37.1	-36.5	-36.6	-36.1	-36.6	-36.1	-36.3
40	-38.3	-37.9	-37.0	-38.0	-37.7	-37.1	-37.0	-37.4	-37.0	-37.1
50	-39.9	-39.3	-38.5	-39.3	-39.4	-38.6	-38.3	-39.0	-38.3	-38.5
60	-42.8	-42.5	-40.7	-41.5	-41.0	-41.1	-40.1	-40.7	-40.1	-40.5
70	-44.1	-42.7	-42.3	-43.7	-42.9	-42.3	-42.3	-43.2	-42.3	-43.2
80	-46.1	-45.7	-44.4	-45.7	-44.7	-44.3	-44.4	-45.2	-44.4	-45.2
90	-47.5	-47.0	-45.9	-47.3	-46.6	-45.7	-45.7	-46.8	-46.0	-46.8
100	-49.4	-48.8	-47.5	-49.3	-47.4	-47.6	-47.7	-48.7	-47,8	-48.8
150	-57.9	-57.9	-56.3	-56.3	<u>-54.9</u>	-54.6	-54.6	-55.5	-54.7	-56.0
200	-61.3	-60.7	-59.3	-60.5	<u>-58.4</u>	-59.3	-59.3	-59.9	-59.1	-60.3
300	-68.5	-67.8	-66.4	-67.6	<u>-62.2</u>	-66.1	-66.8	-67.1	-66.6	-67.7
400	-70.3	-69.8	-68.7	-70.3	-	-69.0	-69.1	-70.0	-69.5	-70.0

Note: Underlined H_2 values were measured at P_{gen} = 0 dBm. H_2 values in parenthesis were measured at P_{gen} = 5 dBm. H_2 values in brackets were measured at P_{gen} = 15 dBm. All other H_2 values were measured at P_{gen} = - 5 dBm.

TABLE B3 (2 of 3)

EXPERIMENTAL VALUES OF $H_2(f_1,-f_2)$ VS RF FREQUENCY f_1
FOR 30 CA081 OP AMPS IN UNITY GAIN BUFFER CIRCUIT

f_1	$20\log_{10}[H_2(f_1,-f_2)$ in $V^{-1}]$									
MHz	#11	#12	#13	#14	#15	#16	#17	#18	#19	#20
0.1	-77.0	-78.3	-77.6	-77.9	[-86.8]	-77.9	-77.6	-77.9	-77.9	(-81.0)
0.2	-73.5	-77.0	-76.2	-76.5	[-76.7]	-76.7	-77.0	-77.0	-76.7	(-77.4)
0.3	-66.7	-70.1	-69.5	-69.5	(-68.9)	-69.8	-70.4	-70.6	-69.4	(-71.1)
0.4	-61.7	-65.4	-64.6	-65.0	(-64.5)	-65.0	-65.4	-65.4	-64.6	(-66.4)
0.6	-54.0	-57.6	-56.7	-56.7	(-57.3)	-57.0	-57.9	-57.6	-57.0	-58.2
0.8	-48.0	-52.3	-51.5	-51.5	-49.5	-51.3	-52.6	-52.1	-51.8	-53.4
1.0	-43.2	-46.9	-46.7	-45.8	-45.2	-45.1	-47.5	-46.6	-47.3	-48.9
1.5	-39.8	-42.5	-41.3	-42.1	-42.1	-42.1	-42.3	-42.6	-41.4	-43.3
2.0	-36.7	-38.7	-38.3	-38.3	-38.5	-38.8	-38.8	-39.1	-38.0	-39.7
3.0	-33.2	-34.3	-34.1	-33.9	-34.2	-34.1	-34.4	-34.8	-34.3	-35.9
4.0	-31.9	-32.2	-32.2	-31.8	-32.5	-31.9	-32.2	-32.4	-32.5	-33.6
6.0	-31.9	-31.8	-32.1	-31.3	-32.3	-31.3	-31.5	-31.6	-31.8	-32.7
8.0	-32.3	-32.4	-32.7	-31.8	-32.7	-31.8	-32.1	-32.0	-32.5	-33.3
10	-32.3	-32.6	-33.2	-32.0	-33.2	-32.1	-32.3	-32.3	-32.7	-33.7
15	-32-2	-32.6	-33.2	-32.1	-33.1	-32.2	-32.5	-32.6	-32.8	-33.9
20	-32.9	-33.4	-33.8	-32.7	33.9	-32.9	-32.9	-33.4	-33.8	-34.5
25	-33.8	-33.8	-34.4	-33.4	-34.5	-33.3	-33.6	-33.8	-34.0	-34.7
30	-34.8	-34.8	-35.4	-34.3	-35.4	-34.1	-34.6	-34.5	-35.0	-35.6
35	-36.5	-36.3	-37.0	-35.7	-36.3	-35.5	-35.9	-35.9	-36.3	-36.5
40	-37.4	-37.1	-37.9	-36.7	-37.4	-36.6	-36.7	-36.9	-37.3	-37.7
50	-39.0	-38.6	-39.1	-38.3	-39.0	-38.2	-38.3	-38.3	-38.6	39.2
60	-40.9	-40.9	-41.5	-39.9	-40.5	-40.1	-40.1	-39.9	-40.7	-40.5
70	-43.3	-42.6	-43.6	-42.1	-42.4	-42.3	-42.4	-42.2	-42.9	-42.6
80	-45.2	-44.7	-45.7	-44.2	-44.1	-44.6	-44.4	-44.3	-45.0	-44.7
90	-46.9	-46.2	-47.3	-45.7	-45.7	-46.0	-46.0	-45.9	-46.5	-46.6
100	-49.0	-47.8	-49.3	-47.7	-46.8	-48.2	-48.0	-47.5	-48.9	-48.1
150	-55.9	-55.8	-56.2	-54.2	<u>-55.0</u>	-55.2	-54.8	-54.7	-55.4	-54.9
200	-60.1	-59.8	-61.0	-59.1	<u>-59.8</u>	-59.7	-59.5	-59.3	-59.9	-59.0
300	-67.3	-70.7	-68.4	-66.3	<u>-61.4</u>	-67.1	-66.7	-66.5	-66.8	<u>-65.5</u>
400	-70.0	-69.7	-71.8	-69.3	<u>-62.2</u>	-70.6	-69.8	-70.0	-70.6	<u>-68.2</u>

Note: Underlined H_2 values were measured at P_{gen} = 0 dBm. H_2 values in parenthesis were measured at P_{gen} = 5 dBm. H_2 values in brackets were measured at P_{gen} = 15 dBm. All other H_2 values were measured at P_{gen} = -5 dBm.

TABLE B3 (3 of 3)

EXPERIMENTAL VALUES OF $H_2(f_1,-f_2)$ VS RF FREQUENCY f_1
FOR 30 CA081 OP AMPS IN UNITY GAIN BUFFER CIRCUIT

f_1	$20\log_{10}[H_2(f_1,-f_2)]$ in V^{-1}									
MHz	#21	#22	#23	#25	#30	#31	#32	#33	#34	#35
0.1	-78.0	-77.0	-77.9	(-82.1)	(-82.1)	[-86.2]	[-85.8]	[-85.4]	[-87.0]	[-86.2]
0.2	-76.7	-75.3	-76.2	(-78.2)	(-76.7)	[-76.0]	[-76.1]	[-75.9]	[-77.2]	[-75.9]
0.3	-70.3	-69.0	-69.0	(-71.1)	(-70.1)	(-68.4)	(-68.4)	(-67.9)	(-70.1)	(-68.4)
0.4	-65.4	-64.3	-64.1	-59.9	(-65.0)	(-64.1)	(-64.1)	(-64.1)	(-65.4)	(-64.1)
0.6	-57.3	-56.7	-56.2	-56.7	-56.7	(-57.0)	(-56.5)	(-56.7)	(-57.5)	(-56.5)
0.8	-51.8	-51.3	-50.6	-53.0	-51.1	-50.7	-50.1	-48.4	-51.4	-50.7
1.0	-46.1	-46.1	-44.8	-47.4	-45.6	-46.2	-45.4	-46.2	-46.6	-45.0
1.5	-42.5	-41.7	-41.4	-43.6	-42.8	-42.4	-42.4	-41.6	-42.9	-41.9
2.0	-39.1	-38.5	-38.5	-39.6	-39.2	-38.5	-38.7	-38.0	-39.6	-38.4
3.0	-34.6	-34.5	-34.3	-35.2	-34.6	-34.4	-34.4	-34.2	-35.2	-34.0
4.0	-32.5	-32.6	-32.5	-32.7	-32.7	-32.3	-32.4	-32.3	-33.2	-32.0
6.0	-31.7	-32.3	-32.1	-32.0	-32.5	-32.0	-32.3	-31.7	-32.5	-31.6
8.0	-32.3	-32.9	-32.8	-32.7	-33.2	-32.4	-32.8	-32.3	-33.2	-32.3
10	-32.5	-33.1	-33.1	-33.1	-33.3	-32.8	-33.1	-32.6	-33.4	-32.7
15	-32.6	-33.4	-33.4	-33.2	-33.4	-33.1	-33.2	-32.6	-33.6	-32.7
20	-33.2	-34.0	-33.9	-34.2	-34.5	-34.1	-34.1	-33.5	-34.2	-33.4
25	-33.8	-34.5	-34.5	-34.6	-35.0	-34.6	-34.7	-33.9	-34.5	-33.7
30	-34.5	-35.5	-35.6	-35.6	-35.5	-35.7	-35.7	-34.7	-35.5	-34.7
35	-35.9	-37.3	-37.6	-36.5	-36.5	-36.9	-36.9	-35.7	-36.5	-35.9
40	-36.9	-38.2	-38.2	-37.7	-37.7	-38.0	-37.9	-37.0	-37.6	-37.2
50	-38.3	-39.3	-39.5	-39.4	-39.0	-39.6	-39.6	-38.5	-39.4	-38.7
60	-40.1	-41.8	-41.3	-40.5	-40.5	-41.4	-41.2	-39.9	-40.5	-40.5
70	-42.3	-43.4	-44.0	-42.6	-42.9	-43.2	-43.8	-42.4	-43.9	-42.9
80	-44.4	-45.4	-46.1	-44.9	-45.0	-45.8	-45.8	-44.4	-46.0	-45.0
90	-45.9	-47.0	-47.8	-46.4	-46.8	-47.4	-47.9	-45.8	-47.7	-46.6
100	-47.9	-49.0	-50.1	-48.1	-48.4	-48.4	-48.9	-47.9	-49.5	-47.9
150	-55.0	-56.3	-56.6	-54.9	-54.9	-55.8	-56.2	-54.4	-56.0	-55.2
200	-59.0	-60.5	-61.1	-59.9	-59.0	-61.4	-60.7	-59.5	-61.4	-60.1
300	-66.8	-67.1	-68.3	-65.5	-66.1	-67.4	-65.5	-64.4	-66.1	-65.5
400	-70.2	-71.1	-72.5	-68.2	-68.2	-69.0	-69.0	-66.1	-68.2	-68.2

Note: Underlined H_2 values were measured at P_{gen} = 0 dBm. H_2 values in parenthesis were measured at P_{gen} = 5 dBm. H_2 values in brackets were measured at P_{gen} = 15 dBm. All other H_2 values were measured at P_{gen} = -5 dBm.

TABLE B4 (1 of 3)

EXPERIMENTAL VALUES OF $H_2(f_1,-f_2)$ VS RF FREQUENCY f_1

FOR 30 LF355 OP AMPS IN UNITY GAIN BUFFER CIRCUIT

f_1	$20\log_{10}[H_2(f_1,-f_2)$ in $V^{-1}]$									
MHz	#1	#2	#3	#4	#5	#6	#7	#8	#9	#10
0.1	-71.3	-71.7	-76.7	-75.1	(-76.1)	-75.5	-76.5	-75.5	-76.2	(-73.9)
0.2	-60.9	-61.3	-72.5	-67.5	(-70.4)	-67.7	-71.1	-68.0	-71.3	(-63.9)
0.3	-53.9	-54.3	-65.4	-60.5	(-64.2)	-60.9	-64.2	-60.9	-64.5	(-57.0)
0.4	-48.8	-49.2	-60.6	-55.4	(-59.4)	-55.9	-59.1	-55.9	-59.3	-51.8
0.6	-41.5	-42.0	-53.1	-47.8	-51.1	-48.5	-51.7	-48.5	-51.8	-44.4
0.8	-36.6	-36.7	-48.3	-42.9	-46.8	-43.6	-46.7	-43.6	-47.1	-39.4
1.0	-32.7	-33.0	-44.4	-39.1	-42.9	-39.7	-42.9	-39.3	-43.3	-35.9
1.5	-26.5	-26.0	-37.4	-32.9	-36.2	-32.9	-35.9	-32.3	-36.5	-29.1
2.0	-25.6	-23.8	-34.3	-30.8	-32.8	-30.2	-32.6	-29.1	-33.6	-26.0
2.5	-27.4	-23.1	-32.2	-51.2	-	-28.4	-30.3	-27.3	-31.8	-
3.0	-43.6	-25.4	-31.5	-35.3	-29.4	-28.7	-29.4	-27.4	-31.8	-23.9
3.5	-22.5	-48.4	-32.5	-51.7	-	-31.2	-30.1	-30.0	-33.8	-
4.0	-15.5	-22.0	-35.6	-28.9	-31.2	-40.1	-32.9	-43.9	-39.5	-33.3
4.5	-14.5	-16.0	-47.5	-22.2	-35.9	-37.3	-40.9	-28.5	-51.5	-52.6
5.0	-15.6	-14.8	-37.7	-19.3	-51.1	-28.0	-41.3	-20.1	-34.6	-22.5
5.5	-17.7	-15.5	-29.3	-19.2	-34.1	-24.3	-30.5	-15.9	-29.3	-18.8
6.0	-20.3	-17.1	-24.6	-20.4	-27.4	-22.1	-25.8	-14.4	-25.7	-17.2
6.5	-23.6	-19.7	-22.1	-22.5	-	-21.6	-23.4	-15.2	-24.2	-
7.0	-27.1	-22.8	-20.7	-25.0	-22.9	-22.1	-22.3	-16.7	-23.6	-18.5
8.0	-37.9	-30.1	-21.5	-31.8	-22.5	-25.2	-22.9	-21.8	-24.8	-22.0
9.0	-48.7	-43.6	-24.7	-43.0	-24.6	-29.8	-25.7	-28.2	-28.0	-27.1
10.	-38.3	-44.5	-29.7	-50.2	-28.2	-36.6	-30.0	-36.7	-32.6	-33.5
11.	-35.5	-37.7	-35.9	-41.3	-32.6	-48.0	-35.7	-57.6	-38.2	-43.8
12.	-34.4	-35.4	-44.8	-38.5	-38.4	-51.5	-43.7	-44.3	-47.4	-51.4
13.	-33.9	-34.5	-79.9	-37.3	-46.6	-43.6	-69.0	-39.8	-62.0	-41.9
14.	-33.8	-34.2	-48.5	-36.6	-54.9	-40.7	-48.5	-38.0	-47.9	-39.0
15.	-33.8	-34.0	-44.5	-36.3	-48.7	-39.3	-44.2	-37.1	-44.3	-37.4
17.	-33.9	-34.1	-41.3	-36.3	-42.9	-38.3	-41.1	-36.5	-41.7	-36.3
20.	-35.3	-35.3	-40.8	-37.7	-41.5	-38.6	-40.5	-37.3	-41.4	-37.0
25.	-36.7	-36.5	-41.3	-39.0	-41.5	-39.5	-41.0	-38.3	-41.7	-37.9
30.	-38.0	-38.0	-42.2	-40.3	-42.6	-40.5	-41.9	-39.4	-42.9	-39.2
35.	-39.7	-39.7	-43.9	-42.3	-43.6	-42.3	-43.9	-41.4	-45.1	-40.4
40.	-40.5	-40.7	-44.7	-43.1	-44.7	-43.2	-44.4	-42.3	-45.4	-41.6
50.	-42.8	-43.0	-46.9	-45.3	-47.0	-45.3	-46.6	-44.6	-47.5	-43.8
60.	-45.2	-45.2	-49.5	-47.7	-49.2	-48.0	-49.0	-47.4	-51.7	-45.6
70.	-47.3	-47.5	-52.1	-50.4	-51.9	-50.3	-58.0	-49.5	-52.1	-49.3
80.	-49.4	-49.7	-54.2	-52.6	-54.1	-52.5	-60.1	-51.7	-54.2	-51.4
90.	-51.1	-51.3	-55.9	-54.3	-55.4	-54.1	-61.5	-53.3	-55.4	-52.9
100	-53.5	-54.1	-58.5	-56.9	-57.0	-56.7	-64.8	-55.9	-57.1	-55.0
150	-61.1	-61.5	-65.2	-63.9	-61.8	-63.9	-72.0	-63.0	-67.5	-62.2
200	-65.5	-65.6	-69.4	-67.3	-63.4	-68.2	-75.5	-67.4	-68.3	-64.9
300	-75.5	-76.7	-82.0	-75.5	-	-78.5	-87.5	-76.2	-76.5	-71.0
400	-79.5	-77.0	-81.5	-79.5	-	-80.7	-87.5	-79.0	-81.1	-

Note: Underlined H_2 values were measured at P_{gen} = 0 dBm. H_2 values in parenthesis were measured at P_{gen} = 5 dBm. All other H_2 values were measured at P_{gen} = - 5 dBm.

TABLE B4 (2 of 3)

EXPERIMENTAL VALUES OF $H_2(f_1,-f_2)$ VS RF FREQUENCY f_1

FOR 30 LF355 OP AMPS IN UNITY GAIN BUFFER CIRCUIT

f_1	$20\log_{10}[H_2(f_1,-f_2)$ in $V^{-1}]$									
MHz	#11	#12	#13	#14	#15	#16	#17	#18	#20	#25
0.1	-73.7	-76.2	-75.1	-76.5	(-73.9)	-76.7	-71.3	-76.9	(-76.7)	(-72.6)
0.2	-64.8	-70.0	-67.8	-70.2	(-65.6)	-72.6	-61.3	-72.0	(-67.9)	(-68.9)
0.3	-57.9	-63.6	-60.7	-63.6	(-58.8)	-65.9	-54.3	-65.2	(-61.1)	(-63.2)
0.4	-52.8	-58.3	-55.6	-58.5	(-53.4)	-60.5	-49.3	-60.2	(-56.1)	(-58.3)
0.6	-45.5	-50.8	-48.3	-50.8	-46.4	-52.8	-41.8	-52.6	-48.4	-49.2
0.8	-40.5	-46.3	-43.3	-46.0	-41.4	-48.1	-36.9	-47.7	-43.9	-45.6
1.0	-36.7	-42.2	-39.3	-42.3	-37.4	-44.3	-33.0	-43.8	-39.7	-41.6
1.5	-30.1	-35.2	-32.0	-35.3	-30.6	-37.3	-26.8	-36.9	-33.9	-34.9
2.0	-27.8	-32.0	-28.5	-32.5	-27.5	-34.0	-25.0	-33.8	-31.3	-31.9
2.5	-27.9	-29.3	-26.0	-30.1	-	-31.4	-25.5	-31.4	-	-
3.0	-31.4	-28.2	-25.0	-29.5	-26.2	-30.1	-30.2	-30.4	-31.9	-28.7
3.5	-61.5	-28.6	-25.8	-30.8	-29.8	-30.3	-36.7	-31.2	-37.0	-29.7
4.0	-27.6	-30.7	-29.3	-34.3	-53.9	-32.2	-22.2	-33.8	-47.2	-33.0
4.5	-21.3	-37.0	-49.6	-46.7	-24.9	-36.9	-17.6	-40.8	-31.6	-45.4
5.0	-18.6	-41.1	-27.8	-37.3	-18.4	-68.0	-16.6	-43.9	-26.2	-34.2
5.5	-18.2	-29.0	-21.3	-29.4	-	-35.6	-17.4	-32.1	-	-
6.0	-19.0	-23.6	-18.0	-25.1	-15.8	-28.7	-19.3	-26.8	-22.6	-22.6
6.5	-20.7	-20.7	-16.9	-23.4	-	-25.4	-21.8	-24.0	-	-
7.0	-23.3	-19.4	-17.1	-22.5	-19.1	-23.4	-25.1	-22.4	-24.2	-20.2
8.0	-29.3	-20.0	-20.1	-23.4	-24.9	-22.5	-33.8	-22.2	-28.5	-21.9
9.0	-37.9	-22.9	-24.8	-26.4	-32.3	-24.4	-59.5	-24.6	-34.4	-25.4
10.	-69.6	-27.3	-30.8	-30.7	-44.4	-27.7	-40.7	-28.5	-43.8	-30.4
11.	-43.9	-32.3	-39.3	-36.5	-47.0	-32.1	-36.7	-33.4	-57.4	-36.3
12.	-39.7	-38.8	-85.5	-44.5	-40.1	-37.9	-35.1	-39.7	-45.0	-45.4
13.	-38.0	-49.0	-44.0	-76.2	-37.7	-46.3	-34.3	-50.4	-41.5	-52.6
14.	-37.1	-56.2	-39.9	-48.8	-36.6	-75.1	-34.1	-54.6	-40.0	-46.2
15.	-36.9	-46.4	-38.2	-44.4	-36.2	-49.0	-33.9	-46.4	-39.3	-43.3
17.	-36.6	-41.9	-37.0	-41.3	-35.9	-42.9	-34.1	-41.9	-38.7	-40.9
20.	-37.6	-41.1	-37.4	-41.1	-36.9	-41.6	-35.4	-41.0	-39.7	-40.9
25.	-38.6	-41.3	-38.3	-41.4	-38.1	-41.7	-36.6	-41.2	-40.6	-41.4
30.	-40.8	-43.1	-39.5	-42.3	-39.5	-42.9	-37.9	-42.3	-42.0	-42.6
35.	-42.6	-45.3	-41.5	-44.3	-40.6	-45.0	-39.6	-44.6	-43.2	-43.8
40.	-42.8	-45.7	-41.8	-44.8	-42.0	-45.4	-40.3	-45.0	-44.5	-44.4
50.	-45.4	-48.2	-44.2	-46.8	-44.2	-48.0	-42.3	-47.4	-46.8	-46.4
60.	-50.7	-54.0	-46.4	-48.8	-46.2	-50.1	-44.3	-49.6	-48.7	-48.1
70.	-48.9	-51.8	-49.3	-51.7	-48.3	-51.9	-47.1	-51.7	-51.0	-51.2
80.	-51.1	-54.1	-51.5	-53.8	-50.3	-54.0	-49.1	-53.8	-52.9	-53.0
90.	-52.2	-55.7	-53.0	-55.4	-51.9	-55.4	-50.6	-55.3	-54.5	-54.7
100	-54.0	-59.0	-55.4	-58.0	-53.6	-57.6	-52.8	-57.6	-56.2	-56.2
150	-64.2	-66.3	-65.2	-66.4	-58.9	-68.3	-62.2	-68.6	-61.1	-61.1
200	-66.1	-69.7	-66.8	-69.3	-60.7	-69.4	-64.8	-72.0	-62.2	-63.0
300	-73.7	-80.3	-73.5	-78.8	-62.2	-76.0	-71.8	-82.5	-	-
400	-77.0	-80.7	-78.2	-81.5	-63.9	-82.0	-77.3	-83.6	-	-

Note: Underlined H_2 values were measured at P_{gen} = 0 dBm. H_2 values in parenthesis were measured at P_{gen} = 5 dBm. All other H_2 values were measured at P_{gen} = -5 dBm.

TABLE B4 (3 of 3)

EXPERIMENTAL VALUES OF $H_2(f_1,-f_2)$ VS RF FREQUENCY f_1

FOR 30 LF355 OP AMPS IN UNITY GAIN BUFFER CIRCUIT

f_1	$20\log_{10}[H_2(f_1,-f_2)$ in $V^{-1}]$									
MHz	#31	#32	#33	#36	#37	#41	#42	#43	#44	#45
0.1	[-76.8]	(-83.5)	(-77.7)	[-83.4]	[-82.6]	-76.7	-72.8	-75.3	-76.7	-76.7
0.2	(-65.0)	(-76.1)	-67.4	(-73.4)	(-73.0)	-74.4	-63.6	-68.0	-71.3	-70.4
0.3	(-60.5)	(-69.5)	-61.4	-65.5	-65.5	-67.6	-56.9	-61.1	-64.5	-63.9
0.4	(-55.7)	-64.4	-56.4	-63.0	-61.1	-62.1	-51.5	-56.0	-59.3	-58.6
0.6	-55.0	-56.8	-47.9	-53.4	-53.0	-55.3	-44.1	-48.5	-52.0	-51.1
0.8	-43.2	-51.9	-43.5	-50.4	-49.5	-50.2	-39.0	-43.5	-46.9	-46.1
1.0	-39.2	-47.7	-39.9	-46.8	-45.6	-46.4	-35.3	-39.6	-43.0	-42.5
1.5	-33.0	-41.4	-33.1	-40.0	-38.7	-39.0	-28.6	-32.5	-35.9	-35.4
2.0	-30.1	-37.4	-30.0	-35.9	-35.0	-35.2	-26.1	-29.3	-32.1	-32.1
2.5	-	-	-	-32.7	-32.5	-31.9	-25.2	-26.8	-29.3	-29.7
3.0	-29.0	-32.7	-27.4	-30.8	-31.3	-29.8	-26.7	-26.4	-27.6	-28.7
3.5	-31.9	-31.9	-28.5	-29.8	-31.3	-28.7	-33.7	-27.5	-27.2	-29.1
4.0	-42.6	-32.3	-32.0	-29.8	-32.7	-28.5	-33.5	-32.4	-28.0	-31.8
4.5	-32.2	-34.1	-44.1	-30.9	-36.9	-29.5	-23.2	-39.5	-31.0	-39.3
5.0	-23.6	-39.0	-34.9	-34.0	-57.4	-33.3	-19.5	-24.2	-40.3	-41.1
5.5	-19.6	-47.9	-27.7	-42.9	-35.7	-55.3	-18.3	-18.2	-36.6	-30.0
6.0	-17.7	-33.4	-24.1	-38.4	-28.3	-31.0	-18.6	-15.3	-27.3	-25.4
6.5	-	-	-	-29.5	-24.5	-24.6	-20.1	-14.8	-23.0	-23.0
7.0	-19.1	-24.1	-22.6	-25.4	-22.1	-22.2	-22.1	-15.9	-21.0	-22.1
8.0	-23.8	-21.2	-24.4	-22.2	-21.3	-22.1	-27.5	-19.9	-20.5	-22.9
9.0	-30.2	-21.9	-28.1	-23.0	-23.6	-24.7	-35.1	-25.7	-22.9	-26.0
10.	-38.8	-25.6	-33.2	-25.8	-27.7	-28.2	-50.6	-32.9	-26.7	-30.2
11.	-49.5	-30.0	-39.6	-29.6	-32.6	-32.5	-45.0	-45.2	-31.8	-35.9
12.	-44.4	-34.9	-52.2	-34.1	-38.5	-37.7	-39.2	-49.0	-38.3	-43.9
13.	-40.1	-41.0	-49.5	-39.8	-47.2	-45.2	-37.4	-41.1	-49.6	-76.2
14.	-38.7	-45.8	-44.1	-47.7	-57.4	-65.9	-36.6	-38.5	-52.9	-48.2
15.	-37.7	-47.9	-41.4	-59.0	-49.5	-50.8	-36.2	-37.3	-45.0	-43.9
17.	-37.4	-45.0	-39.4	-46.6	-43.9	-43.2	-35.9	-36.3	-40.6	-40.7
20.	-37.7	-43.5	-39.8	-43.5	-42.8	-41.4	-36.9	-37.1	-39.9	-40.4
25.	-38.7	-42.9	-40.2	-43.0	-42.8	-41.5	-38.2	-38.2	-40.3	-40.8
30.	-39.9	-43.5	-41.5	-43.9	-43.8	-42.6	-39.6	-39.4	-41.6	-41.9
35.	-41.4	-44.9	-42.6	-44.9	-44.7	-44.9	-41.9	-41.4	-43.8	-44.0
40.	-42.9	-45.4	-43.9	-46.2	-46.2	-45.4	-42.4	-42.2	-44.3	-44.6
50.	-45.2	-47.4	-46.2	-48.4	-47.7	-48.0	-45.1	-44.6	-47.0	-46.8
60.	-47.4	-49.5	-48.1	-50.4	-50.1	-50.6	-46.8	-46.8	-49.3	-49.3
70.	-52.1	-56.4	-51.2	-	-53.8	-52.5	-51.7	-51.9	-53.7	-53.9
80.	-54.1	-59.2	-53.0	-	-55.6	-54.7	-54.0	-54.1	-55.9	-56.2
90.	-55.8	-60.4	-54.5	-	-57.0	-56.2	-55.2	-55.6	-57.3	-57.7
100	-57.4	-62.2	-57.0	-	-59.5	-58.5	-57.1	-57.9	-59.1	-59.9
150	-60.1	-68.2	-61.4	-	-61.8	-68.2	-69.0	-66.4	-69.8	-69.0
200	-	-73.8	-66.1	-	-63.9	-69.5	-69.3	-68.7	-70.6	-70.6
300	-	-78.4	-75.8	-	-	-76.0	-76.2	-75.7	-77.6	-77.6
400	-	-81.4	-78.4	-	-	-81.3	-82.2	-82.5	-83.6	-84.8

Note: Underlined H_2 values were measured at P_{gen} = 0 dBm. H_2 values in parenthesis were measured at P_{gen} = 5 dBm. H_2 values in brackets were measured at P_{gen} = 10 dBm. All other H_2 values were measured at P_{gen} = - 5 dBm.

APPENDIX C

MEASURED VALUES OF DEMODULATION RFI RESPONSES OF THE THREE-STAGE OP AMP LED CIRCUIT

Appendix C contains two tables of experimental results for the 3-stage op amp LED circuit shown in Fig. 5-2. The values for the input resistor R1 = 10 kohm and feedback resistor R2 = 100 kohm were used. The Table C1 data are for the circuit with the RFI suppression capacitors omitted, i.e. $C_4 = C_5 = 0$. The Table C2 data are for the circuit with the RFI suppression capacitors included, i.e. $C_4 = C_5 = 27$ pF. All op amps were 741 op amps. The 741 op amps used for the second and third stages were not changed during the experiment. Thirty-five 741 op amps were used for the first stage.

The data in Tables C1 and C2 are listed in string format. Consider Table C1. The first two rows are

741 - #01
0.1 - 7.0 36.8 1.0 0.15 -10.3 27.5 1. 0.4 -13.0 25.3 1.0 ...

The first row indicates the op amp number which is 741-#01 in this example. The second row contains a data string with numbers being grouped in sets of four. The first number, 0.1, in the first set is the RF frequency f_{RF} in MHz. The second number, -7.0, in the first set is the RF generator available power P_{gen} in dBm. The third number, 36.8, in the first set is the RF rms voltmeter reading V_m^{RF} in mV. The fourth and last number, 1.0, in the first set is the 1 kHz AF rms voltmeter reading V_{03}^{AF} in volts. The next set of four numbers corresponds to: f_{RF} = 0.15 MHz; P_{gen} = -10.3 dBm; V_m^{RF} = 27.5 mV; V_{03}^{AF} = 1.0 V. The third set

of four numbers corresponds to f_{RF} = 0.4 MHz, etc. The data string is continued in subsequent rows. The last set of four numbers for 741 - #01 op amp corresponds to f_{RF} = 150 MHz. The next data which are for op amp 741 - #02 are arranged in the same format. The data for op amps 741 - #03 to 741 - #k32 follow in the same format.

It should be stressed that the values given for V_m^{RF} and V_{03}^{AF} are rms voltage values. Finally, it should be noted again that the RF input voltage V_i^{RF} to the 1st op amp stage is given by $V_i^{RF} = 2 \times V_m^{RF}$.

TABLE C1 (1 of 3)

MEASURED VALUES OF DEMODULATION RFI RESPONSES OF THE THREE-STAGE OP AMP LED CIRCUIT WITHOUT RFI SUPPRESSION CAPACITOR

741 -#01
0.1 -7.0 30.3 1. 0.15 -10.3 27.5 1. 0.4 -13.0 25.3 1. 0.6 -15.9 19.6 1.
0.8 -17.4 15.7 1. 1. -18.1 14.5 1. 1.5 -15.6 19.0 1. 3.0 -20.0 14.2 1.
4.0 -21.2 9.4 1. 6.0 -20.9 9.9 1. 8.0 -20.2 11.2 1. 10.0 -20.9 11. 1.
15.0 -17.0 16.1 1.
20.0 -15.3 19.5 1. 30.0 -14.0 22.5 1. 60.0 -8.0 47.0 1. 80.0 -4.5 56.0 1.
100.0 -3.0 66.5 1. 150.0 -0.5 82.0 1.
741 -#02
0.15 -8.7 32.0 1. 0.6 -15.0 21. 1. 0.8 -16.2 18.0 1.
1. -17.5 14.6 1. 1.5 -16.5 17.0 1. 2.0 -20.0 10.9 1. 3.0 -20.7 10.3 1.
4.0 -20.0 12.1 1. 20.0 -15.3 18.9 1. 30.0 -12.9 25.5 1. 40.0 -10.9 31. 1.
80.0 -4.0 61. 1. 100.0 -3.0 66.0 1. 150.0 0.0 85.0 1.
741 -#03
0.1 -19.9 14.5 1. 0.15 -15.2 15.8 1. 0.2 -17.6 13.5 1. 0.3 -16.6 16.2 1.
0.4 -15.3 19.2 1. 0.6 -5.0 66 1. 0.8 -13.7 23.7 1. 1. -15.5 19.4 1.
1.5 -13.0 22.5 1. 3.0 -23.2 7.8 1. 4.0 -23.2 7.8 1. 6.0 -22.8 8.4 1.
8.0 -21.6 8.3 1. 10.0 -20.4 10.0 1. 15.0 -18.9 12.5 1. 20.0 -16.3 17.1 1.
30.0 -13.7 23.0 1. 40.0 -11.6 29.0 1. 60.0 -8.5 44.5 1. 80.0 -4.9 57.0 1.
100.0 -3.5 63.0 1. 150.0 -0.5 80.0 1.
741 -#04
0.15 -10.2 27.5 1. 0.6 -13.1 25.4 1. 0.8 -15.5 19.5 1. 1. -16.5 17.0 1.
2.0 -6.5 54.0 1. 3.0 -20.2 10.8 1. 4.0 -19.9 9.6 1. 6.0 -18.5 14.1 1.
10.0 -18.4 14.2 1. 20.0 -15.5 19.0 1. 30.0 -13.0 24.5 1. 40.0 -11.1 30.0 1.
60.0 -7.9 46.5 1. 80.0 -4.5 59.0 1. 100.0 -3.5 63.0 1. 150.0 -0.5 81. 1.
741 -#05
0.4 -13.5 23.5 1. 0.6 -17.0 16.8 1. 2.0 -20.4 10.5 1. 3.0 -20.3 10.4 1.
8.0 -20.4 10.6 1. 10.0 -20.1 11.1 1. 15.0 -17.5 15.8 1. 20.0 -15.2 19.4 1.
30.0 -12.1 27.0 1. 40.0 -10.6 32.0 1. 60.0 -8.0 47.0 1. 80.0 -4.0 61. 1.
100.0 -3.0 67.0 1.
741 -#06
0.15 -10.5 27.0 1. 0.6 -13.5 24.6 1. 0.8 -16.2 17.8 1. 2.0 -20.2 10.7 1.
3.0 -21.5 29.0 1. 10.0 -19.0 13.4 1.
4.0 -20.4 10.5 1. 6.0 -20.4 10.5 1. 8.0 -20.0 11. 1. 15.0 -17.0 16.1 1.
20.0 -16.0 18.0 1. 30.0 -13.3 23.5 1. 40.0 -11.5 29.0 1. 60.0 -8.1 45.0 1.
80.0 -4.5 58.0 1. 100.0 -3.2 64.0 1. 150.0 -0.8 80.0 1.
741 -#07
0.4 -9.7 38.0 1. 1.5 -18.4 13.6 1. 8.0 -20.0 10.0 1. 10.0 -19.3 11.8 1.
0.8 -16.3 17.8 1. 1. -17.8 15.2 1. 3.0 -20.7 9.7 1. 4.0 -21.4 9.2 1.
6.0 -20.9 9.8 1. 10.0 -20.7 11.8 1. 20.0 -15.6 18.7 1. 40.0 -11.2 30.0 1.
30.0 -13.2 24.0 1.
60.0 -8.0 46.0 1. 80.0 -4.6 56.0 1. 100.0 -3.5 64.0 1. 150.0 -0.9 76.0 1.
741 -#08
0.6 -15.0 20.6 1. 0.6 -16.5 17.2 1. 1. -12.6 14.7 1. 2.0 -15.6 18.2 1.
3.0 -20.3 10.5 1. 4.0 -20.9 10.1 1. 6.0 -15.7 18.9 1. 10.0 -17.1 15.9 1.
20.0 -15.6 18.7 1. 30.0 -12.9 22.0 1. 40.0 -11.2 30.0 1. 60.0 -8.1 44.2 1.
80.0 -4.2 59.0 1.0 100.0 -3.0 66.0 1. 150.0 -0.4 60.0 1.
741 -#09
0.15 -8.0 36.0 1. 0.6 -15.5 19.7 1. 0.8 -17.0 16.4 1. 1. -18.4 13.5 1.
0.4 -12.0 28.2 1.
2.0 -15.5 19.1 1. 3.0 -20.0 11.8 1. 4.0 -21.1 9.6 1. 6.0 -20.0 10.9 1.
8.0 -19.2 11.8 1. 10.0 -18.0 14.8 1. 20.0 -15.7 18.4 1. 30.0 -13.5 23.5 1.
40.0 -11.7 29.0 1. 60.0 -8.8 39.0 1. 80.0 -4.7 57.0 1. 100.0 -3.7 63.0 1.
150.0 -1. 75.0 1.
741 -#10
0.1 -7.2 35.0 1. 0.15 -0.2 28.1 1. 0.4 -14.1 22.2 1. 0.6 -18.3 13.7 1.
1. -18.8 12.9 1. 3.0 -19.2 12.0 1. 4.0 -21.8 9.0 1. 15.0 -17.3 15.9 1.
8.0 -19.8 11.2 1.
20.0 -16.0 18.0 1. 30.0 -13.0 24.5 1. 40.0 -11.1 30.0 1. 60.0 -7.8 46.0 1.
80.0 -4.0 61. 1. 100.0 -2.9 69.0 1. 150.0 0.0 85.0 1.
741 -#11
0.1 -9.0 27.5 1. 0.15 -12.2 22.5 1. 0.2 -12.1 26.6 1. 0.3 -14.0 22.2 1.
0.4 -15.1 19.6 1. 0.6 -17.1 16.7 1. 0.8 -17.1 16.6 1. 1. -14.9 21. 1.
2.0 -22.0 8.7 1. 3.0 -21.9 8.9 1. 20.0 -14.5 22.0 1.
1.5 -19.5 12.0 1. 6.0 -20.5 10.4 1. 8.0 -19.0 12.2 1. 30.0 -11.2 30.0 1.
40.0 -10.5 35.0 1. 60.0 -8.1 55.0 1. 80.0 -2.1 75.0 1. 100.0 -1. 84.0 1.
150.0 1.9 98.0 1.
741 -#12
0.1 -6.5 38.0 1. 0.15 -9.8 28.0 1. 0.3 -5.1 60.0 1. 0.4 -13.0 25.1 1.
0.6 -15.2 20.3 1. 0.8 -15.5 19.5 1. 1.-14.2 22.1 1. 2.0 -21.8 8.9 1.
3.0 -23.0 7.9 1.
4.0 -22.5 8.3 1. 6.0 -21.1 9.5 1. 8.0 -18.8 12.9 1. 10.0 -17.9 15.0 1.
15.0 -15.6 18.9 1. 30.0 -10.8 30.5 1. 40.0 -9.2 38.0 1. 60.0 -6.1 56.0 1.
80.0 -2.2 75.0 1. 100.0 -1.6 84.0 1.
741 -#13
0.1 -8.9 29.6 1. 0.15 -12.1 22.5 1. 0.2 -12.4 25.6 1. 0.3 -14.6 21.2 1.
0.4 -15.8 18.6 1. 0.6 -16.9 16.8 1. 0.8 -16.4 17.2 1. 1. -14.0 23.3 1.
1.5 -20.2 11. 1. 2.0 -22.5 6.2 1. 3.0 -22.8 6.0 1. 4.0 -22.1 6.8 1.
6.0 -20.5 10.5 1. 8.0 -17.5 15.6 1. 10.0 -18.4 13.1 1. 15.0 -16.0 18.1 1.
20.0 -14.1 22.0 1. 30.0 -11.3 29.0 1. 40.0 -9.2 37.0 1. 60.0 -5.6 59.0 1.
80.0 -2.2 56.0 1. 100.0 -1. 74.0 1. 150.0 2.0 98.0 1.
741 -#14
0.6 -13.0 20.2 1. 0.6 -13.7 24.3 1. 1.5 -20.2 11. 1. 3.0 -22.8 8.1 1.
4.0 -22.1 8.9 1. 6.0 -21. 9.8 1. 8.0 -19.5 11.8 1. 10.0 -18.0 14.5 1.

TABLE C1 (2 of 3)

MEASURED VALUES OF DEMODULATION RFI RESPONSES OF THE THREE-STAGE

OP AMP LED CIRCUIT WITHOUT RFI SUPPRESSION CAPACITOR

```
15.0 -10.0 18.0 1.  20.0 -13.7 24.0 1.  30.0 -11.1 30.0 1.  40.0 -9.1 38.0 1.
60.0 -6.0 57.0 1.  80.0 -2.0 77.0 1.  100.0 -1. 84.0 1.  150.0 1.9 100.0 1.
741 -#35
0.3 -15.5 19.1 1.  0.4 -16.5 17.4 1.  1. -16.8 17.0 1.  1.5 -14.5 21. 1.
2.0 -21.4 8.9 1.
3.0 -23.2 7.7 1.  4.0 -22.6 8.1 1.  6.0 -20.8 10.3 1.  8.0 -19.3 12.0 1.
10.0 -17.6 15.1 1.  15.0 -16.0 18.2 1.  20.0 -14.1 21.5 1.  30.0 -11.1 30.0 1.
40.0 -9.1 38.5 1.  60.0 -6.0 57.0 1.  80.0 -4.0 61. 1.  100.0 -2.9 69.0 1.
150.0 0.0 85.0 1.
741 -#41
0.1 -11. 22.5 1.  0.15 -12.1 22.7 1.  0.2 -14.2 20.6 1.  1. -13.5 24.5 1.
1.5 -14.2 12.2 1.  2.0 -21.8 8.9 1.  3.0 -19.0 12.2 1.  4.0 -16.7 11.2 1.
6.0 -16.5 13.0 1.  8.0 -14.3 12.0 1.  10.0 -18.0 14.2 1.  15.0 -16.2 17.6 1.
20.0 -15.1 19.6 1.  30.0 -12.1 27.0 1.  40.0 -0.2 34.0 1.  60.0 -6.9 52.0 1.
80.0 -4.7 57.0 1.  100.0 -13.7 63.0 1.  150.0 -1. 75.0 1.
741 -#42
0.1 -10.7 23.5 1.  0.8 -11.1 31. 1.
1. -13.1 24.5 1.  1.5 -19.5 11.8 1.  2.0 -21.2 9.5 1.  3.0 -23.0 7.7 1.
4.0 -23.2 7.6 1.  6.0 -22.4 8.5 1.  8.0 -20.8 10.0 1.  10.0 -18.8 13.2 1.
15.0 -16.6 16.7 1.  20.0 -14.1 21.5 1.  30.0 -11.1 29.5 1.  40.0 -11.3 40.0 1.
60.0 -6.7 54.0 1.  80.0 -4.0 63.0 1.  100.0 -3.1 66.0 1.  150.0 -0.4 80.0 1.
741 -#43
0.6 -14.5 22.1 1.  0.8 -15.3 19.8 1.  1. -12.9 26.0 1.  1.5 -20.1 11.1 1.
2.0 -20.4 10.4 1.  6.0 -23.4 7.5 1.  20.0 -15.5 19.5 1.  30.0 -12.7 25.5 1.
40.0 -10.7 32.5 1.  60.0 -6.0 50.0 1.  80.0 -3.0 69.0 1.  100.0 -2.0 76.0 1.
150.0 1.9 98.0 1.
741 -#44
0.15 -12.9 20.8 1.  0.2 -14.8 19.6 1.  0.4 -13.9 22.5 1.  0.6 -13.5 24.7 1.
0.8 -14.1 22.7 1.  1. -15.8 18.8 1.  1.5 -20.2 10.6 1.  2.0 -21.5 9.0 1.
3.0 -23.2 7.5 1.  4.0 -23.8 7.2 1.  6.0 -22.7 8.2 1.  8.0 -21.2 9.6 1.
10.0 -19.8 11.1 1.  15.0 -27.0 16.1 1.  20.0 -25.0 20.0 1.  30.0 -21.8 28.0 1.
40.0 -19.5 36.0 1.  60.0 -6.8 52.0 1.  80.0 -2.6 72.0 1.  150.0 2.0 100.0 1.
741 -#45
0.6 -13.5 24.6 1.  0.8 -13.8 24.3 1.  1.5 -20.8 10.4 1.  2.0 -24.1 7.0 1.
3.0 -25.0 6.4 1.  8.0 -22.0 8.8 1.  10.0 -20.8 10.0 1.  15.0 -17.2 15.6 1.
2 -12.9 24.5 1.  40.0 -10.6 30.5 1.  60.0 -7.6 47.0 1.
80.0 -2.8 70.0 1.  100.0 -1.3 80.0 1.  150.0 1.9 100.0 1.
741 -#51
0.4 -13.6 23.6 1.  0.6 -16.8 17.3 1.  0.8 -18.0 14.7 1.  1. -16.5 13.7 1.
1.5 -9.6 37.5 1.  2.0 -20.0 36.0 1.  3.0 -22.2 8.5 1.  4.0 -22.1 8.7 1.
6.0 -21.6 9.3 1.  8.0 -20.7 10.2 1.  10.0 -20.2 10.9 1.  15.0 -17.9 47.0 1.
20.0 -16.2 5.5 1.  30.0 -14.0 22.0 1.  40.0 -11.9 28.0 1.  60.0 -9.0 38.5 1.
60.0 -4.7 57.0 1.  100.0 -3.2 63.0 1.  150.0 -0.5 79.0 1.
741 -#52
0.1 -10.4 24.0 1.  0.15 -13.2 20.2 1.  0.2 -13.5 22.7 1.  0.3 -15.1 19.6 1.
0.4 -16.8 17.0 1.  0.6 -18.2 14.4 1.  0.8 -20.0 11.5 1.  1. -20.2 11. 1.
2.0 -17.5 15.0 1.  3.0 -21.1 9.7 1.  4.0 -21.5 9.3 1.  6.0 -21.5 9.3 1.
8.0 -21. 10.0 1.  10.0 -19.3 11.9 1.  15.0 -17.9 15.0 1.  20.0 -16.9 16.7 1.
40.0 -11.1 30.5 1.  60.0 -9.1 38.0 1.  80.0 -4.9 55.0 1. 100.0 -3.9 61. 1.
150.0 -1.1 77.0 1.
741 -#53
0.1 -13.2 17.5 1.  0.15 -16.2 14.7 1.  0.3 -17.8 15.0 1.  0.4 -17.9 14.3 1.
0.6 -19.8 11.6 1.  0.8 -20.5 10.6 1.  1. -20.7 10.5 1.  1.5 -16.6 16.0 1.
2.0 -18.9 13.7 1.  3.0 -21.9 8.9 1.  4.0 -22.0 8.7 1.  6.0 -21. 8.9 1.
8.0 -20.9 9.8 1.  10.0 -20.1 11. 1.  15.0 -18.0 14.2 1.  20.0 -16.7 17.0 1.
40.0 -12.0 26.0 1.  60.0 -9.1 38.5 1.
30.0 -13.8 22.5 1.  80.0 -4.9 56.0 1.  100.0 -3.3 63.0 1.  150.0 -0.7 77.0 1.
741 -#54
0.3 -17.8 14.7 1.
0.1 -14.1 15.9 1.  0.15 -14.7 17.5 1.  0.2 -16.5 16.0 1.  0.4 -18.8 13.6 1.
0.6 -20.5 10.8 1.  0.8 -21.1 10.0 1.  1. -21.1 10.0 1.  2.0 -21.3 9.4 1.
3.0 -22.1 8.6 1.  4.0 -22.2 8.5 1.  6.0 -22.0 8.7 1.  8.0 -21.2 9.5 1.
10.0 -20.8 32.5 1.  15.0 -18.0 14.1 1.  20.0 -17.1 15.8 1.  30.0 -14.6 20.5 1.5
40.0 -12.7 25.5 1.  60.0 -9.8 34.5 1.  80.0 -5.0 55.0 1.  100.0 -3.9 61. 1.
150.0 -1. 75.0 1.
741 -#55
0.1 -13.0 18.3 1.  0.15 -16.6 13.9 1.  0.2 -17.5 14.8 1.  0.3 -16.5 13.5 1.
0.4 -19.5 11.6 1.  0.6 -20.9 10.4 1.  0.8 -21.1 10.0 1.  10.0 -21. 10.2 1.
1.5 -9.1 40.5 1.  2.0 -19.4 37.5 1.  3.0 -21.6 9.1 1.  4.0 -21.9 8.5 1.
6.0 -21.9 9.0 1.  8.0 -21. 9.9 1.  10.0 -20.2 34.0 1.  15.0 -16.2 13.03 1.
40.0 -12.0 26.0 1.  60.0 -8.5 41. 1.  80.0 -4.9 56.0 1.  100.0 -3.6 62.0 1.
150.0 -0.4 79.0 1.
741 -#56
0.15 -8.2 34.5 1.  0.4 -12.5 26.5 1.  0.6 -16.6 17.2 1.  0.8 -18.0 14.5 1.
1. -19.2 12.0 1.  2.0 -18.0 43.0 1.  3.0 -21.1 9.6 1.  4.0 -21.9 8.9 1.
6.0 -21.8 8.9 1.  8.0 -20.8 32.0 1.  20.0 -15.9 18.2 1.  30.0 -13.1 24.5 1.
40.0 -11.1 30.0 1.  60.0 -8.2 42.0 1.  80.0 -3.5 64.0 1.  100.0 -2.2 72.0 1.
150.0 0.7 87 1.
741 -#57
0.2 -11.1 29.7 1.  0.6 -12.0 29.2 1.  1.5 -12.1 28.0 1.  2.0 -18.3 37.5 1.
3.0 -21.8 9.0 1.  4.0 -21.8 9.0 1.  6.0 -21. 9.9 1.  8.0 -20.3 10.6 1.
10.0 -19.9 11.1 1.  15.0 -18.0 13.6 1.  20.0 -16.0 18.0 1.  30.0 -13.5 24.0 1.
40.0 -11.2 30.0 1.  60.0 -8.3 41. 1.  80.0 -4.1 60.0 1.  100.0 -3.0 67.0 1.
150.0 0.1 83.0 1.
741 -#58
```

TABLE C1 (3 of 3)

MEASURED VALUES OF DEMODULATION RFI RESPONSES OF THE THREE-STAGE OP AMP LED CIRCUIT WITHOUT RFI SUPPRESSION CAPACITOR

```
0.6 -16.1 18.3 1.  0.8 -17.6 15.4 1.  1. -18.0 14.6 1.  2.0 -20.0 35.0 1.
3.0 -21.9 6.6 1.  4.0 -22.0 8.8 1.  6.0 -13.6 23.5 1.  8.0 -15.0 21. 1.
10.0 -16.1 16.5 1.  30.0 -13.1 24.0 1.  40.0 -11.4 26.5 1.  60.0 -8.4 41. 1.
80.0 -4.1 60.0 1.  100.0 -3.2 65.0 1.  150.0 -0.4 80.0 1.
741 -#24
0.6 -15.8 19.3 1.  0.8 -17.8 15.4 1.  1. -18.1 13.9 1.  1.5 -16.0 14.5 1.
2.0 -19.3 12.0 1.  3.0 -22.8 8.0 1.  4.0 -22.9 8.1 1.  6.0 -22.1 8.7 1.
8.0 -20.8 32.0 1.  10.0 -19.7 36.0 1.  15.0 -16.1 43.0 1.  20.0 -15.9 17.1 1.
30.0 -13.0 24.5 1.  40.0 -10.9 31. 1.  60.0 -7.6 48.0 1.  80.0 -4.1 60.0 1.
100.0 -3.0 67.0 1.  150.0 -0.1 82.0 1.
741 -#00
0.15 -8.8 33.0 1.  0.4 -11.9 28.6 1.  0.6 -14.4 23.2 1.  0.8 -16.0 18.6 1.
1. -16.5 17.1 1.  1.5 -13.3 24.5 1.  2.0 -16.0 17.9 1.  3.0 -19.6 350. .05 1.
4.0 -20.2 34.0 1.  6.0 -20.0 11. 1.  8.0 -18.2 30.0 1.  10.0 -16.1 14.5 1.
20.0 -14.8 20.5 1.  30.0 -12.6 25.5 1.  40.0 -11. 30.5 1.  60.0 -8.0 46.0 1.
80.0 -3.9 62.0 1.  100.0 -2.6 71. 1.  150.0 0.1 87.0 1.
741 -#K06
0.1 -7.3 35.0 1.  0.15 -10.1 28.6 1.  1.5 -15.2 19.4 1.  6.0 -14.3 22.0 1.
8.0 -13.0 23.0 1.  10.0 -12.8 25.5 1.  15.0 -11.7 29.0 1.  20.0 -10.8 32.0 1.
30.0 -9.5 36.0 1.  40.0 -8.7 39.5 1.  60.0 -6.8 53.0 1.  80.0 -5.0 55.0 1.
100.0 -3.6 63.0 1.  150.0 -0.7 78.0 1.
741 -#K14
4.0 -15.5 19.1 1.  6.0 -14.2 22.0 1.  8.0 -13.2 24.5 1.  10.0 -12.4 26.5 1.
15.0 -11.3 30.5 1.  20.0 -10.8 31.5 1.  30.0 -9.4 36.5 1.  40.0 -8.5 4.5 1.
60.0 -6.4 54.0 1.  80.0 -3.0 69.0 1.  100.0 -2.2 73.0 1.  150.0 0.1 85.0 1.
741 -#K20
0.15 -10.4 26.0 1.  2.0 -15.6 18.9 1.  3.0 -15.6 18.9 1.  4.0 -15.1 20.0 1.
10.0 -12.3 27.0 1.
15.0 -11.2 30.0 1.  20.0 -10.9 31.5 1.  30.0 -9.6 35.5 1.  40.0 -8.5 36.0 1.
60.0 -6.2 54.0 1.  80.0 -3.0 68.0 1.  100.0 -2.2 73.0 1.  150.0 0.1 85.0 1.
741 -#K26
1.0 -15.0 20.4 1.  6.0 -15.2 17.2 1.  15.0 -12.5 26.5 1.  20.0 -11.9 26.0 1.
30.0 -10.5 32.5 1.  40.0 -9.2 37.0 1.  80.0 -3.2 67.0 1.  100.0 -2.3 72.0 1.
741 -#K32
10.0 -12.9 25.5 1.  15.0 -11.7 29.5 1.  20.0 -10.9 31.5 1.  30.0 -9.7 35.5 1.
30.0 -9.7 35.5 1.  40.0 -8.4 41.0 1.  60.0 -6.0 56.0 1.  80.0 3.1 66.0 1.
100.0 -2.2 74.0 1.  150.0 0.1 85.0 1.
12.15.03.UCPG, ID22,      0.004 KPGS.
12.15.03.UCLN, ID22,      0.207 KLNS.
12.15.23.UCLP, AA, 033,      0.255KLNS.
```

TABLE C2 (1 of 3)

MEASURED VALUES OF DEMODULATION RFI RESPONSES OF THE THREE-STAGE OP AMP LED CIRCUIT WITH RFI SUPPERSSION CAPACITOR

```
741 -#01
0.3 -8.1 44.5 1.0   0.4 -9.4 36.5 1.0   0.6 -11. 30.5 1.0   0.8 -12.1 27.5 1.0
1.0 -12.4 25.5 1.0
1.5 -9.2 37.2 1.0   2.0 -4.7 62.0 1.0   3.0 -7.2 47.0 1.0   4.0 -5.7 55.5 1.0
6.0 -2.7 78.0 1.0   8.0 -0.8 95.0 1.0   10.0 -0.6 97.0 1.0   15. -3.2 73.5 1.0
20.0 -3.7 66.5 1.0   30. -2.0 80.0 1.0   40. -0.7 94.0 1.0   60. 0.4 106. 1.0
80. 3.9 151. 1.0   100. 4.5 157. 1.0   150. 7.1 195. 1.0
741 -#02
0.3 -7.2 49.5 1.0   0.4 -8.7 41. 1.0   0.6 -10.3 33. 1.0   0.8 -11.2 30. 1.0
1.0 -11.4 28.7 1.0   1.5 -9.3 37. 1.0   3.0 -6.2 52. 1.0   4.0 -5.2 59. 1.0
6.0 -2.4 80. 1.0   8.0 -0.2 102. 1.0   10.0 1.1 128. 1.0   15. -1.3 91.5 1.0
20. -2.0 73.5 1.0   30. -1.0 82. 1.0   40. -0.6 95. 1.0   60. 0.6 107. 1.0
80. 4.2 153. 1.0   100. 4.7 160. 1.0   150. 7.4 202. 1.0
741 -#03
0.1 -11.2 22.4 1.0   0.15 -11.7 24. 1.0   0.2 -13.7 22.8 1.0   0.3 -13. 25.3 1.0
0.4 -11.6 29.5 1.0   0.8 -8.7 41.7 1.0   1.0 -10. 33.5 1.0   1.5 -5. 62.3 1.0
2.0 -10.1 33. 1.0   3.0 -9.2 36.6 1.0   4.0 -7.3 46.7 1.0   6.0 -4.6 63.5 1.0
8.0 -3.4 72.5 1.0   10.0 -3.7 69.5 1.0   15. -5.3 54. 1.0   20. -5.1 56. 1.0
30. -3.1 72. 1.0   40. -1.5 86. 1.0   60. 0.1 102. 1.0   80. 3.6 147. 1.0
100. 4.4 154. 1.0   150. 7.4 197. 1.0
741 -#04
0.6 -8.9 38.8 1.0   0.8 -10.3 33.5 1.0   1.0 -10.8 30. 1.0   1.5 -9.9 34. 1.0
2.0 -1.7 86.5 1.0   3.0 -7.2 46.8 1.0   4.0 -6.3 51.5 1.0   6.0 -3.6 70. 1.0
8.0 -1.3 92. 1.0   10.0 0.8 116.0 1.0   15.0 2.7 151.0 1.0   20.0 -0.9 91. 1.0
30. -2.6 75.5 1.0   40. -1.4 86.5 1.0   60. -0.3 98.5 1.0   80. 3.4 141. 1.0
100. 4.1 149. 1.0   150. 6.9 193. 1.0
741 -#05
0.4 -10.9 32. 1.0   0.6 -12.9 24.8 1.0   0.8 -13.7 22.8 1.0   1.0 -12.5 25.2 1.0
1.5 -9. 37.8 1.0   2.0 -10.4 31.3 1.0   3.0 -8.3 40.3 1.0   4.0 -6.1 52.5 1.0
6.0 -3.2 72.5 1.0   8.0 -1.5 89. 1.0   10.0 -1.6 88. 1.0   15. -4.7 62.5 1.0
20. -4.4 62. 1.0   30. -2.3 78. 1.0   40. -1.1 65. 1.0   60. 0.5 107. 1.0
80. 4.3 157. 1.0   100. 5.1 166. 1.0   150. 7.6 208. 1.0
741 -#06
0.2 -8.0 41.7 1.0   0.3 -4.7 66.5 1.0   0.6 -6.8 39. 1.0   0.8 11.1 30. 1.0
1.0 -11.3 29. 1.0   1.5 -4.9 62.5 1.0   2.0 -9.8 33.5 1.0   3.0 -8.3 40.3 1.0
4.0 -6.0 53.5 1.0   6.0 -2.6 76. 1.0   8.0 -0.6 95. 1.0   10.0 -0.4 100. 1.0
15. -3.3 73. 1.0   20. -3.9 65. 1.0   30. -2.4 77.5 1.0   40. -1.1 64. 1.0
60. 0.0 100. 1.0   80. 3.5 144. 1.0   100. 4.2 151. 1.0   150. 6.9 192. 1.0
741 -#07
0.4 -7.6 49. 1.0   0.6 -9.6 35.8 1.0   0.8 -10.7 31.5 1.0   1.0 -11.3 29. 1.0
1.5 -10.4 32.5 1.0   2.0 -1.7 86.5 1.0   3.0 -7.2 47. 1.0   4.0 -6.2 52. 1.0
6.0 -3.4 72. 1.0   8.0 -1.2 93. 1.0   10.0 0.9 115. 1.0   15. 3.1 136. 1.0
20. -0.8 91.5 1.0   30. -2.8 73.5 1.0   40. -1.6 84. 1.0   60. -0.2 99. 1.0
80. 3.2 139. 1.0   100. 3.8 146. 1.0   150. 6.6 187. 1.0
741 -#08
0.4 -8.3 43.5 1.0   0.6 -10.1 34. 1.0   0.8 -11.2 29.8 1.0   1.0 -11.4 28.7 1.0
1.5 -7.5 47. 1.0   2.0 -4.2 65.5 1.0   3.0 -6.7 50.5 1.0   4.0 -5.0 60. 1.0
6.0 -2.2 82.5 1.0   8.0 -0.6 98. 1.0   10.0 -0.7 97.5 1.0   15.0 -3.1 74.5 1.0
20.0 -3.4 69.5 1.0   30.0 -1.7 82.5 1.0   40.0 -0.5 96.0 1.0   60.0 0.6 108. 1.
80.0 3.8 150. 1.0   100.0 4.5 157.0 1.0   150.0 7.3 197.0 1.0
741 -#09
0.4 -8.4 42.0 1.0
0.6 -10.6 32.0 1.0   0.8 -11.6 28.5 1.0   1.0 -12.0 26.8 1.0   1.5 -9.2 37.2 1.0
2.0 -4.0 67. 1.0   3.0 -7.4 46.5 1.0   4.0 -5.7 55.0 1.0   6.0 -2.7 77. 1.0
8.0 -0.6 98. 1.0   10.0 0.5 111. 1.0   15.0 -1.7 87. 1.0   20. -3.1 71. 1.0
30. -2.2 79. 1.0   40. -0.6 92. 1.0   60. 0.2 102. 1.0
80.0 3.4 140.0 1.0   100.0 3.8 146.0 1.0   150.0 6.6 185.0 1.0
741 -#10
0.3 -9.1 38.5 1.0   0.4 -10.4 33.5 1.0   0.6 -12.2 27.2 1.0   0.8 -13.1 24. 1.0
1.0 -13. 24.3 1.0   1.5 -6.4 54. 1.0   2.0 -9.5 39.2 1.0   3.0 -8.4 46. 1.0
4.0 -6.4 51.5 1.0   6.0 -3.6 71.5 1.0   8.0 -1.2 93. 1.0   10.0 1.6 112. 1.0
15. -1.7 87. 1.0   20. -3.7 67.5 1.0   30. -2.2 79. 1.0   40. -1.0 90. 1.0
60. 0.3 106. 1.0   80. 4.0 152. 1.0 100. 4.7 162. 1.0   150. 7.5 206. 1.0
741 -#11
0.1 -3.7 54.5 1.0   0.2 -5.8 55. 1.0   0.3 -7.1 49. 1.0   0.4 -8.7 41. 1.0
0.8 -9.6 36.3 1.0   1.0 -8.4 52. 1.0   1.5 -10.9 30.5 1.0   2.0 -12.5 25.3 1.0
3.0 -10.7 30.5 1.0   4.0 -8.6 39. 1.0   6.0 -5.1 59.5 1.0   8.0 -2.2 83. 1.0
10.0 0.7 113.0 1.0   15.0 -0.4 99.0 1.0   20.0 -3.4 69.0 1.0 30.0 -1.1 88.0 1.0
40.0 1.1 113.0 1.0   60.0 3.7 159.0 1.0   80.0 6.0 235.0 0.94
100.0 8.0 230.0 0.795
741 -#12
0.1 0.1 81.2 1.0   0.2 -3.1 76.0 1.0   0.3 -5.3 61.3 1.0   0.4 -6.9 51.3 1.0
0.6 -8.5 41.5 1.0   0.8 -8.4 41.8 1.0   1.0 -8.4 54.0 1.0   1.5 -8.6 40.7 1.0
2.0 -12.0 27.2 1.0   3.0 -11.5 28.5 1.0   4.0 -9.5 35.6 1.0   6.0 -6.1 54.5 1.0
8.0 -3.4 73.5 1.0   10.0 -0.8 97.0 1.0   15.0 6.2 223.0 1.0   20.0 -1.4 87.5 1.0
30.0 -1.9 83.0 1.0   40.0 0.4 106.0 1.0   60.0 3.2 153.0 1.0   80.0 7.5 224.0 1.
100.0 8.0 234.0 0.955
741 -#13
0.1 -3.4 54.7 1.0   0.2 -5.2 53.0 1.0   0.3 -8.1 43.3 1.0   0.4 -9.1 39. 1.0
0.6 -10.3 34.0 1.0   0.8 -9.9 35.5 1.0   1.0 -8.0 56.5 1.0   1.5 -11.5 29.3 1.0
2.0 -12.7 25.0 1.0   3.0 -10.9 30.5 1.0   4.0 -8.7 39.0 1.0   6.0 -5.3 60.0 1.0
8.0 -2.4 82.5 1.0   10.0 0.4 112.0 1.0   15.0 -0.8 97.0 1.0   20.0 -3.4 70. 1.0
30. -1.1 91.5 1.0   40.0 1.1 116.0 1.0   60.0 3.8 165.0 1.0   80.0 8.0 232.0 1.0
```

TABLE C2 (2 of 3)

MEASURED VALUES OF DEMODULATION RFI RESPONSES OF THE THREE-STAGE OP AMP LED CIRCUIT WITH RFI SUPPRESSION CAPACITOR

```
1.0.0 3.0 229.0 0.75
741 -834
0.6 -8.7 52.5 1.0   0.8 -9.7 52.5 1.0   1.5 -11.4 24.5 1.0
2.0 -12.8 24.8 1.0   3.0 -11.1 29.8 1.0   4.0 -9.0 38.3 1.0   6.0 -5.6 57.6 1.0
8.0 -2.9 78.0 1.0   10.0 -0.4 104.0 1.0   15.0 3.7 172.0 1.0   20.0 -3.4 72. 1.0
30.0 -1.7 86.5 1.0   40.0 0.8 113.0 1.0   60.0 3.7 162.0 1.0   80.0 7.7 229.0 1.
100.0 8.0 230.0 0.87
741 -835
0.1 -4.0 51.5 1.0   0.15 -6.5 44.5 1.0   0.2 -7.3 47.5 1.0   0.3 -8.6 40.2 1.0
0.4 -9.5 37.5 1.0   0.6 -10.4 35.5 1.0   0.8 -10.3 35.5 1.0   1.0 -9.7 37.5 1.0
1.5 -8.3 55.8 1.0   2.0 -11.6 29.0 1.0   3.0 -11.3 29.0 1.0   4.0 -6.8 35.8 1.0
6.0 -6.2 54.5 1.0   8.0 -3.7 72.0 1.0   10.0 -1.7 90. 1.0   15. 3. 160.0 1.0
20.0 11.2 360.0 1.0   30.0 -3.4 72.5 1.0   40.0 -0.5 99.0 1.0   60. 2.8 144.0 1.
80.0 6.9 210.0 1.0   100.0 7.7 227.0 1.0
741 -841
1.5 -10.6 33.0 1.0   2.0 -11.8 28. 1.0   3.0 -11.6 28.5 1.0   4. -10.1 34.0 1.0
6.0 -6.9 50.8 1.0   8.0 -3.7 73.0 1.0   10.0 0.0 109.0 1.0   15.0 -4.7 65.5 1.0
20.0 -4.8 62.0 1.0   30.0 -0.5 90.0 1.0   40.0 0.5 113.0 1.0   60.0 2.7 152.0 1.
80.0 6.7 206.0 1.0
100.0 7.4 219.0 1.0   150.0 8.0 215.0 0.52
741 -842
1.5 -9.7 36.0 1.0   2.0 -10.8 31.0 1.0   3.0 -10.7 31.5 1.0   4.0 -9.6 36.0 1.0
6.0 -6.7 52.0 1.0   8.0 -3.7 72.0 1.0   10.0 -0.4 105.0 1.0   15.0 -2.3 85.5 1.0
20.0 -3.8 69.0 1.0   30.0 -0.8 97.0 1.0   40.0 1.1 120.0 1.0   60.0 3.2 161.0 1.
80.0 7.5 223.0 1.0   100.0 8.0 233.0 1.0   150.0 8.0 213.0 0.44
741 -843
0.6 -8.3 45.5 1.0   0.8 -9.1 41.0 1.0   1.0 -6. 60.5 1.0   1.5 -11.2 30.6 1.0
2.0 -13.8 22.5 1.0   3.0 -13.0 24.5 1.0   4.0 -11.2 30.4 1.0   6.0 -7.4 48.2 1.0
8.0 -3.7 72.5 1.0   10.0 -0.5 104.0 1.0   15. -0.3 94.5 1.0   20. -2.3 59.0 1.0
30.0 -1.7 88.0 1.0   40.0 0.5 112.0 1.0   60.0 2.7 153.0 1.0   80.0 7.0 212. 1.0
100.0 7.6 224.0 1.0   150.0 8.0 214.0 0.47
741 -844
0.2 -8.8 37.8 1.0   0.3 -8.4 41.2 1.0   1.0 -8.9 41.0 1.0
1.5 -10.7 32.0 1.0   2.0 -11.4 29.3 1.0   3.0 -10.8 31.0 1.0   4.0 -9.5 36.0 1.0
6.0 -6.2 55.0 1.0   8.0 -2.5 82.5 1.0   10.0 -1.2 90.0 1.0   15.0 -3.4 61.0 1.0
20.0 -3.8 69.5 1.0   30.0 -0.9 95.0 1.0   40.0 0.8 116.0 1.0   60.0 3.2 160. 1.0
80. 7.5 223. 1.0   100. 8. 233. 0.44   150. 8. 215. 0.45
741 -845
0.6 -6.9 54.3 1.0   0.8 -5.7 61.5 1.0   1.5 -11.9 26.0 1.0   2.0 -13.5 23.2 1.0
3.0 -12.6 25.7 1.0   4.0 -10.7 31.5 1.0   6.0 -7.0 50.0 1.0   8.0 -3.2 76.0 1.0
10.0 -0.9 98.0 1.0   15.0 -0.3 55.0 1.0   20.0 -4.5 64.0 1.0   30.0 -1.2 93.5 1.
40.0 0.8 160.0 1.0   60.0 3.2 160.0 1.0   80.0 7.4 222.0 1.0   100. 8. 232. 0.44
741 -851
0.4 -9.9 36.8 1.0   0.6 -12.5 28.0 1.0   0.8 -13.5 24.9 1.0   1.0 -13.5 24.7 1.0
1.5 -3.7 73.5 1.0   2.0 -9.0 38.2 1.0   3.0 -8.3 41.5 1.0   4.0 -6.2 54.5 1.0
6.0 -3.1 77.0 1.0   8.0 -1.3 95. 1.0   10.0 -1.4 94. 1.0   15.0 -4.5 67. 1.0
20.0 -4.7 63.5 1.0   30.0 -2.7 76.5 1.0   40.0 -1.3 92. 1.0   60.0 0.1 108. 1.0
80.0 3.6 145. 1.0   100.0 4.1 151. 1.0   150.0 6.8 190.0 1.0
741 -852
0.15 -6.9 32.8 1.0   0.2 -9.6 35. 1.0   0.3 -10.9 31.5 1.0   0.4 -11.9 28.5 1.0
0.6 -14.4 23.3 1.0   0.8 -15. 21.4 1.0   1.0 -14.9 21.6 1.0   1.5 -7.5 46.5 1.0
2.0 -8.2 42.3 1.0   3.0 -7.7 44.5 1.0   4.0 -5.4 59.3 1.0   6.0 -2.8 76. 1.0
8.0 -3.3 76.0 1.0   10.0 -4.9 63.5 1.0   15.0 -6.8 52. 1.0   20.0 -5.9 54.5 1.0
30.0 -3.9 68.5 1.0   40.0 -2.7 74.5 1.0   60.0 -0.8 87.5 1.0   80.0 3.1 136. 1.0
100.0 3.8 146.0 1.0   150.0 6.8 190.5 1.0
741 -853
0.1 -8.7 29. 1.0   0.15 -10.9 26.5 1.0   0.2 -11.7 28.1 1.0   0.3 -12.7 23.8 1.0
0.4 -13.5 23.4 1.0   0.6 -15. 20.7 1.0   0.8 -15.6 19.3 1.0   1.0 -15.5 19.7 1.0
1.5 -9.3 38.0 1.0   2.0 -7.7 46.5 1.0   3.0 -7.7 44.3 1.0   4.0 -5.6 56.8 1.0
6.0 -3.2 76. 1.0   8.0 -2.6 82.5 1.0   10.0 -3.4 74.5 1.0   15.0 -5.4 60.5 1.0
20.0 -4.8 61.5 1.0   30.0 -2.8 77. 1.0   40.0 -1.4 91.0 1.0   60.0 -0.1 106. 1.0
80.0 3.5 144.0 1.0   100.0 4.1 151.0 1.0   150.0 6.9 191.0 1.0
741 -854
0.1 -9.7 25.2 1.0   0.15 -11.8 23.6 1.0   0.2 -13.0 24.2 1.0   0.3 -13.9 22.6 1.
0.4 -14.6 21.2 1.0   0.6 -16.6 18. 1.0   0.8 -16.7 17.4 1.0   1.0 -16.2 18.5 1.0
2.0 -10.2 33.3 1.0   3.0 -8.4 41.2 1.0   4.0 -6.1 54.8 1.0   6.0 -3.5 73.5 1.0
8.0 -3.2 76.5 1.0   10.0 -4.4 67. 1.0   15.0 -6.2 55.5 1.0   20.0 -5.5 57. 1.0
30.0 -3.4 72.5 1.0   40.0 -1.7 86.5 1.0   60.0 -0.3 103. 1.0   80.0 3.3 138. 1.0
100.0 3.8 145.0 1.0   150.0 6.7 186.0 1.0
741 -855
0.1 -8.8 28.1 1.0   0.15 -11. 25.8 1.0   0.2 -12.2 26.5 1.0   0.3 -13.1 24.7 1.0
0.4 -13.9 22.9 1.0   0.6 -15.7 19.6 1.0   0.8 -16. 18.6 1.0   1.0 -15.6 19.7 1.
1.5 -9.2 39.5 1.0   2.0 -8.4 41. 1.0   3.0 -7.2 46.3 1.0   4.0 -5.4 56. 1.0
6.0 -3.2 75.5 1.0   8.0 -3.2 76.5 1.0   10.0 -4.3 68.0 1.0   15.0 -5.7 58.5 1.0
20.0 -4.9 60.0 1.0   30.0 -2.8 77.5 1.0   40.0 -1.3 92.0 1.0   60.0 0.0 107. 1.0
80.0 3.5 143.0 1.0   100.0 4.1 149.0 1.0   150.0 6.8 190.0 1.0
741 -856
0.2 -3.3 56.0 1.0   0.3 -8.2 42.5 1.0   0.4 -9.7 36.3 1.0   0.6 -12.4 28.4 1.0
0.8 -13.4 25.5 1.0   1.0 -13.3 25.5 1.0   1.5 -9.5 37. 1.0   2.0 -5.8 55.5 1.0
3.0 -8.5 40.7 1.0   4.0 -6.8 50.7 1.0   6.0 -4.1 69.0 1.0   8.0 -1.7 89. 1.0
10.0 -0.9 98.0 1.0   15.0 -3.8 71.5 1.0   20.0 -3.7 70.0 1.0   30.0 -1.7 87.0 1.
40.0 -0.8 96.0 1.0   60.0 0.7 116.0 1.0   80.0 4.7 163.0 1.0   100.0 8.4 173. 1.
150.0 8.0 210.0 0.97
741 -857
0.6 -10.3 35.7 1.0   0.8 -11.9 29.5 1.0   1.0 -12.3 28.6 1.0   1.5 -9.1 63. 1.0
```

TABLE C2 (3 of 3)

MEASURED VALUES OF DEMODULATION RFI RESPONSES OF THE THREE-STAGE OP AMP LED CIRCUIT WITH RFI SUPPRESSION CAPACITOR

```
2.0 -6.1 42.5 1.0   3.0 -7.9 45.0 1.0   4.0 -6.0 55.0 1.0   6.0 -3.0 76.0 1.0
8.0 -1.1 97.5 1.0   10.0 -1.0 97.5 1.0   15.0 -4.0 111.0 1.0   20.0 -3.6 69.0 1.0
30.0 -1.7 87.0 1.0   40.0 -0.7 97.5 1.0 60.0 0.3 110.0 1.0   60.0 4.2 153.0 1.0
100.0 4.7 156.0 1.0   150.0 7.4 200.0 1.0
741 -858
0.3 -6.8 52.3 1.0   0.4 -11.4 41.0 1.0   0.6 -12.2 29.6 1.0   0.8 -13.3 25.8 1.0
1.0 -13.3 25.7 1.0   1.5 -2.6 61.0 1.0   2.0 -8.6 34.0 1.0   3.0 -8.2 42.0 1.0
4.0 -8.1 54.5 1.0   6.0 -3.0 77.0 1.0   8.0 -1.3 94.0 1.0   10.0 -1.6 92.0 1.0
15.0 -4.6 86.5 1.0   20.0 -4.2 81.5 1.0   30.0 -2.1 84.0 1.0   40.0 -0.9 95. 1.0
60.0 0.3 111.0 1.0   80.0 4.1 151.0 1.0   100.0 4.7 159. 1.0   150.0 7.4 200. 1.
741 -859
0.2 -3.7 71.0 1.0   0.4 -7.5 49.3 1.0   0.6 -11.9 29.9 1.0   0.8 -13.4 25.4 1.0
1.0 -13.4 25. 1.0   1.5 -6.8 40.3 1.0   2.0 -7.6 45.7 1.0   3.0 -9.0 36.5 1.0
4.0 -7.2 46.6 1.0   6.0 -4.3 87.5 1.0   8.0 -2.1 87.0 1.0   10.0 -1.3 96.0 1.0
15.0 -4.0 70.5 1.0   20.0 -3.9 68.7 1.0   30.0 -1.9 86.0 1.0   40.0 -0.9 95.0 1.
60.0 0.5 114.0 1.0   80.0 4.5 159. 1.0   100.0 5.1 167. 1.0   150.0 7.7 208. 1.0
741 -860
0.4 -7.8 46.5 1.0   0.6 -10.3 35.7 1.0   0.8 -11.2 32.0 1.0   1.0 -11.4 31.5 1.0
1.5 -6.3 55.8 1.0   2.0 -5.0 62.5 1.0   3.0 -6.4 53.3 1.0   4.0 -4.7 64.0 1.0
6.0 -1.8 89.5 1.0   8.0 0.2 111.0 1.0   10.0 0.3 124.0 1.0   15.0 -2.6 82.5 1.0
20.0 -3.0 76. 1.0   30.0 -1.5 91.0 1.0   40.0 -0.3 103. 1.0   60.0 0.4 113. 1.0
80.0 3.9 150.0 1.0   100.0 4.4 156.0 1.0   150.0 6.9 192.0 1.0
741 -8K6
0.1 -0.4 76. 1.0   1.5 -6.7 53.3 1.0   2.0 -5.8 57.0 1.0   3.0 -2.6 73.0 1.0
4.0 -1.2 95.0 1.0   6.0 2.8 169.0 1.0   8.0 5.9 220.0 1.0   10.0 8.4 295.0 1.0
15.0 8.7 305.0 1.0   20.0 5.0 193.0 1.0   30.0 3.3 161.0 1.0   40.0 3.6 168. 1.0
60.0 3.9 174.0 1.0   80.0 6.6 202. 1.0   100.0 6.2 189. 1.0   150.0 7.6 210. 1.0
741 -8K14
1.5 -7.2 50.5 1.0   2.0 -6.3 54.0 1.0   3.0 -4.1 69. 1.0   4.0 -1.7 90. 1.0
6.0 4.5 152.0 1.0   8.0 7.6 214.0 1.0   10.0 8.2 285.0 1.0   15.0 8.7 303.0 1.0
20.0 5.3 202.0 1.0   30.0 3.7 168.0 1.0   40.0 4.0 175.0 1.0   60.0 4.2 179.0 1.
80.0 6.7 207.0 1.0   100.0 5.3 191.0 1.0   150.0 7.7 210.0 1.0
741 -8K20
0.1 -1.1 73. 1.0   0.4 -2.7 65.3 1.0   1.5 -6.6 54.3 1.0   2.0 -5.8 57.0 1.0
3.0 -3.7 72.5 1.0   4.0 -1.3 95.0 1.0   6.0 2.6 158.0 1.0   8.0 5.9 222.0 1.0
10.0 8.3 290.0 1.0   15.0 8.9 310.0 1.0   20.0 5.5 206.0 1.0   30.0 3.6 175.0 1.
40.0 3.8 172.0 1.0   50. 4.1 177.0 1.0   80.0 6.7 205.0 1.0   100.0 6.3 189. 1.0
150.0 7.7 206.0 1.0
741 -8K26
1.0 -8.2 45.0 1.0   1.5 -8.4 42.3 1.0   2.0 -7.1 49.0 1.0   3.0 -4.7 64.5 1.0
4.0 -2.1 86.0 1.0   6.0 2.0 137.0 1.0   8.0 5.3 207.0 1.0   10.0 7.8 273.0 1.0
15.0 8.7 175.0 1.0   20.0 1.4 125.0 1.0   30.0 1.7 130.0 1.0   40.0 2.4 140.0 1.
60. 3.2 160. 1.   80. 6.5 200. 1.   100. 6.4 194. 1.0   150. 8. 213. 0.945
741 -8K32
0.8 -5.2 65.0 1.0   1.0 -6.3 58.0 1.0   1.5 -7.1 51.0 1.0   2.0 -6.2 54.3 1.0
3.0 -4.0 69.5 1.0   4.0 -1.6 91.0 1.0   6.0 2.4 150.0 1.0   8.0 5.5 212.0 1.0
10.0 7.8 275.0 1.0   15.0 8.0 280.0 1.0   20.0 4.4 193.0 1.0   30.0 3.3 162.0 1.
40.0 3.6 169.0 1.0   60.0 4.1 176.0 1.0   80.0 6.8 206.0 1.0   100.0 6.2 189. 1.
150.0 8.0 212.0 1.0
14.02.18.UCPG, 1022,      0.004 KPGS.
14.02.18.UCLN, 1022,      0.219 KLNS.
14.03.08.UCLP, AA, 033,      0.255KLNS.
```

APPENDIX D

NCAP SENSITIVITY ANALYSIS RESULTS FOR THE UNITY GAIN BUFFER AMPLIFIER CIRCUITS

Appendix D contains four tables of NCAP sensitivity analysis results. Tables D1 and D2 contain NCAP sensitivity results for the 741 unity gain buffer amplifier circuit shown in Figure 6-1. Tables D3 and D4 contain NCAP sensitivity results for the LF355 unity gain buffer amplifier circuit shown in Figure 6-5. The effects of the JFET interelectrode parasitic capacitances are included in the circuit simulations. (C_{p1}= 5pF, C_{p2}= 3pF, C_{p3}= 4pF). The standard values in the second column of each table are H_2 values obtained when the original NCAP parameter values are used.

In Table D1 are H_2 values for a +10% and a -10% variation in the value of one BJT model parameter for RF frequencies 0.1 to 100 MHz. Note that H_2 values for the -10% variation in the value of the parameters V_{CB}, μ, I_{Cmax}, a, h_{FEmax}, K, C_2', r_b, and r_c are not listed because the appropriate simulations have not been performed. Also omitted are H_2 values for both +10% and -10% variations in the value of the parameters C_1 and C_2. In Table D2 are H_2 values for a +10% and a -10% variation in the value of one linear macromodel parameter for RF frequencies 0.1 to 500 MHz. Note that H_2 values for the -10% variation in the value of the parameter C_2 are not listed because the appropriate simulations have not been performed. Also omitted are H_2 values for both +10% and -10% variations in the value of the parameters R_2, R_{O1}, R_{O2}, and C_b. In Table D3 are H_2 values for a +10% and a -10% variation in the value of one JFET model parameter for RF frequencies 0.1 to 500 MHz. Note that H_2 values for the -10% variation in the value of the parameters V_p, ρ, Ψ, V_{GS}, and K are

not listed because the appropriate simulations have not been performed. Also omitted are H_2 values for both +10% and -10% variations in the value of the parameters C_{GD}, R_S, m, and V_o. In Table D4 are H_2 values for a +10% and a -10% variation in the value of one linear macromodel parameter for RF frequencies 0.1 to 500 MHz. Note that H_2 values for the +10% and -10% variations in the value of the parameters C_1, R_2, R_{b1}, R_{b2}, and C_b are not listed because the appropriate simulations have not been performed.

TABLE D1(1 OF 4)

NCAP SENSITIVITY ANALYSIS RESULTS FOR 741 UNITY GAIN BUFFER AMPLIFIER
BJT MODEL PARAMETER VARIATION

Values of $20\log_{10}|H_2(f_1,-f_2)|$ vs RF Frequency

Freq	Std.	V_{CBO}		I_C		V_{CB}		C_{je}	
MHz	Value	+10%	-10%	+10%	-10%	+10%	-10%	+10%	-10%
0.10	-58.1	-59.0	-56.3	-59.8	-56.3	-56.5		-58.1	-58.1
0.15	-51.1	-51.9	-49.2	-52.7	-49.2	-49.4		-51.0	-51.2
0.20	-46.1	-47.0	-44.3	-47.8	-44.3	-44.5		-46.1	-46.1
0.30	-39.2	-40.1	-37.3	-41.0	-37.4	-38.0		-39.1	-39.2
0.40	-34.4	-35.4	-32.5	-36.0	-32.7	-33.0		-34.4	-34.4
0.60	-27.9	-29.0	-26.0	-29.4	-26.3	-26.0		-28.0	-28.0
0.80	-23.7	-24.9	-21.4	-25.1	-22.2	-22.0		-24.0	-24.0
1.00	-20.8	-22.1	-20.0	-22.0	-19.5	-19.0		-21.0	-21.0
1.50	-16.7	-18.4	-18.3	-18.0	-16.0	-14.0		-17.0	-17.0
2.00	-15.2	-17.0	-12.0	-16.0	-15.0	-12.1		-15.2	-15.2
3.00	-15.1	-17.0	-11.3	-16.0	-14.4	-12.0		-15.1	-15.1
4.00	-15.6	-17.5	-12.0	-16.4	-15.0	-12.4		-16.0	-16.0
6.00	-14.8	-16.4	-11.5	-16.1	-13.3	-12.0		-15.0	-15.0
8.00	-12.4	-14.0	-09.5	-14.0	-11.0	-09.8		-13.0	-12.4
10.0	-10.4	-12.0	-07.8	-12.0	-09.2	-08.0		-11.0	-10.2
15.0	-07.8	-08.9	-05.9	-09.0	-07.0	-06.1		-08.2	-08.0
20.0	-07.4	-08.3	-06.0	-08.0	-07.0	-06.0		-08.0	-07.0
30.0	-08.7	-09.3	-07.6	-09.1	-08.3	-07.7		-09.3	-08.1
40.0	-10.6	-11.0	-09.8	-11.0	-10.2	-09.9		-11.4	-10.0
60.0	-14.4	-15.0	-14.0	-15.0	-14.0	-14.0		-15.4	-13.4
80.0	-17.8	-18.1	-17.5	-18.1	-17.6	-17.4		-19.0	-17.0
100.	-20.8	-21.0	-21.0	-21.1	-21.0	-21.0		-22.0	-20.0
150.	-27.1								
200.	-32.3								
300.	-40.4								
400.	-46.6								
500.	-51.6								

TABLE D1(2 OF 4)

NCAP SENSITIVITY ANALYSIS RESULTS FOR 741 UNITY GAIN BUFFER AMPLIFIER
BJT MODEL PARAMETER VARIATION

Values of $20\log_{10}|H_2(f_1,-f_2)|$ vs RF Frequency

Freq	Std.	η		μ		I_{Cmax}		a	
MHz	Value	+10%	-10%	+10%	-10%	+10%	-10%	+10%	-10%
0.10	-58.1	-58.5	-58.0	-58.1		-58.1		-58.1	
0.15	-51.1	-51.4	-50.6	-51.1		-51.1		-51.1	
0.20	-46.1	-46.5	-46.0	-46.1		-46.1		-46.1	
0.30	-39.2	-40.0	-38.7	-39.2		-39.2		-39.2	
0.40	-34.4	-34.8	-33.9	-34.4		-34.4		-34.4	
0.60	-27.9	-28.4	-27.4	-27.9		-27.9		-27.9	
0.80	-23.7	-24.2	-23.1	-23.7		-23.7		-23.7	
1.00	-20.8	-21.3	-20.1	-20.8		-20.8		-20.8	
1.50	-16.7	-17.4	-15.9	-17.0		-16.7		-16.7	
2.00	-15.2	-15.9	-14.3	-15.2		-15.2		-15.2	
3.00	-15.1	-15.8	-14.1	-15.0		-15.1		-15.1	
4.00	-15.6	-16.4	-14.7	-16.0		-15.6		-15.6	
6.00	-14.8	-15.5	-13.9	-15.0		-15.0		-15.0	
8.00	-12.4	-13.1	-12.0	-12.4		-12.4		-12.5	
10.0	-10.4	-11.0	-09.7	-10.4		-10.4		-10.4	
15.0	-07.8	-08.3	-07.3	-08.0		-07.8		-07.8	
20.0	-07.4	-08.0	-07.2	-07.3		-07.4		-07.4	
30.0	-08.7	-08.9	-08.4	-09.0		-09.0		-09.0	
40.0	-10.5	-10.8	-10.4	-10.5		-10.6		-10.6	
60.0	-14.4	-15.0	-14.3	-14.3		-14.4		-14.4	
80.0	-17.8	-17.9	-17.7	-18.0		-17.8		-17.8	
100.	-20.8	-20.9	-20.8	-20.7		-20.8		-20.8	
150.	-27.1								
200.	-32.3								
300.	-40.4								
400.	-46.6								
500.	-51.6								

TABLE D1(3 OF 4)

NCAP SENSITIVITY ANALYSIS RESULTS FOR 741 UNITY GAIN BUFFER AMPLIFIER
BJT MODEL PARAMETER VARIATION

Values of $20\log_{10}|H_2(f_1,-f_2)|$ vs RF Frequency

Freq	Std.	h_{FEmax}		K		n		C_2'	
MHz	Value	+10%	-10%	+10%	-10%	+10%	-10%	+10%	-10%
0.10	-58.1	-58.1		-58.1		-57.2	-59.0	-58.1	
0.15	-51.1	-51.1		-51.1		-50.2	-51.9	-51.1	
0.20	-46.1	-46.1		-46.1		-45.3	-47.0	-46.1	
0.30	-39.2	-39.2		-39.2		-38.4	-40.0	-39.2	
0.40	-34.4	-34.4		-34.4		-33.4	-35.2	-34.4	
0.60	-27.9	-27.9		-28.0		-27.3	-28.6	-27.9	
0.80	-23.7	-23.7		-24.0		-23.3	-24.2	-23.7	
1.00	-20.8	-21.0		-20.7		-20.5	-21.1	-20.8	
1.50	-16.7	-16.7		-17.0		-17.0	-16.7	-16.7	
2.00	-15.2	-15.2		-15.2		-15.5	-15.0	-15.2	
3.00	-15.1	-15.1		-15.1		-15.3	-14.7	-15.1	
4.00	-15.6	-15.6		-16.0		-15.6	-16.0	-15.6	
6.00	-14.8	-15.0		-14.9		-14.4	-15.2	-15.0	
8.00	-12.4	-12.4		-13.0		-12.0	-13.0	-12.5	
10.0	-10.4	-10.4		-10.5		-10.2	-10.8	-10.4	
15.0	-07.8	-07.8		-08.0		-08.0	-07.8	-07.9	
20.0	-07.4	-07.4		-07.6		-07.7	-07.1	-07.4	
30.0	-08.7	-09.0		-09.0		-09.2	-08.2	-08.7	
40.0	-10.5	-10.6		-10.9		-11.1	-10.0	-10.1	
60.0	-14.4	-14.4		-15.0		-15.0	-13.8	-14.5	
80.0	-17.8	-17.8		-18.2		-18.5	-17.2	-18.0	
100.	-20.8	-20.8		-21.2		-21.5	-20.1	-21.0	
150.	-27.1								
200.	-32.3								
300.	-40.4								
400.	-46.6								
500.	-51.6								

TABLE D1(4 OF 4)

NCAP SENSITIVITY ANALYSIS RESULTS FOR 741 UNITY GAIN BUFFER AMPLIFIER
BJT MODEL PARAMETER VARIATION

Values of $20\log_{10}|H_2(f_1,-f_2)|$ vs RF Frequency

Freq	Std.	r_b		r_c		C_1		C_2	
MHz	Value	+10%	-10%	+10%	-10%	+10%	-10%	+10%	-10%
0.10	-58.1	-58.1		-58.1					
0.15	-51.1	-51.1		-51.1					
0.20	-46.1	-46.1		-46.1					
0.30	-39.2	-39.2		-39.2					
0.40	-34.4	-34.4		-34.4					
0.60	-27.9	-27.9		-27.9					
0.80	-23.7	-24.0		-23.7					
1.00	-20.8	-21.0		-21.0					
1.50	-16.7	-17.0		-16.7					
2.00	-15.2	-15.1		-15.2					
3.00	-15.1	-15.0		-16.0					
4.00	-15.6	-16.0		-15.6					
6.00	-14.8	-14.8		-15.0					
8.00	-12.4	-13.0		-12.4					
10.0	-10.4	-10.4		-10.4					
15.0	-07.8	-08.0		-07.5					
20.0	-07.4	-07.5		-07.4					
30.0	-08.7	-09.0		-09.0					
40.0	-10.5	-11.0		-10.6					
60.0	-14.4	-14.8		-14.4					
80.0	-17.8	-18.3		-17.8					
100.	-20.8	-21.3		-20.8					
150.	-27.1								
200.	-32.3								
300.	-40.4								
400.	-46.6								
500.	-51.6								

TABLE D2(1 OF 3)

NCAP SENSITIVITY ANALYSIS RESULTS FOR 741 UNITY GAIN BUFFER AMPLIFIER
LINEAR MACROMODEL PARAMETER VARIATION

Values of $20\log_{10}|H_2(f_1,-f_2)|$ vs RF Frequency

Freq	Std.	C_E		R_e		C_2		G_a	
MHz	Value	+10%	-10%	+10%	-10%	+10%	-10%	+10%	-10%
0.10	-58.1	-57.2	-59.0	-58.1	-58.1	-57.3		-59.0	-57.2
0.15	-51.1	-50.2	-52.0	-51.1	-51.2	-50.3		-51.8	-50.2
0.20	-46.1	-45.2	-47.0	-46.1	-46.1	-45.4		-47.0	-45.3
0.30	-39.2	-38.3	-40.1	-39.2	-39.1	-38.5		-39.9	-38.4
0.40	-34.4	-34.0	-35.3	-34.5	-34.3	-34.0		-35.1	-34.0
0.60	-27.9	-27.1	-29.0	-28.1	-28.0	-27.5		-28.5	-27.4
0.80	-23.7	-23.0	-25.0	-23.9	-23.5	-23.4		-24.1	-23.4
1.00	-20.8	-20.0	-22.0	-21.1	-21.0	-20.7		-20.9	-20.7
1.50	-16.7	-15.9	-17.7	-17.2	-16.4	-17.2		-16.4	
2.00	-15.2	-14.4	-16.2	-15.8	-15.0	-15.9		-14.5	-16.0
3.00	-15.1	-14.2	-16.1	-16.0	-15.0	-16.0		-14.2	-16.0
4.00	-15.6	-14.6	-17.0	-16.2	-15.2	-16.2		-15.0	-16.3
6.00	-14.8	-13.6	-16.2	-15.1	-14.5	-14.9		-15.0	-15.0
8.00	-12.4	-11.3	-13.7	-12.7	-12.2	-12.5		-12.4	-12.5
10.0	-10.4	-09.4	-11.6	-10.7	-10.1	-10.4		-10.4	-10.4
15.0	-07.8	-07.1	-08.7	-08.2	-07.5	-07.8		-08.0	
20.0	-07.4	-07.0	-08.1	-07.8	-07.5			-07.4	-07.4
30.0	-08.7	-08.3	-09.2	-09.1	-08.2	-09.0		-09.0	-09.0
40.0	-10.5	-10.3	-11.0	-11.2	-10.1	-10.6		-10.6	-10.6
60.0	-14.5	-14.2	-14.8	-15.1	-14.0	-14.4		-14.4	-14.4
80.0	-17.8	-17.6	-18.2	-18.5	-17.2	-17.8		-18.0	-18.0
100.	-20.8	-20.6	-21.1	-22.0	-20.1	-20.8		-20.8	-20.8
150.	-27.1	-27.0	-27.4	-28.0	-26.3	-27.2		-27.1	-27.2
200.	-32.3	-32.2	-32.5	-33.3	-31.4	-32.3		-32.3	-32.3
300.	-40.4	-40.3	-41.0	-41.5	-39.5	-40.5		-40.5	-40.5
400.	-46.6	-46.6	-47.0	-47.6	-45.7	-46.7		-46.7	-46.7
500.	-51.6	-51.6	-52.0	-52.5	-51.0	-52.0		-52.0	-52.0

TABLE D2(2 OF 3)

NCAP SENSITIVITY ANALYSIS RESULTS FOR 741 UNITY GAIN BUFFER AMPLIFIER
LINEAR MACROMODEL PARAMETER VARIATION

Values of $20\log_{10}|H_2(f_1,-f_2)|$ vs RF Frequency

Freq	Std.	R_C		R_E		C_1		R_2	
MHz	Value	+10%	-10%	+10%	-10%	+10%	-10%	+10%	-10%
0.10	-58.1	-58.9	-57.2	-58.1	-58.1	-58.1	-58.1		
0.15	-51.1	-51.8	-50.2	-51.1	-51.1	-51.0	-51.1		
0.20	-46.1	-46.8	-45.3	-46.1	-46.1	-46.1	-46.1		
0.30	-39.2	-39.9	-38.4	-39.2	-39.2	-39.2	-39.2		
0.40	-34.4	-35.0	-33.7	-34.4	-34.4	-34.4	-34.4		
0.60	-27.9	-28.4	-27.5	-27.9	-27.9	-27.8	-28.0		
0.80	-23.7	-23.9	-23.6	-23.7	-23.7	-23.6	-23.8		
1.00	-20.8	-20.8	-20.9	-20.8	-20.8	-20.7	-20.9		
1.50	-16.7	-16.2	-17.4	-16.8	-16.8	-16.6	-16.9		
2.00	-15.2	-14.5	-16.0	-15.3	-15.3	-15.1	-15.3		
3.00	-15.1	-14.5	-15.7	-15.1	-15.1	-15.3	-14.9		
4.00	-15.6	-15.5	-15.9	-15.7	-15.7	-16.0	-15.3		
6.00	-14.8	-14.9	-14.7	-14.8	-14.8	-15.0	-14.5		
8.00	-12.4	-12.5	-12.4	-12.5	-12.5	-12.5	-12.4		
10.0	-10.4	-10.5	-10.4	-10.4	-10.4	-10.4	-10.4		
15.0	-07.8	-07.9	-07.8	-07.9	-07.9	-07.8	-07.9		
20.0	-07.4	-07.5	-07.3	-07.4	-07.4	-07.4	-07.5		
30.0	-08.7	-08.7	-08.6	-08.7	-08.7	-08.7	-08.7		
40.0	-10.5	-10.6	-10.5	-10.6	-10.6	-10.6	-10.6		
60.0	-14.4	-14.4	-14.4	-14.5	-14.5	-14.5	-14.4		
80.0	-17.8	-17.7	-17.8	-17.8	-17.8	-17.9	-17.8		
100.	-20.8	-20.7	-20.8	-20.9	-20.9	-20.9	-20.8		
150.	-27.1	-27.0	-27.2	-27.2	-27.2	-27.3	-27.1		
200.	-32.3	-32.2	-32.3	-32.4	-32.4	-32.4	-32.2		
300.	-40.4	-40.3	-40.5	-40.5	-40.5	-40.6	-40.3		
400.	-46.6	-46.6	-46.6	-46.7	-46.7	-46.9	-46.5		
500.	-51.6	-51.7	-51.6	-51.7	-51.7	-51.9	-51.5		

TABLE D2(3 OF 3)

NCAP SENSITIVITY ANALYSIS RESULTS FOR 741 UNITY GAIN BUFFER AMPLIFIER
LINEAR MACROMODEL PARAMETER VARIATION

Values of $20\log_{10}|H_2(f_1,-f_2)|$ vs RF Frequency

Freq	Std.	G_{cm}		R_{01}		R_{02}		G_b	
MHz	Value	+10%	-10%	+10%	-10%	+10%	-10%	+10%	-10%
0.10	-58.1	-58.1	-58.1						
0.15	-51.1	-51.1	-51.1						
0.20	-46.1	-46.1	-46.1						
0.30	-39.2	-39.2	-39.2						
0.40	-34.4	-34.4	-34.4						
0.60	-27.9	-27.9	-27.9						
0.80	-23.7	-23.7	-23.7						
1.00	-20.8	-21.0	-21.0						
1.50	-16.7	-16.7	-16.7						
2.00	-15.2	-15.2	-15.2						
3.00	-15.1	-15.1	-15.1						
4.00	-15.6	-15.6	-15.6						
6.00	-14.8	-15.0	-15.0						
8.00	-12.4	-12.4	-12.4						
10.0	-10.4	-10.4	-10.4						
15.0	-07.8	-07.8	-07.8						
20.0	-07.4	-07.4	-07.4						
30.0	-08.7	-09.0	-09.0						
40.0	-10.5	-10.6	-10.6						
60.0	-14.4	-14.4	-14.4						
80.0	-17.8	-17.8	-17.8						
100.	-20.8	-20.8	-20.8						
150.	-27.1	-27.2	-27.2						
200.	-32.3	-32.3	-32.3						
300.	-40.4	-40.5	-40.5						
400.	-46.6	-46.7	-46.7						
500.	-51.6	-52.0	-52.0						

TABLE D3(1 OF 2)

NCAP SENSITIVITY ANALYSIS RESULTS FOR LF355 UNITY GAIN BUFFER AMPLIFIER
JFET MODEL PARAMETER VARIATION

VALUES OF $20\log_{10}|H_2(f_1,-f_2)|$ vs RF FREQUENCY

Freq	Std.	V_p		I_{Dmax}		ρ		Ψ	
MHz	Value	+10%	-10%	+10%	-10%	+10%	-10%	+10%	-10%
0.10	-74.0	-75.0		-76.0	-72.1	-74.1		-72.9	
0.15	-67.3	-68.4		-69.0	-65.5	-67.5		-66.3	
0.20	-61.9	-63.0		-63.5	-60.2	-62.0		-60.9	
0.30	-55.3	-56.4		-57.0	-54.0	-55.4		-54.3	
0.40	-50.2	-51.3		-51.7	-48.6	-50.1		-49.3	
0.60	-43.9	-45.0		-45.2	-43.0	-44.0		-43.0	
0.80	-40.1	-41.2		-41.1	-38.9	-39.9		-39.3	
1.00	-38.0	-39.3		-39.0	-37.4	-38.0		-37.5	
1.10	-37.8	-39.0		-37.6	-37.1	-36.8		-37.0	
1.20	-37.8	-39.2		-38.0	-38.4	-37.2		-38.0	
1.30	-39.8	-41.5		-39.0	-42.3	-38.7		-40.8	
1.40	-46.1	-49.0		-42.0	-74.4	-43.4		-51.7	
1.50	-59.0	-54.9		-49.5	-42.3	-59.1		-47.0	
1.60	-35.3	-36.0		-41.0	-31.5	-37.0		-32.9	
1.70	-29.1	-30.2		-32.1	-27.3	-29.6		-27.9	
1.80	-25.4	-27.0		-27.0	-25.1	-25.3		-25.0	
1.90	-23.5	-25.0		-24.0	-24.6	-22.8		-23.8	
2.00	-23.2	-24.8		-22.4	-25.2	-22.0		-24.0	
2.10	-24.2	-26.0		-22.0	-27.3	-23.0		-25.7	
2.20	-26.1	-28.1		-23.2	-30.0	-24.3		-28.0	
2.30	-29.0	-30.8		-25.3	-33.4	-27.0		-31.0	
2.40	-32.0	-34.2		-28.0	-37.8	-29.7		-34.8	
2.50	-35.2	-37.6		-30.5	-42.9	-33.0		-38.7	
3.00	-49.0	-45.1		-60.2	-41.0	-47.8		-41.8	
4.00	-35.0	-36.1		-35.3	-34.3	-34.4		-34.4	
5.00	-34.4	-36.0		-35.0	-34.2	-33.9		-34.2	
6.00	-34.4	-35.7		-34.4	-34.3	-33.8		-34.2	
8.00	-35.2	-36.6		-35.3	-35.2	-35.0		-35.1	
10.0	-36.2	-38.0		-36.2	-36.2	-35.6		-36.0	
15.0	-38.9	-40.3		-39.0	-39.0	-38.4		-38.8	
20.0	-40.5	-42.0		-40.5	-40.5	-39.9		-40.4	
30.0	-44.5	-46.0		-44.5	-44.5	-43.9		-44.4	
40.0	-47.2	-48.5		-47.1	-47.2	-47.0		-47.1	
60.0	-52.2	-54.0		-52.2	-52.2	-51.6		-52.1	
80.0	-56.3	-57.7		-56.3	-56.4	-55.7		-56.2	
100.	-60.0	-61.1		-60.0	-59.8	-59.2		-59.7	
150.	-67.1	-68.5		-67.1	-67.1	-66.5		-67.0	
200.	-71.4	-72.8		-71.4	-71.5	-70.8		-71.3	
300.	-79.0	-80.0		-78.5	-78.6	-78.0		-78.5	
400.	-84.0	-85.0		-84.0	-83.7	-83.1		-83.6	
500.	-87.6	-89.0		-88.0	-87.7	-87.0		-87.6	

TABLE D3(2 OF 2)

NCAP SENSITIVITY ANALYSIS RESULTS FOR LF355 UNITY GAIN BUFFER AMPLIFIER
JFET MODEL PARAMETER VARIATION

VALUES OF $20\log_{10}|H_2(f_1,-f_2)|$ vs RF FREQUENCY

Freq	Std.	V_{GS}		K	
MHz	Value	+10%	-10%	+10%	-10%
0.10	-74.0	-72.9		-74.0	
0.15	-67.3	-66.3		-67.3	
0.20	-61.9	-60.9		-61.9	
0.30	-55.3	-54.3		-55.3	
0.40	-50.2	-49.3		-50.3	
0.60	-43.9	-43.0		-44.0	
0.80	-40.1	-39.2		-40.2	
1.00	-38.0	-37.3		-38.2	
1.10	-37.2	-36.6		-37.5	
1.20	-37.8	-37.3		-38.2	
1.30	-39.8	-39.7		-40.5	
1.40	-46.1	-48.0		-48.0	
1.50	-59.0	-51.2		-53.0	
1.60	-35.3	-33.6		-34.5	
1.70	-29.1	-28.0		-28.6	
1.80	-25.4	-24.7		-25.0	
1.90	-23.5	-23.2		-23.2	
2.00	-23.2	-23.2		-22.9	
2.10	-24.2	-24.5		-24.0	
2.20	-26.1	-27.0		-26.0	
2.30	-29.0	-29.5		-28.6	
2.40	-32.0	-33.0		-31.9	
2.50	-35.2	-36.5		-35.1	
3.00	-49.0	-43.0		-45.1	
4.00	-35.0	-34.1		-34.9	
5.00	-34.4	-33.8		-35.0	
6.00	-34.4	-34.0		-35.0	
8.00	-35.2	-35.0		-35.5	
10.0	-36.2	-35.6		-36.4	
15.0	-38.9	-38.4		-39.2	
20.0	-40.5	-39.9		-40.8	
30.0	-44.5	-43.9		-45.0	
40.0	-47.2	-47.0		-48.0	
60.0	-52.2	-51.6		-52.6	
80.0	-56.3	-55.7		-56.7	
100.	-60.0	-59.2		-60.2	
150.	-67.1	-66.5		-67.5	
200.	-71.4	-71.0		-72.0	
300.	-79.0	-78.0		-79.0	
400.	-84.0	-83.1		-84.1	
500.	-87.6	-87.1		-88.1	

TABLE D4 (1 of 2)

NCAP SENSITIVITY ANALYSIS RESULTS FOR LF355 UNITY GAIN BUFFER AMPLIFIER
LINEAR MACROMODEL PARAMETER VARIATION

VALUES OF $20\log_{10}|H_2(f_1,-f_2)|$ vs RF FREQUENCY

Freq.	Std.	R_d		G_a		R_s		C_2	
MHz	Value	+10%	-10%	+10%	-10%	+10%	-10%	+10%	-10%
0.10	-74.0	-75.0	-73.0	-75.0	-73.0	-74.0	-74.0	-73.1	-75.0
0.15	-67.3	-68.2	-66.4	-68.2	-66.4	-67.3	-67.3	-66.5	-68.3
0.20	-61.9	-63.0	-61.0	-63.0	-61.0	-61.9	-61.9	-61.1	-63.0
0.30	-55.3	-56.2	-54.4	-56.2	-54.4	-55.3	-55.3	-54.4	-56.3
0.40	-50.2	-51.1	-49.3	-51.1	-49.3	-50.2	-50.2	-49.3	-51.2
0.60	-43.9	-45.0	-43.0	-45.0	-42.8	-43.9	-43.9	-42.9	-45.0
0.80	-40.1	-41.3	-38.8	-41.2	-38.8	-40.0	-40.0	-38.9	-41.3
1.00	-38.0	-39.8	-36.4	-39.5	-36.5	-38.0	-38.0	-36.6	-39.6
1.10	-37.2	-39.7	-35.2	-38.9	-35.4	-37.3	-37.2	-36.0	-39.1
1.20	-37.8	-41.7	-35.0	-40.0	-36.0	-38.0	-38.0	-35.7	-40.3
1.30	-39.8	-49.0	-35.5	-43.2	-36.6	-39.9	-39.7	-37.0	-44.0
1.40	-46.1	-47.0	-36.9	-59.1	-39.6	-47.0	-46.0	-40.0	-62.5
1.50	-59.0	-38.0	-40.3	-46.3		-56.6	-62.3	-47.7	-45.7
1.60	-35.3	-27.8	-52.9	-32.4	-44.0	-35.0	-36.0	-42.4	-32.2
1.70	-29.1	-22.7	-43.3	-27.0	-35.1	-28.8	-29.4	-34.4	-26.4
1.80	-25.4	-19.1	-35.8	-22.2	-31.6	-25.1	-25.6	-30.9	-22.0
1.90	-23.5	-17.1	-33.0	-19.2	-30.5	-23.3	-24.0	-29.7	-19.0
2.00	-23.2	-17.1	-32.0	-18.1	-30.6	-23.0	-23.4	-30.0	-17.6
2.10	-24.2	-18.7	-32.1	-18.0	-33.0	-24.1	-24.3	-32.0	-17.2
2.20	-26.1	-21.3	-33.6	-19.4	-35.5	-26.1	-26.2	-34.5	-18.6
2.30	-29.0	-24.3	-36.2	-22.0	-40.0	-29.0	-29.0	-38.3	-20.9
2.40	-32.0	-27.7	-40.0	-24.5	-46.6	-31.9	-32.1	-44.4	-24.0
2.50	-35.2	-30.9	-44.2	-27.1	-60.0	-35.1	-35.4	-53.4	-26.3
3.00	-49.0	-49.1	-41.4	-53.9	-39.0	-45.2	-44.5	-39.3	-50.1
4.00	-35.0	-35.0	-34.4	-35.5	-34.2	-35.0	-34.6	-34.2	-35.6
5.00	-34.4	-34.6	-34.2	-35.0	-34.2	-34.5	-34.3	-34.2	-34.7
6.00	-34.4	-35.0	-34.2	-34.5	-34.2	-34.5	-34.3	-34.3	-34.5
8.00	-35.2	-35.4	-35.1	-35.3	-35.2	-35.4	-35.1	-35.2	-35.3
10.0	-36.2	-36.3	-36.0	-36.2	-36.1	-36.3	-36.0	-36.1	-36.2
15.0	-38.9	-39.0	-39.0	-39.0	-39.0	-39.2	-38.7	-38.9	-39.0
20.0	-40.5	-40.5	-40.5	-40.5	-40.5	-41.0	-40.2	-40.5	-40.5
30.0	-44.5	-44.5	-44.5	-44.5	-47.1	-44.8	-44.2	-44.5	-44.5
40.0	-47.2	-47.2	-47.2	-47.2	-44.5	-47.5	-47.0	-47.1	-47.2
60.0	-52.2	-52.2	-52.2	-52.2	-52.2	-52.6	-51.7	-52.2	-52.2
80.0	-56.3	-56.3	-56.3	-56.3	-56.3	-56.8	-55.8	-56.3	-56.3
100.	-60.0	-59.7	-60.0	-60.0	-59.7	-60.3	-59.2	-59.7	-60.0
150.	-67.1	-67.1	-67.1	-67.1	-67.1	-68.0	-66.5	-67.1	-67.1
200.	-71.4	-71.4	-71.4	-71.4	-71.4	-71.9	-70.9	-71.4	-71.4
300.	-79.0	-79.0	-79.0	-79.0	-79.0	-79.0	-78.1	-79.0	-79.0
400.	-84.0	-84.0	-84.0	-84.0	-84.0	-84.1	-83.2	-84.0	-84.0
500.	-87.6	-87.6	-87.6	-87.6	-87.6	-88.0	-87.2	-87.6	-87.6

TABLE D4 (2 of 2)

NCAP SENSITIVITY ANALYSIS RESULTS FOR LF355 UNITY GAIN BUFFER AMPLIFIER
LINEAR MACROMODEL PARAMETER VARIATION

VALUES OF $20\log_{10}|H_2(f_1,-f_2)|$ vs RF FREQUENCY

Freq.	Std.	C_s		G_{cm}	
MHz	Value	+10%	-10%	+10%	-10%
0.10	-74.0	-73.5	-74.4	-74.0	-74.0
0.15	-67.3	-66.8	-67.8	-67.3	-67.3
0.20	-61.9	-61.4	-62.4	-61.9	-61.9
0.30	-55.3	-54.8	-56.0	-55.3	-55.3
0.40	-50.2	-50.0	-51.0	-50.2	-50.2
0.60	-43.9	-43.5	-44.2	-43.9	-43.9
0.80	-40.1	-39.7	-40.4	-40.0	-40.0
1.00	-38.0	-37.8	-38.3	-38.0	-38.0
1.10	-37.2	-37.2	-37.4	-37.2	-37.2
1.20	-37.8	-38.0	-37.8	-37.8	-37.8
1.30	-39.8	-40.3	-40.0	-39.8	-39.8
1.40	-46.1	-48.1	-45.0	-46.1	-46.1
1.50	-59.0	-52.2	-82.1	-59.0	-59.0
1.60	-35.3	-34.1	-36.4	-35.3	-35.3
1.70	-29.1	-28.3	-29.9	-29.1	-29.1
1.80	-25.4	-24.7	-26.0	-25.4	-25.4
1.90	-23.5	-22.9	-24.0	-23.5	-23.5
2.00	-23.2	-23.0	-24.0	-23.2	-23.2
2.10	-24.2	-23.7	-24.6	-24.2	-24.2
2.20	-26.1	-25.7	-26.5	-26.1	-26.1
2.30	-29.0	-28.4	-29.1	-29.0	-29.0
2.40	-32.0	-32.0	-32.4	-32.0	-32.0
2.50	-35.2	-35.0	-36.0	-35.2	-35.2
3.00	-49.0	-44.5	-45.2	-45.0	-44.8
4.00	-35.0	-34.4	-35.0	-35.0	-35.0
5.00	-34.4	-34.1	-35.0	-34.4	-34.4
6.00	-34.4	-34.0	-34.7	-34.4	-34.4
8.00	-35.2	-34.8	-36.0	-35.2	-35.2
10.0	-36.2	-35.7	-36.6	-36.2	-36.2
15.0	-38.9	-38.5	-39.4	-38.9	-38.9
20.0	-40.5	-40.0	-41.0	-40.5	-40.5
30.0	-44.5	-44.1	-45.0	-44.5	-44.5
40.0	-47.2	-46.8	-48.0	-47.2	-47.2
60.0	-52.2	-52.0	-52.5	-52.2	-52.2
80.0	-56.3	-56.1	-56.5	-56.3	-56.3
100.	-60.0	-59.6	-60.0	-60.0	-60.0
150.	-67.1	-67.0	-67.2	-67.1	-67.0
200.	-71.4	-71.4	-71.5	-71.4	-71.4
300.	-79.0	-78.5	-79.0	-79.0	-78.6
400.	-84.0	-84.0	-84.0	-84.0	-83.7
500.	-87.6	-87.6	-87.6	-87.6	-87.6

APPENDIX E

DISCUSSION: SUPPRESSION OF RFI RESPONSES IN INVERTING AMPLIFIER

In Chapter 5, we have presented experimental results showing how RFI demodulation responses in an op amp inverting amplifier can be suppressed by including a 27 pF capacitor in the feedback path. Here we attempt to apply the approach used by Goedbloed, Riemens and Stienstra[31] to calculate theoretically the amount of RFI suppression. The calculated values will be compared to the experimental values in Figure 5-5.

Shown in Figure E-1 is the circuit diagram of an inverting amplifier. We define:

V_i = input voltage containing a desired signal and an interference signal,

V_{in} = desired signal,

V_{RF} = interference signal,

Z_i = differential input impedance of the op amp,

Z_o = output impedance of the op amp,

A = op amp open-loop voltage gain,

V_o = output voltage,

Z_L = load impedance.

The voltage at the inverting node and the non-inverting node of the op amp are denoted as V_1 and V_2 respectively. We assume that the non-inverting node is connected to ground so that $V_2 = 0$. Following the approach used by Goedbloed et al.,[31] we first determine the voltage ratio V_1/V_i. Applying Kirchhoff's current law at the inverting input node, we have

$$(V_i-V_1)/R_1 = (V_1/Z_1) + (V_1-V_o)/Z_2 \qquad \text{(E-1)}$$

where $Z_2 = R_2 \| C_4 = R_2/(1+j\omega R_2 C_4)$. Rearranging Eq.(E-1) so that only V_o

RFI Suppression in the inverting amplifier

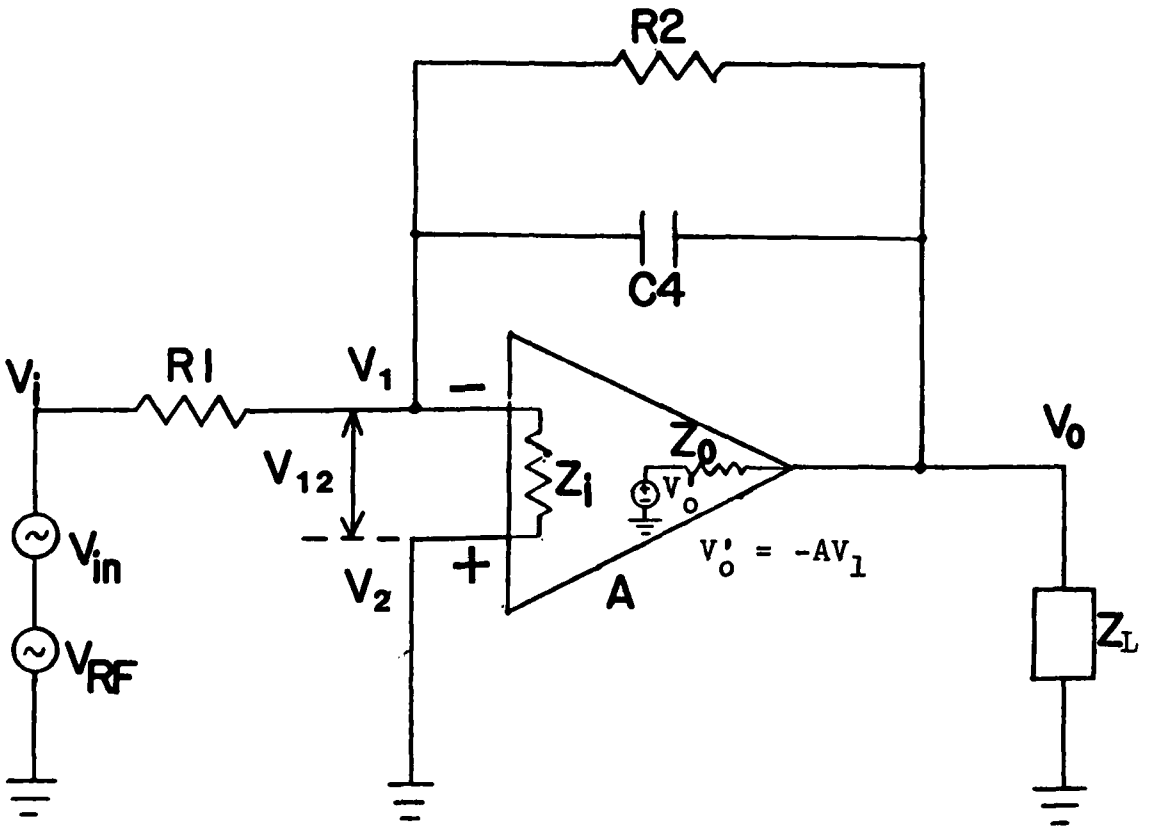

Fig. E-1. RFI suppression in the inverting amplifier.

appears on the left-hand side, we have

$$(V_i/R_1) - (V_1/R_1) = (V_1/Z_i) + (V_1/Z_2) - (V_o/Z_2) \qquad (E\text{-}2)$$

$$(V_o/Z_2) = V_1[(1/Z_i)+(1/Z_2)+(1/R_1)] - (V_i/R_1) \qquad (E\text{-}3)$$

$$V_o = V_1Z_2[(1/Z_i)+(1/Z_2)+(1/R_1)] - V_iZ_2/R_1 \qquad (E\text{-}4)$$

Applying Kirchhoff's current law at the output node, we have

$$(-AV_1-V_o)/Z_o + (V_1-V_o)/Z_2 = V_o/Z_L \qquad (E\text{-}5)$$

Rearranging Eq.(E-5) so that only V_o appears on the left-hand side, we have

$$(-AV_1/Z_o) - (V_o/Z_o) + (V_1/Z_2) - V_o/Z_2 = V_o/Z_L \qquad (E\text{-}6)$$

$$V_o[(-1/Z_o)-(1/Z_2)-(1/Z_L)] = V_1[A/Z_o-(1/Z_2)] \qquad (E\text{-}7)$$

$$V_o = V_1[A/Z_o-(1/Z_2)]/[(-1/Z_o)-(1/Z_2)-(1/Z_L)] \qquad (E\text{-}8)$$

Note that the voltage dependent voltage source, V_o', is in general a nonlinear function of V_1. The nonlinear function can be expressed as a power series and AV_1 is the linear term. In writing Eq. (E-5), we have assumed that the nonlinear terms in the power series are small compared to the linear term. Equating the right-hand sides of Eqs. (E-4) and (E-8), we have

$$V_1Z_2[(1/Z_i)+(1/Z_2)+(1/R_1)]-V_iZ_2/R_1 = V_1[A/Z_o-(1/Z_2)]/[(-1/Z_o)-(1/Z_2)-(1/Z_L)] \qquad (E\text{-}9)$$

Rearranging Eq.(E-9) to obtain the voltage ratio V_1/V_i, we have

$$V_1[(Z_2/Z_i)+1+(Z_2/R_1)+(A/Z_o-1/Z_2)/(1/Z_o+1/Z_2+1/Z_L)] = V_iZ_2/R_1 \qquad (E\text{-}10)$$

$$V_1/V_i = (Z_2/R_1)/[(Z_2/Z_i)+1+(Z_2/R_1)+(A/Z_o-1/Z_2)/(1/Z_o+1/Z_2+1/Z_L)] \qquad (E\text{-}11)$$

In order to simplify the calculation, we assume that Z_i is relatively

large compared to the impedances of other elements and Z_o is relatively small. This assumption may not be justified at high frequencies where the open-loop voltage gain, A, is small. Rewriting Eq.(E-11) with $Z_o \rightarrow 0$ and $Z_i \rightarrow \infty$, we have

$$V_1/V_i = (Z_2/R_1)/[1 + (Z_2/R_1) + A] \qquad \text{(E-12)}$$

When the RFI suppression capacitor C_4 is not included, then $Z_2 = R_2$, and Eq.(E-12) reduces to

$$(V_1/V_i)\big|_{C_4 = 0} = (R_2/R_1)/[1 + (R_2/R_1) + A] \qquad \text{(E-13)}$$

The amount of RFI suppression at the inverting input node of the op amp can be obtained by dividing Eq.(E-12) by Eq.(E-13):

$$\text{RFI suppression at inverting input node} = \frac{|(Z_2/R_1)/[1 + (Z_2/R_1) + A]|}{|(R_2/R_1)/[1 + (R_2/R_1) + A]|} \equiv S \qquad \text{(E-14)}$$

The amount of suppression of second-order RFI responses at the output node of the op amp can be obtained by taking the square of Eq.(E-14):

$$\text{Second-order RFI suppression at output node} = \left\{\frac{|(Z_2/R_1)/[1 + (Z_2/R_1) + A]|}{|(R_2/R_1)/[1 + (R_2/R_1) + A]|}\right\}^2 = S^2 \qquad \text{(E-15)}$$

To facilitate the calculation of Eq.(E-15), an op amp having only a single time constant is considered here. Therefore the open-loop voltage gain, A, is given by

$$A = A_o/(1 + jf/f_o) \qquad \text{(E-16)}$$

where A_o is the dc open-loop voltage gain and f_o the upper half-power frequency. (In practice, the effects caused by additional time constants may show up at higher frequencies. It is believed that these effects are small enough to be ignored.) Assuming typical parameter values for a 741 op amp, we have

$$A_o = 200{,}000 , \qquad f_o = 10 \text{ Hz}$$

Also, we assume that $R_1 = 10$ kΩ, $R_2 = 100$ kΩ, and $C_4 = 27$ pF. We insert these values in Eq.(E-15) and calculate S^2 at frequencies 0.1 MHz, 1 MHz, and 10 MHz. The results are tabulated in Table E-1. Also shown in Table E-1 are experimental values from Figure 5-5.

TABLE E-1

CALCULATED VALUES OF SECOND-ORDER RFI SUPPRESSION AT OUTPUT NODE

f MHz	Calculated Suppression $20\log_{10}(S^2)$ dB	Experimental Suppression dB	Discrepancy dB
0.1	-13.1	-10.7	2.4
1.0	-25.0	-11.6	13.4
10.	-48.1	-36.2	11.9

The calculated values of RFI suppression using Eq.(E-15) are larger than experimental values by 2.4 dB to 13.4 dB and thus overpredict the amount of RFI suppression. It does not seem possible to compare directly our agreement between calculated and experimental values of RFI suppression with that obtained by Goedbloed et al.[31] For RFI frequencies 10 kHz to 2 MHz, they obtained agreement within 3 dB for suppression of RFI-

induced dc voltage shifts in an inverting amplifier with R1 = 4.7 kΩ and R2 = 150 kΩ. However, for RFI frequencies 0.2 to 5 MHz they obtained discrepancies from 0 to 20 dB for suppression of RFI-induced 1 kHz demodulation voltages in a non-inverting op amp circuit.

The linear theory proposed by Goedbloed, Riemens, and Stienstra[31] focuses on the linear suppression of the RFI signal at the op amp input terminals. They used a simple one time constant model for the op amp because it yields a simple formula for the RFI suppression which can be evaluated using a hand-held calculator. This simplifies the EMC design process. That is why they ignored the effects of additional time constants. The 741 op amp macromodel used in this dissertation accounts for excess phase shifts effects caused by additional time constants. The 741 macromodel could be used to calculate the RFI suppression, but the calculations would have to be made on a computer. An additional advantage of using the computer to calculate the RFI suppression would be that it would not be necessary to assume that the input impedance $Z_i = \infty$ and the output impedance $Z_o = 0$. Furthermore, the frequency dependent behavior of Z_i and Z_o would also be accounted for. We have not yet attempted to use the op amp macromodel to calculate RFI suppression in the manner described.

REFERENCES

1. G. Kaplan, "Computer Aided Design," IEEE Spectrum, Vol. 12, pp. 40-46, October 1975.

2. D. D. Weiner and J. F. Spina, "Sinusoidal Analysis and Modeling of Weakly Nonlinear Circuits with Applications to Nonlinear Interference Effects." New York: Van Nostrand Reinhold Co., 1980.

3. "Nonlinear Circuit Analysis Program Documentation," Tech. Rep. RADC-TR-79-245, Vols. I-III, Rome Air Development Center, Griffiss AFB, New York 13441, September 1979. J. F. Spina, C. A. Paludi, Jr., D. D. Weiner and J. J. Whalen, Engineering Manual, Vol. I, J. Valente and S. Stratakos, User's Manual, Vol. II, J. B. Valente and S. Stratakos, Programer's Manual, Vol. III.

4. K. N. Chen, "Nonlinear Modeling of Metal-Oxide-Semiconductor Field-Effect-Transistor with Application to Radio Frequency Interference Analysis," Ph.D. Dissertation, State University of New York at Buffalo, Amherst, New York 14226, February, 1982.

5. K. N. Chen and J. J. Whalen, "A Nonlinear Incremental Model For Predicting EMI In MOS Transistors And Integrated Circuits," International Conf. on Electromagnetic Compatibility, 21-23 Sept., 1982, The University of Surrey - IERE Publication No. 56.

6. T. F. Fang, "Nonlinear System Analysis in Bipolar Integrated Circuits," Ph.D. Dissertation, State University of New York at Buffalo, Amherst, NY 14226, February, 1979.

7. T. F. Fang and J. J. Whalen, "Application of the Nonlinear Circuit Analysis Program NCAP to Predict RFI Effects in Linear Bipolar Integrated Circuits," in Proc. 3rd Symp. Tech. Exhibition on Electromagnetic Compatibility, Rotterdam, pp. 263-268, May 1-3, 1979.

8. T. F. Fang, J. J. Whalen and G. K. C. Chen, "Using NCAP to Predict RFI Effects in Operational Amplifiers," in 1979 IEEE Int. Electromagnetic Compatibility Symp. Rec., San Diego, California,

pp. 96-103, October 9-11, 1979.

9. T. F. Fang, J. J. Whalen and G. K. C. Chen, "Using NCAP to Predict RFI Effects in Linear Bipolar Integrated Circuits," IEEE Trans. Electromagnetic Compatibility, Vol. EMC-22, pp. 256-262, November, 1980.

10. C. A. Paludi, Jr. and J. J. Whalen, "The NCAP Nonlinear T Model for Bipolar Junction Transistors at UHF Frequencies," Record of the 1979 IEEE International Symposium on Electromagnetic Compatibility, (IEEE Pub. No. 79CH1383-9), pp. 112-117, San Diego, CA, October 9-11, 1979.

11. G. R. Boyle, B. M. Cohn, D. O. Pederson and J. E. Solomon, "Macromodeling of Integrated Circuit Operational Amplifiers," IEEE J. Solid-State Circuits, Vol. SC-9, pp. 353-363, December, 1974.

12. G. K. C. Chen, "A Nonlinear Macromodel of the Bipolar Integrated Circuit Operational Amplifier for Electromagnetic Interference Analysis," Ph.D. Dissertation, State University of New York at Buffalo, Amherst, New York 14226, February, 1981.

13. K. N. Chen, G. K. C. Chen and J. J. Whalen, "Using Macromodels to Compare RFI in Bipolar and FET-Bipolar Operational Amplifiers," in Proc. 4th Symp. Tech. Exhibition on Electromagnetic Compatibility, Zurich, pp. 157-162, March 10-12, 1981.

14. G. Krajewska and F. E. Holmes, "Macromodeling of FET/Bipolar Operational Amplifiers," IEEE J. Solid-State Circuits, Vol. SC-14, pp. 1083-1087, December, 1979.

15. J. W. Graham and L. Ehrman, "Nonlinear System Modeling and Analysis with Application to Communication Receivers," Technical Report RADC-TR-73-178, Rome Air Development Center, Griffiss Air Force Base, New York, 1973.

16. J. J. Bussgang L. Ehrman and J. W. Graham, "Analysis of Nonlinear Systems with Multiple Inputs," Proc. IEEE, Vol. 62, pp. 1088-1119, August, 1974.

17. J. J. Whalen, C. A. Paludi and T. F. Fang, "Application of the Nonlinear Circuit Analysis Program NCAP," 1977 IEEE International Electromagnetic Compatibility Symposium Record, pp. 467-474, Seattle, Washington, August 2-4, 1977.

18. J. E. Solomon, "The Monolithic Op Amp: A Tutorial Study," IEEE Journal of Solid-State Circuits, Vol. SC-9, No. 6, December, 1974.

19. "μA LINEAR - 1982 Linear Division Products" Fairchild Camera and Instrument Corporation, Mountain View, CA 94042, 1982.

20. P. E. Gray and C. L. Searle, "Electronic Principles - Physics, Models, and Circuits." New York: John Wiley & Sons, Inc., 1969.

21. J. Millman and C. C. Halkias, "Integrated Electronics - analog and digital circuits and systems." New York: McGraw Hill Book Company.

22. S. Narayanan, "Intermodulation Distortion of Cascaded Transistors," IEEE Journal of Solid State Circuits, Vol. SC-4, pp. 97-106, June, 1969.

23. S. Narayanan, "Application of Volterra Series to Intermodulation Distortion Analysis of Transistor Feedback Amplifiers," IEEE Trans. on Circuit Theory, Vol. CT-17, pp. 518-527, November, 1970.

24. J. F. Spina, J. Lexa, and D. D. Weiner, "Computer Modeling of Solid State VHF Tuner Using the Nonlinear Transfer Function Approach," Technical Memorandum, Rome Air Development Center, Griffiss Air Force Base, New York, 1974.

25. R. B. Fair, "Harmonic Distortion in the Junction Field-Effect Transistor with Field-Dependent Mobility," IEEE Trans. Electron Devices, Vol. ED-19, No. 1, pp. 9-13, Jan., 1972.

26. P. R. Gray and R. G. Meyer, "Recent Advances In Monolithic Operational Amplifier Design," IEEE Trans. Circuits and Syst., Vol. CAS-21, pp. 317-327, May, 1974.

27. Y. H. Sutu and J. J. Whalen, "A Comparison of RFI in Operational Amplifiers," Proc. of the 5th Symposium and Technical Exhibition

on Electromagnetic Compatibility, pp. 477-482, Zurich, Switzerland, March 8-10, 1983.

28. G. K. C. Chen and J. J. Whalen, "Macromodel Predictions for EMI in Bipolar Operational Amplifiers," IEEE Trans. Electromagnetic Compatibility, Vol. EMC-22, pp. 262-265, November, 1980. Also see Proc. Conf. on Electromagnetic Compatibility, University of Southampton, pp. 363-375, September, 1980.

29. G. K. C. Chen and J. J. Whalen, "Comparative RFI Performances of Bipolar Operational Amplifiers," 1981 IEEE International Electromagnetic Compatibility Symposium Record, pp. 91-95, Boulder, Colorado, August 18-20, 1981.

30. K. N. Chen and J. J. Whalen, "MOSFET Nonlinear Incremental Model For NCAP," 1982 IEEE International Electromagnetic Compatibility Symposium Record, pp. 66-73, Santa Clara, California, September 8-10, 1982.

31. J. J. Goedbloed, K. Riemens and A. J. Stienstra, "Increasing the RFI Immunity of Amplifiers with Negative Feedback," 5th Symp. and Tech. Exh. on EMC, Zurich, March 8-10, 1983.

32. J. J. Whalen, "Notes on Electronic Circuits," Vol. 1, p. 283, Dept. of Electrical and Computer Engineering, SUNY/Buffalo, NY 14226, Spring, 1984.

33. J. J. Whalen, "DC Offsets in Op Amps," Memo., July 14, 1983.

34. J. J. Whalen and C. Paludi, " Computer-Aided Analysis of Electronic Circuits - the Need to include Parasitic Elements," International J. of Electronics, Vol. 43, pp. 501-511, November, 1977.

35. J. B. Valente, "The Nonlinear Circuit Analysis Program," 1977 IEEE International Electromagnetic Compatibility Symposium Record, pp. 461-466, Seattle, Washington, August 2-4, 1977.

36. L. W. Nagel, "SPICE2 : A Computer Program to Simulate Semiconductor Circuits," Memo. No. ERL-M520, Electronic Research Lab., College of Engineering, U. C. Berkeley, California 94720, May, 1975.

37. J. G. Tront, J. J. Whalen, C. E. Larson and J. M. Roe, "Computer Aided Analysis of RFI Effects in Operational Amplifiers," Proc. of the 3rd Symp. and Tech. Exh. on EMC, pp. 269-274, Rotterdam, The Netherlands, May 1-3, 1979.

38. W. L. Nagel and D. O. Pederson, "SPICE - Simulation Program with Integrated Circuit Emphasis," Technical Memorandum No. ERL-M382, Electronic Research Laboratory, University of California, Berkeley, CA 94720, April 12, 1973.

39. "LM10/LM10B(L)/LM10C(L) Op Amp and Voltage Reference," National Semiconductor, December, 1978.

40. CA081 BiMOS Operational Amplifiers Data Sheet, RCA Solid State.

41. J. J. Whalen, "Goals of 3-stage Op Amp LED Experiment," Memo., Dept. of Electrical Engineering, SUNY/Buffalo, NY 14226, June 8, 1983.

42. C. R. Paul and J. W. McKnight, "Prediction of Crosstalk Involving Twisted Pairs of Wires - Part I: A Transmission-Line Model for Twisted Wire, IEEE Trans. on EMC, Vol. EMC-21, p. 92, May 1979.

43. C. R. Paul and J. W. McKnight, "Prediction of Crosstalk Involving Twisted Pairs of Wires - Part II: A Simplified Low-Frequency Prediction Model," IEEE Trans. on EMC, Vol. EMC-21, p. 105, May 1979.

44. "LF155/LF156/LF157 Series Monolithic JFET Input Operational Amplifiers," National Semiconductor, 1980.

MISSION
of
Rome Air Development Center

RADC plans and executes research, development, test and selected acquisition programs in support of Command, Control Communications and Intelligence (C^3I) activities. Technical and engineering support within areas of technical competence is provided to ESD Program Offices (POs) and other ESD elements. The principal technical mission areas are communications, electromagnetic guidance and control, surveillance of ground and aerospace objects, intelligence data collection and handling, information system technology, ionospheric propagation, solid state sciences, microwave physics and electronic reliability, maintainability and compatibility.

END

FILMED

7-85

DTIC